Institute of Pharmacy and Biomedical Sciences

Molecular analysis of MAP kinase kinase signalling in *Leishmania*

Basmah Massad Alenzi

Thesis presented in fulfilment of the requirement for the degree of

Doctor of Philosophy (PhD)

June 2019

Declaration of Authenticity and Author's Rights

This thesis is the result of the author's original research. It has been composed by the author and has not been previously submitted for examination which has led to the award of a degree.

Signed: Basmah Massad Alenzi

Date: 28-06-2019

Acknowledgment

I would like to express my deepest appreciation to my supervisor, Dr Martin Wiese, who demonstrates the attitude of a genius: he continually and convincingly conveys the spirit of adventure with regards to research and of passion with regards to teaching. Without his guidance and persistent help, this dissertation would not have been possible.

I would like to thank Dr Chris Carter for her advice and help during the animal infection experiment, which was essential for the drug screening aspect of this work. Moreover, I am indebted to many of my colleagues in the 'Wiese group', for their support.

I would also like to thank my Dada, my Mum and my husband, Maher Alharbi, for their immense support, patience and understanding during this journey. Finally, I would like to thank my siblings for their unending support.

Abstract

Mitogen-activated protein kinase patways play important roles in *L. mexicana* cell biology. This research characterised two yet unstudied MAP2Ks (LmxPK3 and LmxPK6) in *Leishmania* and studied putative signal transduction between MAP2Ks and MAPKs involved in regulating flagellum length. LmxPK6 is closely related to the STE7 kinase family, and LmxPK3 is related to CAMK. Recombinant GST-LmxPK6 could not be obtained, but GST-LmxPK3 could be purified in sufficient amounts to prove kinase activity by phosphorylation of the generic substrate MBP. Only single allele deletion mutants could be generated for *LmxPK6.* Multiple attempts to obtain a null mutant were unsuccessful. This might suggest that LmxPK6 is an essential kinase of *L. mexicana*. However, an LmxPK3 null mutant was successfully generated, relying on the LmxMPK12 flanking regions to guarantee sufficient neomycin phosphotransferase resistance marker gene expression. GFP fused to LmxPK3 at either the C-terminus or the N-terminus showed that LmxPK3 localised in the cytosol and flagellum. A null mutant of LmxPK3 showed similar lesion development in BALB/c mice as wild type *L. mexicana,* and the lesion-derived amastigotes differentiated back to promastigotes and grew in culture suggesting that LmxPK3 does not play a role in *Leishmania* differentiation. Hence, LmxPK3 is not a drug target against leishmaniasis. Interactions between LmxPK4 and LmxMPK3 were investigated *in vitro* by co-expression of the two kinases in *Escherichia coli* followed by purification and kinase assays. MS/MS analysis showed that LmxPK4 phosphorylates LmxMPK3 at SER183, THR194 and TYR196 of the TDY motif. Using split-GFP for the first time in *Leishmania* promastigotes showed an interaction between LmxPK4 and LmxMPK3 *in vivo* by fluorescence in distinct areas of the cytosol and formation of normal length flagella when expressed in the LmxMPK3 null mutant. A hypothesis of how LmxPK4 and LmxMKK can jointly regulate intraflagellar transport was generated.

Abbreviations

Aa	Amino acids
AP	Alkaline phosphatase
APKs	Atypical PKs
ATP	Adenosine triphosphate
Bla	Blasticidin S
bps	Base pairs
C	Degree Celsius
CaMKs	Calcium / calmodulin-dependent protein kinases
cAMP	cyclic adenosine monophosphate
CaBP	Ca^{2+} binding proteins
CD	domain common docking domain
C. elegans	*Caenorhabditis elegans*
cDNA	complementary DNA
cGMP	cyclic guanosine monophospha
C. reinhardtii	*Chlamydomonas reinhardtii*
CL	Cutaneous leishmaniasis
ddH_2O	Double distilled water
DMSO	Dimethyl sulfoxide
DNA	Deoxyribonucleic acid
dNTP	Deoxyribonucleotide triphosphate
DTT	1, 4-dithiothreitol

DIC	Differential interference contrast microscopy
ePK	Eukaryotic protein kinase
E. coli	*Escherichia coli*
EDTA	Ethylenediamine tetra acetic acid
EtBr	Ethidium bromide
g	Gram
× g	times gravity
gDNA	genomic DNA
gRNA	guide RNA
GS	glutamine synthetase
GFP	Green fluorescent protein
GST	Glutathione-S-transferase
GTP	Guanosine Triphosphate
GDP	Guanosine Diphosphate
h	hours
HCl	hydrochloric acid
HYG	Hygromycin B resistance marker gene
His	histidine
HPLC	high performance liquid chromatography
InsP	Inositol phosphate
InsP3	inositol 1,4,5-triphosphate
JNK	c-Jun N-terminal kinase
IPTG	Isopropyl-β-D-thiogalactopyranoside
L	Litres

kb	Kilo base pairs
kDa	Kilo Dalton
L.	*Leishmania*
LB	Luria-Bertani (broth)
L. major	*Leishmania major*
MAPKs	Mitogen-activated protein kinases
MAP2K or MPKK	MAP kinase kinase
MP3K or MAPKKK	MAP kinase kinase kinase
MBP	Myelin basic protein
MCL	Mucocutaneous leishmaniasis
DHFR-TS	dihydrofolate reductase-thymidylate synthase
MOPS	Morpholinopropane sulfonic acid
mRNA	messenger RNA
MS	mass spectrometry
MS/MS	tandem MS
NaCl	Sodium chloride
NaOH	Sodium hydroxide
NEO	Neomycin resistance marker gene
OD	optical density
ORF	Open reading frame
PBS	Phosphate-buffered saline
PCR	Polymerase chain reaction
PKA	Protein kinase A
PKs	Protein kinases
RNA	Ribonucleic acid

rpm	Revolutions per minute
RT	Room temperature
s	Seconds
SAP	shrimp alkaline phosphatase
SDS	sodium dodecyl sulphate
SDS-PAGE	sodium dodecyl sulphate-polyacrylamide gel electrophoresis
SL	SL spliced leader
T. brucei	*Trypanosoma brucei*
T. cruzi	*Trypanosoma cruzi*
TEMED	N, N, N′, N′-tetramethylethylenediamine
TMB	3 ,3',5,5'-Tetramethylbenzidine
U	units
UTR	untranslated region
V	volt
v/v	Volume per volume
VL	Visceral leishmaniasis
w/v	Weight per volume
WHO	World Health Organisation
-/-	double-allele deletion
+/-	single-allele deletion

Contents

Figures

Tables

Chapter 1: General Introduction

1.1 *Leishmania* and leishmaniasis

Leishmaniasis is a parasitic disease caused by protozoan parasites belonging to the genus *Leishmania* (Alvar et al., 2012). People in more than 98 countries suffer from leishmaniasis. Each year, the number of new cases worldwide ranges from 700,000 to 1,000,000, and between 20,000 and 30,000 deaths occur (World Health Organization [WHO], 2018).

1.2 Epidemiology and clinical manifestations

Leishmaniasis is characterised by a spectrum of clinical manifestations, including cutaneous leishmaniasis (CL), which presents with multiple non-ulcerative nodules. CL is considered a group of diseases, because CL presents with various clinical manifestations, which depend on the parasite species and the host's level of immunity (Reithinger et al., 2007). Localised CL occurs when ulcerative skin lesions develop at the site of a sand fly bite. Mucosal CL occurs when symptoms include destructive mucosal inflammation (Reithinger et al., 2007). The most notable clinical feature of CL is the development of a nodule, which subsequently develops into an ulcer with a sharply incised central crater and indurate-raised margins, which progresses over a period of several months (Reithinger et al., 2007). The lesions, which result from leishmaniasis, are typically painless until a secondary infection develops (Bari, 2012). Although CL causes disfiguring lesions, it is not a life-threatening condition. However, patients with CL often experience psychological and social ramifications, which can include depression, anxiety and a reduced quality of life (Kassi et al., 2008). Figure 1.1 A shows the distribution of CL in 2016.

Visceral leishmaniasis (VL) is the most severe form of leishmaniasis. However, VL has a more limited distribution than CL (Figure 1.1 B), with 90% of VL cases occurring

in Sudan, Brazil, India and Nepal (Hussain et al., 2014). The species which cause VL are *L. donovani*, *L. chagasi* and *L. infantum* (Murray et al., 2005). VL, also known as kala-azar, can be fatal if left untreated. VL is characterised by irregular bouts of fever, weight loss, the enlargement of the spleen and liver, and anaemia (WHO, 2018). Post-kala-azar dermal leishmaniasis is a complication of VL characterised by a typical nodular rash in patients who have recovered from VL but are otherwise healthy. The rash usually starts around the mouth and can spread to other parts of the body, depending on the severity of the condition (Zijlstra, 2016).

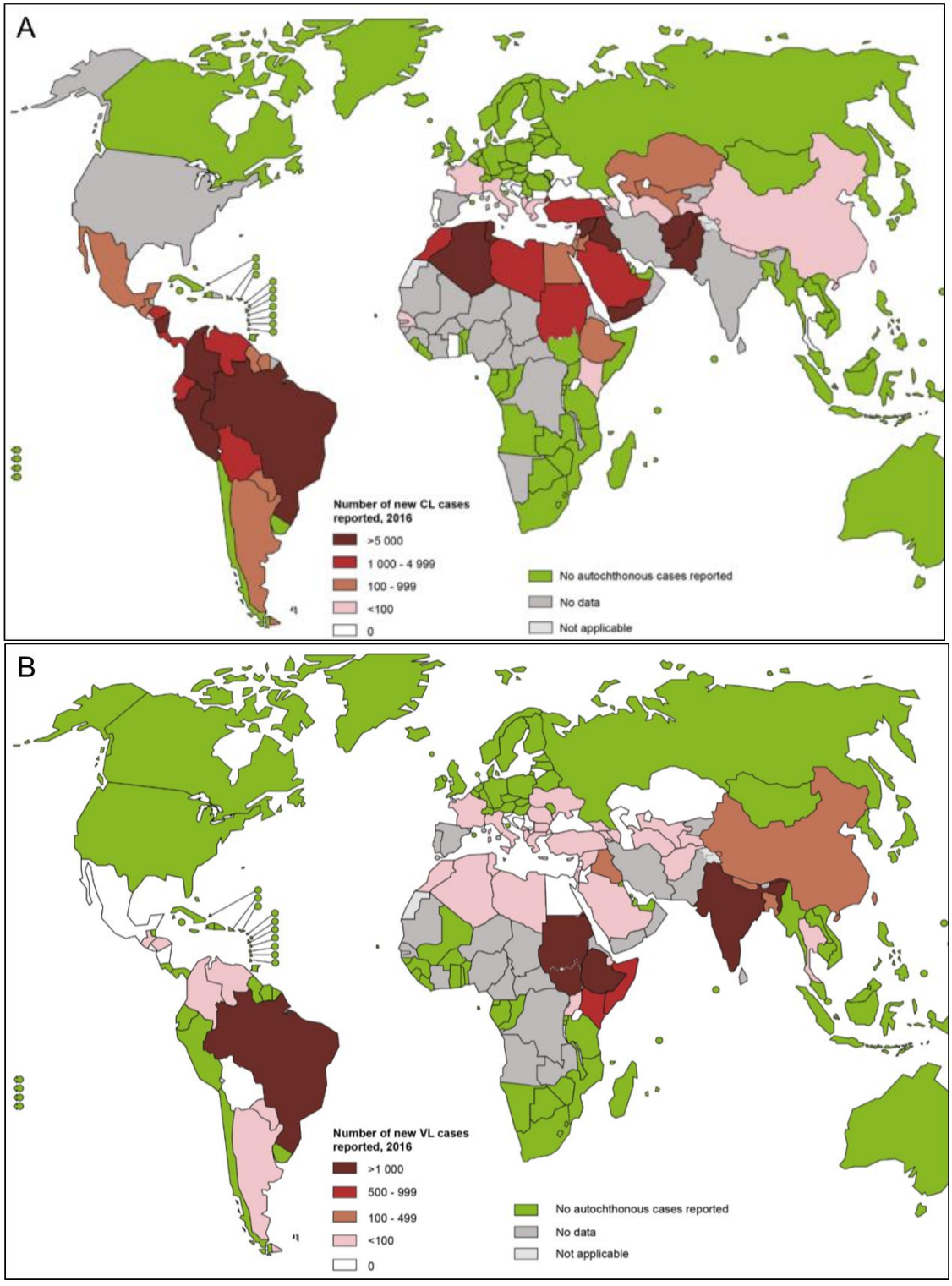

Figure 1.1. Worldwide distribution of leishmaniasis in 2016. Panel A shows the countries affected by cutaneous leishmaniasis. Panel B shows the countries affected by visceral leishmaniasis (WHO, 2018).

1.3 Treatment and prevention of leishmaniasis

Determining the *Leishmania* species responsible for leishmaniasis is important in selecting the appropriate drug treatment. However, species identification can be difficult in many endemic countries, as several species of *Leishmania* may be found in these locations. The form of the disease and the body parts affected can also be used to determine the appropriate treatment (Murray et al., 2005). Antimonial chemotherapy of leishmaniasis has been used as a first-line treatment for the past 60 years and can cause DNA fragmentation in *Leishmania* species. However, the exact mechanisms of action in these drugs remain unknown (Dorlo et al., 2012). The compounds of pentavalent antimoniates, such as sodium stibogluconate and meglumine antimoniate (MA), are antileishmanial for VL and CL under different conditions. Systemic antimonial and intralesional drugs are recommended by the WHO to treat CL (Minodier and Parola, 2007; Reithinger et al., 2007). The WHO also recommends intra-lesion antimony treatment, in which the drug is injected at the edge of the lesion every two to seven days for up to 30 days (Minodier and Parola, 2007). Antimonial drugs have been shown to temporarily affect the liver enzymes by increasing aspartate aminotransferase (AST) and alanine aminotransferase (ALT) in patients treated with MA, and animal experiments showed that the activity of cytochrome P1A decreased in the livers of mice (Ghorbani et al., 2018). Many studies have also reported increased resistance to the MA drug. Studies of Indian patients who suffer from VL showed that they did not respond to pentavalent antimonial (Sb^{5+}) treatment indicating resistance of the parasite (Croft et al., 2006; Nare et al., 2009). The drug also led to renal and cardiac toxicity in leishmaniasis patients (de Moura et al., 2016).

The second line of treatment is Fungizone®, an antifungal treatment containing amphotericin B, which is used to treat both VL and mucosal CL (Adler-Moore et al., 1993). The amphotericin B drug is limited in its use as a treatment, because the side effects are chronic and acutely adverse, for example myocarditis, chills, fever, hypokalaemia and even death. Amphotericin B has low solubility in aqueous solutions and therefore has a low bioavailability. It is used intravenously in systemic infections. Clinical isolates of *L. donovani* have been shown to be resistant to amphotericin B (Croft et al., 2003). *Leishmania* strains showing resistance to amphotericin B show significantly decreased reactive oxygen species (ROS) accumulation has led to an increase of components of the tryparedoxin cascade. These pathways could play an important role in the antioxidative defence against ROS in kinetoplastids (Dorlo et al., 2012). Proteomic analysis of the amphotericin B resistant (AmB-R) strain of *L. infantum* showed upregulation of members of the tryparedoxin cascade (Dorlo et al., 2012). AmB resistance was also associated with ATP depletion and led to an increase in ion leakage. Other studies also found that the ATP-binding cassette family of transporters and various Ras isoforms might have important roles in AmB-R strains of *Leishmania* (Brothertonet et al., 2014; Purkait et al., 2012). To conclude, the second-line treatment is effective in inhibiting *Leishmania* growth, but due to the higher toxicity and treatment resistance, its use is limited.

AmBisome is a unique liposomal formulation of amphotericin B, which circulates in the body for a long time and penetrates tissues efficiently, due to its small size. Moreover, it displays reduced toxicity. However, AmBisome is expensive, especially in developing countries (Wasan et al., 2010).

Miltefosine is the third-line treatment and was originally developed as an anticancer agent but is now used to treat VL and CL. The benefit of this treatment is a short

course, and the most common side effect reported is gastrointestinal discomfort. Miltefosine treatment of *Leishmania* showed high bioavailability in *in vitro* experiments (Croft et al., 2003). Miltefosine was shown to inhibit the synthesis of phosphatidylcholine and the cytochrome c oxidase, the latter affecting the parasite mitochondrion. It was also shown to be able to activate a Ca^{2+} channel in the plasma membrane and to affect acidocalcisomes (Pinto-Martinez et al., 2018). Promastigotes could become resistant to miltefosine as a result of a mutation of the miltefosine transporter gene due to loss of drug internalisation, which is considered a resistance mechanism (Ghorbani et al., 2018). It was suggested that miltefosine transporter activity is vital and that inactivation of the transporter led to miltefosine resistance in parasites (Maran et al., 2016; Perez-Victoria et al., 2003). The side effects of miltefosine limit its clinical use in the treatment of leishmaniasis.

Chemotherapy is the most effective treatment of leishmaniasis; however, the major drawbacks of such treatment are a long lifespan, teratogenicity and high costs (Maran et al., 2016). Therefore, alternative therapeutic methods were sought. Vaccination is the most economical way to prevent infection. There are many forms of vaccine used against viruses such as killed virus, recombinant subunits, attenuated virus, or DNA (Soni et al., 2015). Vaccines use the induction of an immune response to produce memory lymphocytes to control infection. Vaccines can stimulate humoral and cellular immunity, especially a strong Th1 response, as well as cell cytotoxicity to eliminate the infection (McMichael and Koff, 2014; Soni et al., 2015). However, leishmaniasis does not have a vaccine for prevention yet.

A first-generation vaccine against leishmaniasis is composed of killed whole parasites and can be produced in developing countries at a low cost. Fructose mannose ligand and saponins were used as adjuvants in the first vaccines designed for canine VL

containing purified *L. donovani* (Ghorbani et al., 2018). This vaccine suppresses the transmission of zoonotic VL in an immunoprotective role with a purified *Leishmania* extract, which is widely used in the experimental model (Afrin et al., 2002). The first-generation vaccine in human clinical trials was evaluated for three forms of leishmaniasis caused by *L. major*, *L. amazonensis* and *L. mexicana* (Noazin et al., 2008). However, there are many issues to be addressed for a vaccine derived from cultured parasites, for example standardisation and large-scale *in vitro* culture (Ghorbani et al., 2018).

A recombinant protein vaccine would be low-cost compared to other vaccines, because distribution does not need a cold chain and is flexible, combining several different genes into the product. Generation of immune responses via activation of the innate immunity is the mode of action of DNA vaccines (Palatnik-de-Sousa et al., 2008). Vaccination with plasmids were attempted, but there are no available Phase III data on these vaccines (Ghorbani et al., 2018). It has been shown that a DNA vaccine composed of the genes for thiol-specific antioxidant antigen (TSA) or *L. major* stress-inducible protein 1 (LmSTI1) can protect against CL in mice via a CD4+ Th1 response. However, clinical trial Phases I and II and animal trials of the DNA vaccine were not promising (Velashjerdi Farahani et al., 2016).

To conclude, current vaccination and drug therapies are far from being perfect therapeutic methods to eliminate leishmaniasis, and more research is needed. As a result, the most effective prevention for leishmaniasis is not to experience bites by a sand fly (Alexander and Maroli, 2003).

1.4 Life cycle of *Leishmania*

Leishmania parasites undergo a digenetic life cycle, differentiating from the promastigote form within the insect vector, the phlebotomine sand fly, to the amastigote form within the lysosomal compartment of mammalian macrophages (Figure 1.2). The insect-stage promastigotes appear as spindle-shaped cells 11–20 µm in length and 2 µm in diameter, with a kinetoplast, a large central nucleus, a projecting form of flagellar pocket and longe flagellum. Promastigotes have a single flagellum at their anterior pole which is at least the length of their cell bodies. The flagellum reaching up to 20 µm in length, protruding from the flagellar pocket at the anterior end of the cell (Wiese et al., 2003b). This flagellum propels the cell forward and mediates cell attachment to the surface of the insect gut. Amastigotes are smaller spherical cells 4–5 µm in length, with their short flagellum almost entirely buried inside the flagella pocket.

The *Leishmania* life cycle begins when a female sand fly takes a blood meal from an infected mammal. When the sand fly produces a small wound in the mammal's skin, it leads to the release of amastigotes into the blood pool and macrophages in the gut of the sand fly (Lane, 1993). The change in the parasite's condition (a decrease in temperature, increase in pH) leads to a differentiation into different stages. Also, it has been shown that different cell surface glycoconjugates play an important role in the parasite's strategy to survive. Lipophosphoglycan, produced during different stages of the *Leishmania* life cycle, is a glycoconjugate which represents the primary cell surface component of promastigotes and binds to the lectin receptors on the gut

epithelium of the sand fly, preventing the expulsion of the parasite during the excretion of the blood meal (Kamhawi, 2006).

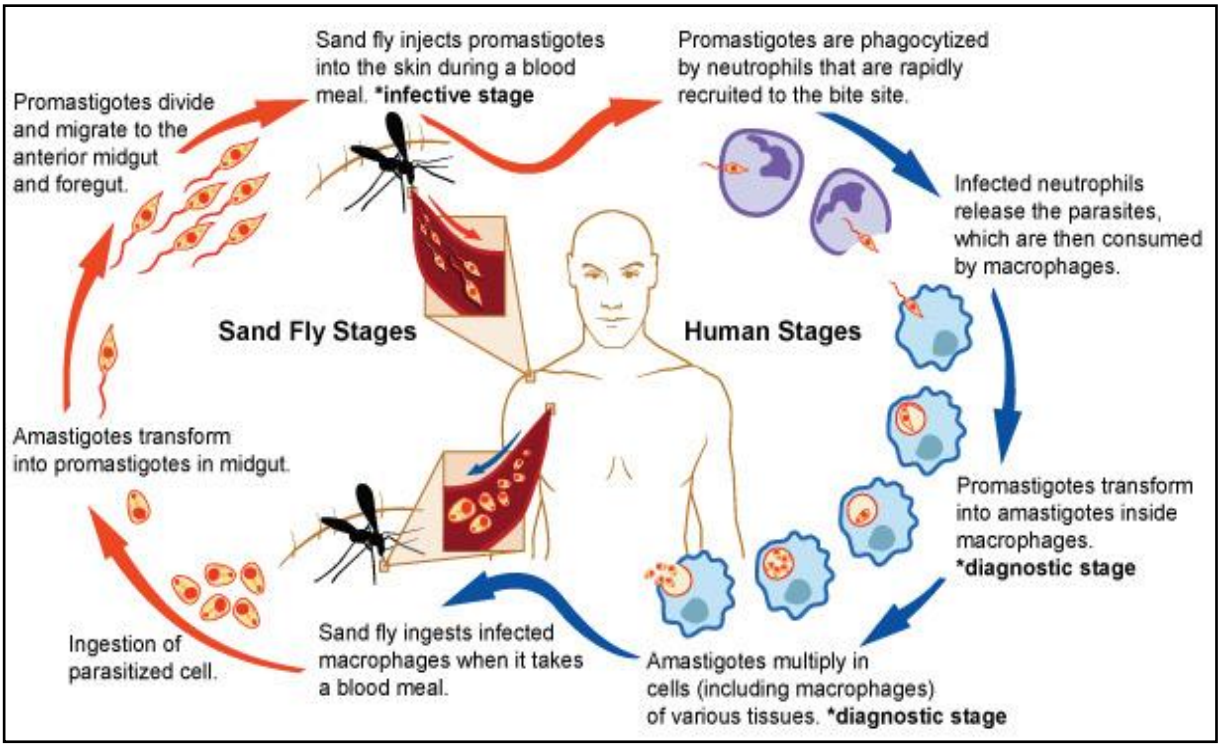

Figure 1.2. The life cycle of *Leishmania* (Adapted from NIAID, 2015).

Four promastigote forms have been identified in the sand fly. The first occurs when the amastigotes transform into procyclic promastigotes within 48 h after the blood meal and present in the midgut of the female sand fly, still enclosed by the peritrophic membrane (PM) protecting the parasite from digestion (Pimenta et al., 1997). The procyclic promastigotes are an oval-shaped, flagellated, weakly motile replicative form (Bates and Rogers, 2004; Teixeira et al., 2013). Within 24 h, the slow procyclic forms generate long flagella, which allow rapid movement. The resulting slender, non-dividing and strongly motile cells are known as nectomonads, the second form of promastigotes (Schlein et al., 1991). Replication and transformation into the non-dividing, long, slender and strongly motile nectomonad promastigotes, which escape from the PM via secretion of a chitinase (Schlein et al., 1991), allows them to anchor

themselves to the midgut epithelium. They subsequently migrate towards the anterior midgut until reaching the stomodeal valve located at the junction between the midgut and foregut. By day four, the nectomonads develop into leptomonads, the third form of promastigotes, a shorter form of the parasite; the leptomonads produce a promastigote secretory gel (PSG), which functions to block the anterior midgut of the sand fly, ensuring the transmission of the parasite to the mammalian host. PSG plays a role in biological transmission, acting as a sieve that retains immature parasites to produce a final metacyclic form. The immature and mature promastigote parasites were observed to have differences in movement within the PSG plug (Rogers et al., 2002; Saraiva et al., 1995). After day five, the leptomonad promastigotes differentiate into mammalian-infective, non-dividing metacyclic promastigotes and develop a metacyclic form, the fourth form, between days five and seven, with an expanded short flagellum and a tip which mediates the attachment of the parasite to the cuticle-lined surface of the stomodeal valve (Kamhawi, 2006). Whether the non-motile promastigote develops from the nectomonads or leptomonads remains unknown. However, both attach to the stomodaeal valve and form a parasite plug (Rogers et al., 2002).

The metacyclic stage is adapted for transmission from the insect to mammals. Metacyclic promastigotes are transmitted through the skin of the mammalian host. Regurgitation of metacyclic promastigotes is induced by the PSG plug during the blood meal (Rogers et al., 2002). It was also observed that another form of promastigotes with short flagella, known as haptomonads, was attached to the stomodaeal valve of the sand fly directly before the next blood meal (Kamhawi, 2006). The PSG plug must be regurgitated by the female sand fly, thereby transmitting the metacyclic promastigotes into the skin of the mammalian host. It is assumed that induced enzymatic damage of the stomodeal valve, an occurrence of parasites in the

salivary glands, and an excretion of parasites from the anus of the infected sand flies additionally contribute to the transmission of the parasite (Kamhawi, 2006; Figure 1.3).

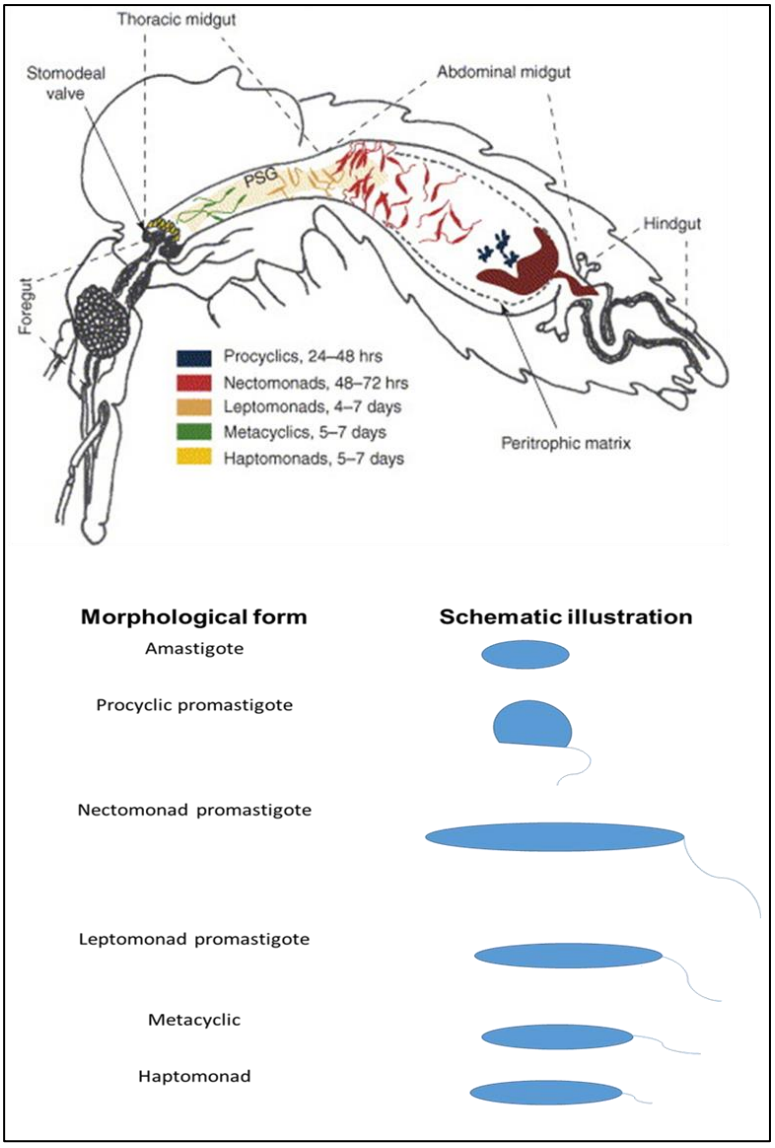

Figure 1.3. Differences between the stages of promastigotes in sand flies (Adapted from Kamhawi, 2006).

1.4.1 *Leishmania* flagellum structure and function

The most distinguishing feature of a *Leishmania* promastigote is the flagellum. The flagellum plays a critical role in the retention of *Leishmania* within the sand fly (Bates, 2007). The flagellum is located at the anterior end of the cell and propels the cell from the gut to the mouth of the sand fly (Bates, 2007). One function of the flagellum is attaching the cell to the midgut epithelium to prevent excretion by attaching, through the flagellum tip. The flagellum tip contains hemidesmosomal structures, which facilitate the anchoring of the parasite to the cuticle-lined portions of the foregut, hindgut and stomodaeal valve (Bates, 2007).

Another theory suggests that the flagellum can be inserted between two epithelial cells to anchor the *Leishmania* cell to the gut lining through receptor-ligand interactions (Dostalova and Volf, 2012). Flagella are well-conserved cell structures, which can be found in entities from protists to mammals, and these organelles are functionally involved with many biological processes, such as fluid movement, sensory reception and single-cell movement inside complex multicellular organisms (Parsons et al., 2005). Flagella typically form from a cell surface and are composed of a microtubule backbone (axoneme) surrounded by a membrane contiguous with the plasma membrane. The motile “9+2” type is composed of nine microtubule doublets surrounding a central pair of single microtubules. The “9+0” type is non-motile, and its nine microtubule doublets do not surround a central pair of single microtubules (Fisch and Dupuis-Williams, 2011).

A feature of flagella in trypanosomatids is the presence of a paraflagellar rod (PFR) which runs along the length of each flagellum and attaches to the axoneme, presenting a lattice-like structure in an electron microscope (Gull, 1999). PFRs have been identified in three groups of protists: kinetoplastids, euglenoids and

dinoflagellates. PFRs are plate-like structures, composed of intermediate domain filaments and proximal distal domains linked in parallel, and the proximal domains of the PFR connect with axonemal microtubules at doublets four to seven (Ridgley et al., 2000). Forty proteins have been associated with PFRs by using immunological, biochemical and bioinformatics techniques. The PFR is demonstrated to be involved in regulatory, metabolic and signalling functions, although its precise role has not yet been determined (Portman and Gull, 2010).

Flagellar proteins play potential roles during environmental sensing and intracellular signal transduction (Paindavoine et al., 1992). The flagellar membrane of *T. brucei* contains the adenylate cyclase, ESAG4, and the flagellar membrane has functions in signalling pathways (Paindavoine et al., 1992). An EF-hand flagellar Ca^{2+}-binding protein (FCaBP) is associated with the flagellar membrane in a Ca^{2+}-dependent manner in *T. cruzi* (Engman et al., 1989). An analogous mechanism was found in the plasma membrane of mammalian retinal rod cells, where an EF-hand Ca^{2+}-binding protein mediates signal transduction through changes in intracellular Ca^{2+} levels (Calvert et al.,1995). ISO1 was identified as a flagellum-specific glucose transporter (Piper et al., 1995). Yeast and human orthologues of ISO1 are involved in glucose sensing (Bandyopadhyay et al., 2000; Ozcan et al., 1996). The flagellum of trypanosomes is involved in regulating the size, shape, polarity and division of the cell (Kohl et al., 2003). The flagellar attachment zone, which is exclusively found in trypanosomes, and the flagellar attachment to the cell body mediate the function of the flagellum. However, *Leishmania* does not have similar functions as those performed by unattached flagella (Kohl et al., 2003). A desmosome-like thickening may prevent the free flow of materials into and out of the flagella pocket membrane; however, macromolecules have been shown to pass through this border (Landfear and Ignatushchenko, 2001).

The mechanism for transporting macromolecules within mature and nascent flagella is known as intraflagellar transport (IFT); however, IFT has also been observed in the basal bodies of cilia (Absalon et al., 2008). The flagellar pockets of *T. brucei* are the only sites within the cell where both endocytosis and protein secretion occur, and membrane proteins are first delivered to the flagellar pocket, after which they are differentially targeted to different membrane domains (Bastin et al., 2000). The sub-proteome identified from the purified flagella of *Chlamydomonas reinhardtii* contains 93 signal transduction proteins, including 21 protein kinases and 32 flagellar phosphoproteins, such as DYF-5, which regulates flagellar length in *C. elegans* (BurgHoorn et al., 2007).

Many proteins have been suggested to play roles in the control of flagellar length, including the following: the aurora protein kinase (CALK) (Pan et al., 2004); the cyclin-dependent kinase (CDK)-related kinase, long flagella 2 (LF2) (Tam et al., 2007); the never in mitosis gene A (NIMA)-related kinase Cnk2p (Bradley and Quarmby, 2005); and glycogen synthase kinase (GSK)3β (Wilson and Lefebvre, 2004). Moreover, the following members of MAPK pathways LmxMPK9 (Bengs et al., 2005), LmxMPK14 (Scholz, 2008), LmxPK4 (Kuhn and Wiese, 2005), LmxMPK13, LmxMKK and LmxMPK3 (Wiese et al., 2003b) were shown to be involved in the regulation of flagellar length.

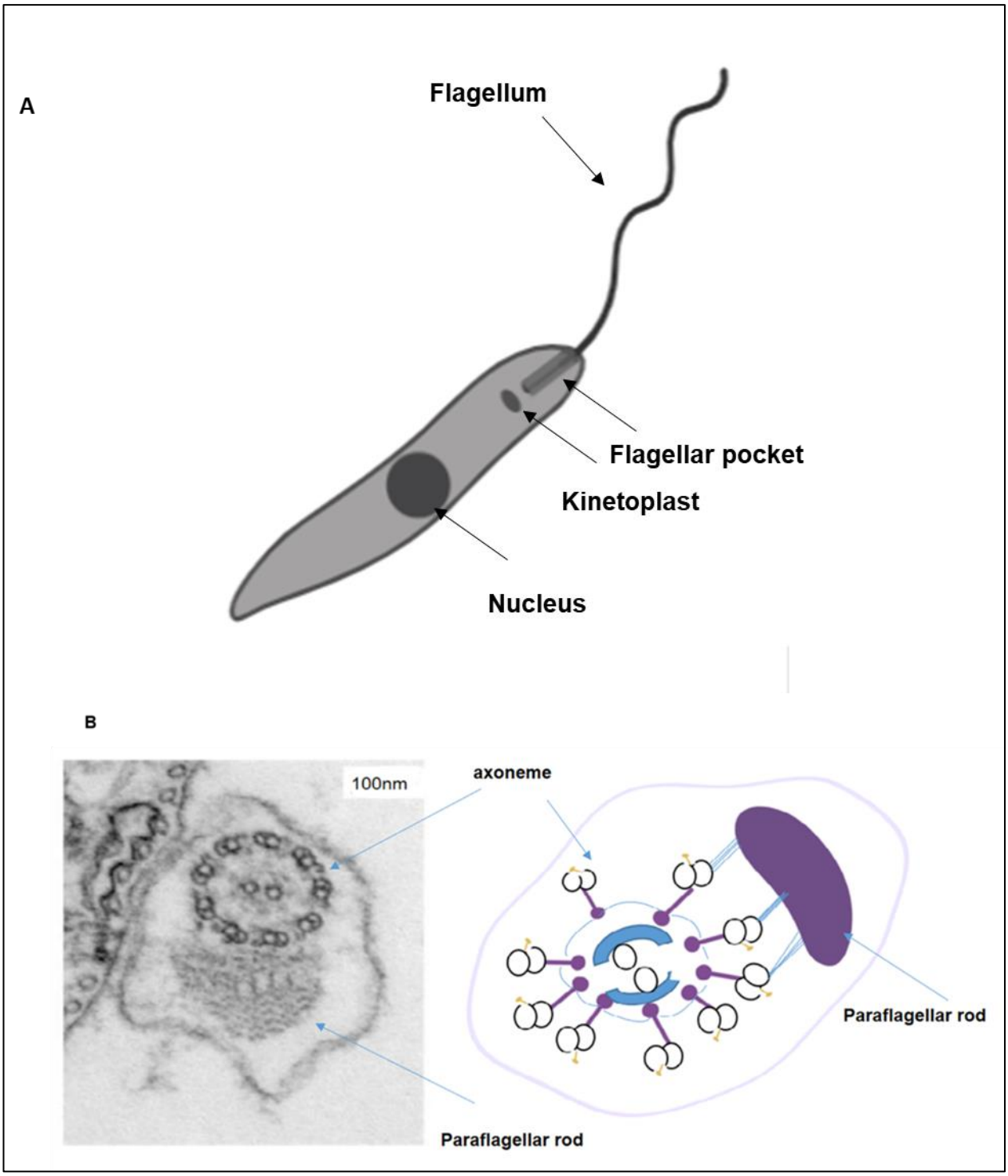

Figure 1.4. Flagellum structure of trypanosomatids. A) Structural organisation of the *Leishmania* promastigote. **B)** Flagellum structure; cross section and drawing of axoneme and PFR (Adapted from Branche et al., 2006; Teixeira et al., 2013).

1.5 Taxonomy

The modern taxonomy of *Leishmania* is shown in Figure 1.4. *Leishmania* is a single-celled organism which belongs to the *Trypanosomatidae* family and includes all kinetoplastid flagellates of the genus *Leishmania.* In 1994, the *Leishmania* Genome Network was established in Rio de Janeiro, Brazil (Ivens and Blackwell, 1999). There are 30 different species in the genus *Leishmania*, and 20 of these species cause leishmaniasis in humans (Banuls et al., 2002) The genus *Leishmania* is divided into three sub-genera (*Sauroleishmania*, *Leishmania* and *Vannia*), based on the presence of a developmental phase in the hindgut of sand flies (Chauhan et al., 2015). *L. mexicana* is the species studied in our investigation.

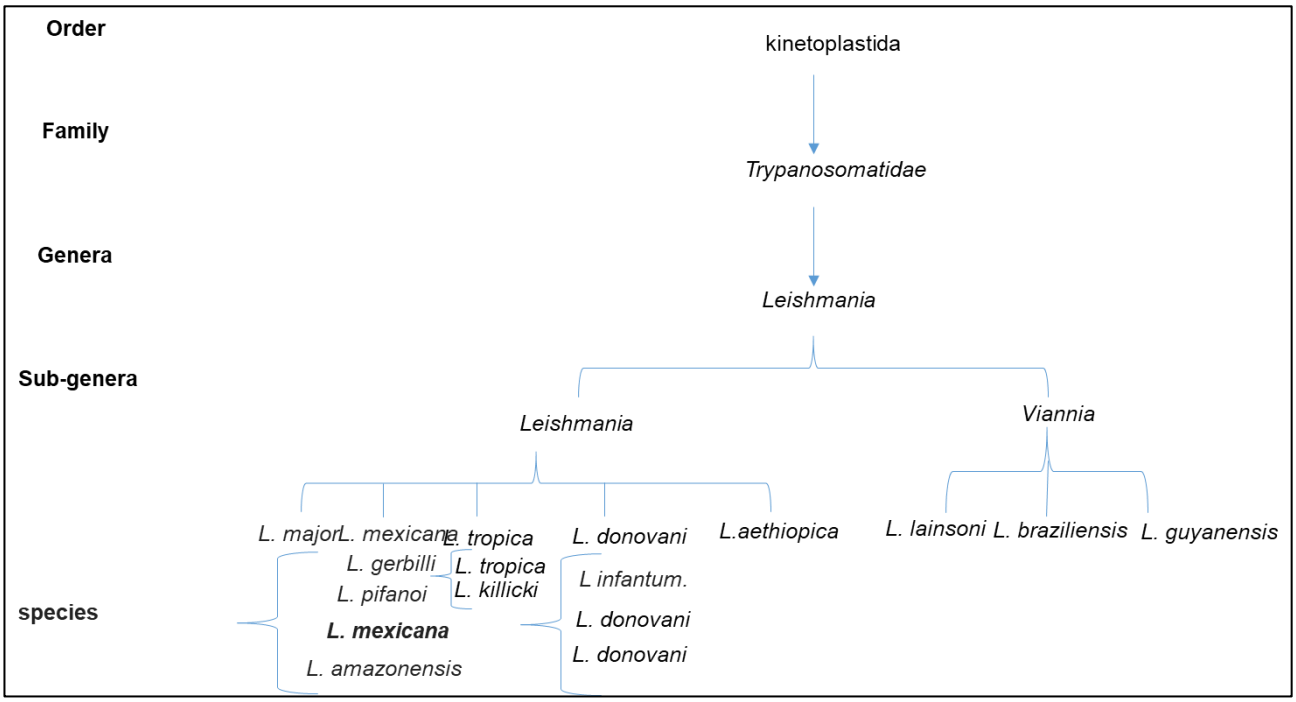

Figure 1.5. Taxonomy of *Leishmania* (Adapted from Chauhan et al., 2015).

1.6 Gene regulation in *Leishmania*

The sequencing of *L. major* began in 1994, supported by the WHO and the *Leishmania* Genome Network, and was finished in 2003 (Ivens et al., 2005). The *Leishmania* haploid genome contains 3.2–5 × 10^7 base pairs (bp), arranged on 34 to 36 chromosomes, depending on the *Leishmania* species (Britto et al., 1998). Like other eukaryotes, *Leishmania* have telomeric sequences at the ends of their chromosomes, but they lack the typical centromeric sequences (Myler et al., 1999). *L. major* has chromosome sizes, which range from 0.3–2.8 × 10^7 bp; however, the sizes and numbers of chromosomes can change rapidly, because repetitive DNA sequences can cause the amplification or deletion of DNA regions (up to 30% of the genome) through homologous intramolecular recombination (Myler et al., 1999). *L. mexicana* undergoes homologous gene recombination in chromosomes 8, 29, 20 and 36 (Sterkers et al., 2012). The genomic DNA (gDNA) of *Leishmania* is located in the nucleus and in kinetoplast DNA (kDNA). kDNA is located in single, large mitochondria found in *Leishmania* parasites. It constitutes 10% to 15% of the total cellular DNA and consists of thousands of circular, non-supercoiled DNA molecules, which form a highly condensed planar network (Lukes et al., 2005). kDNA contains two types of DNA molecules, called minicircles and maxicircles. Minicircles range from 0.5 to 2.8 kilobase (kb) pairs, and parasites generally contain 500 to 10,000 non-identical copies per cell (Lukes et al., 2005). Minicircles are thought to encode guide RNA (gRNA), which is involved in the editing of maxicircle transcripts (Lukes et al., 2005). Maxicircles, which exist as 25 to 50 identical copies per cell ranging from 20 to 39 kb, encode rRNA, mitochondrial proteins and a small number of gRNAs (Lukes et al., 2005).

Leishmania genes do not contain introns; therefore, cis-splicing mechanisms are not expected to occur (Peacock et al., 2007). However, trypanosomatids have four genes subject to cis-splicing, including RNA helicase. One-third of *Leishmania* protein-coding genes can be clustered into families of related genes (Ivens et al., 2005). Genes from larger families consist of single genes and tandem arrays spread across multiple loci and representing *Leishmania*-specific genes, while smaller gene families are likely to have developed through tandem gene duplication (Ramirez et al., 2012). Genes of highly expressed proteins, such as transporters, surface proteins, heat shock proteins, α- and β-tubulins, flagellar proteins and proteases, are present in multiple copies (Ramirez et al., 2012). Genes are organised as direct tandem repeats, which most likely serves as a mechanism for increasing the abundance of primary transcripts (Ramirez et al., 2012).

Intracellular protein concentrations have been correlated with the number of gene copies for some heat shock proteins in *Leishmania* promastigotes (Brandau et al., 1995; Hubel et al., 1995). However, the chromatin-remodelling activities and the mechanisms, which regulate RNA polymerase II-directed transcription in trypanosomatids, appear to differ strongly from those in other eukaryotes (Ivens et al., 2005). The chromosomes are organised into directional gene clusters containing tens to hundreds of genes with unrelated predicted functions and can reach up 1,259 kb in size (Ivens et al., 2005). These clustered genes are co-transcribed, generating polycistronic pre-mRNA. A common spliced leader (SL) sequence of 39 nucleotides, also known as a miniexon, is attached to the 5'-end of all messages by a mechanism called trans-splicing. Approximately 200 gene copies encoding SL-RNAs are predominantly organised in tandem arrays (Papadopoulou et al., 2003). The 5'-end of the SLs have a 7-methylguanosine cap essential for the splicing reaction. Trans-splicing is controlled by polypyrimidine (CT) tracts in the 5'-untranslated region (UTR)

of each gene and usually occurs at the first AG dinucleotide downstream of the CT tract (Ullu et al., 1993). The 3'-end polyadenylation of *Leishmania*, resulting in mono-cistronic mRNA, has been reported to be coupled with the trans-splicing of a downstream neighbour gene (Ullu et al., 1993). Polyadenylation occurs 100 to 500 nucleotides upstream of the splice-acceptor site.

Leishmania is different from other eukaryotes, because the selection of poly(A) sites is not determined by consensus about poly(A) signal sequences in *Leishmania*. The 5'- and 3'-UTRs of *Leishmania* transcripts are longer than in other eukaryotes and can reach up to 688 bp and 2,973 bp, respectively (Clayton, 2002; Stiles et al., 1999). The initiation mechanism for RNA polymerase II-directed transcription in *Leishmania* is unusual, as the promoter for RNA polymerase II precedes multiple reading frames for individual mRNAs, including the primary transcript, a 39-bp poly(A) tail and a 59-bp trans-splicing sequence (Michaeli, 2011). The high number of gene-encoding proteins with potential RNA-binding properties suggests that trypanosomatid gene expression is regulated at the post-transcriptional level (Ivens et al., 2005). This is in contrast with higher eukaryotes, in which gene expression is controlled by the regulation of transcription factors. The transcription levels rely on the sequences of the 3'-UTRs, which are also known to control translation efficiency (Stiles et al., 1999). In some cases, post-translational modifications affect intracellular protein levels (Clayton, 2002). The downstream intergenic regions which affect mRNA processing and/or stability are mediated by labile protein factors (Stiles et al., 1999). Trypanosomatids are also characterised by a process known as RNA editing, during which extensive sequence modifications of mitochondrial transcripts occur to produce mature mRNAs ready for translation.

A comparative analysis of genomic gene expression between *L. mexicana* promastigote and amastigote forms was performed using Illumina sequencing of polyA selected RNA. A total of 9,169 protein-coding genes were identified in the *L. mexicana* genome, approximately 936 of which were novel. In the gene expression model, 3,832 genes were identified as being differentially expressed between amastigotes and promastigotes (Fiebig et al., 2015). Several undefined genes encoding proteins, transporters and peptidases, representing 239 of the 936 novel genes, were upregulated; chromosome 30 in *L. mexicana* is tetraploid and contains genes that are upregulated in amastigotes (Fiebig et al., 2015).

1.7 Differences in signal transduction between higher eukaryotes and trypanosomatids

Cells can detect and respond to any changes in their environments, which is essential for all cells. In multicellular organisms, growth, homeostasis and responses to pathogens are controlled by endocrine signalling during circuit regulation processes which involve protein kinases, phosphatases, G proteins and second messengers which respond to external signals, environmental changes and initial homeostatic or cycling mechanisms by altering their activities (Parsons and Ruben, 2000). During the life cycle of *Leishmania,* parasites must undergo morphological and biochemical changes to survive in both the insect vector and the mammalian host. The mechanisms underlying the environmental signalling in *Leishmania* cells, either to sense environmental changes or transmit these changes to the cell, remain unknown; however, the differentiation of *Leishmania* is regulated by discrete signalling events (Parsons and Ruben, 2000). There is a lack of information regarding the types of

extracellular molecules, which induce signal transduction or their responses, and there is currently no existing gene database of protein interaction pathways in trypanosomatids (Parsons and Ruben, 2000). Kinetoplastids express a large number of adenylyl cyclases (ACs), integral membrane proteins which are class II cyclases, which are exclusive to protozoa (Laxman and Beavo, 2007). The primary signalling receptor in kinetoplastids has been suggested as an AC (Seebeck et al., 2004). ACs contain a transmembrane domain which links diverse extracellular ligand-binding domains with a cytoplasmic adenylyl cyclase domain. When ACs are stimulated, cyclic AMP (cAMP) levels increase in most eukaryotes (Tagoe et al., 2015). cAMP activates protein kinase A (PKA), which phosphorylates and activates Phosphoinositide 3-kinases (PI3K) (Bao et al., 2008). Receptor-type AC and cAMP-specific phosphodiesterases (PDEs) regulate cAMP levels in *T. brucei* (Seebeck et al., 2004). In *T. brucei*, TbPDEB2 is distributed within the cell, whereas TbPDEB1 is localised to the flagellum (Oberholzer et al., 2007); PDEs hydrolyse cAMP (Alonso et al., 2006). The *Trypanosoma* genome encodes proteins known to participate in second messenger systems (Parsons and Ruben, 2000). Like other eukaryotes, Ca^{2+} is an important “second messenger” in trypanosomatids (Parsons and Ruben, 2000). The endoplasmic reticulum, plasma membrane, and mitochondrial membranes possess the ability to transport Ca^{2+} ions (Nolan et al., 1994) to maintain low cytosolic Ca^{2+} concentrations (Xiong and Ruben, 1998). Acidocalcisomes are well-characterised organelles involved in Ca^{2+} homeostasis and are also involved in the regulation of intracellular pH levels (Docampo and Moreno, 1999).

Numerous Ca^{2+}-binding proteins (CaBPs) can convert Ca^{2+} signals into physiological outcomes in trypanosomatids (Ersfeld et al., 2005). CaBPs contain an acetylation motif with an unknown function and a PKA-binding motif, which could play a role in scaffolding (Ersfeld et al., 2005). Ca^{2+}/calmodulin-dependent protein kinase (CAMK)

could also play a role in the differentiation in *T. cruzi* from the blood-borne form to the epimastigote form (Souza et al., 2009). Ca^{2+} concentrations in the cytoplasm change during the cell development of *T. brucei* and during host cell invasion by *T. cruzi* (Stojdl and Clarke, 1996), whether extracellular signals induce Ca^{2+} signalling pathways remains unclear (Docampo and Moreno, 1999). However, Ca^{2+}could enter the trypanosomatid cell via Ca^{2+} channels (Docampo and Huang, 2015). Inositol phosphate acts as a second messenger, and it is involved in the phosphorylation of membrane-bound phosphatidylinositol (PtdIns). The phosphoinositol cascade includes phosphatidylinositol 3-kinase (PI3K), which generates phosphatidylinositol phosphates (PtdInsPs), which are then cleaved by phospholipase C to produce cytoplasmic inositol phosphates (InsPs) (Parsons and Ruben, 2000). Genes encoding the putative C-terminal half of PI3K have been identified in *T. brucei* (Bringaud et al., 1998), and phospholipase has been identified in *T. cruzi* (Nozaki et al., 1999*).* Inositol 1,4,5-triphosphate (InsP3) triggers the release of intracellular Ca^{2+} in most eukaryotes (Moreno et al., 1992). It has been found that inositol 1,4,5-trisphosphate receptor (IP3 R) binds IP3, which leads to release of Ca^{2+} from acidocalcisomes in *T. brucei* (Docampo and Huang, 2015). Pleckstrin homology (PH) domain-containing proteins are capable of interacting with different PtdInsPs and InsPs (Shaw, 1996), and these interactions result in the specific targeting of PH domain-containing proteins to membranes to modulate the PH domain function. Many protein kinases in trypanosomatids contain PH domains (Parsons and Ruben, 2000), for example the Akt-like proteins UBMC1 and UBMC4 of *Leishmania panamensis* (Tirado-Duarte et al., 2018).

There are many similarities between the signalling pathways of mammals and trypanosomatids. Some secreted proteins have been reported to affect the physiological activity of either trypanosomatids or their hosts, such as growth factors (Hide et al., 1989), cytokines (Barcinski et al., 1992) and adrenergic ligands (De Castro and Luz, 1993). cAMP can be also digested by PDEs in trypanosomatids (al-Chalabi et al., 1989). However, trypanosomatids show significant differences in signal transduction compared with higher eukaryotes. Little is known regarding the types of extracellular molecules involved in signal transduction in trypanosomatids. They lack receptor tyrosine kinases, heterotrimeric G proteins, and seven-helix receptors (Parsons and Ruben, 2000), although a small number of protein kinases with transmembrane domains have been predicted to be present in trypanosomatids. However, it has been suggested that some proteins act as ectokinases, which phosphorylate molecules in the extracellular environment instead of mediating sensory functions (Parsons et al., 2005).

The SH3 protein interaction domain is also rarely found in trypanosomatids, and the SH2 protein interaction domain has not yet been identified within the trypanosomatid database. Unlike in higher eukaryotes and despite the presence of MAP kinase signalling pathways (Figure1.6), the signalling cascade in trypanosomatids is not likely to conclude in the activation of transcription factors, and the regulation of gene expression in parasites appears to be regulated at the post-transcriptional level (Parsons et al., 2005). This finding is consistent with the observation of stage-specific changes in protein phosphorylation (Aboagye-Kwarteng et al., 1991; Dell and Engel, 1994). Genomic analyses identified 199 protein kinases in *L. major*, including 20 atypical protein kinases, which lacked twelve conserved subdomains found in eukaryotic proteins; 176 kinases, including 17 atypical kinases, were identified in *T.*

brucei, and 190 kinases, including 19 atypical kinases, were identified in *T. cruzi* (Parsons et al., 2005).

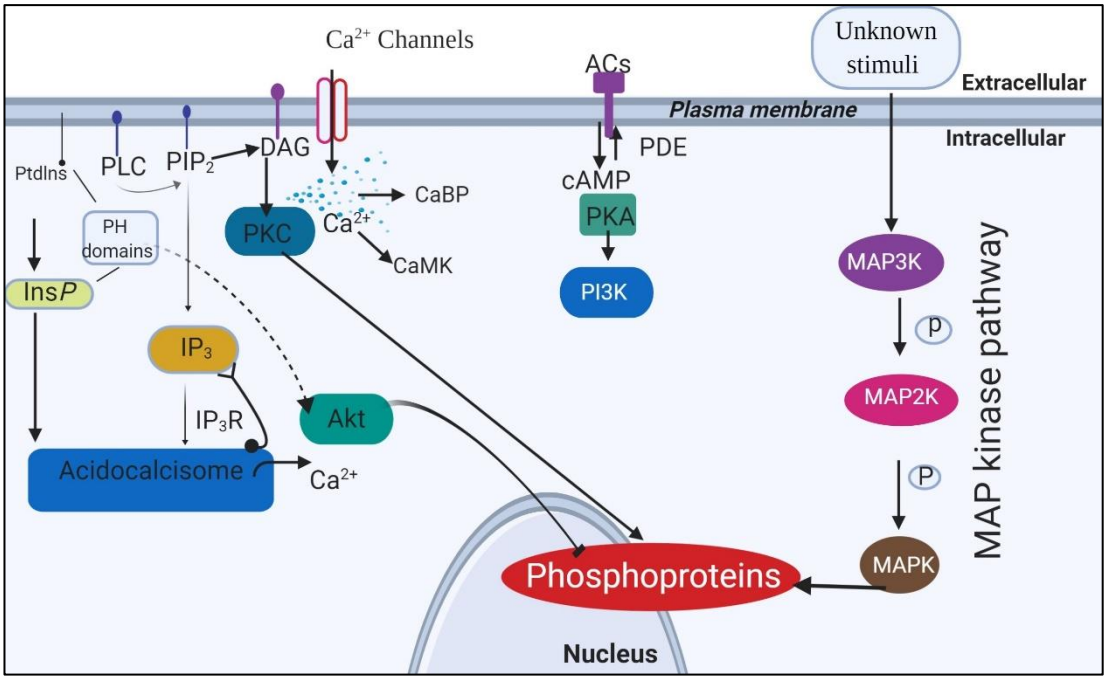

Figure 1.6. Signal transduction pathways in trypanosomatids. The solid arrows indicate signals and dashed arrows indicate signals predicted in trypanosomatids. The types of extracellular molecules involved in signal transduction in trypanosomatids are not known. However, Ca^{2+} could enter via the Ca^{+2} channel. Once Ca^{2+} is inside the cell, it could bind to Calcium-binding proteins (CaBP) and calcium/calmodulin-regulated kinases (CAMKs). Phosphatidylinositol phosphates (PtdInsPs) are cleaved to produce cytoplasmic inositol phosphates (InsP) which can interact with pleckstrin domains (PH) of various protein kinases. This interaction might activate the Akt-like pathway. Inositol 1,4,5-trisphosphate (IP_3) is generated by the hydrolysis of PIP_2, catalysed by phosphoinositide-specific PLC (PI-PLCs), which also generates DAG activating PKC. IP_3 binds to the IP_3 receptor to release Ca^{2+} from acidocalcisomes. Moreover, when adenylyl cyclases (ACs) were stimulated, the generated cyclic Amp (cAMP) stimulates protein kinase A (PKA), which leads to activation of phosphoinositide 3-kinases (PI3K). MAP3Ks are activated by yet unknown stimuli leading to activated MAP2K followed by phosphorylation of MAPKs (adapted from Parsons and Ruben, 2000; Parsons et al., 2005; Alonso et al., 2006; Bao et al., 2008; Docampo et al., 2015; Tirado-Duarte et al.,2018).

1.8 Protein kinases

Protein kinases play key roles in signalling cascades. Kinases regulate cell proliferation, apoptosis, differentiation and metabolism. Protein kinases represent highly dynamic, accurate and unique control molecules for biological processes through the reversible phosphorylation of their substrates (Taylor and Kornev, 2011). Humans express more than 500 protein kinases, which regulate many natural events in cells (Manning et al., 2002a). Protein kinases and protein phosphatases are important post-translational modification proteins involved in a broad spectrum of biological events (Cheng et al., 2011). Protein phosphorylation occurs through the transfer of the γ-phosphate from ATP to a hydroxyl group on the substrate and can lead to the creation of recognition sites for the recruitment of other proteins (Johnson and Lewis, 2001) (Figure 1.7).

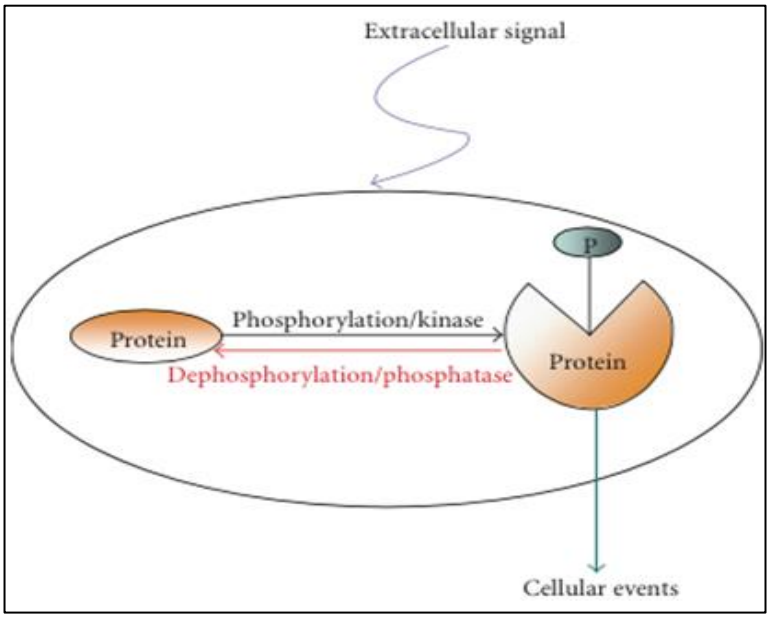

Figure 1.7. General principle of signal transduction by kinases, showing the phosphorylation of a protein by a kinase and the dephosphorylation of the same protein by a phosphatase. Phosphorylation usually causes a conformational change in the protein (adapted from Chen et al., 2015).

The general structure of protein kinases is highly conserved. Protein kinases are composed of two domains, the ATP- and substrate-binding domains, linked by a hinge region (Cheng et al., 2011). The catalytic domain (290 residues) in serine/threonine- and tyrosine-specific kinases displays a common fold composed of a larger, mostly α-helical C-terminal lobe and a smaller N-terminal lobe, which contains five antiparallel β-strands and two α-helices. One of these, the α-C-helix, is critically involved in ATP-binding. Connected by a linker, which features an activation lip (Endicott et al., 2012), these domains are responsible for the binding and orientation of the substrate (Krupa et al., 2004). The C-terminal lobe is responsible for the binding and orientation of substrates following phosphorylation and for activation of the protein kinase. During this process, the protein structure changes to an active conformation and masks binding motifs, which changes the subcellular localisation of the protein (Hanks and Hunter, 1995). The catalytic residue interacts with the OH group on the substrate (Endicott et al., 2012) (Figure 1.8).

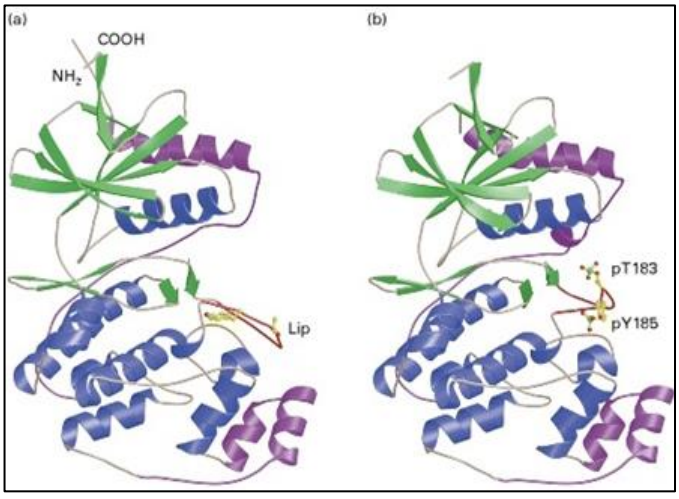

Figure 1.8. Three-dimensional structures of unphosphorylated and phosphorylated MAPK. The N-terminal domain (residues 1-109 and 320-358) consists of five β-strands (green), two α-helices, helix C (blue), and helix αL 16 (magenta). The phosphorylation lip (red) lies between the N-terminal and C-terminal lobes. The C-terminal lobe (residues 110–319) is composed of α-helices (blue), two of which (magenta) are typical for MAPK. (a) Unphosphorylated MAPK; (b) phosphorylated MAPK. Phosphorylation occurs on threonine 183 (THR183) and tyrosine 185 (TYR185), inducing a conformational change in the phosphorylation lip (red line), which improves the binding of the substrate and promotes the dimerisation of the kinase (adapted from Canagarajah et al., 1997).

Protein kinases are subdivided based on whether they phosphorylate serine, threonine and tyrosine (dual-specificity kinases), serine and threonine (serine/threonine kinases), or tyrosine only (tyrosine kinases) (Hubbard and Cohen, 1993; Johnson and Hunter, 2005). Protein kinases are further grouped into atypical protein kinases and eukaryotic protein kinases (Manning et al., 2002b). Atypical protein kinases lack sequence similarity with the eukaryotic protein kinase domain. The initial classification of eukaryotic protein kinases was based on amino acid sequences, dividing them into seven subfamilies: casein kinase I (CKI), protein kinase A/protein kinase G/protein kinase C (AGC), the sterile kinases (STE), protein tyrosine kinases (TKs), tyrosine kinase-like kinases (TKLs), calcium/calmodulin-regulated kinases (CAMKs), and and primarily proline-directed serine/threonine kinases such as cyclin-dependent kinases (CDKs), mitogen-activated protein kinases (MAPK), GSK3 and CDK-like kinases (CDKL) forming the CMGC group (Manning et al., 2002a). Protein kinase genes constitute approximately 2–4% of a typical eukaryotic genome (Wang et al., 2013). Protein kinases are involved in many diseases, because they play roles in the regulation of cell movement, cell death and cell growth.

1.8.1 The structure of protein kinases

Protein kinases contain 12 subdomains separated by amino acid inserts of variable lengths (Hanks and Hunter, 1995) (Figure 1.9). The C-terminal lobe encompasses subdomains VIA to XI, whereas the N-terminal lobe includes subdomains I to IV. Subdomain I contains a glycine-rich loop defined by the GxGxxG motif, which forms the phosphate anchor ribbon. Subdomains II and III are linked by a salt bridge between a lysine in subdomain II and a glutamate in subdomain III, involved in the stabilisation of the interaction between the kinase and the α- and β-phosphates of

ATP. Mutations of this lysine result in the disruption of the salt bridge and the inactivation of the kinase, because the kinase is no longer able to orient ATP into the correct position for phosphate transfer (Gibbs and Zoller, 1991). Subdomain VIB contains a catalytic loop with the invariant DxxxxN motif. During the phosphotransferase reaction, the invariant aspartate acts as the catalytic base, accepting a proton from the attacking substrate hydroxyl group. Subdomain VII assists with ATP orientation via its DFG motif, while subdomains VIII and IX stabilise the C-terminal lobe. Subdomain VIII comprises the activation lip and extends from the conserved DFG to the APE motif. The phosphorylation of the activation lip leads to a change in conformation, which allows the recognition of the substrate (Hanks and Hunter, 1995).

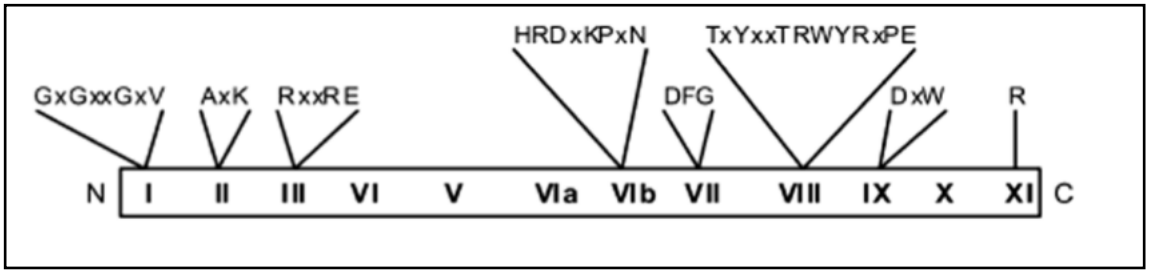

Figure 1.9. Twelve subdomains of MAPKs with conserved motifs in *Leishmania* (adapted from Wiese et al., 2003a).

1.9 Mitogen-activated protein kinase signal transduction

1.9.1 Mitogen-activated protein kinases

MAPKs are serine/threonine (Ser/Thr)-specific protein kinases, which play important roles in intracellular signalling pathways in eukaryotic cells (Shadab and Ali, 2011). These kinases belong to the CMGC subfamily of eukaryotic protein kinases (Kultz, 1998). MAPKs are important proteins for cell signalling and are involved in essential

processes, such as apoptosis, proliferation and differentiation. MAPKs contain a catalytic domain of approximately 300 amino acids, which can be divided into 12 typical subdomains, with a known catalytic core structure and a particular amino acid insertion between subdomains X and XI (Krupa et al., 2004).

1.9.2 The MAPK family

There are two types of MAPKs: conventional MAPKs and atypical MAPKs. MAPK signalling cascades contain three sequentially activated kinases: a MAP3K, a MAP2K, and a MAPK (Brumlik et al., 2011; Cargnello and Roux, 2011). The extracellular signal activates a MAP3K via a cell membrane receptor, which interacts with a small GTP-binding protein of the Ras/Rho family to activate the MAP3K via phosphorylation (Cargnello and Roux, 2011). The MAP3K then activates a MAP2K via the phosphorylation of two threonine/serine residues; MAP2Ks contain docking sites (D-sites) in their N-termini, which bind to the CD domains of MAPKs (Brumlik et al., 2011). Most eukaryotic MAP2Ks contain a consensus motif [K/R]2–3-X1–6-[L/I]-X-[L/I] (Grewalet et al., 2006). MAP2Ks phosphorylate MAPKs on THR and TYR residues in the conserved THR-X-TYR motif located in the activation loop of kinase subdomain VIII (Cargnello and Roux, 2011). Tyrosine phosphorylation leads to the subsequent phosphorylation of a neighbouring threonine residue in the TXY motif of the MAPK (Payne et al., 1991). The phosphorylated tyrosine and threonine residues in the MAPK change the conformation of the lip region, which allows ATP and the substrate to bind to the catalytic site (Wu et al., 1992). Atypical MAPKs can be activated by mono-phosphorylation (Brumlik et al., 2011). MAPKs can be inactivated by the removal of phosphate groups by dual-specificity phosphatases from either one or both of the phosphothreonine or phosphotyrosine residues within the activation lip (Jeffrey et al., 2007). *Leishmania* lacks transcription factors; thus, the *Leishmania*

MAPK substrates are currently unknown (Wiese, 2007). Protein kinases are likely candidates to influence gene expression and differentiation, as *Leishmania* parasites have been found to undergo stage-specific changes in protein phosphorylation patterns (Dell and Engel, 1994).

1.9.3 MAPK pathways in *Leishmania*

A large number of protein kinases in *Leishmania* have been identified in both stages of the parasite's life cycle (Parsons et al., 2005). The *Leishmania* genomes contain 15 MAPKs, 7 MAP2Ks and 23 MAP3Ks, which represent more MAPKs than are found in other eukaryotes (Pearson et al., 2001). In *Leishmania,* as in other eukaryotes, MAPKs consist of a large kinase domain divided into 12 kinase subdomains (Wiese, 2003a). Attempts at deleting the interferon-γ activating MAPK (Kfr1) gene from *T. brucei* failed, suggesting that the protein is essential for the proliferation of the parasite (Hua and Wang, 1997). The functions of MAP2K and MAP3K activators have not been well-studied in trypanosomatids. The mechanisms for initiating MAPK signalling in trypanosomatids and the downstream targets and activators remain unknown (Parsons et al., 2005). Degenerate oligonucleotide primers identified eight MAPKs (LmxMPK2–9) containing the MAPK activation lip (Wiese et al., 2003a). MAPKs were cloned from a genomic DNA library of *L. mexicana* (Wiese et al., 2003a). Three MAPKs (LmxMPK1, 2, and 4) have been identified as suitable drug targets, because when these proteins are absent from amastigotes, they are unable to proliferate (Wiese, 1998; Wiese, 2007). The LmxMPK1 gene was found in the intergenic region between two genes for secreted acid phosphatases and was the first LmxMPK1 to be identified in *L. mexicana*. LmxMPK1 was shown to be essential for amastigote proliferation and survival in infec ted macrophages and mice (Wiese, 1998). LdMPK1

in *L. donovani* and KFR1 in *T. brucei* are homologues of LmxMPK1 in *L. mexicana* (Ashutosh et al., 2012; Brumlik et al., 2011).

LmMPK2, the *L. major* homologue of LmxMPK2 influences the activity of aquaglyceroporin (Mandal et al., 2012). A null mutant of LmxMPK2 demonstrated that LmxMPK2 is necessary to establish an infection in a mammalian host. Morphological defects were not observed during the promastigote stage in LmxMPK2 null mutants (Wiese, 2007).

LmxMPK3 has been identified in *L. mexicana* and has been demonstrated to be involved in MAPK signalling, both *in vivo* and *in vitro* (Erdmann et al., 2006). LmxMPK3 deletion mutants have reduced flagellar lengths indicating involvement in the regulation of intraflagellar transport (Figure 1.10). The re-expression of LmxMPK3 in the deletion mutant led to the regeneration of wild type flagella (Erdmann et al., 2006). A mouse infection experiment showed that LmxMPK3 is not essential for lesion development and promastigote null mutants were able to cause lesions in infected mice (Erdmann et al., 2006).

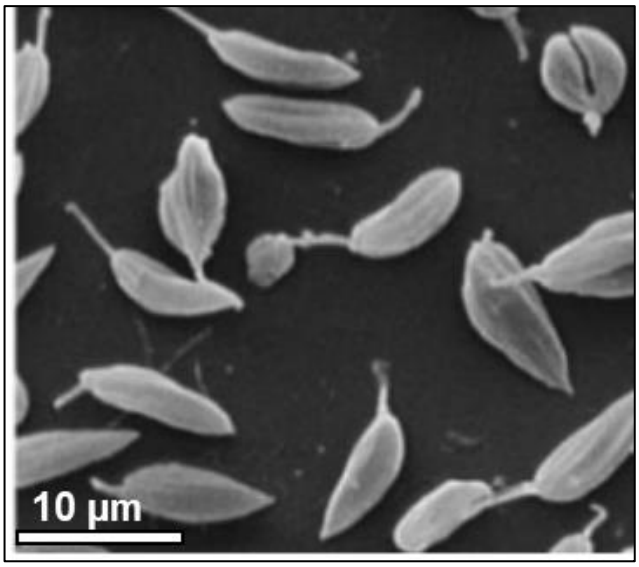

Figure 1.10. LmxMPK3 null mutant promastigotes (ΔLmxMPK3$^{-/-}$ HN6). Scanning electron microscopy micrograph of LmxMPK3 null mutants (ΔLmxMPK3$^{-/-}$ HN6), showing short flagella (adapted from Erdmann et al., 2006).

LmxMPK4 is essential for both life cycle stages of *L. mexicana*, and this null mutant can be rescued by a plasmid expressing the extra copy of LmxMPK4 during a knockout approach (Wang et al., 2005). LmxMPK4 is homologous with TbMAPK2 in *T. brucei*, and GST-LmxMPK4 was able to phosphorylate MBP *in vitro* (Wang et al., 2005). Tandem mass spectrometry (MS/MS) results showed that LmxMPK4 could be activated by LmxMKK5-mediated phosphorylation at T190 and T192 of the activation loop TQY motif (John von Freyend et al., 2010).

While the longest N-terminal extensions can be found in LmxMPK5 (Wiese et al., 2003a), the LmxMPK5 deletion mutants maintain the ability to infect mice but do not produce lesions containing active parasites at the inoculation site (Wanders, 2004). LmxMPK5 is homologous with TbMAPK5, which is involved in the differentiation of the stumpy form of the parasite, and the null mutant of TbMAPK5 results in a 16-fold reduction in parasitaemia (Pfister et al., 2006).

LmxMPK6, the homologue for TbECK1 in *T. brucei*, has a long C-terminal extension, which might be involved in the regulation of kinase activity (Ellis et al., 2004). LmxMPK6 plays a role in the proliferation of parasite cells and exhibits phosphotransferase activity (Brumlik et al., 2011).

LmxMPK7 and 8 have been identified in *L. mexicana*, but they do not appear to have homologues in *T. brucei* or *T. cruzi.* LmxMPK7 caused delayed lesion development in knockout mice (Bleicher, 2019). The longest N-terminal extensions can be found in LmxMPK7 and LmxMPK8 (Wiese et al., 2003a). All 12 kinase subdomains are present in LmxMPK7 and LmxMPK8; these contain an insertion in the core kinase domain (Wiese et al., 2003a).

LmxMPK9 is expressed exclusively during the promastigote stage of *L. mexicana* (Wiese et al., 2003b). The deletion of LmxMPK9 resulted in promastigotes with elongated flagella, whereas the overexpression of the LmxMPK9 gene led to shorter flagella in promastigotes (Bengs et al., 2005). The LmxMPK9 deletion mutants maintain the ability to infect mice and to develop lesions (Bengs et al., 2005).

LmxMPK10 is homologous to LmjMPK10 in *L. major*. LmjMPK10 has been shown to play a role during the amastigote stage. LdMPK10 in *L. donovani* was identified in the phosphoprotein fraction of axenic amastigotes. Uniquely, LdMPK10 appears to exhibit increased activity during the transition from the promastigote to amastigote stages and is phosphorylated only on tyrosine of the TQY motif (Cayla et al., 2014).

Homozygous deletion mutants of LmxMPK11 and LmxMPK12, generated in promastigotes, remained infectious in mouse experiments. Therefore, they are likely not essential for *Leishmania* (Windelberg, 2007). TbMAPK4, which is the homologue of LmxMPK12 in *T. brucei*, was shown to be necessary for differentiation and division,

using a null mutant, which also resulted in enhanced sensitivity to temperature increases (Guttinger et al., 2007). LmxMPK12 has all 12 kinase subdomains, and these contain an insertion in the core kinase domain (Wiese et al., 2003a).

Deletion of LmxMPK13 also resulted in the elongation of flagella. LmxMPK13 is the homologue of LF4 in *C. reinhardtii*, which showed a long flagellar phenotype after deletion of the gene (Berman et al., 2003). The null mutants of LmxMPK13 and LmxMPK14 also generated elongated flagella in promastigotes compared with wild type *L. mexicana* (Scholz, 2008).

The *Leishmania* MAPKs, LmxMPK3, LmxMPK9, LmxMPK11, LmxMPK12 and LmxMPK13, are not suitable as drug targets, because parasites lacking any one of these kinases remain infective in BALB/c mice (Bengs et al., 2005; Erdmann et al., 2006; Wiese, 2007). The role of MPK15 has not yet been studied.

		Phenotype of null mutant			
MAPKs TriTrypDB	**Generation of null mutant**	**Infectivity**	**Flagella length**	**Functions**	**Drug target**
LmxMPK1 **LmxM.20_36.6470**	**-**	**-**	**-**	Essential for survival of amastigotes	Suitable
LmxMPK2 **LmxM.36.0720**	**+**	**-**	**-**	Necessary to establish an infection in mammalian host.	Suitable
LmxMPK3 **LmxM.10.0490**	**+**	**+++**	**Short flagella**	Might regulate IFT	Not suitable
LmxMPK4 **LmxM.19.1440**	**+(extra copy gene)**	**-**	**-**	Essential for both life cycle stages of *L. mexicana*	Suitable
LmxMPK5 **LmxM.29.2910**	**+**	**+**	**-**	Unknown	Not suitable
LmxMPK6 **LmxM.31.3250**	**-**	**Unknown**	**Unknown**	Unknown	Unknown
LmxMPK7 **LmxM.13.1640**	**+**	**++**	**-**	Delayed lesion development	Not suitable
LmxMPK8 **LmxM.28.0580**	**-**	**Unknown**	**Unknown**	Unknown	Unknown
LmxMPK9 **LmxM.19.0180**	**+**	**+++**	**Long flagella**	Exclusively during the promastigote stage; appears to regulate IFT	Not suitable
LmxMPK10 **LmxM.10.0200**	**-**	**Unknown**	**Unknown**	Plays a role during the amastigote stage	Not suitable
LmxMPK11 **LmxM.32.1380**	**+**	**+++**	**-**	Likely not essential for *Leishmania*	Not suitable
LmxMPK12 **LmxM.29.0370**	**+**	**+++**	**-**	Likely not essential for *Leishmania*	Not suitable
LmxMPK13 **LmxM.34.5010**	**+**	**+++**	**Long flagella**	Might regulate IFT	Not suitable
LmxMPK14 **LmxM.27.0100**	**+**	**Unknown**	**Long flagella**	Might regulate IFT	Unknown

LmxMPK15 **LmxM.32.2070**	**-**	**Unknown**	**Unknown**	Unknown	Unknown

Table 1. 1. Summary of all 15 MAPKs. (**-**) No generation of null mutant, and (**+**), Generation of null mutant; phenotype of null mutants ((**-**). no lesion (**+**), no lesion, but parasites surviving at inoculation site; and (**++**), delayed lesion development; (**+++**), lesion development in BALB/c mice); functions and whether suitable as drug target. TriTrypDB accession number.

1.9.4 MAP2K pathways

Scaffolding interactions and a variety of docking mechanisms are involved in MAPK pathways (Miller and Turk, 2018; Raman et al., 2007). Scaffolds lead to conformational changes in substrates, which promote phosphorylation (Miller and Turk, 2018). MAPK CD domains interact with the D domain of MAP2K or MAPK substrates (Takekawa et al., 2005). This docking interaction leads to conformational changes in the proteins, resulting in increased accessibility of the activation loop (Goldsmith et al., 2007). Only those kinases and phosphatases with the correct docking motif can unlock the activation loop; therefore, this conformational change contributes to pathway fidelity (Min et al., 2009). The docking interaction between MP2K and MAPK is allosteric, readying the MAPK activation loop for processing by kinases and phosphatases (Zhou et al., 2006). MAP2K adopt an inactive configuration, even in the absence of substrates, which sequesters the activation loop from the activities of other kinases and phosphatases (Zhou et al., 2006). MP2Ks have been shown to move in and out of the nucleus carrying active MAPKs, which require translocation to the nucleus to phosphorylate nuclear targets (Yao and Seger, 2009).

1.9.4.1. MAP2K pathways in *L. mexicana*

Seven MAP2Ks have been identified by bioinformatics (Pearson et al., 2001). In our laboratory, different MAP2Ks from *L. mexicana* were cloned, namely LmxMKK,

LmxMKK2 (LmxPK2), LmxMKK3 (LmxPK3), LmxMKK4 (LmxPK4), LmxMKK5 (LmxPK5), LmxMKK6 (LmxPK6) and LmxMKK7 (LmxPK7). The phylogenetic relationships in the radial tree shown in Figure 1.11 demonstrate that LmxPK3 and LmxPK4 cluster together with four of the stress-activated MAP2Ks from *Arabidopsis thaliana* (AtMKK1, AtMKK2, AtMKK3, and AtMKK6). *C. reinhardtii* and *Dictyostelium discoideum* contain MAP2Ks, which are homologous with those expressed in *L. mexicana*.

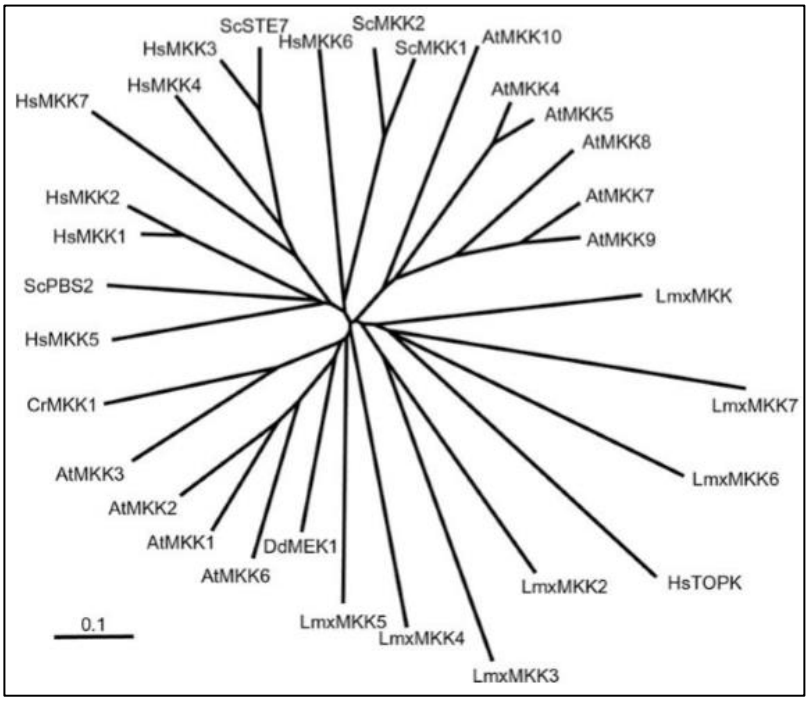

Figure 1.11. Phylogenetic tree of the catalytic domains for MAP2Ks from different organisms (*C. reinhardtii*, *D. discoideum* and *L. mexicana*) (Parsons et al., 2005).

LmxPK2, LmxPK6 and LmxPK7 are large proteins, due to N-terminal extensions in LmxPK6 and LmxPK7 and a C-terminal extension in LmxPK2 (Melzer, 2007).

LmxMKK is the first MAP2K homologue identified in *L. mexicana*. LmxMKK phosphorylates and activates LmxMPK3 *in vitro*. Both LmxMPK3 and LmxMKK

regulate flagellar length in *L. mexicana* (Erdmann et al., 2006; Wiese et al., 2003b). LmxMPK3 and LmxMKK deletion mutants have reduced flagellar lengths compared to wild type cells. TbMEKg, the homologue of LmxMKK in *T. brucei,* demonstrated no phenotype in the deletion mutant (Pfister et al., 2006). A delayed lesion onset of null mutant LmxMKK was observed in mice infected with the LmxMKK null mutant (Wiese et al., 2003b).

The amino acid sequence of LmxPK4 reveals a typical protein kinase domain (L73-I331) with 11 highly conserved subdomains, which exhibit strong homology to MAP2Ks from other organisms (Kuhn and Wiese, 2005). The deletion of LmxPK4 from the *L. mexicana* genome results in the elongation of flagella in promastigotes, which suggests that LmxPK4 plays a role in promastigote-to-amastigote differentiation (Kuhn and Wiese, 2005). It was shown that LmxMKK activates LmxMPK3 and LmxMKK5 activates LmxMPK4 *in vitro* (Erdmann et al., 2006; John von Freyend et al., 2010). MAP2Ks could be responsible for regulating the length of the flagellum, as demonstrated by the deletion of LmxMKK from *L. mexicana* (Wiese et al., 2003b).

		Phenotype of null mutant			
MAP2Ks TriTrypDB	**Generation of null mutant**	**Infectivity**	**Flagella length**	**Functions**	**Drug target**
LmxMKK (LmxPK) LmxM.08_29.2320	**+**	**++**	**short flagella**	1) Regulates flagella length 2) physiological activator for LmxMPK3 in vitro	Not suitable
LmxMKK2 (LmxPK2) LmxM.13.0440	**-**	**Unknown**	**Unknown**	Unknown	Unknown
LmxMKK3 (LmxPK3) LmxM.17.0060	**+ this study**	**+++ this study**	**short flagella this study**	Not essential in amastigotes and cultured promastigotes	Not suitable; this study
LmxMKK4 (LmxPK4) LmxM.24.2320	**+**	**++**	**Long flagella**	1) differentiation from promastigote to amastigote 2) physiological activator for LmxMPK3 *in vitro and in vivo* (this study)	Not suitable
LmxMKK5 (LmxPK5) LmxM.36.0860	**-**	**Unknown**	**Unknown**	physiological activator for LmxMPK4 in vitro	Unknown
LmxMKK6 (LmxPK6) LmxM.31.1020	**- this study**	**Unknown**	**Unknown**	Unknown	Unknown
LmxMKK7 (LmxPK7) LmxM.07.0250	**-**	**Unknown**	**Unknown**	Unknown	Unknown

Table 1. 2. Summary of all MAP2Ks. (**-**), no Generation of null mutant, and (**+**), generation of null mutant; phenotypes of null mutants ((**-**). no lesion, (**++**), and delayed lesion development; (**+++**), lesion development in BALB/c mice); Functions and whether suitable drug target. TriTrypDB accession number**.**

1.10 Project aims

One aim of this project was to identify and characterise new MAP2Ks (LmxPK3 and LmxPK6) of *L. mexicana*. LmxPK3 and LmxPK6 have not been studied in *Leishmania*

before; hence, investigating these kinases could lead to the validation of new drug targets. The second aim was to study the putative signal transduction between a MAP2K and a MAPK and its function in *Leishmania* by the interaction between LmxPK4 and LmxMPK3, involved in flagellum length regulation. The objectives are as follows:

- **Study the function and localisation of LmxPK3 and LmxPK6, both *in vivo* and *in vitro.***
  - Molecular characterisation of LmxPK3 and LmxPK6.
  - Protein purification and kinase activity assays for recombinant protein kinases.
  - LmxPK3 and LmxPK6 knockouts in *L. mexicana* for validation as drug targets.
  - Phenotypic analysis of knock out parasites.
  - Localisation of protein kinases in *L. mexicana* by fluorescence microscopy of tagged proteins.
- **Analysis of the interaction between MAP2K and MAPK by examining the activity of LmxPK4 on LmxMPK3, *in vivo* and *in vitro.***
  - Recombinant expression and purification of different forms of LmxMPK3 and assessment of their kinase activity.
  - Phosphorylation analysis of LmxMPK3 co-expressed with LmxPK4.
  - Use of a split-green fluorescent protein (-GFP) to confirm the interaction between LmxMPK3 and LmxPK4 *in vivo*.

Chapter 2: Materials and Methods

2.1 Materials

2.1.1 Laboratory Equipments

Centrifuge 5424	Eppendorf, Hamburg, Germany
Centrifuge 5415R	Eppendorf, Hamburg, Germany
HERMLE Z 400 K	Hermle Labortechnik,Wehingen,Germany
Power supply: Consort E734	Consort, Turnhout, Belgium
Power supply: Gene Power Supply GPS 200/400	Amersham Biosciences, Freiburg, Germany
Thermomixer 5436 Eppendorf	Eppendorf, Cambridge, UK
Microscopes Axiovert 25	Carl Zeiss, Jena
Microscopes Axiostar plus	Carl Zeiss, Jena
Nikon eclipse E600	Nikon Instruments, Derby, UK
Epifluorescence Microscope Nikon EclipseE600	Woburn, Massachusetts, U.S.A.
Digital MDs camera Hamamatsu	Hamamatsu Photonics
Digital-pH-Meter CG 82	Hannah Instruments, UK
Innova 4230/4400	New Brunswick Scientific, Edison, NJ, USA
Branson Sonifier 250	Branson, Danbury, CT, USA
Nucleofector II	Amaxa Biosystems, Gaithersburg, MD, USA
IKA-VIBRO-FIX VF2	IKA Labortechnik, Staufen, Germany
VWR Genosmart	VWR International, Lutterworth, UK
High Performance UV	UVP, Cambridge, UK
Gene Amp PCR System 9700	PE Applied Biosystems, Weiterstadt, German
KODAK M35-M X-OMAT	New York, United States
Amersham Typhoon 9200 Image	Eastman Kodak Company, Rochester
Transilluminator	GE Healthcare Bio-Sciences, USA
Water bath GFL 1083	GFL, Burgwedel, Germany Heidolph Electro, Kehlheim, Germany

2.1.2 Chemicals

Chemicals	**Companies**
[γ-^{32}P]-ATP	Hartmann Analytics, GmbH, Germany
Acetic acid	Carl Roth, Karlsruhe, Germany
Acrylamide 30% (w/v)/Bis-acrylamide 0.8% (w/v)	VWR, Lutterworth, UK
Agar-Agar	Roche Diagnostics, Sussex, UK
Agarose (electrophoresis grade)	Techmate Ltd, Milton Keyes, UK

Ammonium persulfate (APS)	VWR, Lutterworth, UK
Ampicillin	Sigma-Aldrich, Steinheim, Germany
Boric acid	Techmate Ltd., Milton Keyes, UK
Bovine serum albumin (BSA)	Sigma-Aldrich, Steinheim, Germany
Carbenicillin	Sigma-Aldrich, Steinheim, Germany
Calcium chloride	Techmate Ltd., Milton Keyes, UK
Cobalt chloride	Carl Roth, Karlsruhe
Coomassie Brilliant Blue R250	Techmate Ltd., Milton Keyes, UK
Coomassie Brilliant Blue G250	Carl Roth, Karlsruhe
Chelating sepharose fast flow	GE Healthcare, Little Chalfont, UK
Dimethyl sulfoxide DMSO	Techmate Ltd., Milton Keyes, UK
dNTP mix	Bioline, UK
Disodium hydrogenphosphate	Merck, Darmstadt,UK
1,4-Dithiothreito(DTT)	Biomol, Hamburg, Germany
EDTA disodium dehydrate	Techmate Ltd., Milton Keyes, UK
Ethanol	Techmate Ltd., Milton Keyes, UK
Ethidium bromide	Sigma-Aldrich, Steinheim, Germany
Formaldehyde 37% (Formaline)	Carl Roth, Karlsruhe, Germany
Fetal calf serum	Gibco BRL
Glucose	Techmate Ltd., Milton Keyes, UK
Glycerol	Techmate Ltd., Milton Keyes, UK
Glycine	Techmate Ltd., Milton Keyes, UK
Glutathione, reduced	Sigma-Aldrich, Steinheim,Germany
Glutathione Sepharose 4B	GE Healthcare, UK
N-2-Hydroxyethylpiperazine- N′-2-ethanesulfonic acid (HEPES)	Techmate Ltd., Milton Keyes, UK
Hydrochloric acid	Techmate Ltd., Milton Keyes, UK
Hygromycin B	InvivoGen, San Diego, California,USA
Hemin	Sigma-Aldrich, Steinheim, Germany
Imidazole	Techmate Ltd., Milton Keyes, UK
Isopropyl-β-D-thiogalactopyranoside IPTG	Sigma-Aldrich, Steinheim, Germany
Isopropanol	Techmate Ltd., Milton Keyes, UK
Kanamycin sulfate	VWR, Lutterworth, UK
Magnesium chloride hexahydrate	Techmate Ltd., Milton Keyes, UK
Manganese chloride	Merck, Darmstadt, Germany
MBP dephosphorylated	Millipore, UK
Methanol	Carl Roth, Karlsruhe, Germany
Morpholinopropane sulfonic acid (MOPS)	Sigma-Aldrich, Gillingham, UK
Mowiol 4-88	Merck, Darmstadt
Neomycin (G418)	Roche Diagnostics, Mannheim
Penstrep (1000 U/mL Penicillin, 10 mg/mL Streptomycin)	PAN Biotech, Aidenbach
Phleomycin (Bleocin)	Merck Biosciences, Schwalbach
Poly-L-Lysine hydrobromide	Sigma-Aldrich, Steinheim
Potassium chloride	Sigma-Aldrich, Gillingham, UK
Puromycin dihydrochloride	Invivogen, San Diego, California,USA
Potassium acetate	Techmate Ltd, Milton Keyes, UK
SDM-79 medium	Bio & Sell GmbH, Germany

Sodium acetate trihydrate	Techmate Ltd., Milton Keyes, UK
Sodium chloride	Sigma-Aldrich, Gillingham, UK
Sodium dihydrogen phosphate	Merck, Darmstadt, Germany
Sodium dihydrogen phosphate	Merck, Darmstadt, Germany
Sodium dodecyl sulfate (SDS)	Fischer Scientific, Loughborough, UK
Sodium hydroxide	Techmate Ltd., Milton Keyes, UK
TEMEDN,N,N′,N′Tetramethylethylenediamine	Sigma-Aldrich, Steinheim, Germany
Tetracycline	Sigma-Aldrich, Steinheim, Germany
Triton X-100	Techmate Ltd., Milton Keyes, UK
Xylenecyanol	Sigma Aldrich,Steinheim,Germany
Yeast extract	Fluka, Gillingham, UK

2.1.3 Culture media, stock and buffer solutions

2.1.3.1 Buffers

Agarose gel loading buffer (10×)	0.1 M EDTA pH 8.0 0.1% (w/v) bromophenol blue 0.1% (w/v) xylenecyanol 0.5× TBE 50% (v/v) glycerol
Coomassie R250 destaining solution	30% (v/v) methanol 10% (v/v) acetic acid 50
Coomassie R250 staining solution	0.1% (w/v) Coomassie Brilliant Blue R250 40% (v/v) methanol 10% (v/v) acetic acid Filtered through fluted filter
Complete EDTA-free protease inhibitor	1 tablet complete EDTA-free (Roche) in 15 mL PBS
Fixing solution for *Leishmania* cell counting	3.7% (w/v) formaldehyde in 1× PBS
Cryo medium for *Leishmania*	90% (v/v) iFCS 10% (v/v) DMSO
PBS (10×)	137 mM NaCl 2.7 mM KCl 10.1 mM Na_2HPO_4 1.8 mM KH_2PO_4
Fixing solution for *Leishmania*	3.7% (w/v) formaldehyde in 1× PBS
Gel drying solution	20% (v/v) ethanol 10% (v/v) glycerol
GST elution buffer	10 mM reduced glutathione in 50 mM Tris/HCl pH8.0 (Buffer needs to be freshly prepared)
Hemin stock solution	2.5 mg/mL in 50 mM NaOH
His-purification binding buffer	50 mM Tris-HCl pH 8.0 1 M NaCl 10% (v/v) glycerol 20 mM imidazole

His-purification elution buffer	50 mM Tris-HCl pH 8.0 300 mM NaCl 10% (v/v) glycerol 500 mM imidazole 1 mM PMSF
His-purification washing buffer	50 mM Tris-HCl pH 8. 0.1 M NaCl 10% (v/v) glycerol 10 mM imidazole
MPK3 Kinase Buffer (10×)	0.5 M MOPS pH 7.2 1 M NaCl 100 mM MgCl
DNA loading buffer (10×)	0.5× TBE 0.1 M EDTA pH 8.0 0.1% (w/v) bromophenol blue 0.1% (w/v) xylenecyanol 50% (v/v) glycerol
Mowiol/DABCO	2.4 g Mowiol 6 g glycerol 0.2 M Tris-HCl pH 8.5 6 mL ddH_2O
RF1	100 mM RbCl 50 mM MnCl2 10 mM CaCl2 30 mM potassium acetate 15% (v/v) glycerol adjusted to pH 5.8, filter-sterilised
RF2	10 mM RbCl 75 mM $CaCl_2$ 10 mM MOPS 15% (v/v) glycerol adjusted to pH 6.8, filter-sterilised
SDS-PAGE electrophoresis buffer	0.25 M Tris base 1.92 M glycine 1% (w/v) SDS pH8.3
SDS-PAGE sample buffer	62.5 mM Tris-HCl pH6.8 20% (v/v) glycerol 2% (w/v) SDS 0.001%(w/v) bromophenol blue 200 mM DTT
SDS-PAGE resolving gel buffer (4×)	1.5 M Tris base 0.4% (w/v) SDS Adjusted to pH 8.8
SDS-PAGE stacking gel buffer (4×)	0.5 M Tris base 0.4% (w/v) SDS Adjusted to pH 6.8
Standard kinase reaction buffer (10×)	0.5 M MOPS pH 7.2 1 M NaCl 100 mM $MgCl_2$ 20 mM $MnCl_2$

TBE (5×)	0.45 M Trizma 0.45 M boric acid 10 mM EDTA pH 8.0
TENS	10 mM Tris-HCl pH 8. 0.1 mM EDTA pH 8.0 10 mM NaOH 0.5% (w/v) SDS

2.1.3.2 Media

Media names	**Preparation**
Cryo medium for *Leishmania*	90% (v/v) iFCS 10% (v/v) DMSO
LB medium	10 g tryptone 5 g yeast extract 10 g NaCl dissolved in 1000 mL ddH_2O, autoclaved for sterilisation. If required, antibiotics were added after LB medium, had cooled to reach 50°C
SDM medium complete	10% (v/v) iFCS 1% (v/v) penstrep 7.5 µg/mL hemin in SDM
LB agar with carbenicillin	15 g agar-agar in 1000 mL LB medium autoclaved for sterilisation antibiotic was added (Carbenicillin100 µg/mL, after LB agar, had cooled to reach 50°C)

2.1.3.3 Gel preparation

Gel names	**Preparation**
SDS-PAGE 14%	12.25 mL ddH_2O 8.75 mL Resolvingbuffer 4× 14 mL 30% Acrylamide/Bisacrylamide Solution 17.5 µL TEMED 105 µL 10% APS
Agarose gel 0.8%	0.8g agarose 100 mL 0.5× TBE buffer 7 µL Ethidium Bromide 10mg/mL

2.1.4. Enzymes

Alkaline phosphatase, shrimp	Roche Diagnostics, Mannheim, Germany
Klenow enzyme	New England Biolabs, Hitchin, UK
Restriction endonucleases	New England Biolabs, Hitchin, UK
RNase A (bovine pancreas)	New England Biolabs, Hitchin, UK

2.1.5 strains

2.1.5.1 Bacterial (*E. coli*) strains

***E. coli* Strain**	**Genotype**
BL21 (DE3)	[pAPlacIQ] hsdS gal (λclts857 ind 1 Sam7 nin5 lacUV5- T7 gene 1) [pAPlacIQ]
GM2929 Dam-methylation negative	araC14, leuB6(Am), fhuA13, lacY1, tsx-78, glnX44(AS), galK2(Oc), galT22, λ-, mcrA0, dcm-6, hisG4(Oc), rfbC1, rpsL136(strR), dam-13: Tn9, xylA5, mtl1, recF143, thiE1, mcrB9999, hsdR2
DH5α	F2huA∆(argF-lacZ)U169phoA glnV44Ø80∆(lacZ)M15yrArecA1enddA1

2.1.5.2 *Leishmania* strains

Leishmania mexicana mexicana MNYC/BZ/62/M379, clone 2.

2.1.5.3 Mouse strain

8 to 12 weeks old, female Balb/c mice bred in-house and supplied by the University of Strathclyde colony. The animal licence number PPLPF669CAE8.

2.1.6 DNA vectors and plasmid constructs

They were generated throughout the project (plasmid maps drawn using Clone Manager 9.1; see Appendix 9.1).

Plasmid Name	**Backbones**	**Insert**
pGEX-KGSP	pGEX-KGSP	None
pTH6cGFPn	pTH6cGFPn	None
pB5KXLmxPK6upds	pBSKII(+)	LmxPK6upds
pBAX7Dlmkin24	pBSKII(+)	LmxPK3
pBAX14Dlmkin24neo	pBSKII(+)	LmxPK3upneods
pB-LmxPK4-3	pBSKII(+)	LmxPK4-3
pBLmxPK4NheI	pBSKII(+)	LmxPK4
pBNELmxPK6upBlads	pBSKII(+)	LmxPK6upBlads
pBNELmxPK6upPhleods	pBSKII(+)	LmxPK6upPhleods
pCR2.1Phleo	pCR2.1-TOPO	Phleo
pEXBla-ATa-AR	pEX	Bla
pJC1LmxMPK3	pJC-duet	LmxMPK3

pJC2LmxMPK3KM	pJC	LmxMPK3KM
pJC7MPK3KMMKKMut2	pJC	LmxMPK3-LmxMKKmut2
pJC-duetlinker	pJC-duetlinker	None
pJCLmxMPK3PK4	pJC	LmxMPK3LmxPK4
pSSUPacTriGFP	pSSUPac	TriGFP
pSSUPacTriGFP10MKKMPK3GFP11	pSSUPacTriGFP	LmxMKK-LmxMPK3
pSSUPacTriGFP10PK4	pSSUPacTriGFP	LmxPK4
pGEX-KGSPLmxPK3	pGEX-KGSP	LmxPK3
pTHBsdGFPTEVLmxPK3	pTHBsd	GFPTEVLmxPK3
pTHBsdGFPTEVLmxPK3His	pTHBsd	GFPTEVLmxPK3His
pTHBsdHisTEVLmxPK3GFP	pTHBsd	HisLmxPK3GFPTEV
pCR2.1LmxPK6	pCR2.1-TOPO	LmxPK6
pX14polNcoIPAC	pX14polNcoIPAC	None

2.1. 7 Oligonucleotides

The following oligonucleotides were synthesised by Life Technologies.

Description	**Nucleotide sequence**	**Use**
LmxPK3up.for	5'-CTCTCTTAGTGTCCATCAAGG-3'	Proof of LmxPK3 deletion
Neoint.rev	5'-CATTCAGGGCACCGGACAGG-3'	Proof of LmxPK3 deletion
Hygint.rev	5'-GCAATAGGTCAGGCTCTCGC-3'	Proof of LmxPK3 deletion
LmxPK3int.rev	5'-GCGTCTCCAGTTCAGACACG-3'	Proof of LmxPK3 deletion
LmxPK3ds.rev	5'-TCGTATGTTGTGTGGAATTG-3'	Proof of LmxPK3 deletion
NeoC.for	5'-CATCGCCTTCTATCGCCTTC-3'	Proof of LmxPK3 deletion
Phleo.for2	5'-GCAACTGCGTGCACTTCGTG-3'	Proof of LmxPK3 deletion
LmxMPK12.for	5'-CGTCGCCGTGGCTGGCTGTTGAT-3'	Proof of LmxMPK12 deletion
Phleomycin_int.for	5'-TCGGAGGTCGTGTCCACGAA-3'	Proof of LmxPK6 deletion
PK6.6rev	5'-CGCAGCAGAACTGCTGAACT-3'	Proof of LmxPK6 deletion
Blasticidin_int.for	5'-CTGGGGGACCTTGTGCAGAA-3'	Proof of LmxPK6 deletion
PK6.6rev	5'-GAAGACGCGCATCCACGCAA-3'	Proof of LmxPK6 deletion
pXPhleo2	5'-AAACCGCTCGCGTGTGTT-3'	Proof of LmxPK6 deletion
PK6.5rev	5'-CGACGCCCACGGATTCGCGAT-3'	Proof of LmxPK6 deletion

2.1.8 Antibiotics

Antibiotics	Stock concentration	Final Concentration
Neomycin	14.7 mg/mL	10 µg/mL
Phleomycin	5 mg/mL	10 µg/mL
Blasticidin	10 mg/mL	10 µg/mL
Hygromycin	100 mg/mL	20 µg/mL
Puromycin	10 mg/mL	20 µg/mL

2.1.9 Molecular biology kits

Name of Kit	Origin
Human T Cell Nucleofector Kit	Amaxa Biosystems, Gaithersburg, USA
M&N NucleoSpin Extract II Kit	Macherey & Nagel, Düren, Germany
M&N NucleoSpin Plasmid Kit	Macherey & Nagel, Düren, Germany
The ISOLATE II DNApurification Kit	Qiagen ,UK
QIAquick Gel Extraction Kit	Macherey & Nagel, Düren, Germany

2.1.10 DNA and protein molecular weight markers

Markers	Origin
1 kb DNA Ladder	New England Biolabs, Hitchin, UK
Prestained Protein Marker, Broad Range.	New England Biolabs, Hitchin, UK

2.2 Molecular biology

2.2.1 Restriction enzyme analysis

2.2.1.1 Restriction analysis of DNA using restriction endonucleases

All restriction endonucleases were purchased from New England Biolabs (NEB) and were used according to the manufacturer's instructions. Restriction analysis were conducted in a total volume of 15 µL, using 1-4 µL of eluted plasmid DNA from mini-preparations and 5–10 U of the enzyme. Restriction analysis were incubated for two or three hours at the appropriate temperatures.

2.2.1.2 Preparative cleavage of DNA using restriction endonucleases

DNA was cleaved in a total volume of 100 µL. The relevant 10× NEB buffer (10 µL), 5-10 U of each restriction enzyme, and 10–15 µL of plasmid DNA (1–1.5 mg/mL) were mixed with double-distilled water (ddH_2O) to bring the volume to a total of 100 µL. The solutions were combined in the following order: ddH_2O, buffer, DNA, and enzymes. The reaction mixture was incubated in a thermomixer at the appropriate temperature (for most enzymes, 37°C) for 2–3 h. Later, 5 µL of the DNA was removed, while the rest of the digest was further incubated. The sample was then mixed with 10 µL of ddH_2O and 1.5 µL of a 10× gel loading dye and run for 45 min at 120 V on a 0.8% agarose gel using a 1 kb DNA ladder as a size marker. The gel was analysed using a UV light and a camera.

2.2.2 Agarose gel electrophoresis

2.2.2.1 Analytical agarose gel

Agarose gels were prepared at concentrations of 0.7–1.2% (w/v) agarose. The DNA samples were mixed with a 1/10 volume of 10× agarose gel loading buffer, loaded into the gel wells, and separated at 1.4–10 V/cm. UV illumination was used to visualise nucleic acids with intercalated EtBr. The use of a DNA marker allowed the estimation of the lengths and concentrations of separated DNA fragments.

2.2.2.2 Isolation of DNA fragments from agarose gels

Once the preparative cleavage of the respective plasmid was confirmed to have reached completion, 10× gel loading dye was added to generate a final concentration of 1×, and the cleaved DNA was resolved on a 0.8% agarose gel. The DNA fragments were visualised using a low-energy UV transilluminator (360 nm), and the band of interest was removed using a clean scalpel and transferred into a sterile 2 mL tube. DNA was extracted from the gel following the gel extraction kit protocol of the manufacturer (Macherey & Nagel, Germany). The final elution was performed twice with 30 µL of sterile ddH_2O.

2.2.2.3 Complete fill-in of a 5'-overhang using Klenow enzyme to create blunt end DNA

DNA from plasmid was extracted using the gel extraction kit protocol of the manufacturer (Macherey & Nagel, Germany). The extracted DNA, 1 µL dNTPs, and 1.5 U Klenow enzyme and up to 50 µL ddH_2O were added, followed by incubation for 15 minutes at 25°C.

2.2.2.4 Shrimp alkaline phosphatase (SAP) treatment.

DNA fragments carrying the regions relevant for the maintenance and replication of plasmids in bacterial cells (vector, as opposed to insert) were treated with SAP to remove terminal phosphate residues and to prevent religation. Isolated DNA (60 µL) was added to 6.8 µL of a 10× SAP buffer and 1.5 U of SAP, mixed, and incubated in a thermomixer at 37°C for two hours. After incubation, the SAP was inactivated by heating the solution to 65°C in a thermomixer for 20 minutes. Finally, the solution was collected at the bottom of the tube with a quick spin, and a 5 µL sample was withdrawn for analysis on a 0.8% agarose gel.

2.2.4 DNA ligation

For ligation, the concentrations of the DNA fragments to be ligated were assessed by running an aliquot of the samples on an agarose gel. From this gel, the required volumes of the inserts and vectors (ratio 3:1) were estimated, and the volume of ddH_2O required to bring the total reaction mixture to 15 µL was calculated. ddH_2O, DNA fragments,1.5 µL of 10× T4-Ligase buffer, and 1 U of T4-Ligase were combined in the stated order in a polymerase chain reaction (PCR) tube and incubated overnight at 13°C in a PCR machine.

2.2.5 *E. coli* transformation

2.2.5.1Culturing of *E. coli*

2.2.5.1.1 Culturing on ager plates

A maximum volume of 200 µL of transformed *E. coli* cells were evenly distributed on LB agar plates containing the required antibiotics using a sterile spreader. Antibiotics were used to select positive clones at concentrations of 100 µg/mL (Carbenicillin) or 40 µg/mL (kanamycin). The inoculated agar plates were incubated upside down overnight at 37°C.

2.2.5.1.2 Culturing in liquid medium

A single colony of *E. coli,* selected from freshly incubated agar plates using a sterile 100 µL pipette tip, or an aliquot of a pre-cultured liquid, with a volume of no more than 1% (v/v) of the final concentration, were used to inoculate an appropriate volume of LB medium. Antibiotics were added at appropriate concentrations when needed. The cultures were incubated in a shaking incubator at 37°C at 220 ×g until they reached the required optical densities.

2.2.5.1.3 Preparation of bacterial glycerol stocks

A volume of 500 µL was taken from an overnight culture and carefully mixed with 500 µL of sterile glycerol in a sterile cryotube. The mixture was incubated for 10 minutes on ice and subsequently stored at -80°C.Plasmid DNA (1–3 µL) along with 4–5 µL of a ligation solution were used to transform *E. coli* competent cells. DH5α *E. coli* cells (100 µL) were defrosted at room temperature and mixed briefly with the DNA solution by vortexing. The cells were then incubated on ice for one hour. Then, they were heat shocked for 90 s in a 42°C water bath and transferred onto ice for 5 minutes. LB medium (800 µL) was added, and the suspension was incubated in a thermomixer at 37°C for one hour with shaking. Then, 100 µL and 200 µL of the solution were plated on LB agar plates containing the corresponding antibiotic for the selection of cells carrying the plasmid and incubated overnight at 37°C.

2.2.5.2 Preparation of competent bacteria cells

A single *E. coli* colony was selected from an LB agar plate. The colony was used to inoculate 3 mL of LB broth. The culture was grown in a shaking incubator at 37°C overnight. Subsequently, 500 µL of the culture was added to 100 mL of fresh LB broth. Cultures were grown until they reached an optical density of 0.2 at a wavelength of 600 nm (OD_{600}). The cultures were maintained on ice for 15 minutes, divided into two 50 mL tubes, and centrifuged at 3,500 ×g at 4°C for 15 minutes. The pelleted cells were carefully resuspended in 16 mL of a filter-sterilised RF1 solution. The cells were pooled and incubated on ice for 90 minutes. Later, they were pelleted and resuspended in 8 mL of a sterile RF2 solution (pH6.8), and incubated on ice for 15 minutes. Finally, competent cells were aliquoted (100 µL) into 1.5 mL sterile microcentrifuge tubes, snap-frozen in liquid nitrogen, and stored at -80°C until required (Hanahan et al., 1983).

2.2.6 DNA Isolation

2.2.6.1 Isolation of genomic DNA from *E. coli*

2.2.6.1.1 DNA mini-preparation

A single colony selected from a plate of transformed *E. coli* was used to inoculate 5mL of LB broth containing the appropriate antibiotic. The culture was incubated overnight at 37°C with shaking at 225 ×g in a shaking incubator. The next day, the culture was streaked on LB agar plates, and 1.5 mL of the cultures were transferred into 1.5 mL tubes and centrifuged at 11,000 ×g at room temperature for 30 s. The majority of the supernatant was decanted, and the cell pellet was resuspended in the remaining LB medium (approximately 100 µL) by vortexing vigorously. Then, 300 µL of TENS solution was added to the vortexed medium and once again vortexed for 4 s. The tube was placed on ice. To this tube, 150 µL of 3 M sodium acetate (pH5.2) was added, after which, the solution was vortexed for 3 s and the samples were kept on ice until all samples were processed. The mixtures were then centrifuged at 11,000 ×g at 4°C for 15 minutes. The supernatant was transferred to a new 1.5 mL tube and checked to ensure that it was particle-free. If not, the centrifugation step was repeated. Subsequently, 900 µL of ice-cold 100% ethanol was mixed with the solution to precipitate the DNA. Following centrifugation under the same conditions described above, the obtained pellet was washed with 1 mL of 70% ethanol and centrifuged at 11,000 ×g and 4°C for 15 minutes. The supernatant was discarded. Finally, the pellet was air-dried before being resuspended in 40 µL of sterile ddH_2O (Zhou et al., 1990).

2.2.6.1.2 DNA midi-preparation

LB medium (100 mL) with the appropriate antibiotic was inoculated with a single bacterial colony and incubated at 37°C overnight. A glycerol stock of the grown culture was prepared by mixing 500 µL of the cell suspension with 500 µL of sterile glycerol in a 1.5 mL tube. The mixture was kept on ice for 5 minutes and then transferred to

-80°C for storage. Cells were harvested by dividing the culture between two 50 mL tubes and centrifuging the tubes at 4,000 ×g for 15 minutes at 4°C. The manufacturer's protocol for "high-copy plasmid purification kit" was followed until the DNA elution step (Macherey & Nagel). At this stage, the DNA was eluted from the column using 5 mL of an elution buffer and collected in a 50 mL tube. The eluate was distributed between six 1.5 mL tubes (833 µL per tube). Then, 583 µL of isopropanol were added to each tube, and the samples were mixed by vortexing. The tubes were centrifuged for 30 minutes at 15,800 ×g at 4°C. The supernatants were then discarded, and the pellets were washed with 1 mL of 70% ethanol. The pellets were centrifuged again for 15 minutes at 11,500 ×g at room temperature. The obtained pellets were air-dried to remove the ethanol, dissolved in 30 µL of ddH_2O, and combined into a single tube.

2.2.6.2 Isolation of genomic DNA from *Leishmania*

A total of 1 mL, corresponding to 3×10^7 cells, was harvested from the *Leishmania* culture by centrifugation for 2 minutes at 5,600 ×g at 4°C. The ISOLATE II Genomic DNA Kit was then used to purify the DNA, according to the manufacturer's instructions.

2.2.6.3 Determination of DNA concentration

A Nanodrop 2000c (Thermo Scientific) instrument was set to measure nucleic acids and blanked using 2 µL of ddH_2O. DNA solution (2 µL) was added directly to the micro-volume pedestal to determine the DNA concentration.

2.2.7 Polymerase chain reaction (PCR)

PCRs were performed using the MyTaq™ PCR System (Bioline). Reactions were performed in a volume of 25 µL in a PCR tube using a thermocycler:

1- **Reaction mixture:** The reaction mixture was prepared with the DNA template (10–200 ng), 1.0 µL forward primer (100 µM), 1.0 µL reverse primer (100 µM), 5 µL 10× MyTaq™ DNA polymerase buffer, and 0.8 µL MyTaq™ DNA polymerase and ddH_2O add up to 25 µL.

2- **PCR program for 30 cycles**

The following protocol was used: as showen in table below

Step	PCR Steps	Time	Temperature
1	DNA denaturation 1	5 minutes	95°C
2	DNA denaturation 2	30 s	95°C
3	Primer annealing	30 s	45-61°C
4	DNA elongation 1	30 s – 60 s	72°C
5	DNA elongation 2	7 minutes	72°C
6	storage	unlimited time	4°C

Table 2.1. Protocol for PCR to detect the knockout mutants. DNA denaturation for 5 minutes at 95°C, DNA denaturation for at 95°C, primer annealing for 30 s, DNA elongation for 30 s to one minute at 72°C, DNA elongation for 7 minutes at 72°C, and cooling for an unlimited time at 4°C. Steps 2 -4 were repeated 30 times before moving on to steps 5 and 6. The elongation time depended on the length of the DNA fragment to be amplified. The annealing temperature depended on the melting temperature of the oligonucleotides and was adjusted according to the manufacturer's recommendations.

2. 2.8 DNA sequencing Plasmid

Sequencing was performed by the company SourceBioscience, UK, using stock primers or our own primers.

2.3 Protein Biochemistry

2.3.1 *E. coli* transformation for protein expression

Competent *E. coli* [paPlaclQ] cells were transformed, as described in section 2.2.5. After incubating the transformed cells for one hour at 37°C with shaking, the solution

was centrifuged for 2 minutes at 16,200 ×g, and the supernatant was discarded. The pellet was resuspended in 100 µL LB medium, then plated onto LB agar containing 100 µg/mL carbenicillin and 40 µg/mL kanamycin. The plates were then incubated overnight at 37°C.

2.3.2 Protein purification

On the following day, 100 mL of LB medium containing 100 µg/mL carbenicillin and 40 µg/mL kanamycin were prepared in a 1 L Erlenmeyer flask. The transformed *E. coli* [paPlaclQ] colonies were flushed off the plate using 5–10 mL of this solution, which was then transferred into the flask. The inoculated flask was incubated at 37°C at 215 ×g in an incubator/shaker until the solution reached an OD_{600} of 0.9. The solution was then cooled to 18°C on ice, and isopropyl β-D-1-thiogalactopyranoside (IPTG) was added to generate a final concentration of 1 mM. The bacterial culture was incubated at 18°C overnight at 215×g in an incubator/shaker. The next day, cells were centrifuged at 3,000×g at 4°C for 15 minutes, after which the supernatant was removed. Cells were resuspended in 10 mL ice-cold 1× phosphate buffered saline (PBS) and centrifuged at 3,000 ×g at 4°C for 15 minutes, and then the supernatant was again removed. Cells were then resuspended in 5 mL ice-cold 1× PBS, transferred into 15 mL tubes and lysed on ice with a Branson sonifier, using 4–6 30 s constant pulses at a pulse intensity of four. Then, 600 µL 10% (v/v) Triton X-100 was added to each lysate, and the samples were rotated at 4°C for a one hour before the cell debris was removed by sedimentation at 15,800 ×g at 4°C for 30 minutes.

2.3.3 Isolation of hexahistidine-tagged proteins

The appropriate volume of 50% sepharose stock solution was centrifuged for 2 minutes at 750 ×g and 4°C, and the supernatant was discarded. The sepharose pellet was then washed twice more with ice-cold ddH_2O and sedimented under the same

conditions. Then, 200 µL 0.1 M $CoCl_2$ was added to the tube, rolled for 5 minutes at 4°C, centrifuged for 2 minutes at 750 ×g at 4°C, and the supernatant discarded. The pellets were then washed three more times with 1 mL ddH_2O. Then, 200 µL cold binding buffer was added, rolled for 5 minutes at 4°C, centrifuged for 2 minutes at 750 ×g at 4°C, and the supernatant discarded. To remove free $CoCl_2$, the beads were washed twice with ice-cold ddH_2O. Then, 200 µL of the beads were added to 100 mL of culture in a 15 mL tube and incubated overnight. Then, the beads were centrifuged at 750 ×g for 2 minutes at 4°C, and the supernatant was discarded. The beads were then rolled for one hour at 4°C, centrifuged for 2 minutes at 750 ×g at 4°C, and the supernatant was discarded. Then, 6 mL ice-cold wash buffer was added, rolled for 10 minutes at 4°C, centrifuged for 2 minutes at 750 ×g at 4°C, and the supernatant was removed. Then, 3 mL of ice-cold binding buffer was added, rolled for 10 minutes at 4°C, centrifuged for 2 minutes at 750 ×g at 4°C and the supernatant was discarded. Once more, 3 mL of wash buffer was added, rolled for 10 minutes at 4°C, centrifuged for 2 minutes at 750 ×g and 4°C and the supernatant was discarded. Finally, the beads were resuspended in 1 mL ice-cold wash buffer. Then, 100 µL of the beads were placed in a 1.5 mL tube and centrifuged at 750 ×g for 2 minutes Then, 70 µL of the supernatant was removed, 25 µL of 1× SSB/DTT was added, and the solution was resuspended and boiled for 10 minutes at 95°C, followed by a final quick spin before loading 25 µL of the supernatant on an SDS-PAGE to analyse the bound proteins.

2.3.4 Isolation of Glutathione S-transferase tagged proteins

Using a 200 µL bed volume of glutathione sepharose, the appropriate volume of 50% sepharose stock solution was centrifuged for 2 minutes at 750 ×g and 4°C, and the supernatant discarded. Glutathione sepharose was then washed with 1 mL 1× PBS, rolled for 5 minutes at 4°C, centrifuged for 2 minutes at 750 ×g at 4°C, and the

supernatant discarded. This step was repeated four times. The beads were resuspended in 1 mL 1× PBS, stored at 4°C, centrifuged for 2 minutes at 750 ×g at 4°C, and the supernatant removed. The beads were then resuspended in 900 µL 1× PBS. The cell lysate was added to the sepharose, and the bead suspension was rotated at 4°C for one hour before being centrifuged, as described above. The sepharose was then washed three times with ice-cold 1× PBS. To elute the protein 200 µL of 10× elution buffer was placed in a fresh 2 mL tube, and 1.8 mL ddH_2O was added to create a 1× elution buffer. The GST fusion protein was finally eluted twice with a one bead volume of GST elution buffer. The beads were first centrifuged for 2 minutes at 750 ×g at 4°C, and the supernatant removed from the beads. Then, 300 µL of elution buffer was added by rotation at 4°C for 30 minutes, followed by a subsequent centrifugation under the same conditions as before. Finally, samples for SDS-PAGE analysis were prepared by moving 20 µL of the eluate into a 1.5 mL tube, adding 5 µL of 5× SSB+DTT and heating this for 10 minutes at 95°C. This was followed by a final quick spin, 25 µL of the supernatant was subjected to SDS-PAGE for the analysis of protein content.

2.3.5 Sodium dodecyl sulfate polyacrylamide gel electrophoresis (SDS-PAGE)

14% SDS-PAGE gels were prepared at 25°C with a 4% stacking gels and various concentrations of resolving gels 14%. Separation was performed at 30 mA per gel, until the blue dye just ran off of the resolving gel. At the end of the electrophoresis process, the gel was stained for 30 minutes using a Coomassie R250 staining solution. The gel was destained at room temperature using a Coomassie R250 destaining solution until clear bands were visible.

2.3.2 Radiometric kinase assay

The amount of purified kinases used in the enzymatic assays was determined by SDS-PAGE analysis of the purified kinases (See 2.3.5). Kinase assays were performed in a total volume of 50 µL per tube, with 2.5 µL of 500 cpm/pmol [γ-^{32}P] ATP, 5 µL of a 10× kinase buffer, and 5 µL myelin basic protein (4.5 µg/µL MBP, artificial substrate). Sterile water was added to attain a final volume of 50 µL. The reaction mixture was incubated in a rotary incubator at 27°C for one hour. The reaction was stopped by the addition of 12.5 µL 5× SSB containing 50 mM DTT and boiling for 10 min. The assay was resolved by SDS-PAGE, and the gel was stained as described in section 2.3.5.

2.3.2.1 Gel drying and exposure to film

The Coomassie-stained kinase assay gels were incubated in a gel drying solution for at least 30 minutes before being dried between soaked cellulose-membrane sheets. A cellulose membrane was soaked in water and placed over the base of the gel drying frame. The gel was then placed on top of this membrane. A second water-soaked sheet was placed on top of the gel to ensure that all trapped air bubbles were removed. A frame was then firmly affixed to the top of the final sheet to hold the gel and membranes in place. The gel was left to dry overnight at room temperature or in a gel drier for two hours. The dried gel was exposed to X-ray films at -80°C for various time periods. Then X-ray films was incubated at 37°C for 30 minutes and developed in an automatic developer KODAK M35-M X-OMAT processor. After developing the X-ray films, dark bands appeared where radioactivity was present in the gel.

2.3.2.2 Phosphorimaging

Gels from the radiometric kinase assay were sealed and exposed to radiographic screens in a radiographic cassette. Screens were then scanned using an Amersham

Typhoon 9200 Image for analysis. Radiographic screens produce ionising radiation emissions from [γ-^{32}P] ATP. The amounts of radioactivity in the samples were measured using laser-induced light from the storage phosphor screen, and recorded on the scans. The ImageQuant TL software was used to quantify the subtle signal intensity differences from the digital images over a wide dynamic range.

2.4 *Leishmania* Cultures

2.4.1 Culturing of *L. mexicana promastigotes*

L. mexicana promastigotes were cultivated at 27°C in SDM-79 medium (Brun et al., 1979), containing antibiotics if required. Cultures were passaged every three to four days (upon reaching the late log to early stationary phase) by inoculating a fresh culture at a ratio of 1:500 to 1:1,000.

2.4.2. Preparation of *Leishmania* cryostabilates

Cryo medium (2 mL/culture) was prepared and chilled on ice. withen 5 days a standard 10 mL late log-phase promastigote culture (4–5 × 10^7 cells/mL) was sedimented by centrifugation for 10 minutes at 5,200 ×g at 4°C; the supernatant was then removed, and the cell pellet was resuspended in 2 mL cryo medium and distributed into four cryo tubes (500 µL/tube). The cryo tubes were placed in the gas phase of liquid nitrogen overnight and then transferred to an -80˚C refrigerator in the liquid phase for long-term storage.

2.4.3. Defrosting and re-culturing of *Leishmania* stabilates

Cryo tubes containing frozen cells were removed from liquid nitrogen and rapidly defrosted in a water bath at 37°C, then transferred to 10 mL SDM-79 containing antibiotics, if required. The cultures were incubated overnight at 27°C, and then used to inoculate 10 mL fresh SDM-79.

2.4.4. Transfection of *Leishmania* promastigotes

A volume corresponding to 3 × 10^7 cells was harvested from the culture by centrifugation for 2 minutes at 5,600 ×g at 4°C. The supernatant was completely removed by careful pipetting, and the pellet obtained was resuspended in 100 µL Human T Cell Nucleofector solution, containing an Amaxa Nucleofector II buffer supplemented with 1–5 µg of the DNA fragment or plasmid. The cell suspension was transferred to a precooled electroporation cuvette. The solution was then electroporated using the Amaxa Nucleofector II programme V-033, followed by the incubation of the cuvette on ice for five minutes. The solution was then transferred into 10 mL SDM-79 and incubated for 24 hours at 27 °C. The next day, cells were plated on a 96-well plate (200 µL/well) at two different dilutions (1:2 and 1:40). The cell suspension (10 mL) was diluted by adding 11 mL SDM-79 (containing the selective antibiotic; 1:2 dilution). This diluted solution (1 mL) was then mixed with 19 mL of medium (containing the selective antibiotic; 1:40 dilution), and both dilutions were plated on 96-well plates (200 µL/well). The plates were wrapped with parafilm and incubated at 27°C for 10–15 days until antibiotic-resistant cells had grown. Scaling up of transgenic cell lines occurred each week, and the turbidity of the 96-well plate was checked using an inverted microscope to confirm the growth of *Leishmania* cells and to identify positive clones. Four cell lines were transferred to 12-well plates containing 2 mL supplemented SDM-79 and antibiotic. The 12-well plates were incubated at 27°C for three days, until the turbidity was high enough to warrant the inoculation of 10 mL cultures. Forty microliters of the cultures grown in the 12-well plates were used for the inoculation of 10 mL SDM-79 containing antibiotic in a culture flask. The inoculated media were then incubated at 27°C for three days, until the culture reached the late logarithmic growth phase (5–7 × 10^7 cells/mL).

2.5 Microscopy

2.5.1 Preparation of fixed cells in *L. mexicana*

Leishmania cultures at log-phase were centrifuged at 5,600 ×g for 2 min, cells were washed with 1 mL ice-cold 1× PBS and subsequently resuspended in 300 µL ice-cold 1× PBS. At the same time, a 10-well microscope slide was coated with Poly-L-lysine by incubation with 20 µL 0.1 mg/mL Poly-L-lysine in 1× PBS per well for 15 min at room temperature. The wells were then washed twice with 50 µL 1× PBS before 20 µL cell suspension left to dry then added 100% ice-cold methanol to each well. Then, 20 µL 4% paraformaldehyde was added to each well, and fixation was allowed to proceed for 15 minutes. Cells were finally embedded in Mowiol/DABCO and covered with a cover slip without trapped air bubbles. The cells were viewed using an Epifluorescence Microscope.

2.5.2 Green fluorescence Microscopy

Cells were viewed with an Epifluorescence microscope (Nikon Eclipse E600), and fluorescence images were captured by a Nikon Eclipse E600 camera. Fluorescence was detected using a FITC filter (λ=540 nm), and pictures were typically taken with an exposure time of 100–200 ms. Fluorescence confirmed the expression of GFP-tagged proteins in the *L. mexicana* promastigoate cultures. Localisation of kinases was performed through fluorescence microscopy using cells in the logarithmic growth phase (2–4 × 10^7cells /mL).

2.5.3 Bright field microscopy

The sample technique facilitates the determination of *L. mexicana* promastigote phenotypes. A late log-phase *Leishmania* promastigote culture (50–100 µL) was centrifuged at 5,600 × g for 2 minutes. Pellets were resuspended in 50 µL fixation

solution; 4 µL of the suspension was added to a slide and covered with a cover slip, without trapping air. Bright field microscopy was used to examine the cells at 40× and 100× magnification, and 15–20 fields were examined. Images were captured using a Nikon Eclipse E600 camera. A total of 200 cells for each clone were imaged, and Image J Software Version 1.51p was used. Flagellar lengths were measured using the freehand tool to draw lines along the flagella, while cell lengths were measured using separate lines extending between the distal cell tips, which were defined as the maximum distances. The widths of cells were measured by drawing lines between the two lateral ends.

2.5.4 *Leishmania* cell counting

To count the cells, 5 µL of the *Leishmania* cultures were diluted in a fixing solution to the appropriate ratio, and the cell suspension was loaded onto a Neubauer chamber (0.1 mm, 0.0025 mm^2) for cell counting using a light microscope. The number of cells in the whole area (two large squares) was counted, and the average value was used to calculate the cell density, using the following formula: number of cells/mL=number of counted cells × dilution factor × 10,000.

2.6 Animal infection experiment

The animal experiment was performed, in accordance with local ethical approval and received United Kingdom Home Office approval. Five female six- to ten-weeks-old BALB/c mice were used to test each *Leishmania* clone for this infection study. Late log-phase promastigotes were harvested at 5,600 ×g for 20 s, then washed with ice-cold 1× PBS and resuspended in 1× PBS to a final density of 3.3×10^6 cells/mL. Subsequently, 30 µL of this cell suspension, containing 1×10^7 promastigotes, were injected into the right hind foot pad of a mouse using a 0.3 mm × 13 mm needle. Using

a calliper gauge, the infected foot pad was measured every week and compared to the non-infected foot pad. The experiment was terminated after 12 weeks.

2.6.1 Isolation of *Leishmania* amastigotes from mouse lesions

The foot pad with the developing lesion was sterilised with 70% ethanol and cut into pieces that were transferred into 10 mL ice-cold PBS. Next, a sharp surgical scalpel was used to disassociate the tissue to release amastigotes. Debris was collected in a petri dish with PBS and the suspension was transferred to a sterile centrifugation tube. Following centrifugation for 10 min at 150 ×g at 4°C, cell debris was removed. The suspension was centrifuged again at 1,500 ×g at 4°C for 10 min to sediment amastigotes. Amastigotes were resuspended in 10 mLl ice-cold PBS and cultured in 10 mL SDM-79 to obtain promastigotes.

Chapter 3: Function and localisation of LmxPK6

Abstract

Mitogen-activated protein kinase kinases (MAP2K) are an important component of the MAP kinase signal transduction pathway in *Leishmania*; however, little is known about them in the parasite. This project studies a novel MAP2K (LmxPK6) by molecular characterisation of the recombinant protein followed by a knockout experiment. The amino acid sequence of LmxPK6 was analysed for localisation signals and binding sites. However, no clear nuclear export signal could be identified for LmxPK6, but putative D-sites were revealed for interaction with substrates, most likely MAP kinases. Expression in *E. coli* did not result in LmxPK6 expressed as a Glutathione-S-transferase fusion protein. On the other hand, the generation of a single allele knockout for LmxPK6 was successful and confirmed by PCR, but a double allele knockout could neither be obtained in the standard knockout approach nor in the presence of the LmxPK6 gene on a plasmid, indicating that LmxPK6 could be an essential kinase in *L. mexicana* promastigotes and requires tight regulation of gene expression by its own gene flanking regions.

3.1 Introduction

This study investigates MAP kinase kinases in *Leishmania* signal transduction. Genome analysis suggested that there are seven MAP kinase kinase homologues in *Leishmania* (Pearson et al., 2001). MAP2K signalling has been studied looking at LmxPK4 (Kuhn and Wiese, 2005), LmxMKK (Erdmann et al., 2006) and LmxMKK5 (John von Freyend et al., 2010). Two of these MAP2 kinases, LmxMKK and LmxPK4, play a role in flagellum length control in *L. mexicana* (Wiese et al., 2003b). In this chapter, the putative MAP2 kinase LmxPK6 from *L. mexicana* will be analysed by

recombinant protein expression and purification from *E. coli,* and the generation of a knockout for LmxPK6 in *L. mexicana* will be attempted.

3.2. Results

3.2.1 Molecular characterisation of LmxPK6

LmxPK6 is encoded by a 2436 bp open reading frame, which when translated results in and is a protein of 811 amino acids with a molecular weight of 89.6 kDa. The full-length amino sequence of LmxPK6 (GenBank: DQ812909) was used in a BLAST identity search in TriTrypDB (https://tritrypdb.org/tritrypdb/), resulting in 99% identity with a putative kinase located on chromosome 31 in *L. mexicana* MHOM/GT/2001/U1103 of the genome strain (LmxM.31.1020). A single nucleotide exchange from G to A is responsible for an amino acid change from glycine 516 in *L. mexicana* MNYC/BZ/M379, clone 2 (the strain used in the lab) to aspartate in MHOM/GT/2001/U1103. Whether this mutation influences the activity of the kinase in the two strains has not been determined. Using an NCBI BLAST search identified the kinase as showing homology to plant-like PKc-domain-containing MAP kinase kinases. The LmxPK6 has a long N-terminus with 381 amino acids and the kinase domain is located between amino acids 382 and 732, with a length of 351 amino acids. The sequence of LmxPK6 illustrates a typical protein kinase domain (I382–N732), with 12 highly conserved subdomains. The protein kinase domain contains the phosphate anchor ribbon (G383–G385) and a conserved lysine residue in subdomain II (K403), which are involved in ATP binding and the phosphotransferase reaction. MKKs are activated by phosphorylation of serine and/or threonine residues in their activation loop between subdomains VII and VIII. LmxPK6 contains the conserved DFG and APE motifs. There is a single serine residue, which could serve as a

phosphorylation site, following on from the DFG motif. However, the nearest threonine is after a further 17 residues and forms part of another motif. LmxPK6 has no obvious nuclear export signal but has eight putative D-sites, which are characterised by one or two basic amino acid residues separated by between two and six amino acid residues from the motif (L/I/V-X-L/I/V), (AAARRTKQ**I**S**V**), (KRETPMPE**V**L**L**), (NKFF**I**D**V**), (KELTM**I**T**L**), (KKQLSIL**I**E**L**), (KRETPMPE**V**L**L**), (KLKQFVQR**L**E**V**), and (KEQ**I**L**L**) (Figure 3.1).

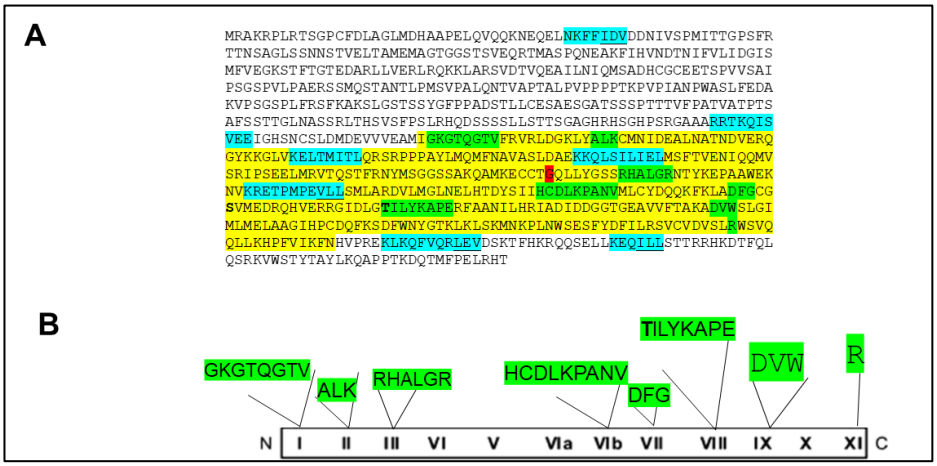

Figure 3.1. Amino acid sequence of LmxPK6 (GenBank: DQ812909). A) amino acid sequence of LmxPK6; yellow: kinase domain; green: conserved motifs; blue: D-sites; and red: glycine 516 (Genbank submission by Melzer and Wiese, 2006). **B)** Schematic of conserved motifs of LmxPK6.

Clustal Omega 1.2.4 analysis of the kinase domain of LmxPK6 with its homologues in *L. major*, *T. brucei, T. cruzi, A. thaliana*, *S. cerevisiae*, *Homo sapiens* and *D. discoideum* is shown in Figure 3.2. The sequence identities range from 96% to 70% and 55% for *L. major*, *T. brucei* and *T. cruzi*, respectively. The other species showed identities ranging from 29% to 48%.

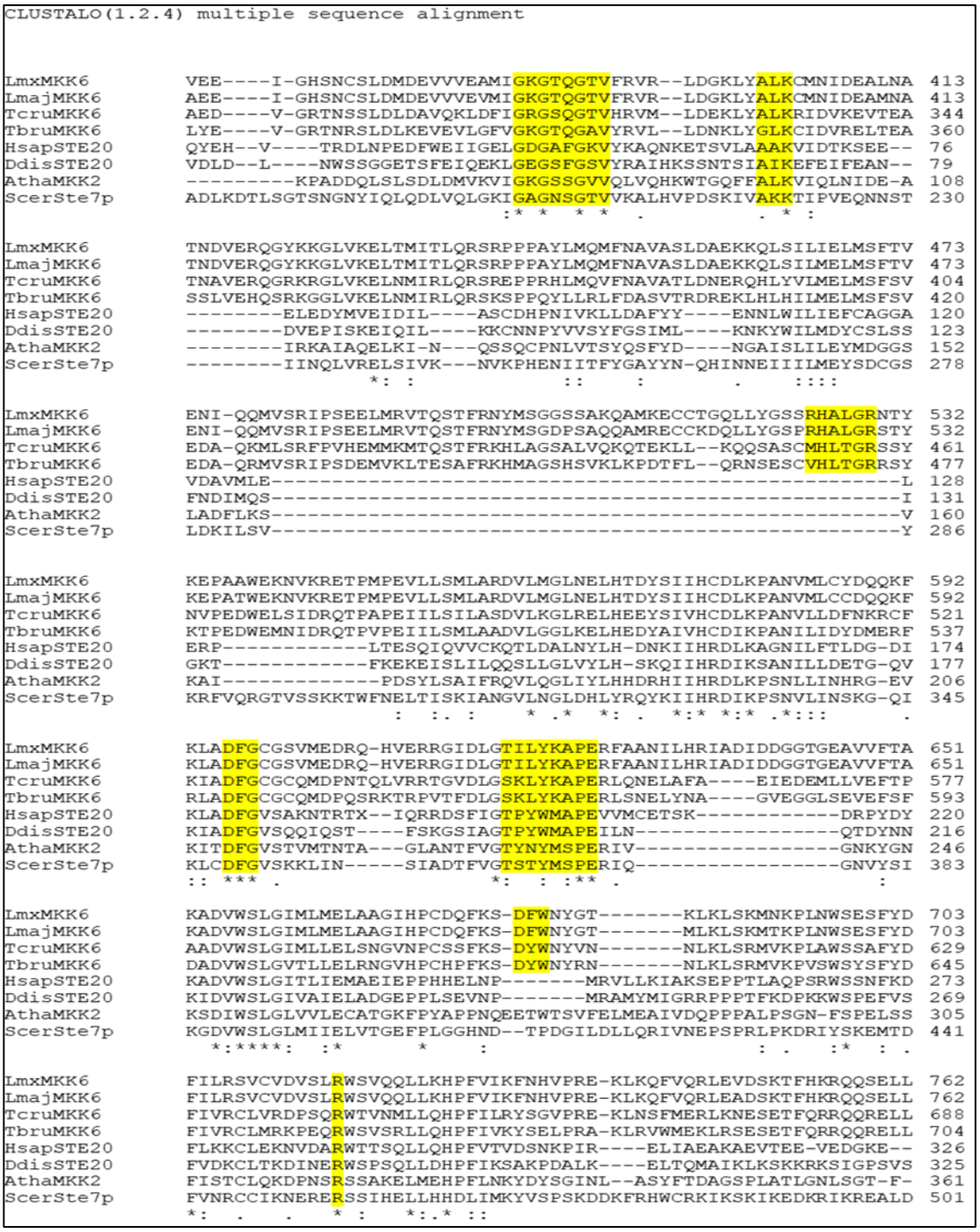

Figure 3.2. Amino acid sequence alignment of the kinase domain of LmxPK6 from *L. mexicana* (382–732 aa) with the closest homologues from various organisms. Sequences were aligned using Clustal Omega (1.2.4). **Numbering** corresponds to the primary sequence of LmxPK6; numbers shown in parentheses indicate numbers of amino acids preceding and following the shown sequences. **Dashes** represent gaps introduced for optimal alignment. **Asterisks** indicate positions which have a single, fully conserved residue. **Colons** indicate conservation between groups of strongly similar properties - scoring > 0.5 in the Gonnet PAM 250 matrix. **Periods** indicate conservation between groups of weakly similar properties - scoring = < 0.5 in the Gonnet PAM 250 matrix. *L. mexicana* MKK6 homologue

(Accession No. DQ812909); *L. major* MKK6 homologue (Accession No. NC_007273); *T. brucei* MKK6 homologue (Accession No. NT_165288); *T. cruzi* MKK6 homologue (Accession No. NW_001849566); *Homo sapiens* STE20 homologue (Accession No. GCA_000001635.6); *Saccharomyces cerevisiae* STE20 homologue (Accession No. CP004731); *A. thaliana* MKK2 homologue (Accession No. NC_003075.7); and *D. discoideum* STE20 homologue (Accession No. NC_007088).

3.2.2 Protein purification of recombinant of LmxPK6

3.2.2.1 Generation of pGEX-KGSPLmxPK6

In order to test the kinase activity of LmxPK6, it was cloned into the bacterial expression plasmid pGEX-KG to generate pGEX-KGLmxPK6 (Melzer, 2007). However, protein expression was extremely low, and no kinase activity was observed using this construct. Sequencing resulted in the discovery of four mutations in LmxPK6 in the expression construct compared to the sequence derived from the genomic DNA library. Therefore, a part of the kinase gene carrying the mutation had to be replaced by a non-mutated LmxPK6 kinase sequence. First, in Figure 3.3, pCR2.1LmxPK6ds carrying the corrected sequence for LmxPK6 and its downstream region was generated. pBSKPK681X6 containing the correct sequence for LmxPK6 was cleaved with AgeI and SpeI resulting in 3377 bp and 7393 bp DNA fragments. The pCR2.1TOPOLmxPK6 with *LmxPK6* from the DNA library, containing four mutations in *LmxPK6*, was cleaved with AgeI and XbaI, resulting in 2247 bp and 4146 bp DNA fragments (Figure 3.4 A). The 3377 bp DNA fragment from pBSKPK681X6 and 4146 bp DNA fragment from pCR2.1TOPOLmxPK6 (Figure 3.4 B) were isolated, ligated and transformed into *E. coli* DH5α to generate pCR2.1LmxPK6ds. The plasmid was analysed by restriction analysis with XhoI, to generate 3364 bp, 4159 bp; with HindIII, resulting in 1854 bp and

5669 bp; and with NdeI, resulting in 7523 bp DNA fragments, to confirm the identity of pCR2.1LmxPK6ds (Figure 3.4 C).

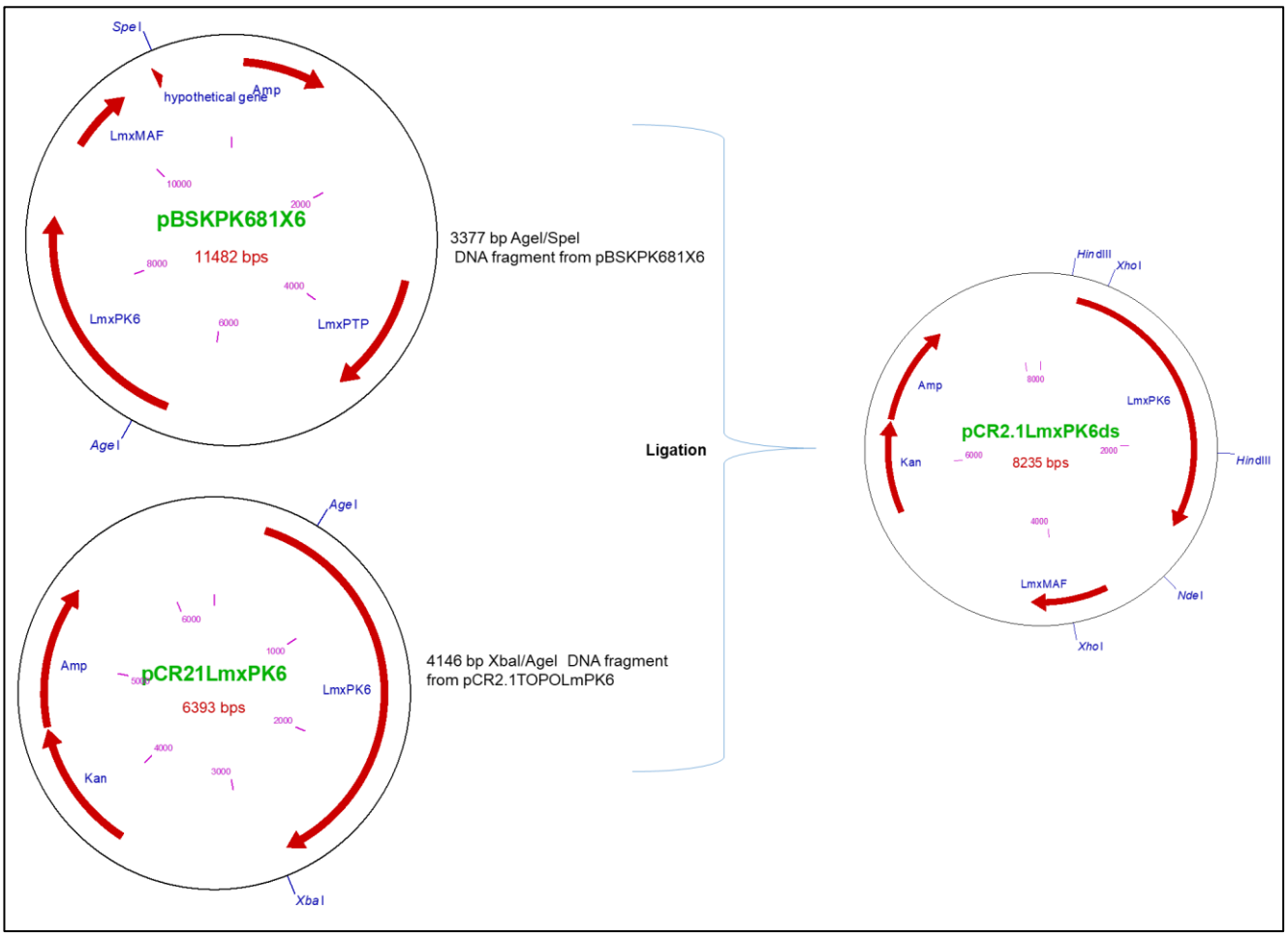

Figure 3.3. Cloning history for the generation of pCR2.1LmxPK6ds. The 3377 bp AgeI/SpeI fragment from pBSKPK681X6 was ligated with the 4146 bp XbaI/AgeI fragment from pCR2.1TOPOLmxPK6 to generate pCR2.1LmxPK6ds. Amp, ampicillin selectable marker; Kan, kanamycin antibiotic resistance gene.

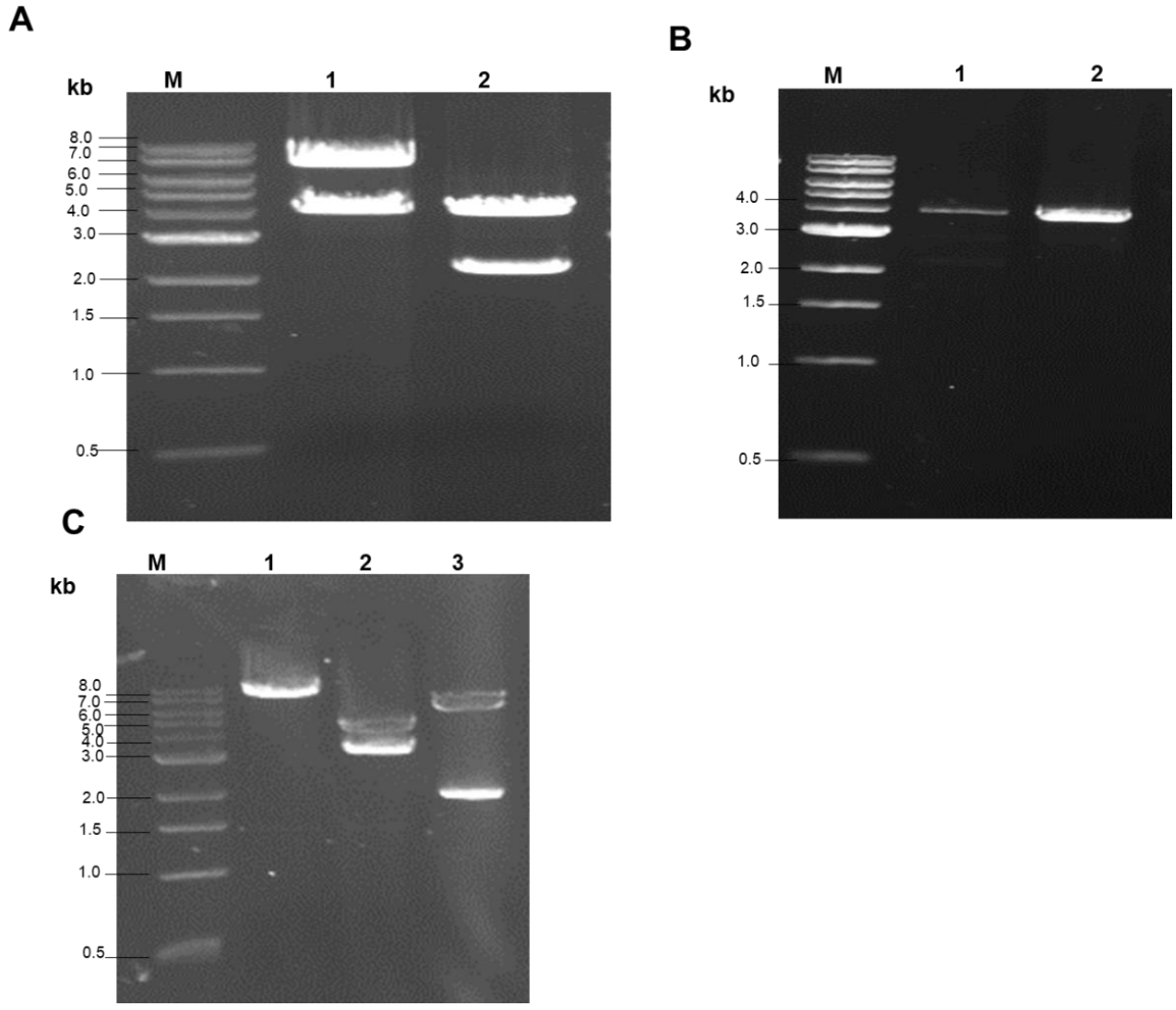

Figure 3.4. Generation of pCR2.1LmxPK6ds. A) Preparative cleavage of pBSKPK681X6 and pCR2.1TOPOLmxPK6. Lane 1, 3377 bp and 7393 bp DNA fragments generated by cleavage of pBSKPK681X6 with AgeI and SpeI; lane 2, 2247 bp and 4146 bp DNA fragments generated by cleavage of pCR2.1TOPOLmxPK6 with AgeI and XbaI. **B)** Isolated DNA fragments from pCR2.1TOPOLmxPK6 and pBSKPK681X6. Lane 1, 4146 bp XbaI/AgeI DNA fragment from pCR2.1TOPOLmxPK6; lane 2, 3377 bp AgeI/SpeI DNA fragment from pBSKPK681X6. **C)** Restriction analysis of pCR2.1LmxPK6ds. Lane 1, NdeI resulting in 7523 bp DNA fragment; lane 2, XhoI, 3364 bp and 4159 bp DNA fragments; lane 3, HindIII resulting in 1854 bp, 5669 bp DNA fragments. M, DNA size marker.

The second step of the cloning history was the generation of pCR2.1LmxPK6cor carrying the corrected kinase sequence of LmxPK6 (Figure 3.5). pCR2.1LmxPK6 was cleaved with AgeI, MluI and BsrGI to generate 452 bp, 1609 bp and 4332 bp DNA fragments, while

pCR2.1LmxPK6ds was cleaved with AgeI and MluI, to generate 714 bp ,1063 bp, 2061 bp and 4397 bp (not shown). The 4332 bp MluI/AgeI DNA fragment of pCR2.1LmxPK6 was isolated and dephosphorylated (Figure 3.6 A). The 2061 bp AgeI/MluI DNA fragment of pCR2.1LmxPK6ds was isolated (Figure 3.6 B). Both fragments were ligated and transformed into *E. coli* DH5α to generate pCR2.1LmxPK6cor. The identity of pCR2.1LmxPK6cor was confirmed by cleavage with EcoRV (2477 bp, 3916 bp), HindIII (1854 bp, 4539 bp), and XhoI (2284 bp, 4109 bp) (Figure 3.6 C), followed by DNA sequencing.

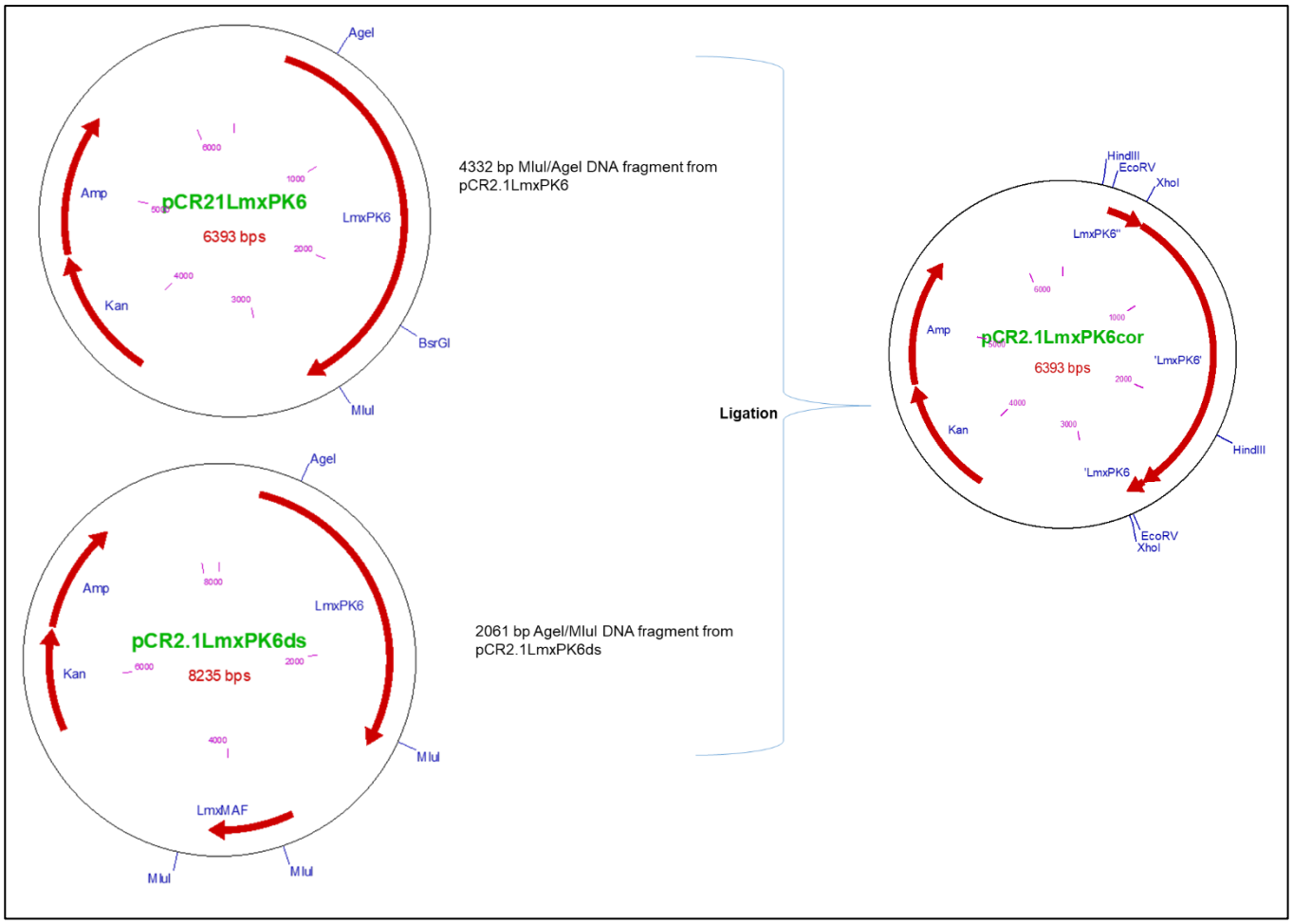

Figure 3.5. Cloning history for the generation of pCR2.1LmxPK6cor. The 4332 bp MluI/AgeI DNA fragment from pCR2.1LmxPK6 was ligated with the 2061 bp AgeI/MluI DNA fragment from pCR2.1LmxPK6ds to generate pCR2.1LmxPK6cor, which carries the correct *LmxPK6*. Amp, ampicillin selectable marker; Kan, kanamycin antibiotic resistance gene.

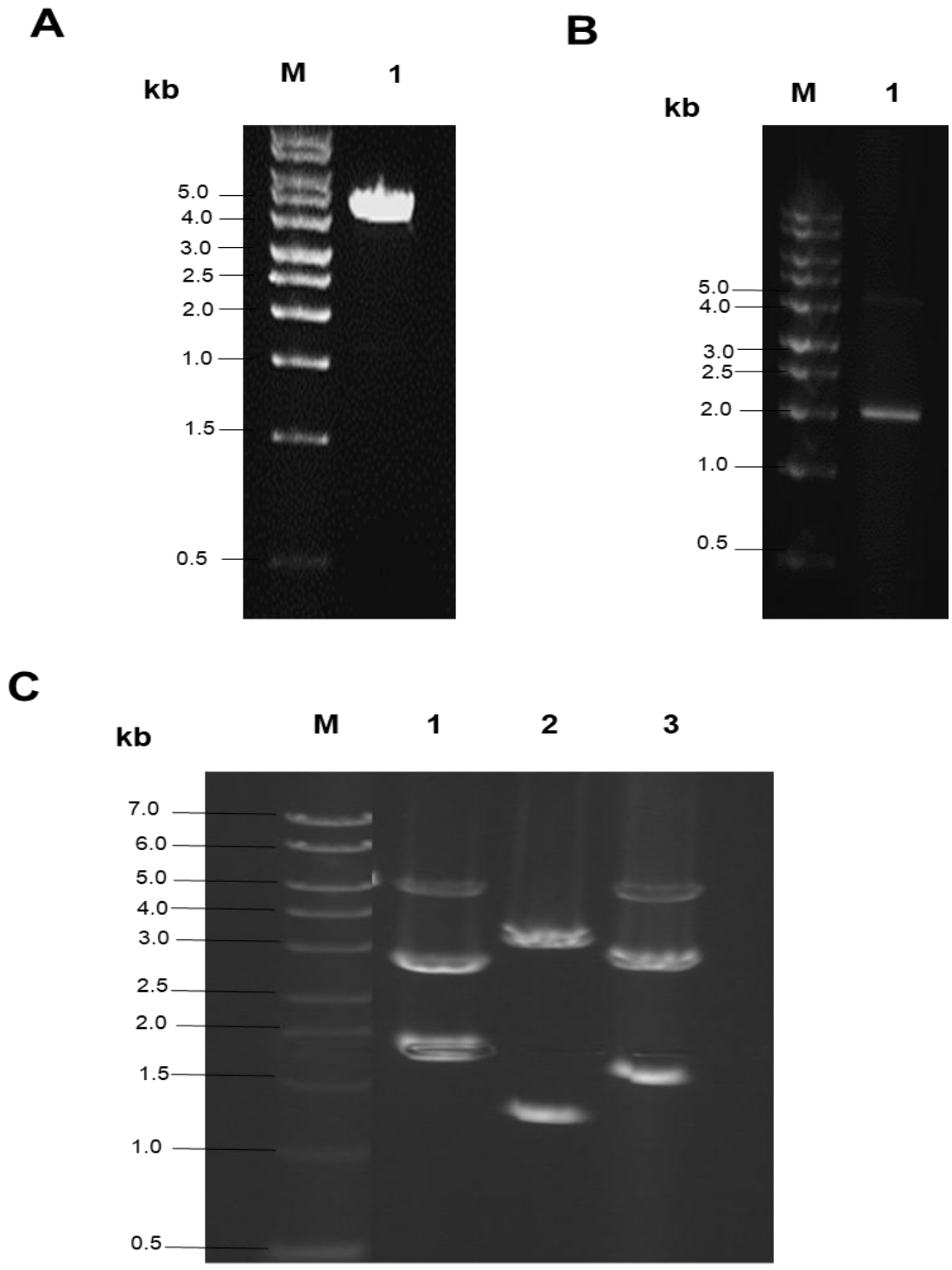

Figure 3.6. Generation of pCR2.1LmxPK6cor. A) Isolated DNA fragment from pCR2.1LmxPK6. Lane 1, 4332 bp MluI/AgeI DNA fragment from pCR2.1LmxPK6. **B)** Isolated DNA fragment from pCR2.1LmxPK6ds. Lane 1, 2061 bp AgeI/MluI DNA fragment from pCR2.1LmxPK6ds. **C)** Restriction analysis of pCR2.1LmxPK6cor. Lane 1, EcoRV (2477 bp, 3916 bp); lane 2, HindIII (1854 bp, 4539 bp), and lane 3, XhoI (2284 bp, 4109 bp). M, DNA size marker.

The third step of the cloning history is the generation of pGEX-KGSPLmxPK6 containing the correct sequence to be used to express LmxPK6 as a glutathione S-transferase (GST) fusion protein (Figure 3.7) pCR2.1LmxPK6cor, was cleaved with BspHI, SnaBI, and NcoI to generate 1155 bp, 1207 bp, 1591 bp, and 2440 bp DNA fragments (not shown). pGEX-KGSP was cleaved with NcoI and Eco53KI to generate 16 bp and 4987 bp fragments (not shown). The 2440 bp BspHI/SnaBI DNA fragment from pCR2.1LmxPK6cor and the 4987 bp NcoI/Eco53KI DNA fragment from pGEX-KGSP were isolated and the latter was dephosphorylated (Figure 3.8 A). Both fragments were ligated and transformed into *E. coli* DH5α to generate pGEX-KGSPLmxPK6. The identity of pGEX-KGSPLmxPK6 was confirmed by cleavage with ScaI (3310 bp, 4117 bp), HindIII (666 bp, 6761 bp), and XbaI (7427 bp) (Figure 3.8 B).

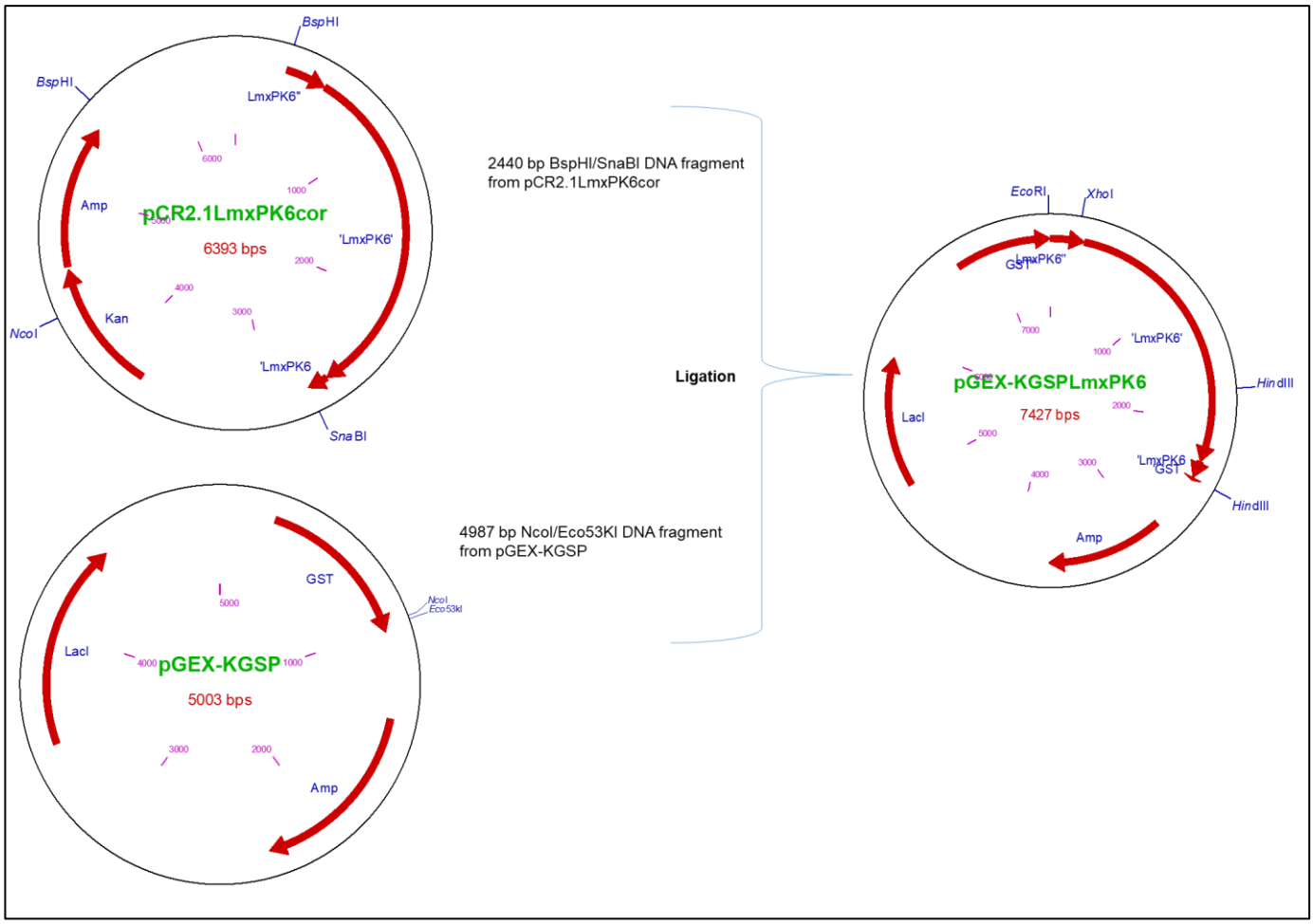

Figure 3.7. Cloning history for the generation of pGEX-KGSPLmxPK6. The 2440 bp BspHI/SnaBI DNA fragment from pCR2.1LmxPK6cor was ligated with the 4987 bp NcoI/Eco53KI DNA fragments from pGEX-KGSP to generate pGEX-KGSPLmxPK6. Amp, ampicillin selectable marker; Kan, kanamycin antibiotic resistance gene; LacI, lac repressor.

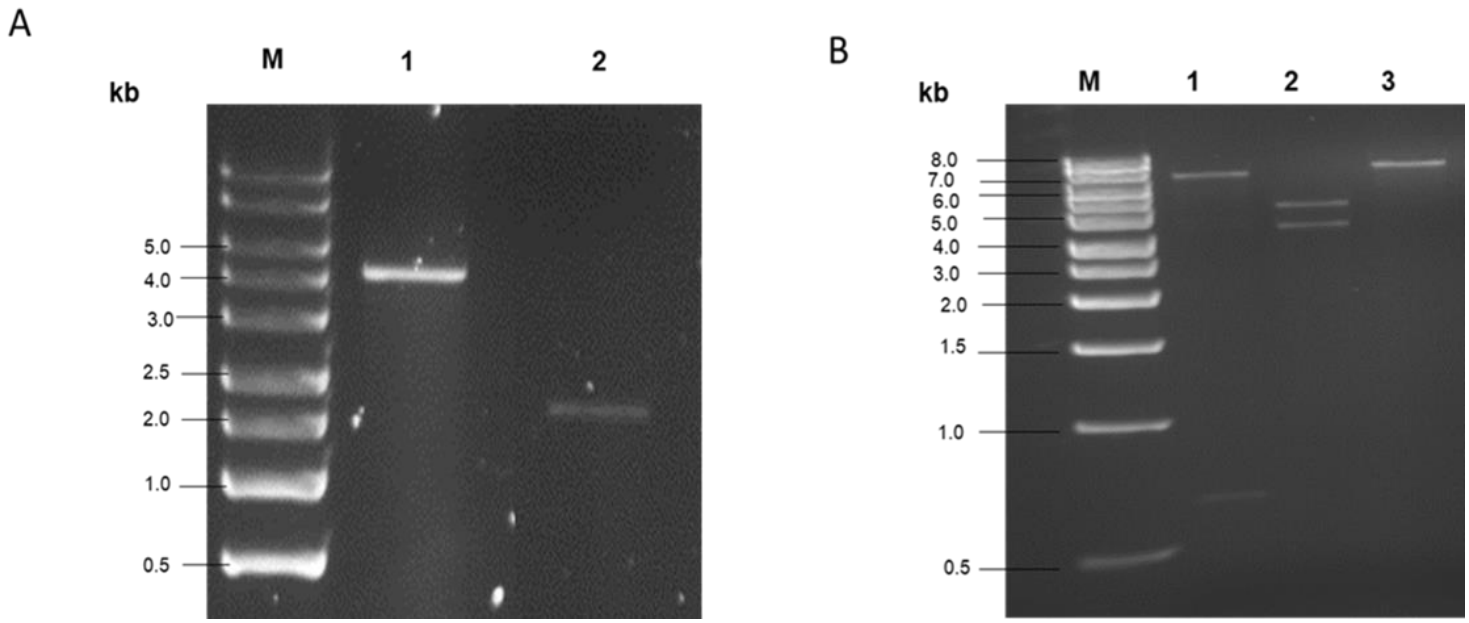

Figure 3.8. Generation of pGEX-KGSPLmxPK6. A) Isolated DNA fragments from pCR2.1LmxPK6cor and pGEX-KGSP. Lane 1, 4987 bp NcoI/Eco53KI DNA fragment from pGEX-KGSP; lane 2, 2440 bp BspHI/SnaBI DNA fragment from pCR2.1LmxPK6cor. **B)** Restriction analysis of pGEX-KGSPLmxPK6. Lane 1, HindIII resulting in 666 bp and 6761 bp DNA fragments; lane 2, ScaI generated 3310 bp and 4117 bp DNA fragments; lane 3, XbaI resulting in 7427 bp DNA fragment. M, DNA size marker.

3.2.2.2 Protein purification of recombinant GST-tagged LmxPK6

The pGEX-KGSPLmxPK6 was used for protein expression. Proteins were purified via their N-terminal GST-tag by binding to glutathione sepharose. GST-tagged proteins were eluted using reduced glutathione and analysed by 14% SDS-PAGE. Recombinant GST-LmxPK6 was expected at a size of 89.7 kDa. However, no proteins of this size were visible on the gel (Figure 3.9). Hence, no further kinase assay experiment could be conducted.

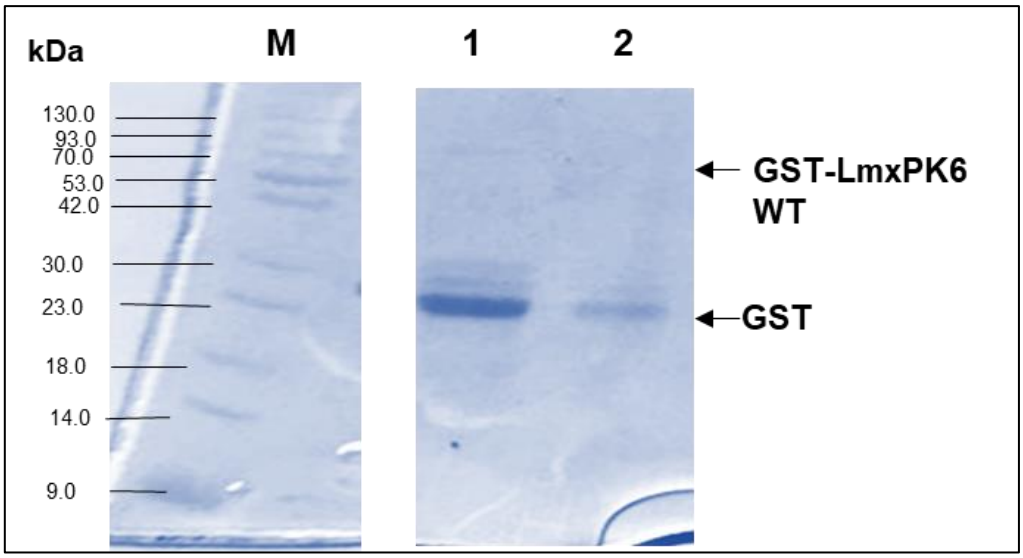

Figure 3.9. Purified recombinant GST-tagged LmxPK6 on Coomassie-stained 14% SDS-PAGE. Lane 1, elution 1 of GST-LmxPK6 showed no band of LmxPK6 visible on the gel, 89.7 kDa; lane 2, elution 2 of GST-LmxPK6 was not visible on the gel with expected size 89.7 kDa. GST with expected size 27 kDa was visible. M, protein size marker. The image is a composite image, because there were four unrelated samples in between the marker and the samples for LmxPK6.

3.2.3 Knockout of LmxPK6 in *L. mexicana*

In this experiment, an attempt was made to generate a null mutant for LmxPK6. A null mutant can be obtained by sequentially replacing the two alleles of LmxPK6 with different resistance marker genes, phleomycin (*Phleo*) and blasticidin (*Bla*), in two consecutive rounds of electroporation and homologous recombination (Figure 3.10).

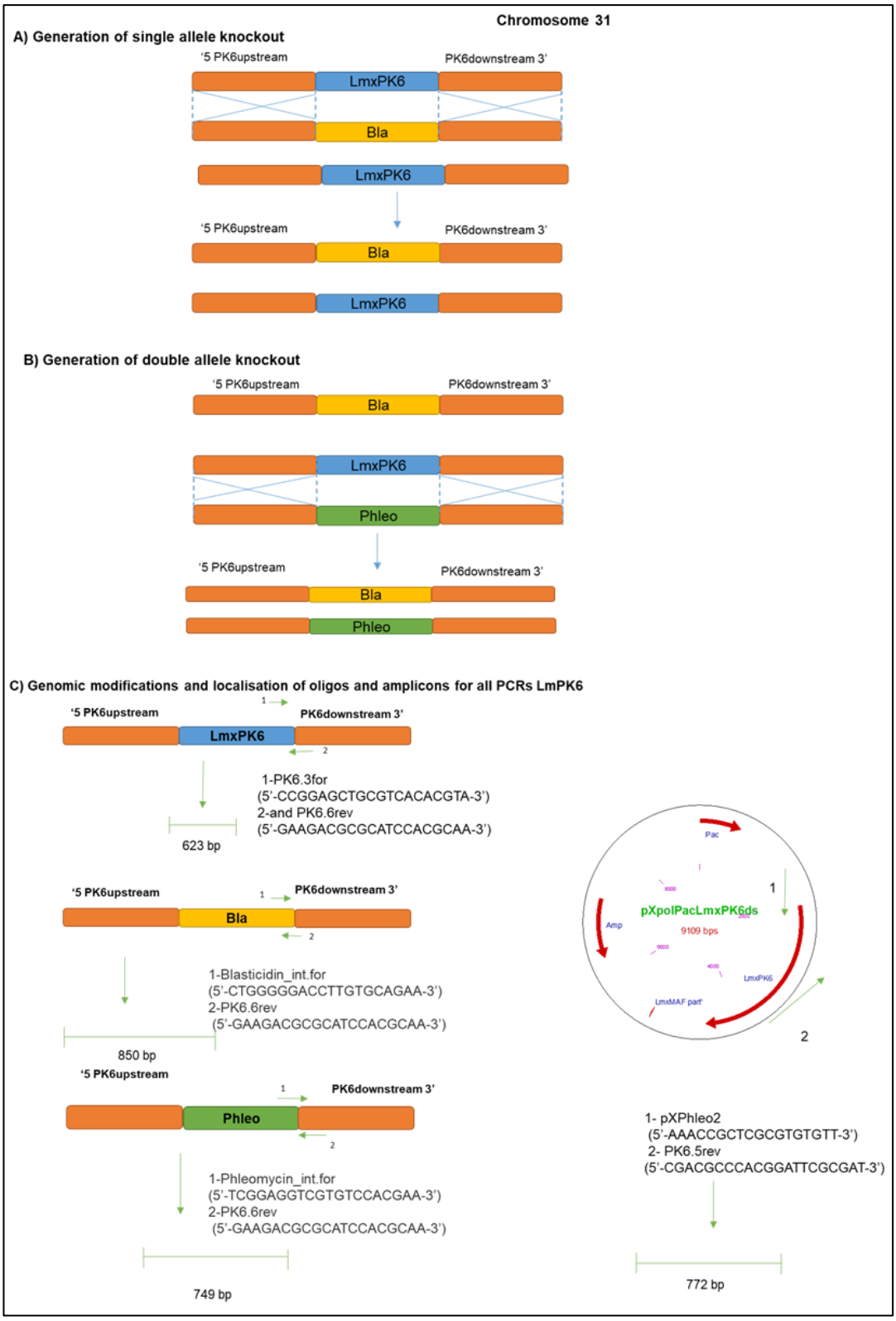

Figure 3.10. Knockout strategy for LmxPK6. A) Generation of single allele knockout with resistance marker gene (*Phleo* or *Bla*). **B)** Generation of double allele deletion of LmxPK6 with

two different resistance marker genes, *Phleo* and *Bla*. **C)** Genomic modifications and localisation of oligos and amplicons for all PCRs of LmxPK6.

3.2.3.1 Generation of *LmxPK6* deletion constructs pBNELmxPK6upBlads and pBNELmxPK6upPhleods

Figure 3.11 shows the cloning history for the generation of the knockout constructs of pBNELmxPK6upBlads, with the LmxPK6 upstream and downstream regions flanking the blasticidin gene. The plasmid pB5KXLmxPK6upds with LmxPK6 upstream and downstream regions. These were already available in the group and were cleaved with NcoI and NheI to produce DNA fragments of 4089 bp and 12 bp (Figure 3.12 A; the 12 bp fragment was too small to be visualised on the gel). The plasmid pEXBla-ATa-AR was cleaved with NcoI and NheI to produce a 401 bp DNA fragment carrying the blasticidin gene (not shown). The 4089 bp NcoI/NheI DNA fragment from the pB5KXLmxPK6upds was isolated, dephosphorylated and used for ligation with the 401 bp NcoI/NheI DNA fragment from pEXBla-ATa-AR. The ligated fragments were transformed into *E. coli* DH5α to generate pBNELmxPK6upBlads. The identity of pBNELmxPK6upBlads was confirmed by cleavage with different restriction enzymes; NruI, which would only result in one band due to dam-methylation preventing cleavage at the 1505 bp NruI site, but not the 1166 bp site (4490 bp), NotI (25 bp, 1533 bp, 2932 bp), EcoRI (1519 bp and 2971 bp), and EcoRV (28 bp and 4462 bp) (Figure 3.12 B; the small bands of 25 and 28 bp are not visible on the gel).

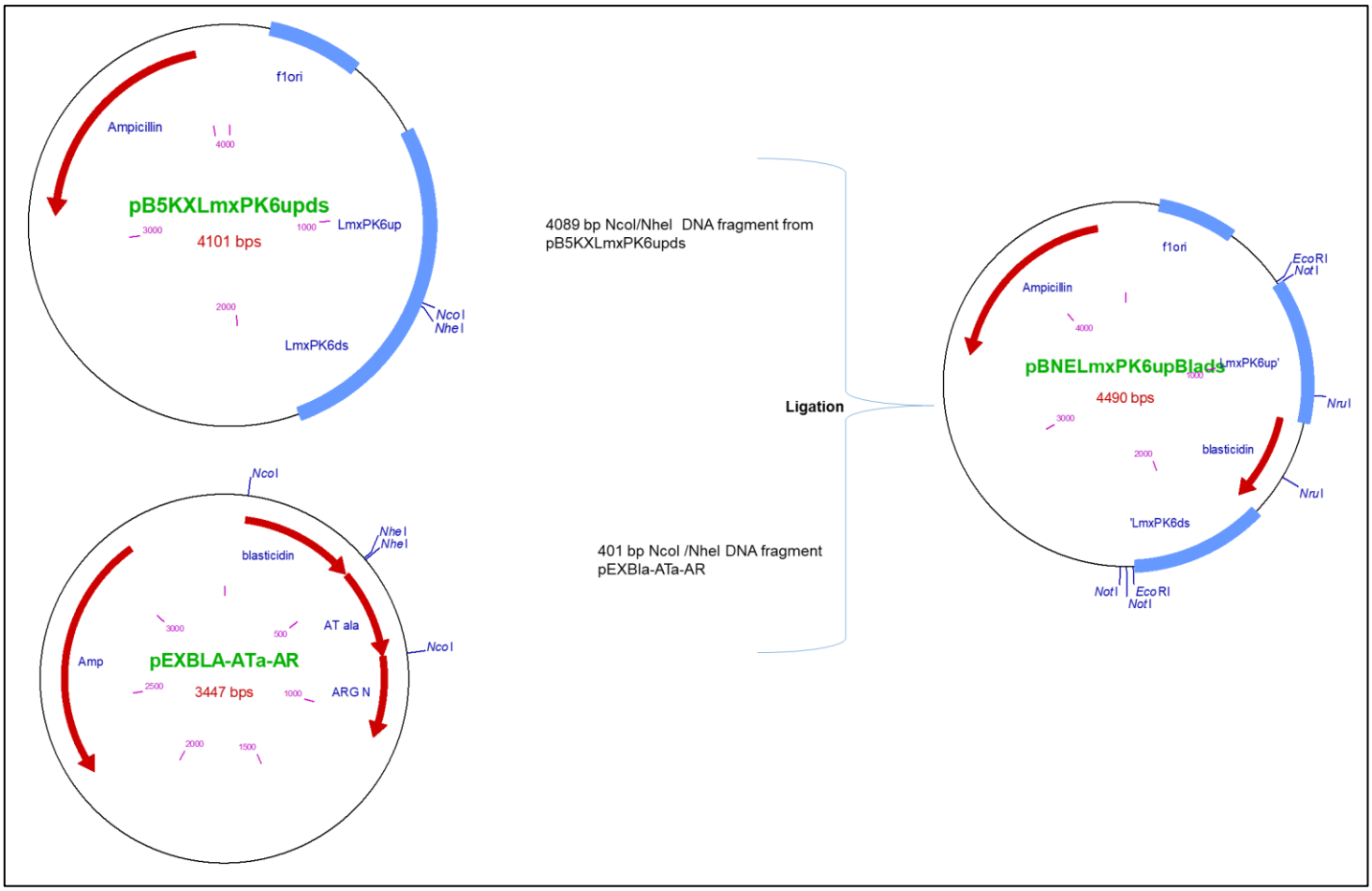

Figure 3.11. Cloning history for the generation of pBNELmxPK6upBlads. The 4089 bp NcoI/NheI DNA fragment from pB5KXLmxPK6upds was ligated with the 401 bp NcoI/NheI DNA fragment from pEXBla-ATa-AR to generate pBNELmxPK6upBlads. Amp, ampicillin selectable marker; f1ori, F1 origin of replication; ATala and ARG N are unrelated gene fragments.

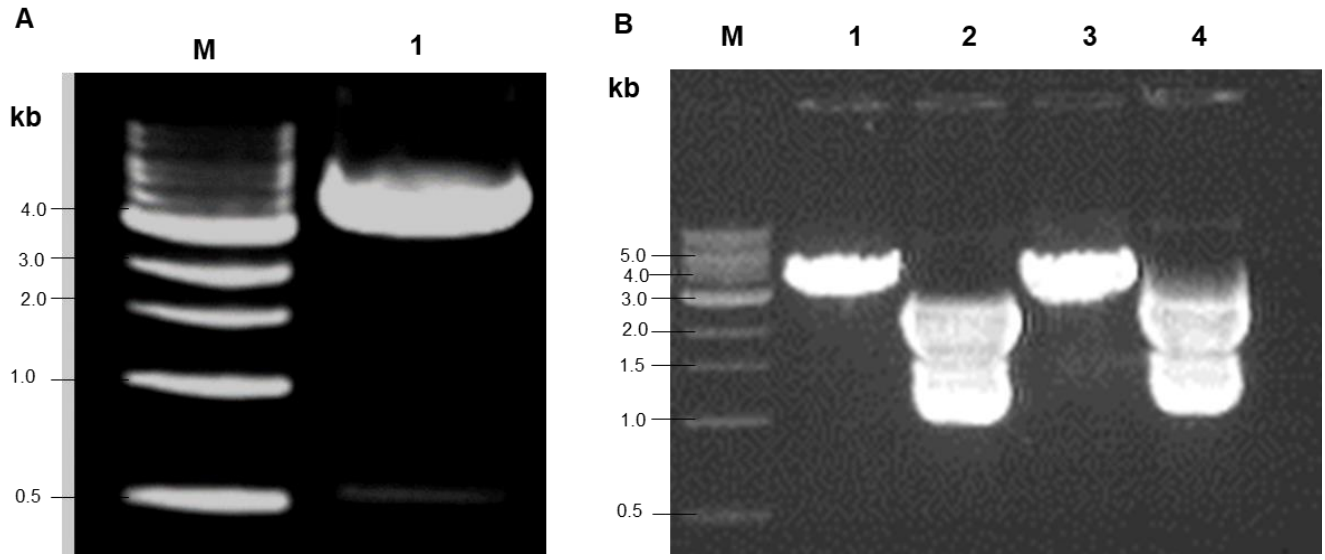

Figure 3.12. Generation of pBNELmxPK6upBlads. A) Preparative cleavage of pB5KXLmxPK6upds. Lane 1, pB5KXLmxPK6upds cleaved with NcoI and NheI resulting in 4089 bp and 12 bp DNA fragments. **B)** Restriction analysis of pBNELmxPK6upBlads. Lane 1; NruI resulting in 4151 bp DNA fragment; lane 2, EcoRI generated 1519 bp and 2971 bp DNA fragments; lane 3, EcoRV resulting in 28 bp and 4462 bp DNA fragments; lane 4, NotI resulting in 25 bp, 1533 bp and 2932 bp DNA fragments. M, DNA size marker.

Figure 3.13 shows the cloning history for the generation of the knockout construct pBNELmxPK6upPhleods, with LmxPK6 upstream and downstream regions flanking the phleomycin gene. The plasmid pCR2.1phleo was cleaved with NcoI and AvrII to generate a 377 bp DNA fragment containing the phleomycin gene (not shown). The 4089 bp NcoI/NheI DNA fragment from pB5KXLmxPK6upds (Figure 3.12 A) was used for ligation with the 377 bp NcoI/AvrII DNA fragment from pCR2.1phleo and was transformed into *E. coli* DH5α to generate pBNELmxPK6upPhleods. The identity of pBNELmxPK6upPhleods was confirmed by cleavage with NruI (4466 bp), HincII (3615 bp, 851 bp), EcoRI (1495 bp and 2971 bp) and EcoRV (28 bp and 4438 bp) (Figure 3.14; the small bands of 28 bp are not visible on the gel) (Figure 3.14).

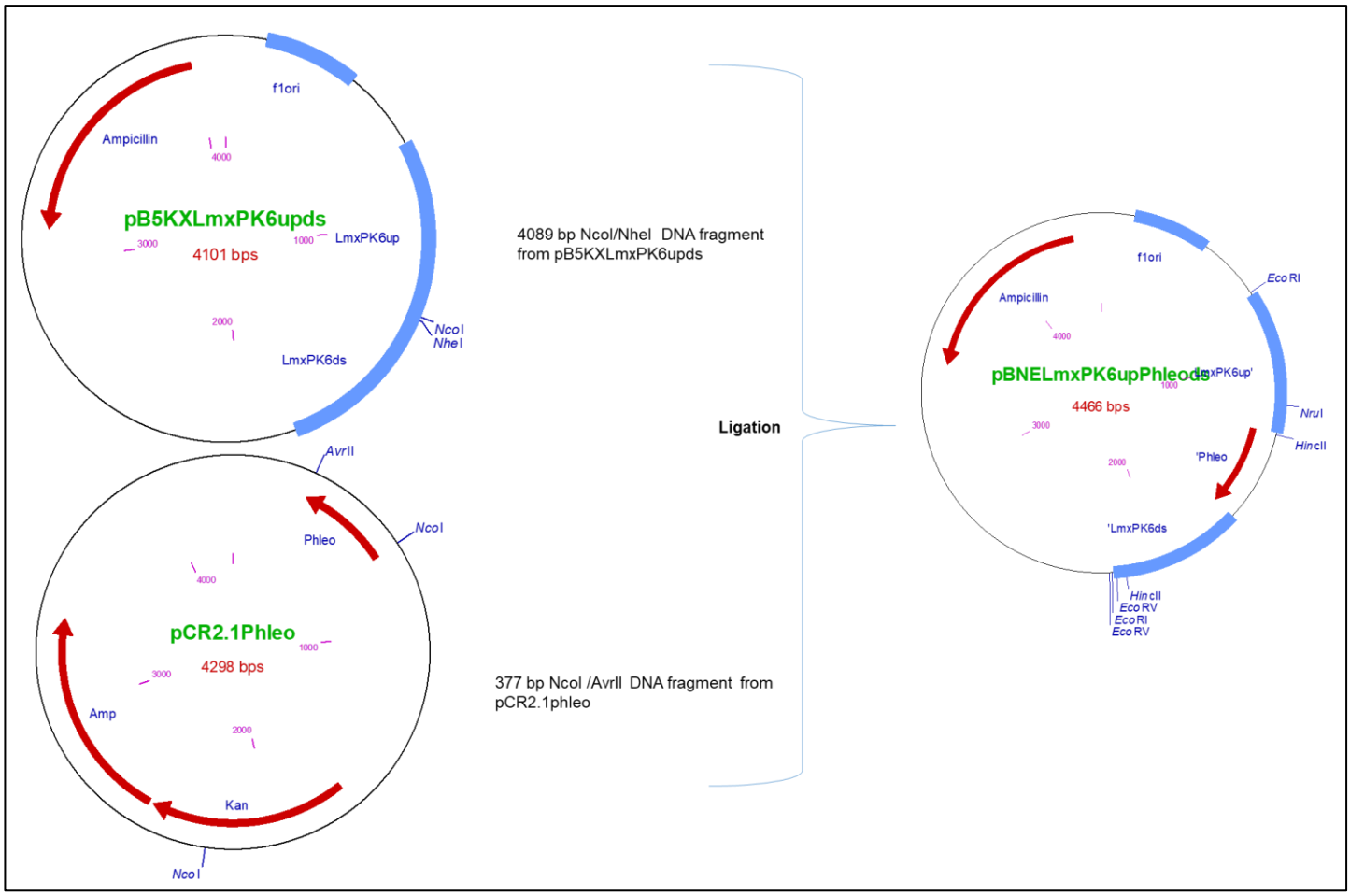

Figure 3.13. Cloning history for the generation of pBNELmxPK6upPhleods. The 4089 bp NcoI/NheI DNA fragment from pB5KXLmxPK6upds was ligated with 377 bp the NcoI/AvrII DNA fragment from pCR2.1phleo to generate pBNELmxPK6upPhleods. Amp, ampicillin selectable marker; Kan, kanamycin antibiotic resistance gene.

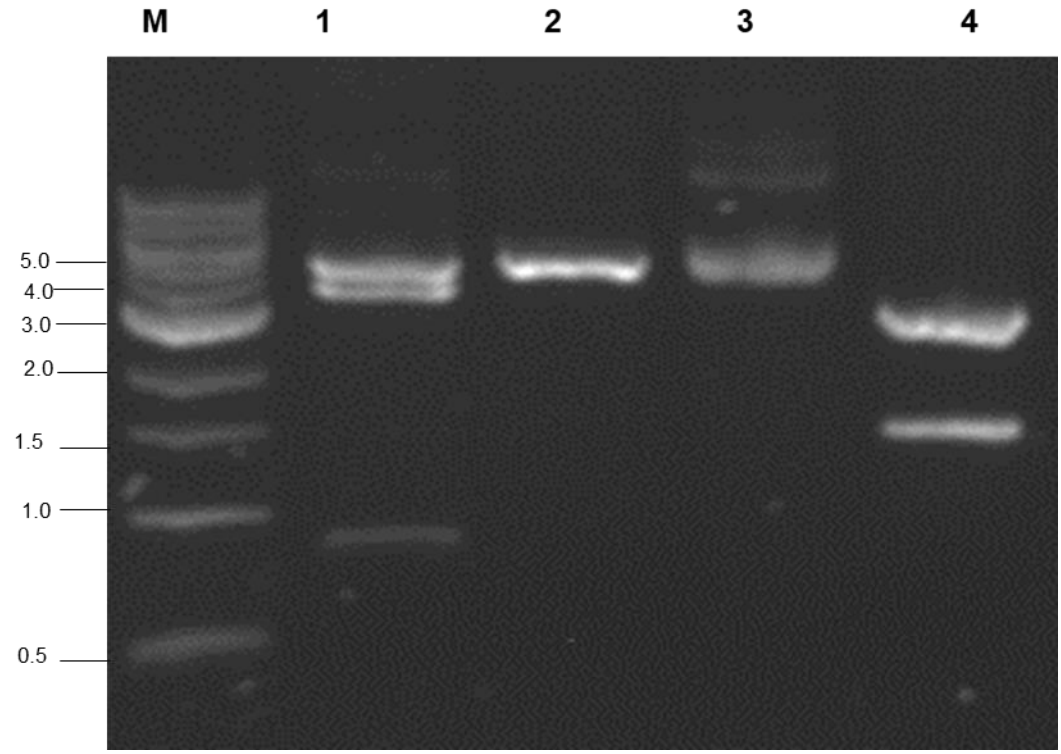

Figure 3.14 Restriction analysis of pBNELmxPK6upPhleods. Lane 1, HincII resulting in 3615 bp and 851 bp DNA fragments; lane 2, NruI resulting in 4466 bp DNA fragment; lane 3, EcoRV resulting in 28 bp and 4438 bp DNA fragments; lane 4, EcoRI resulting in 1495 bp and 2971 bp DNA fragments. M, DNA size marker.

In preparation for the LmxPK6 knockout construct, both plasmids pBNELmxPK6upBlads and pBNELmxPK6upPhleods were cleaved using EcoRV and NotI, with expected bands of 1466 bp, 2932 bp, 15 bp, 28 bp and 25 bp for pBNELmxPK6upPhleods and 2932 bp, 1490 bp, 15 bp, 28 bp and 25 bp for pBNELmxPK6upBlads (Figure 3.15 A). The 1466 bp EcoRV/NotI DNA fragment from pBNELmxPK6upPhleods and the 1490 bp EcoRV/NotI DNA fragment from pBNELmxPK6upBlads were isolated under sterile conditions and tested on 0.8% agarose gel (Figure 3.15 B). Fragments were used for electroporation into *L. mexicana* wild type promastigotes.

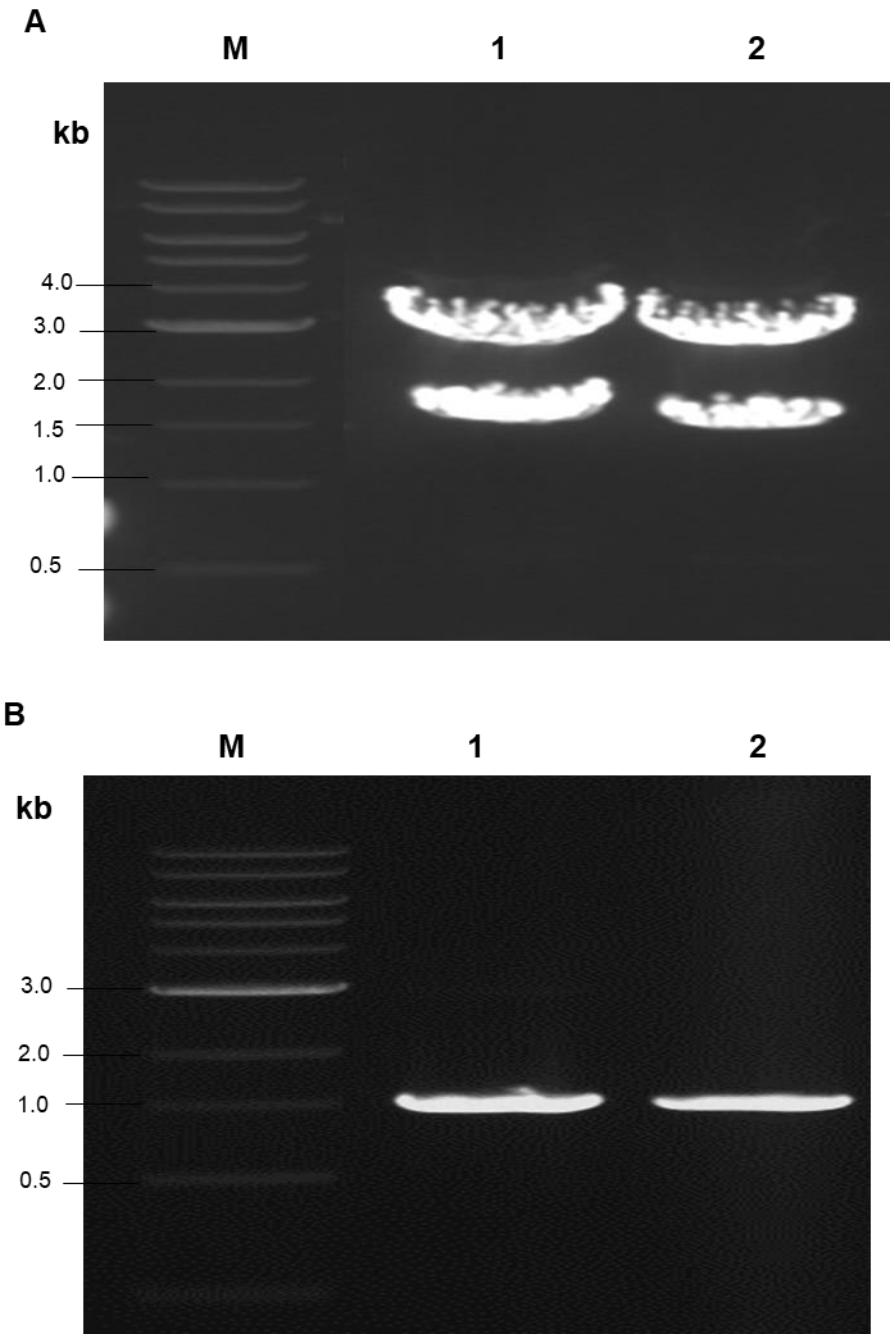

Figure 3.15. Preparation of the *LmxPK6* knockout DNA fragments. A) Preparative cleavage of pBNELmxPK6upPhleods and pBNELmxPK6upBlads with EcoRV and NotI. Lane 1, pBNELmxPK6upBlads resulting in 2932 bp, 1490 bp, 15 bp, 28 bp, and 25 bp DNA fragments; lane 2, pBNELmxPK6upPhleods resulting in 2932 bp, 1490 bp, 15 bp, 28 bp, and 25 bp DNA fragments. The small bands of 15 bp, 25 bp, 28 bp were not visible on the gel. **B)** Isolated DNA fragments from pBNELmxPK6upPhleods and pBNELmxPK6upBlads after cleavage with EcoRV and NotI. Lane 1, 1490 bp EcoRV/NotI DNA fragment from pBNELmxPK6upBlads; lane 2, 1466 bp EcoRV/NotI DNA fragment from pBNELmxPK6upPhleods. M, DNA size marker.

3.2.3.2 Transfection of *L. mexicana* wild type promastigotes to generate single allele deletion mutants

L. mexicana wild type promastigotes (3×10^7 late log-phase cells) were used in the knockout experiment. The wild type of *L.* mexicana has two alleles of LmxPK6. Efforts were made to replace one allele with a resistance marker gene, phleomycin (*Phleo*) or blasticidin (*Bla*). Electroporation was used to introduce the 1490 bp pBNELmxPK6upBlads fragment carrying the blasticidin (Bla) resistance gene or the 1466 bp pBNELmxPK6upPhleods fragment carrying the phleomycin (*Phleo*) resistance gene into wild type promastigotes of *L. mexicana.*

For the generation of single allele deletion mutants containing the resistance markers for blasticidin or phleomycin, the number of positive wells showing visible turbidity in the 96-well plate after incubation at 26 °C for 10−15 days was 70 wells positive for ΔLmxPK6+/-Bla and 65 for ΔLmxPK6+/-Phleo for the 1:2 dilutions and 30 for ΔLmxPK6+/-Bla and 25 for ΔLmxPK6+/-Phleo for the 1:40 dilution. Clones were selected from the 1:40 dilution from both cell lines, ΔLmxPK6+/-Phleo (G4, D4) and ΔLmxPK6+/-Bla (B2, H10, and F4). The cells were transferred to 12-well plates for scaling up. Subsequently, the cells were transferred to a 10 mL culture, and the identity of the clones was confirmed by PCR.

3.2.3.2.1 PCR analysis of LmxPK6+/- single allele deletion mutants

The genomic integration of the relevant constructs leading to ΔLmxPK6+/-Phleo and ΔLmxPK6+/-Bla was tested by PCR. PCR analysis with the oligos (Phleomycin_int.for and PK6.6rev) was used to prove the correct integration of the *Phleo* construct with an expected DNA fragment size of 749 bp. Two single allele mutants (ΔLmxPK6+/-Phleo G4 and ΔLmxPK6+/-Phleo D4) were confirmed (Figure 3.16 A). Whether

LmxPK6 was also still present in the single allele deletion mutants, ΔLmxPK6+/-Phleo was tested by PCR analysis with the oligos (PK6.3for and PK6.6rev). An amplicon of 623 bp was observed for all clones, as expected (Figure 3.16B).

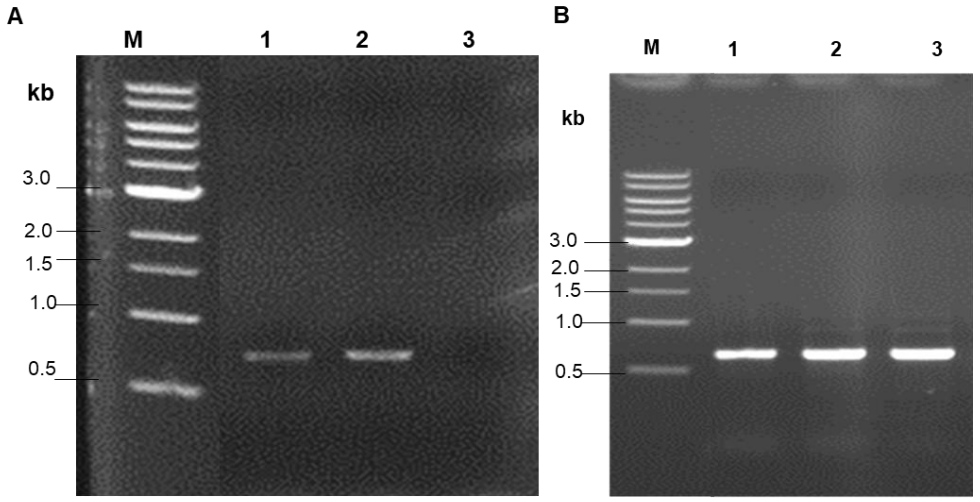

Lanes	Clones	Expected DNA fragment size
1	ΔLmxPK6+/-Phleo G4	749 bp
2	ΔLmxPK6+/-Phleo D4	749 bp
3	*L. mexicana* wild type	-

Lanes	Clones	Expected DNA fragment size
1	ΔLmxPK6+/-Phleo G4	623 bp
2	ΔLmxPK6+/-Phleo D4	623 bp
3	*L. mexicana* wild type	623 bp

Figure 3.16. Single allele deletion mutants of LmxPK6 +/-Phleo. A) Confirmation of the presence of phleomycin gene in ΔLmxPK6+/-Phleo by PCR analysis. Lane 1, ΔLmxPK6+/-Phleo G4; lane 2, ΔLmxPK6+/-Phleo D4; lane 3, *L. mexicana* wild type. The expected size was 749 bp. **B)** Confirmation of the presence of LmxPK6 in ΔLmxPK6+/-Phleo by PCR analysis. Lane 1, ΔLmxPK6+/-Phleo G4; lane 2, ΔLmxPK6+/-Phleo D4; lane 3, *L. mexicana* wild type with expected size 623 bp. M, DNA size marker.

The PCR analysis with the oligos (blasticidin_int.for and PK6.6rev) to prove the correct integration of blasticidin gene and generation of ΔLmxPK6+/-Bla was expected to yield a band of 850 bp. Three positive single allele mutants (ΔLmxPK6+/-Bla B2, ΔLmxPK6+/-Bla H10, and ΔLmxPK6+/-Bla F4) were identified (Figure 3.17 A). PCR analysis with the oligos (PK6.3for and PK6.6rev) was used to test whether *LmxPK6*

was still present in the single allele deletion mutants ΔLmxPK6+/-Bla. An amplicon of 623 bp was observed for all clones, as expected (Figure 3.17 B).

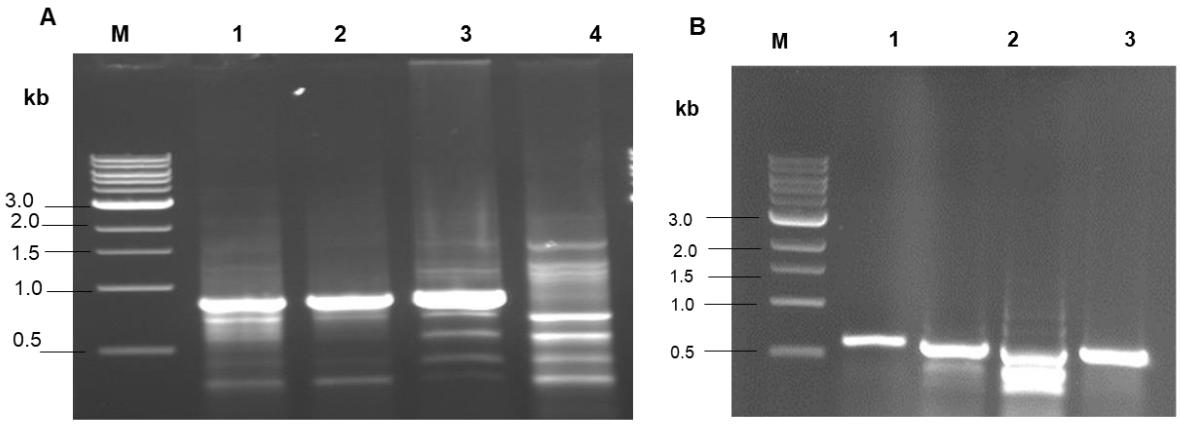

Lanes	Clones	Expected DNA fragment size
1	ΔLmxPK6+/-Bla B2	850 bp
2	ΔLmxPK6+/-Bla H10	850 bp
3	ΔLmxPK6+/-Bla F4	850 bp
4	*L. mexicana* wild type	-

Lanes	Clones	Expected DNA fragment size
1	ΔLmxPK6+/-Bla B2	623 bp
2	ΔLmxPK6+/-Bla H10	623 bp
3	ΔLmxPK6+/-Bla F4	623 bp
4	*L. mexicana* wild type	623 bp

Figure 3.17. Confirmation of single allele deletion mutants ΔLmxPK6+/-Bla by PCR analysis. A) Lane 1, ΔLmxPK6+/-Bla B2; lane 2, ΔLmxPK6+/-Bla H10; lane 3, ΔLmxPK6+/-Bla F4 and lane 4, *L. mexicana wild* type. The expected size was 850 bp. **B)** Confirmation of the presence of LmxPK6 in ΔLmxPK6+/-Bla. Lane 1, ΔLmxPK6+/-Bla B2; lane 2, ΔLmxPK6+/-Bla H10; lane 3, ΔLmxPK6+/-Bla F4; lane 4, *L. mexicana wild* type with expected size 623bp. M, DNA size marker.

Out of the five single allele deletion mutant clones for *LmxPK6* (two for ΔLmxPK6+/-Phleo and three for ΔLmxPK6+/-Bla), ΔLmxPK6+/-Phleo D4 and ΔLmxPK6+/-Bla B2 were selected for the generation of a full knockout.

3.2.3.3. Transfection of single allele deletion mutants of LmxPK6 to obtain a null mutant

In order to obtain double allele null mutants of LmxPK6, a second transfection was performed. Two L. mexicana single knockout clones, already carrying the phleomycin or Blasticidin resistance marker gene instead of one allele of LmxPK6 (∆LmxPK6+/-Phleo D4 and ∆LmxPK6+/-Bla B2), were used for electroporation with linear fragments derived from pBNELmxPK6upBlads or pBNELmxPK6upPhleods constructs (Figure3.15), respectively. Electroporation and selection using both antibiotics should lead to double allele deletion mutants containing both resistance markers. Four attempts of electroporation were performed to obtain an *L. mexicana* null mutant cell line. ∆LmxPK6-/-Phleo/Bla did not result in any turbidity for either of the dilutions plated after electroporation, while four putative clones for ∆LmxPK6-/-Bla/Phleo (∆LmxPK6-/-Bla/Phleo A12, ∆LmxPK6-/-Bla/Phleo B12, ∆LmxPK6-/-Bla/Phleo C12 and ∆LmxPK6-/-Bla/Phleo D12) grew in the 1:40 dilution and were selected. The cells were transferred to 12-well plates for scaling up. Subsequently, the cells were transferred to a 10 mL culture and analysed by PCR.

3.2.3.3.1 PCR analysis of double allele deletion mutants of *LmxPK6*

PCR reactions were set up under the same optimised conditions as before (section 3.2.3.3.1) to confirm the correct gene replacement in the double allele knockout. ∆LmxPK6-/-Bla/Phleo A12, ∆LmxPK6-/-Bla/Phleo B12, ∆LmxPK6-/-Bla/Phleo C12 and ∆LmxPK6-/-Bla/Phleo D12 clones showed an amplicon with an expected size of 749 bp for the presence of Phleo (Figure 3.18A) The absence of LmxPK6 in the double allele deletion mutants ∆LmxPK6-/-Bla/Phleo was tested by PCR analysis. PCR reactions were set up under the same optimised conditions as before (section 3.2.3.3.1) (Figure 3.18 B). ∆LmxPK6-/-Bla/Phleo A12, ∆LmxPK6-/-Bla/Phleo B12,

ΔLmxPK6-/- Bla/Phleo C12 and ΔLmxPK6-/-Bla/Phleo D12 all still carried LmxPK6. As result, the standard knockout strategy could not generate a null mutant of LmxPK6.

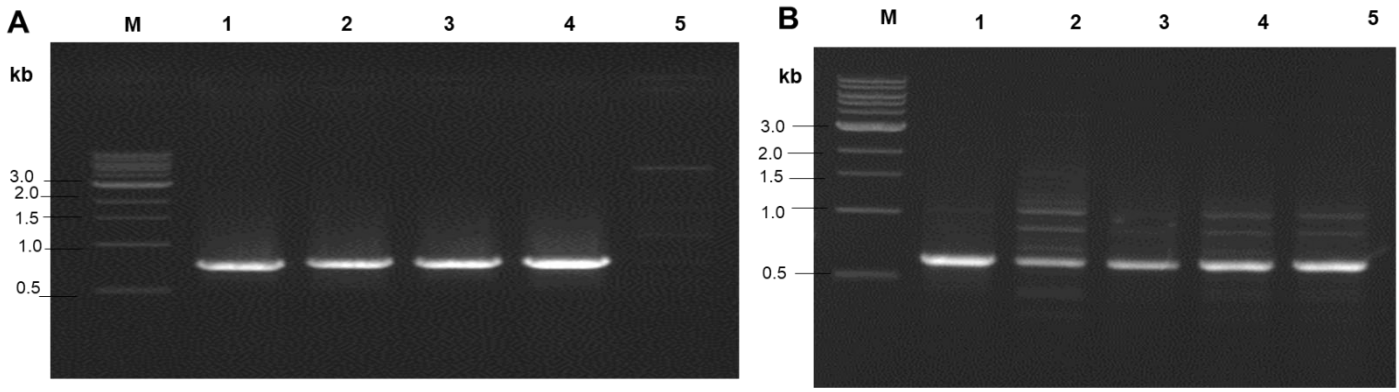

Lanes	Clones	Expected DNA fragment size
1	ΔLmxPK6-/-Bla/Phleo A12	749 bp
2	ΔLmxPK6-/-Bla/Phleo B12	749 bp
3	ΔLmxPK6-/-Bla/Phleo C12	749 bp
4	ΔLmxPK6-/-Bla/Phleo D12	749 bp
5	*L. mexicana* wild type	749 bp

Lanes	Clones	Expected DNA fragment size
1	ΔLmxPK6-/-Bla/Phleo A12	623 bp
2	ΔLmxPK6-/-Bla/Phleo B12	623 bp
3	ΔLmxPK6-/-Bla/Phleo C12	623 bp
4	ΔLmxPK6-/-Bla/Phleo D12	623 bp
5	*L. mexicana* wild type	623 bp

Figure 3.18. Confirmation of null mutants of LmxPK6. A) PCR analysis to detect the correct integration of the Phleo construct in putative ΔLmxPK6-/-Bla/Phleo clones by PCR analysis. Lane 1, ΔLmxPK6-/-Bla/Phleo A12; lane 2, ΔLmxPK6-/-Bla/Phleo B12; lane 3, ΔLmxPK6-/-Bla/Phleo C12; lane 4, ΔlmxPK6-/-Bla/Phleo D12; lane 5, wild type *L. mexicana*. **B)** Confirmation of absence of LmxPK6 from ΔLmxPK6-/-Bla/Phleo clones by PCR analysis. Lane 1, ΔLmxPK6-/-Bla/Phleo A12; lane 2, ΔLmxPK6-/-Bla/Phleo B12; lane 3, ΔLmxPK6-/-Bla/Phleo C12; lane 4, ΔLmxPK6-/-Bla/Phleo D12; lane 5, *L. mexicana* wild type. M, DNA size marker.

3.2.4 Alternative procedure to obtain a genomic null mutant for *LmxPK6*

In this experiment, an alternative procedure was tried to generate a null mutant for *LmxPK6* in *L. mexicana*. It was anticipated that a genomic allele null mutant could be

obtained by adding a plasmid with an extra copy of the LmxPK6 gene, followed by sequentially replacing both alleles of LmxPK6 with different resistance marker genes for phleomycin (*Phleo*) or blasticidin (*Bla*) in three consecutive rounds of electroporation.

3.2.4.1 Generation of LmxPK6 into pX14polNcoIPac

Figure 3.19 shows the cloning strategy for the generation of pXpolNcoIPacLmxPK6ds. Plasmid pCRLmxPK6ds (section 3.4.2.1) was cleaved with BspHI and NcoI, resulting in 3241 bp, 2284 bp, 1207 bp, 1155 bp and 348 bp DNA fragments (Figure 3.20 A). The 3241 bp fragment was isolated, and the 5'-overhangs were filled-in using Klenow polymerase. Then pX14polNcoIPac, with the intergenic region of the DHFR-TS gene, was linearised with EcoRV with an expected size of 5864 bp (Figure 3.20 A). The 5864 bp DNA fragment from pX14polNcoIPac was dephosphorylated using SAP treatment. After that, the 3241 bp DNA fragment from pCRLmxPK6ds and 5864 bp DNA fragment from pX14polNcoIPac were ligated to generate pXpolNcoIPacLmxPK6ds and were transformed into *E. coli* DH5α. Restriction analysis was done to confirm the generation of pXpolNcoIPacLmxPK6ds using NsiI (3057 bp, 6052 bp), HindIII (4274 bp, 4835 bp) and BglII (2678 bp, 6431 bp) (Figure 3.20 B).

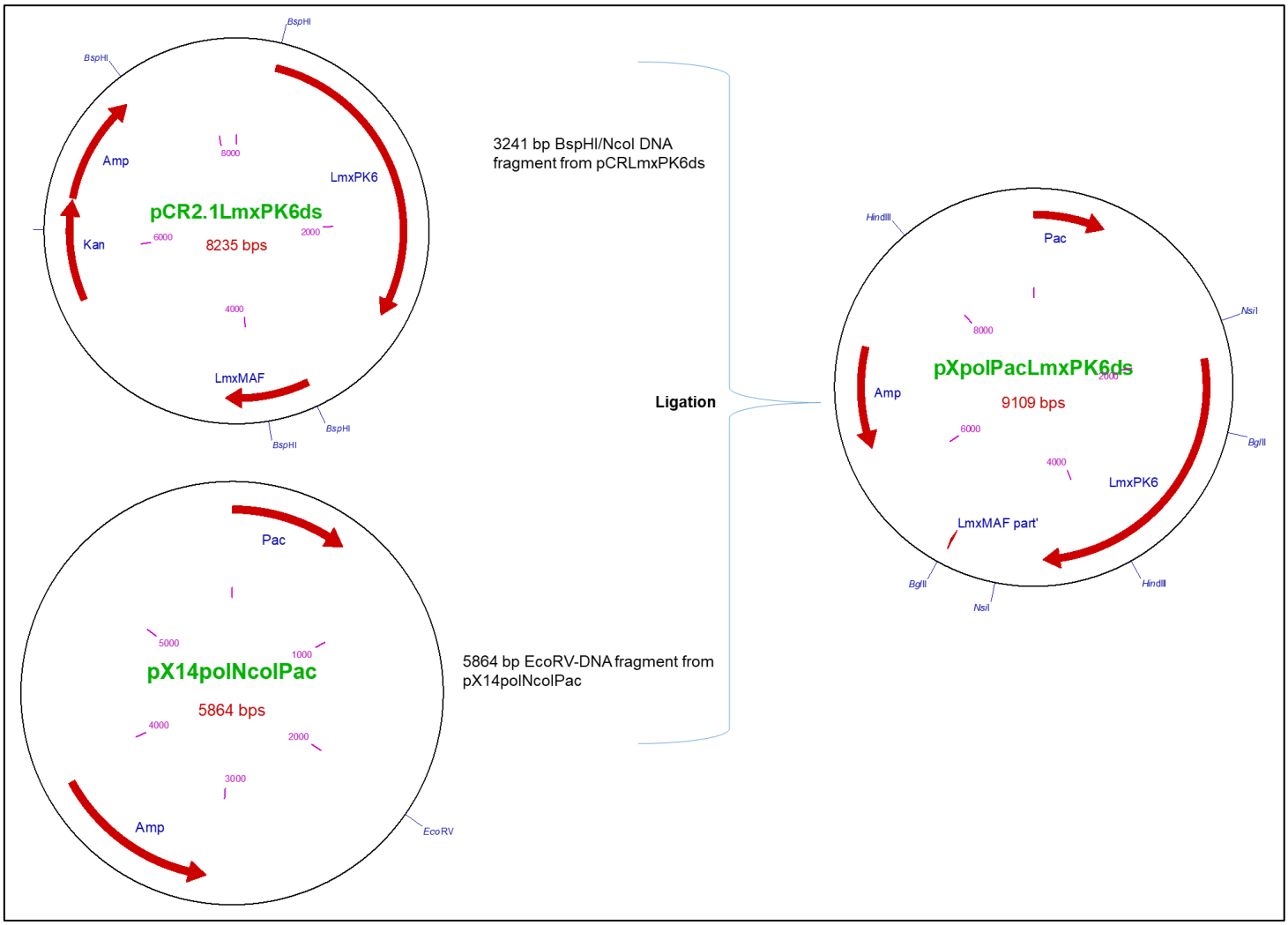

Figure 3.19. Cloning history for the generation of pXpolNcoIPacLmxPK6ds. The 3241 bp BspHI DNA fragments from pCRLmxPK6ds were ligated with 5864 bp DNA fragments of pX14polNcoIPac to generate pXpolNcoIPacLmxPK6ds, Amp selectable marker, Kan antibiotic resistance gene.

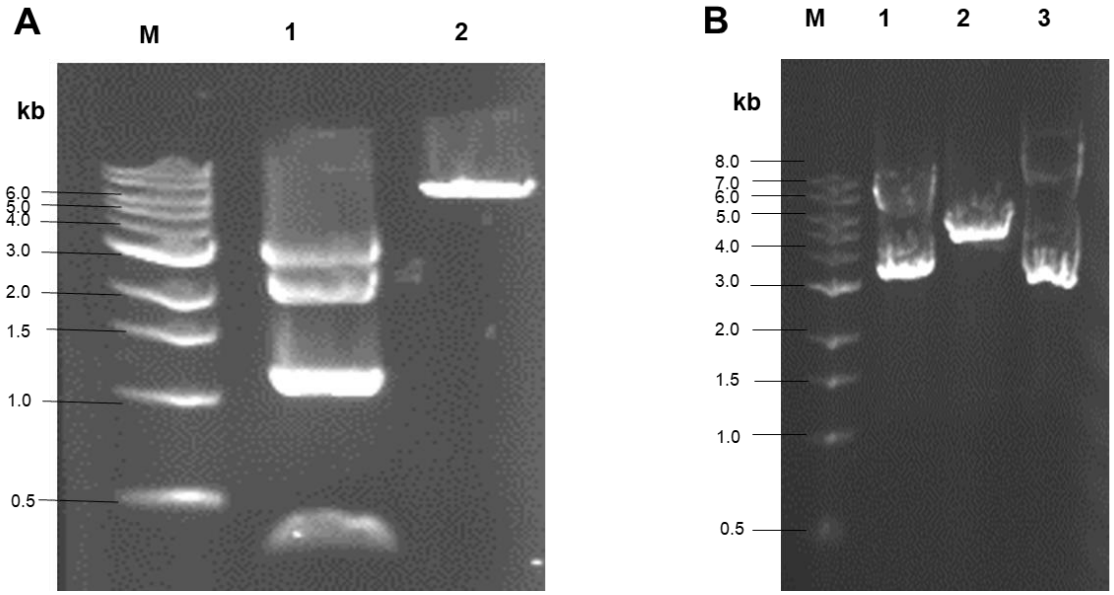

Figure 3.20. Generation of pXpolNcoIPacLmxPK6ds. A) Preparative cleavage of pCRLmxPK6ds and pX14polNcoIPac. Lane 1, pCRLmxPK6ds cleaved with BspHI and NcoI resulting in 3241 bp, 2284 bp, 1207 bp, 1155 bp, and 348 bp; lane 2, pX14polNcoIPac cleaved with EcoRV with expected size 5864 bp. **B)** Restriction analysis of pXpolNcoIPacLmxPK6ds. Lane 1, NsiI resulting in 3057 bp, 6052 bp; lane 2, HindIII resulting in 4274 bp and 4835 bp DNA fragments; lane 3, BglII resulting in 2678 bp, 6431 bp DNA fragments. M, DNA size marker.

3.2.4.2 Transfection of pXpolNcoIPacLmxPK6ds into *L. mexicana* wild type promastigotes

Figure 3.21 shows an overview of the deletion procedure to obtain a null mutant of *LmxPK6* using the alternative method for the knockout using plasmid pXpolNcoIPacLmxPK6ds. Transfection of pXpolNcoIPacLmxPK6ds into *L. mexicana* wild type promastigotes was followed by electroporations in an attempt to delete the genomic copies of LmxPK6.

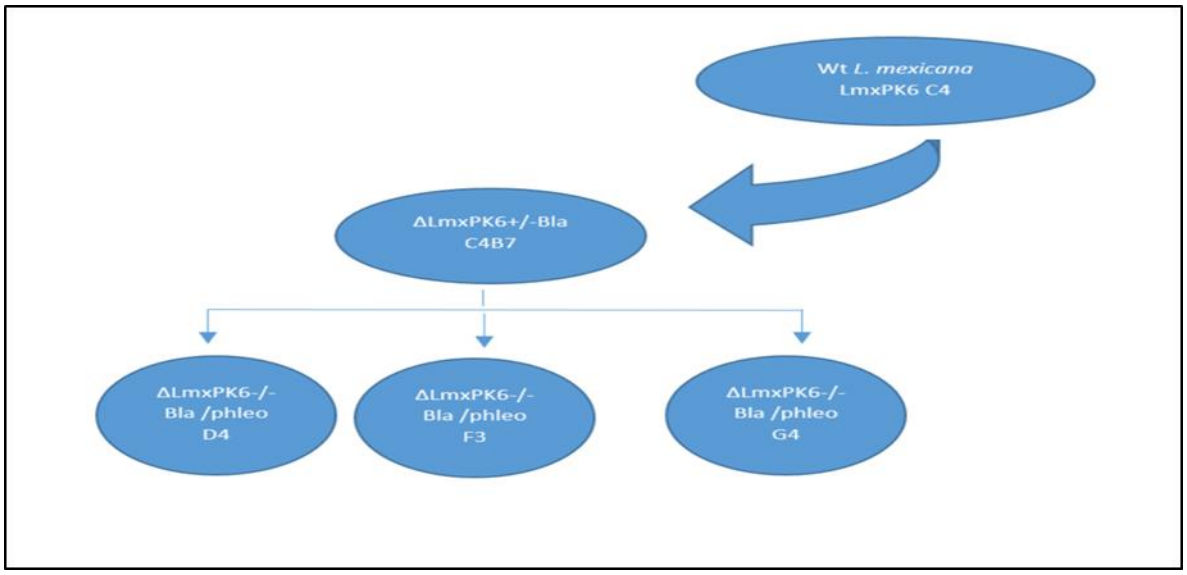

Figure 3.21. Overview of the deletion procedure of *LmxPK6*. The pXpolNcoIPacLmxPK6ds was transfected in *L. mexicana* promastigotes (C4); single allele deletion mutant carrying pXpolNcoIPacLmxPK6ds (LmxPK6+/-C4B7). Genomic null mutants of *LmxPK6* carrying pXpolNcoIPacLmxPK6ds (LmxPK6-/-Bla/Phleo D4, LmxPK6-/-Bla/Phleo F3 and LmxPK6-/-Bla/Phleo G4).

In order to obtain a double allele null mutant for *LmxPK6*, wild type *L. mexicana* promastigotes were used. In the first electroporation, the plasmid pXpolNcoIPacLmxPK6ds was transfected into *L. mexicana* wild type, and positive clones were selected using puromycin. The number of positive wells showing visible turbidity in the 96-well plate after incubation at 26 °C for 10−15 days was 55 wells for the 1:2 dilutions and 23 for the 1:40 dilution. Three clones were selected from the 1:40 dilution. Four cell lines were selected from the 1:40 dilution (LmxPK6 C4; LmxPK6 F5; LmxPK6 H10; and LmxPK6 E6) and were analysed further.

3.2.4.2.1. PCR analysis to prove the presence of pXpolNcoIPacLmxPK6ds in *L. mexicana* promastigotes

The presence of pXpolPacLmxPK6ds after transfection and selection using puromycin in *L. mexicana* wild type was tested by PCR using the oligos (pXPhleo2 and PK6.5rev); an amplicon of 772 bp indicates the presence of the plasmid. All four clones (LmxPK6 C4, LmxPK6 F5, LmxPK6 H10 and LmxPK6 E6) showed the expected band and therefore carried pXpolPacLmxPK6ds (Figure 3.22). LmxPK6 C4 was selected for further electroporation.

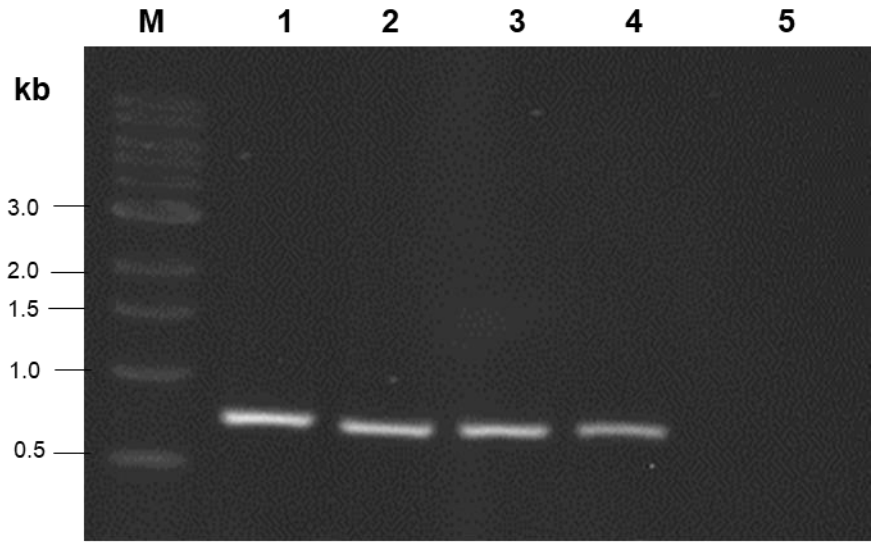

Lanes	Clones	Expected DNA fragment size
1	LmxPK6 C4	772 bp
2	LmxPK6 F5	772 bp
3	LmxPK6 H10	772 bp
4	LmxPK6 E6	772 bp
5	*L. mexicana* wild type	-

Figure 3.22. Confirmation of the presence of the plasmid pXpolPacLmxPK6ds in *L. mexicana* by PCR analysis. Lane 1, LmxPK6 C4; lane 2, LmxPK6 F5; lane 3, LmxPK6 H10; lane 4, LmxPK6 E6; and lane 5, *L. mexicana* wild type. The expected fragment size is 772 bp. M, DNA size marker.

3.2.4.3 Transfection of pXpolPacLmxPK6ds containing *L. mexicana* promastigotes to generate genomic single allele deletion mutants

The clone LmxPK6 C4 was chosen to generate a single genomic allele deletion mutant for *LmxPK6* using a 1490 bp fragment derived from pBNELmxPK6upBlads (Figure 3.15). Puromycin and blasticidin were used as selectable markers. On the 96-well plate with the 1:40 dilution, ten wells showed a growth of parasites, indicating putative positive clones. LmxPK6+/-Bla C4B7 was chosen for PCR analysis of the replacement of genomic LmxPK6 by blasticidin.

3.2.4.3.1 PCR analysis of LmxPK6+/- single allele deletion mutant

The single allele knockout of *LmxPK6* was tested for the presence of pXpolPacLmxPK6ds and the replacement of a genomic allele of LmxPK6 by PCR analysis. PCR reactions for the plasmid were set up under the same optimised conditions as before (section 3.2.3.3.1). ΔLmxPK6+/-Bla C4B7 led to the amplification of a 772 bp fragment confirming the presence of pXpolPacLmxPK6ds (Figure 3.23 A). To prove the single allele deletion, the presence of the blasticidin gene was tested by PCR analysis, using the optimised conditions shown in section 3.2.3.3.1 (Figure 3.23 B). This resulted in the amplification of the expected 850 bp DNA fragment.

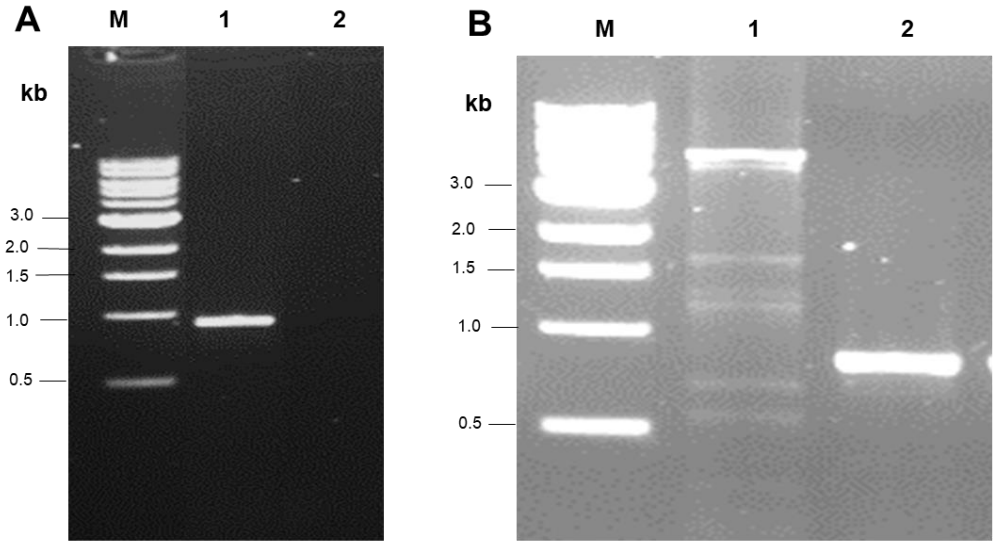

Lanes	Clones	Expected DNA fragment size
1	LmxPK6+/-Bla B7	772 bp
2	*L. mexicana* wild type	-

Lanes	Clones	Expected DNA fragment size
1	*L. mexicana* wild type	-
2	ΔLmxPK6+/-Bla B7	850 bp

Figure 3.23. Confirmation of single allele for LmxPK6+/-with alternative strategy. **A)** Confirmation of single allele LmxPK6Bla+/- C4B7 still carrying LmxPK6 on a plasmid by PCR analysis. Lane 1, ΔLmxPK6+/-Bla C4B7; lane 2, *L. mexicana* wild type. The expected size was 772 bp. **B)** Confirmation of the presence of the blasticidin gene in single allele LmxPK6+/-Bla C4B7 by PCR analysis. Lane 1, *L. mexicana* wild type; lane 2, ΔLmxPK6+/-Bla C4B7. The expected size was 850 bp. M, DNA size marker.

3.2.4.4 Transfection of the single allele deletion mutant LmxPK6+/-Bla C4B7 to obtain a genomic null mutant

In the third round of electroporation, a genomic double allele deletion mutant of LmxPK6 should be generated. The 1466 bp fragment from pBNELmxPK6upPhleods (Figure 3.15) was used for electroporation of LmxPK6+/-Bla C4B7, and putative positive clones were selected using phleomycin, blasticidin and puromycin in the culture media. Three clones, ΔLmxPK6-/-Bla/Phleo D4, ΔLmxPK6-/-Bla/Phleo F3 and

ΔLmxPK6-/-Bla/Phleo G4, were selected from the 1:40 dilution for scaling up. Subsequently, cells were transferred to 10 mL culture and analysed by PCR.

3.2.4.4.1 PCR analysis of putative genomic null mutants of LmxPK6

PCR analysis was used to confirm the double allele knockout of LmxPK6. PCR reactions were set up under the same optimised conditions as before (section 3.2.3.3.1). The putative double allele knockouts ΔLmxPK6-/-Bla/Phleo F3, ΔLmxPK6-/-Bla/Phleo D4 and ΔLmxPK6-/-Bla/Phleo G4 all carried pXpolPacLmxPK6ds, as shown by a PCR fragment of the expected size of 772 bp (Figure 3.24 A). ΔLmxPK6-/-Bla/Phleo D4, ΔLmxPK6-/-Bla/Phleo F3 and ΔLmxPK6-/-Bla/Phleo G4 were tested for the presence of the blasticidin gene instead of one allele of LmxPK6, using PCR and expecting a fragment of 850 bp. The reaction was set up under the same optimised conditions as in section 3.2.3.3.1 and resulted in the expected fragments (Figure 3.24 B). Finally, PCR reactions were set up under the same optimised conditions as before (section section 3.2.3.3.1) to confirm replacement of the second genomic allele of LmxPK6 by the phleomycin gene in the double allele knockout. The double allele knockout ΔLmxPK6-/-Bla/Phleo F3 showed the successful integration of the phleomycin gene with an amplicon of the expected size of 749 bp, while the other clones showed no replacement of LmxPK6 by the phleomycin gene (Figure 3.24 C). Finally, the absence of *LmxPK6* in the putative double allele deletion mutants ΔLmxPK6-/-Bla/Phleo was tested by PCR analysis, and PCR reactions were set up under the same optimised conditions as before (section 3.2.3.3.1). Surprisingly, all cell lines still kept one copy of *LmxPK6* in the genome, as shown by the amplification of a 623 bp fragment (Figure 3.24 D). Hence, the generation of a null mutant for LmxPK6 was still not successful. This strongly suggests that LmxPK6 is essential for *L. mexicana* promastigotes (Table 3.1).

A

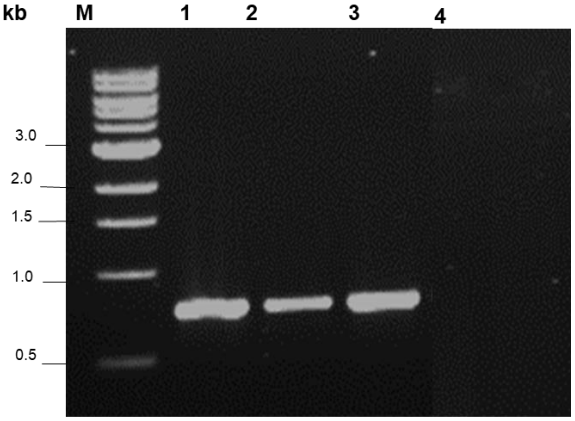

Lanes	Clones	Expected DNA fragment size
1	ΔLmxPK6-/-Bla/Phleo F3	772 bp
2	ΔLmxPK6-/-Bla/phleo D4	772 bp
3	ΔLmxPK6-/ -Bla/Phleo G4	772 bp
4	*L. mexicana* wild type	-

B

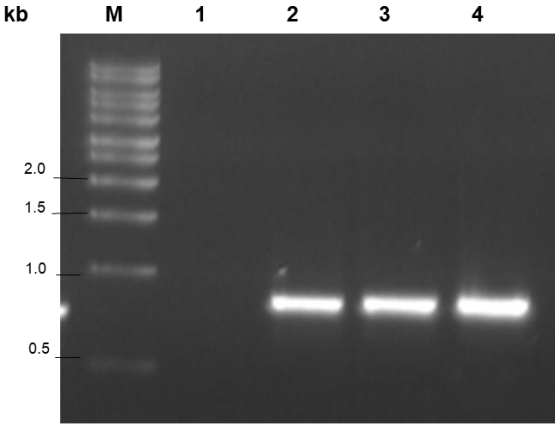

Lanes	Clones	Expected DNA fragment size
1	*L. mexicana* wild type	-
2	ΔlmxPK6-/-Bla/Phleo D4	850 bp
3	ΔLmxPK6-/-Bla/Phleo G4	850 bp
4	ΔLmxPK6-/-Bla/Phleo F3	850 bp

C

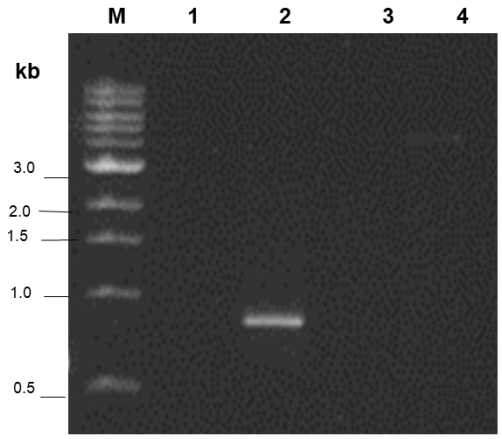

Lanes	Clones	Expected DNA fragment size
1	ΔLmxPK6-/-Bla/Phleo D4	-
2	ΔLmxPK6-/-Bla/Phleo F3	749 bp
3	ΔLmxPK6-/-Bla/Phleo G4	-
4	*L. mexicana* wild type	-

D

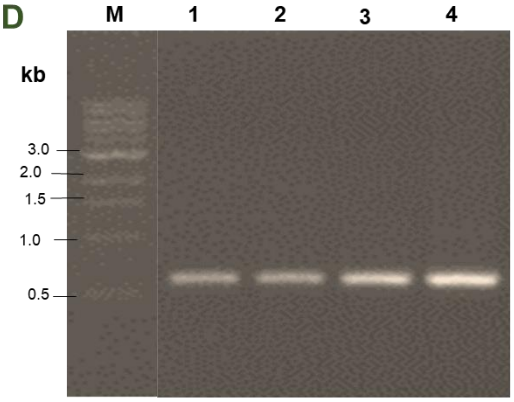

Lanes	Clones	Expected DNA fragment size
1	ΔLmxPK6-/-Bla/Phleo F3	623 bp
2	ΔlmxPK6-/-Bla/Phleo D4	623 bp
3	ΔLmxPK6-/-Bla/Phleo G4	623 bp
4	*L. mexicana* wild type	623bp

Figure 3.24. Confirmation of generation null mutant of LmxPK6 by alternative procedure to obtain a genomic null mutant for LmxPK6. A) Presence of pXpolPacLmxPK6ds in putative genomic null mutant for LmxPK6 using PCR analysis. Lane 1, ΔLmxPK6-/-Bla/Phleo F3; lane 2, ΔLmxPK6-/-Bla/Phleo D4; lane 3, ΔLmxPK6-/-Bla/Phleo G4; lane 4, *L. mexicana* wild type. The expected size was 772 bp. **B)** Confirmation of the presence of the blasticidin gene by PCR analysis**.** Lane 1, *L. mexicana* wild type; lane 2, ΔLmxPK6+/-Bla D4; lane 3, ΔLmxPK6+/-Bla G4; lane 4, ΔLmxPK6+/-Bla F3. The expected size was 850 bp. **C)** Confirmation of correct replacement of LmxPK6 by the phleomycin gene in the genomic double allele mutant of LmxPK6 using PCR analysis. Lane 1, ΔLmxPK6-/-Bla/Phleo D4; lane 2, ΔLmxPK6-/-Bla/Phleo F3; lane 3, ΔLmxPK6-/-Bla/Phleo G4; lane 4, *L. mexicana* wild type**.** The expected size was 749 bp. **D)** PCR analysis for the absence of LmxPK6 gene in null mutant generation ΔLmxK6-/-Bla/Phleo. Lane 1, ΔLmxPK6-/-Bla/Phleo F3; lane 2, ΔLmxPK6-/-Bla/Phleo D4; lane 3, ΔLmxPK6-/-Bla/Phleo G4; lane 4, *L. mexicana* wild type with expected size of 623 bp. M, DNA size marker.

Name of clone ΔLmxPK6-/-Bla/phleo	Detected LmxPK6 gene	Detected Plasmid pXpolPacLmxPK6ds	Detected Blasticidin gene	Detected Phleomycin gene
D4	Positive	Positive	Positive	Negative
F3	Positive	Positive	Positive	Positive
G4	Positive	Positive	Positive	Negative

Table 3.1. 1.Summary of the results of the PCR analyses for the alternative procedure to obtain a genomic null mutant of LmxPK6.ΔLmxPK6-/-Bla/Phleo D4; ΔLmxPK6-/-Bla/Phleo F3; ΔLmxPK6-/-Bla/Phleo G4. All clones still carry a copy of the LmxPK6 gene.

3.3 Discussion

LmxPK6 (LmxM.31.1020) is a putative kinase and an MKK homologue in *L. mexicana.* LmxPK6 homologues can also be found in other *Leishmania* species and trypanosomes, as was found by aligning the kinase domains. *LmxPK6* mRNA has been found to be expressed in all life cycle stages (Fiebig et al., 2015). However, this analysis provides no information about whether the protein is actually present throughout the life cycle. LmxPK4 and LmxMKK proteins were both found to be absent in lesion-derived amastigotes, but their mRNAs were found to be present in all stages (Erdmann et al., 2006; Fiebig et al., 2015; Kuhn and Wiese, 2005).

LmxPK6 contains the classical kinase domain, with an N-terminal phosphate anchor, which contains the sequence G-K-G-T-Q-G, matching the consensus sequence (G-X-G-X-X-G) and an invariant lysine residue at position 403. LmxPK6 has eight putative D-sites, composed of one or two basic amino acids sometimes preceded by another hydrophobic amino acid and separated from a hydrophobic amino acid, any amino acid, hydrophobic amino acid motif by 2–6 variable residues (X-ØH-X2-(Arg/Lys)1-2-(X)2-6-ØA-X-ØB). MAP2K D-sites were demonstrated to be important for high-affinity MAPK binding (Bardwell and Thorner, 1996; Ho et al., 2006), and docking can be prevented by mutating residues or by blocking the binding site with D-

site peptides, which can substantially inhibit the ability of the MAP2Ks to phosphorylate and activate downstream MAPKs (Bardwell et al., 2001; Remenyi et al., 2005). Whether any of the potential D-sites of LmxPK6 are functional has not been determined but should be determined once a substrate is known, most likely one of the 15 MAPK of *L. mexicana*. LmxPK6, does not contain potential regulatory phosphorylation sites with the consensus sequence S/TXXXXXS/T for plants or S/TXXXS/T for animals. However, there are two putative phosphorylation sites in the activation loop between the DFG and APE motifs: serine 601 (S601) and threonine 618 (T618). Phosphoproteomic analysis of promastigotes, axenic amastigotes and lesion-derived amastigotes has not identified any phosphorylated peptides of LmxPK6 (Rosenqvist, 2011), but that does not mean they are absent. Phosphoproteomics will always only detect a subset of phosphorylated peptides, depending on factors such as size, charge and amount. However, other protein kinases of *L. mexicana* showed phosphorylation on threonine residues preceding the APE motif by 5 and 9 residues, suggesting that LmxPK6 could be regulated by phosphorylation on T618, which is at position -5 relative to the APE motif. The catalytic kinase domain of LmxPK6 shares an identity with human MKKs at the amino acid level. SLK (AAI11566) functions as a regulator of the cell cycle, cell spreading and cell adhesion and is the closest *Homo sapiens* homologue of LmxPK6 (65/189; 34% amino acid identities); 92/189 (48%) amino acid similarities in the kinase domain). It was found to show autophosphorylation at residues T183 and S189 when the kinase domain (K19 to E321) was recombinantly expressed in *E. coli* (Pike et al., 2008). T183, S189 and T193 have also been found to be phosphorylated in phosphoproteomics studies (Luhovy et al., 2012). LmxPK6 also shares homology with the plant-like PKc-domain-containing MAP2Ks, which suggests that plants and kinetoplastids may share similar signalling pathways.

E. coli protein expression systems are most widely used because of low costs and a high level of expression. However, recombinant GST-LmxPK6 could not be purified (Figure3.9). This might have several reasons. First, LmxPK6 is considered a large protein with a molecular mass of 89 kDa, which could be difficult to express in *E. coli.* The presence of GST at the N-terminus should have promoted the expression of the protein. Due to time constraints it was not checked whether there was any formation of inclusion bodies, which would have resulted from aggregation of surface-exposed hydrophobic patches. This will need to be tested in the future. If inclusion bodies had formed the protein still could have been isolated using urea to make it soluble. Alternatively, a truncated version lacking the long N-terminus could have been expressed (Henriquez et al., 2010). Preventing the formation of inclusion bodies could also be performed by controlling the growth conditions, such as the pH of the culture. Exchanging the promoter or the host strain could help as well. Moreover, the addition of non-metabolisable sugars to the medium or by the induction at a different temperature could improve the yield (Baneyx, 1999).

Another reason for the difficulty of purifying a recombinant protein such as LmxPK6 was that it was tagged to GST as protein fusion tag. The GST could be a disadvantage as a poor solubility enhancer (Bird, 2011; Hammarstrom et al., 2006), which leads to a low expression of the recombinant protein. Another possibility is that LmxPK6 expression could also be toxic in *E. coli,* resulting in cell death, as described for the oxoglutarate-malate transport protein (OGCP) (Miroux and Walker, 1996). This suggests that the problem of expressing eukaryotic proteins in *E. coli* could lead to a combination of fast synthesis and slow folding, which favours aggregation (Widmann and Christen, 2000). The protein could also have suffered from partial proteolytic degradation. Hence, future recombinant LmxPK6 may require a different expression system, such as yeast.

Knockout approaches could provide information about genes encoding signalling proteins in parasites. A single allele deletion mutant containing one LmxPK6 wild type allele was generated and a replacement of the second allele with a cassette conferring phleomycin (*Phleo*) or blasticidin (*Bla*) resistance was achieved successfully and was confirmed by PCR (Section 3.2.3). However, a null mutant of LmxPK6 could not be produced by simple replacement of the second allele (Section 3.2.3). This might be because LmxPK6 is required in *L. mexicana* promastigotes. Therefore, an alternative method was attempted (Section 3.2.4), utilising the plasmid pXpolNcoIPacLmxPK6ds, which carries a copy of wild type *LmxPK6* (Section 3.2.4.1). The presence of this plasmid in *Leishmania* should allow deletion of the genomic copies of the gene if it were essential. The plasmid used is based on a pX plasmid, which contains the flanking DNA regions of dihydrofolate reductase-thymidylate synthase (DHFR-TS) from *Leishmania* (Beverley, 1991). The function of DHFR-TS in *L. major* has been studied, and it was found by generating the null mutant for DHFR-TS in the presence of thymidine nutritional supplementation that it confers thymidine auxotrophy. As a result, removing thymidine supplementation led to a delay in cell growth. It was demonstrated that DHFR-TS was important for parasite survival (Beverley, 1991; Gueiros-Filho et al., 1996). An episome expressing DHFR-TS restored wild type growth level and showed that the loss of this gene could be complemented genetically and chemically (Cruz and Beverley, 1991). However, even in the presence of pXpolNcoIPacLmxPK6ds, which carries the LmxPK6 wild type gene, double knockout promastigotes could not be generated. Instead, one clone was generated containing the plasmid, a replacement of one LmxPK6 allele with *Bla* and a replacement of the second allele with *Phleo*, but still carried a wild type copy of LmxPK6. LmxPK6 is located on chromosome 31, which is a diploid chromosome; while, in other *Leishmania* species chromosome 31 shows aneuploidy, such as *L. major*, *L.infantum*

and *L. donovani* (Dumetz et al., 2017; Rogers et al., 2011).Therefore, it was suggested that the number of chromosome copies can change as a result of genetic manipulation of essential genes or after genetic exchange and following drug selection (Akopyants et al., 2009; Cruz et al., 1993; Hassan et al., 2001; Martinez-Calvillo et al., 2005). This indicates that either the full chromosome 31 carrying *LmxPK6* or a part of it has been duplicated. Additionally, two other clones were positive for the plasmid, *Bla* and *LmxPK6* as detected in PCRs, but they did not show a positive PCR for *Phleo*. However, they were still resistant to the antibiotic, most likely meaning that the Phleo gene cassette was integrated somewhere else in the genome. This was not further analysed. Overall, these results suggest that LmxPK6 is essential for the promastigote stage of *L. mexicana*. Other proteins like CRK3 protein kinase and DHFR-TS were found to be essential in *Leishmania,* leading to a change of chromosome copy number (ploidy) when the generation of a null mutant was attempted (Cruz et al., 1993; Hassan et al., 2001).

Chapter 4: Function and localisation of LmxPK3

Abstract

The MAPK pathway is a three-tiered signalling pathway in *Leishmania.* LmxPK3 shows homology to MAP2Ks and as such is most likely one component of a MAPK pathway MAP2K. This chapter characterises LmxPK3 using a recombinantly produced enzyme to assess its phosphotransferase activity. The generation of a null mutant of LmxPK3 allowed to test whether the kinase influences the promastigote morphology or has an effect on the infectivity in BALB/c mice. The latter could indicate whether this kinase is a suitable drug target. Fusion of LmxPK3 to GFP allowed to analyse the localisation of the kinase in *Leishmania* promastigotes. Recombinant forms of LmxPK3 expressed as Glutathione-S-transferase fusion proteins were purified from *E. coli* and were shown to phosphorylate MBP, even though only small amounts of protein were generated. Generation of an LmxPK3 double allele knockout was successful under control of the LmxMPK12 flanking regions, resulting in the ΔLmxPK3-/-H/N D8 cell line. Phenotypic analysis of the null mutant of LmxPK3 in *Leishmania* promastigotes demonstrated obvious differences in body shape and flagellum length between the knockout mutants and wild type *L. mexicana.* Mouse infection with the LmxPK3 null mutant led to lesion development, and amastigotes isolated from the lesions differentiated and grew as promastigotes in culture. Hence, LmxPK3 is neither required in *Leishmania* promastigotes in culture nor amastigotes in the infected mouse and is not involved in the differentiation from one life stage into the other. Therefore, LmxPK3 is not a drug target against leishmaniasis. Moreover, fluorescence microscopy analyses using GFP fused to LmxPK3 at either the C-terminus or the N-terminus showed that LmxPK3 was localised in the cytosol and the flagellum of recombinant promastigotes.

4.1 Introduction

This chapter investigates the putative MAP2K known as LmxPK3 from *L. mexicana.* It was analysed by recombinant protein expression and purification from *E. coli,* followed by analysis of the phosphotransferase activity. The generation of a knockout for LmxPK3 in *L. mexicana* was attempted, followed by phenotypic analysis and localisation of N- or C-terminally GFP-tagged LmxPK3 in *L. mexicana* using fluorescence analysis.

4.2 Results

4.2.2. The phosphotransferase activity of LmxPK3 *in vitro*

4.2.2.1 Molecular characterisation of LmxPK3

LmxPK3 was cloned from a genomic DNA library of *L. mexicana* MNYC/BZ/M379, clone 2 and sequenced. It is comprised of a 1413 bp open reading frame, which, when translated, results in a protein of 470 amino acids with a molecular weight of 52.6 kDa. The full-length amino sequence of LmxPK3 was deposited in GenBank with the accession number AJ293291. This sequence was used in a BLAST identity search in TriTrypDB (kinetoplastids genomic resources web site), resulting in 100% identity with a putative kinase located on chromosome 17 in *L. mexicana* MHOM/GT/2001/U1103 (LmxM.17.0060), which is a diploid chromosome (Rogers et al., 2011). Using BLAST on the NCBI database identified the kinase as showing homology to the catalytic domain of CAMK family serine/threonine kinases. The kinase domain is located between amino acids 28 and 285 with a length of 257 residues. Typical features of the protein kinase domain are the phosphate anchor ribbon (G36–G41) and lysine 59

of subdomain II (K59), which are involved in ATP-binding and the phosphotransfer reaction.

MKKs possess serine and/or threonine residues as part of their activation loop between subdomains VII and VIII. LmxPK3 and its homologues in other kinetoplastids contain putative regulatory phosphorylation sites similar to the consensus sequence S/TXXXXXS/T (**S**VFAGNKQCL**TT**CCG**T**). There are also two more threonine residues in the activation loop, which could serve as phosphorylation sites. The conserved DFG and APE motifs were found in LmxPK3 (Figure 4.1). LmxPK3 has four putative D-sites, RNSKSGGSSDT**V**D**V**, L**K**VV, RHPSLQS**I**D**L** and RSI**V**R**L**.

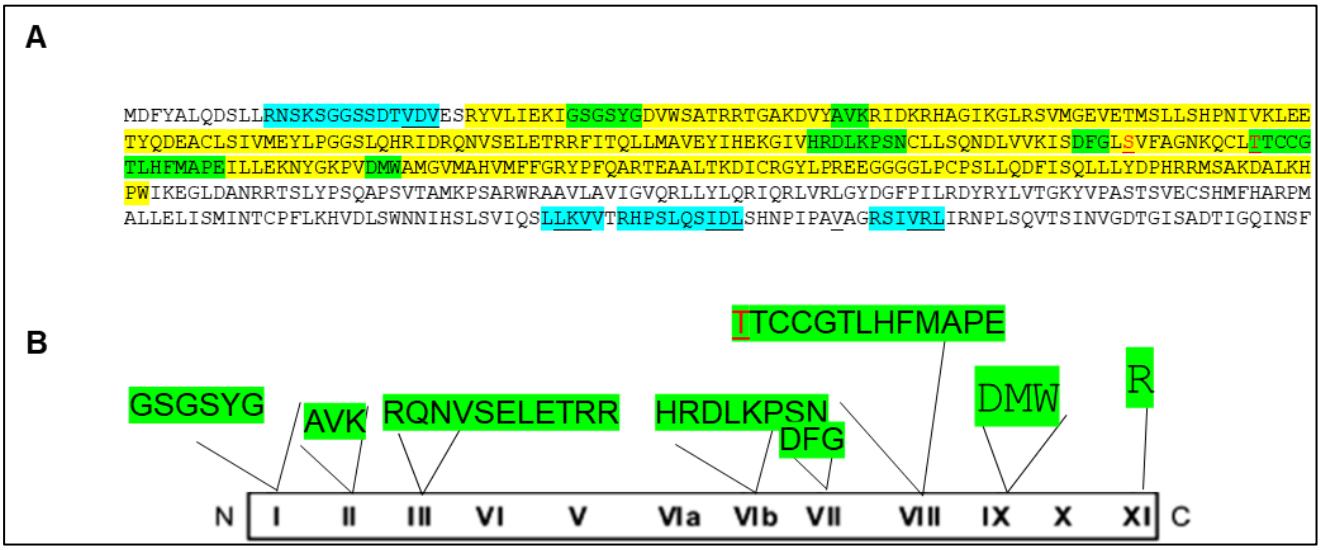

Figure 4 .1. Amino acid sequence of LmxPK3 (AJ293291). A) Yellow, kinase domain; green, conserved motifs; and blue, D-sites. **B)** Schematic of conserved motifs of LmxPK6.

An alignment of the catalytic domain of LmxPK3 with its homologues in *L. major*, *T. brucei, T. cruzi, A. thaliana*, *Homo sapiens* and *Dictyostelium discoideum* using Clustal Omega 1.2.4 is shown in Figure 4.2. The sequence identities range from 95% to 50% and 48% for the *L. major, T. brucei* and *T. cruzi* kinase domains, respectively; the other species show identities down to 27%.

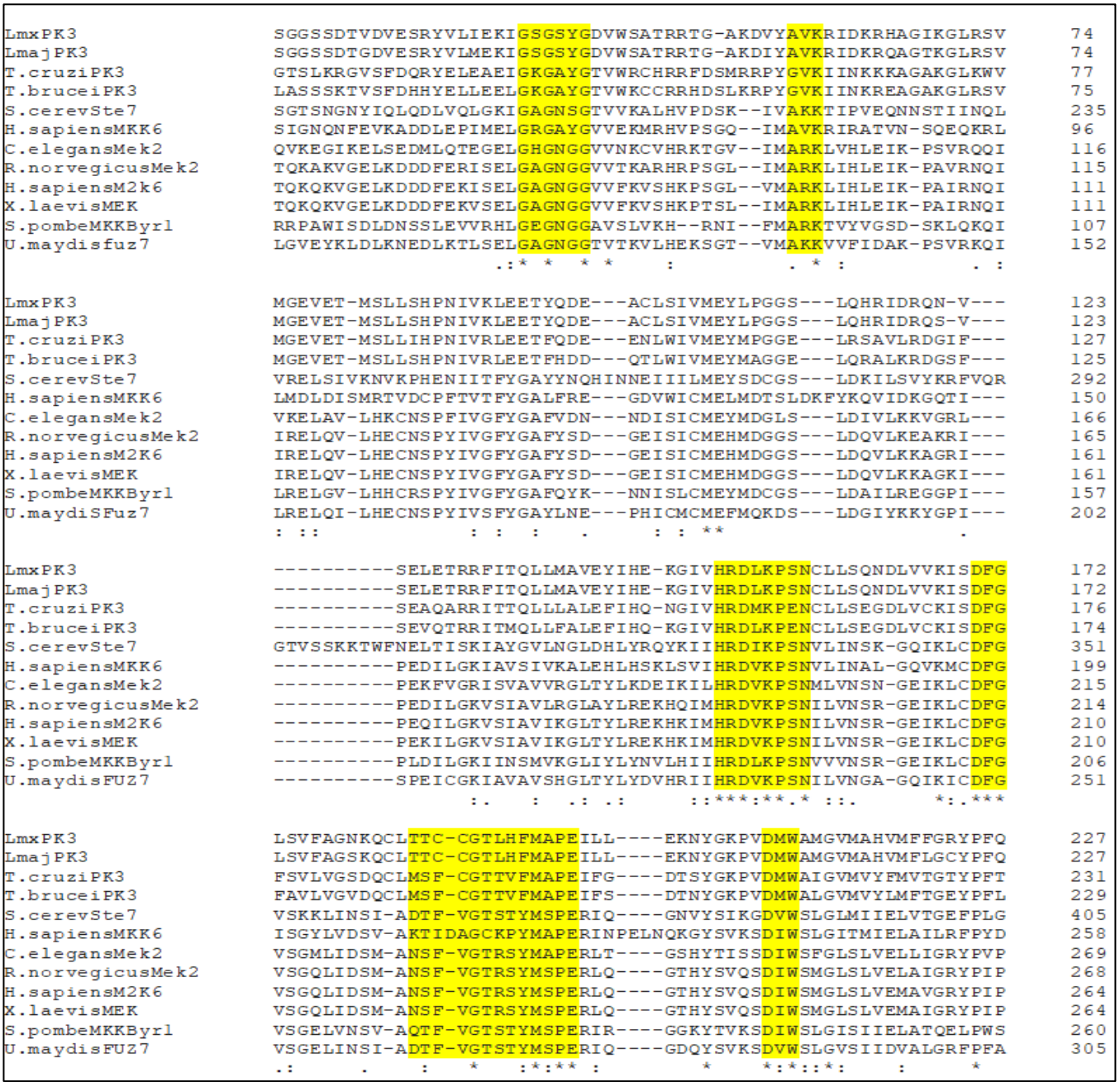

Figure 4.2. Amino acid sequence alignment of catalytic domain 28–285 aa of LmxPK3 from *L. mexicana* with homologues from various organisms. Sequences were aligned using Clustal Omega (1.2.4). **Numbering** corresponds to the primary sequence of LmxPK3; numbers shown in parentheses indicate numbers of amino acids preceding and following the shown sequences. **Dashes** represent gaps introduced for optimal alignment; **asterisks** indicate positions which have a single fully conserved residue. **Colons** indicate conservation between groups of strongly similar properties - scoring > 0.5 in the Gonnet PAM 250 matrix. **Periods** indicate conservation between groups of weakly similar properties - scoring < 0.5 in the Gonnet PAM 250 matrix. LmxPK3, *L. mexicana* MKK homologue (Accession No. AJ293291); *L. major* MKK3 homologue (Accession No ; XM_001682204); *T. brucei* MKK3 homologue (Accession No; XM_011776809); *T. cruzi* MKK3 homologue (Accession No;

MKQG01000152); MAPK kinase STE7 [*Saccharomyces cerevisiae* S288C] (Accession No: NP_010122); MAP kinase kinase Byr1 [*Schizosaccharomyces pombe*] (Accession No: NP_ NP_593026); Dual-specificity MAPK kinase mek-2 [*Caenorhabditis elegans*] (Accession No: NP_491087.1); dual-specificity MAPK kinase 1 [*Bos taurus*] (Accession No: NP_001124224); dual-specificity MAPK kinase 1 [*Xenopus laevis*] (Accession No: NP_001080299); serine/threonine/tyrosine kinase [*Ustilago maydis*] (Accession No: AAA62242); MAPK kinase 6, partial [*Homo sapiens]* (Accession No: AAQ02601); dual-specificity mitogen-activated protein kinase kinase 2 [*Rattus norvegicus*] (Accession No: NP_579817).

4.2.2.2 Generation of pGEX-KGSPLmxPK3

To test the phosphorylation activity of LmxPK3 the gene was cloned into the bacterial expression plasmid pGEX-KGSP to generate pGEX-KGSPLmxPK3 (Figure 4.3). pJCBMPKTEVLmxPK3 containing the LmxPK3 gene (already available in the group) was cleaved with HindIII and EcoRI to generate the 1470 bp and 3002 bp DNA fragments (not shown), followed by the isolation of the 1470 bp HindIII/EcoRI DNA fragment (Figure 4.4 A). pGEX-KGSP was cleaved with HindIII and EcoRI to generate 32 bp and 4971 bp DNA fragments (not shown). The 4971 bp HindIII/EcoRI DNA fragment from pGEX-KGSP was isolated and dephosphorylated (Figure 4.4 B). The 1470 bp HindIII/EcoRI DNA fragment from pJCBMPKTEVLmxPK3 and the 4971 bp HindIII/EcoRI DNA fragment from pGEX-KGSP were ligated and transformed into *E. coli* DH5α to generate pGEX-KGSPLmxPK3. Restriction analysis was done to confirm the generation of pGEX-KGSPLmxPK3 by cleavage with HindIII and EcoRI (1470 bp, 4971 bp) and PstI (1416 bp, 5025 bp) (Figure 4.4 C). pGEX-KGSPLmxPK3 was sequenced, and a duplicated sequence was found compared to the DNA sequence of *LmxPK3* in the databases (TriTrypDB, GenBank). This sequence had been introduced accidentally and had to be replaced with a wild type sequence (Figure 4.5).

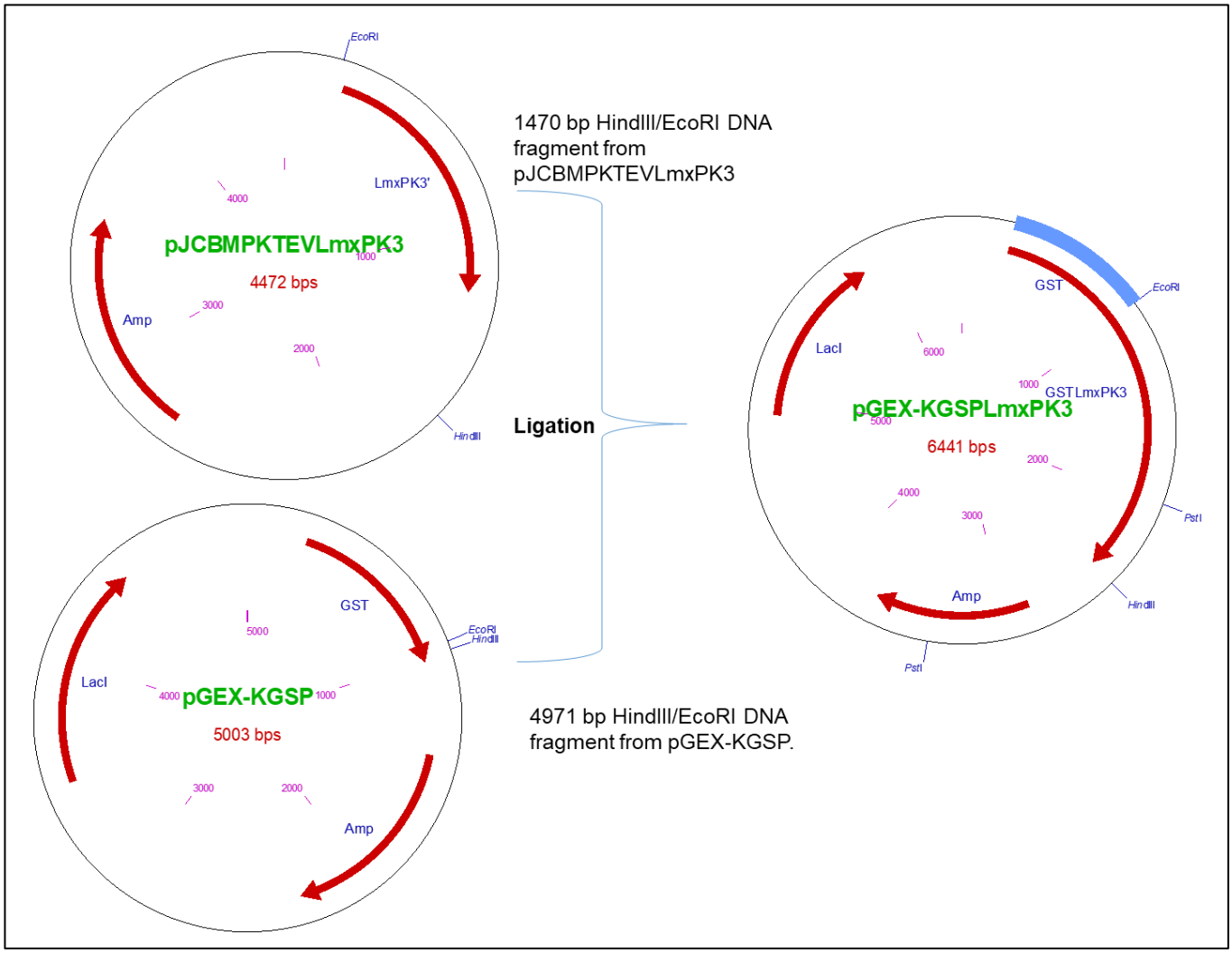

Figure 4.3. Cloning history for the generation of pGEX-KGSPLmxPK3. The 1470 bp HindIII/EcoRI DNA fragment from pJCBMPKTEVLmxPK3 was ligated with the 4971 bp HindIII/EcoRI DNA fragment from pGEX-KGSP to generate pGEX-KGSPLmxPK3. Amp, ampicillin selectable marker

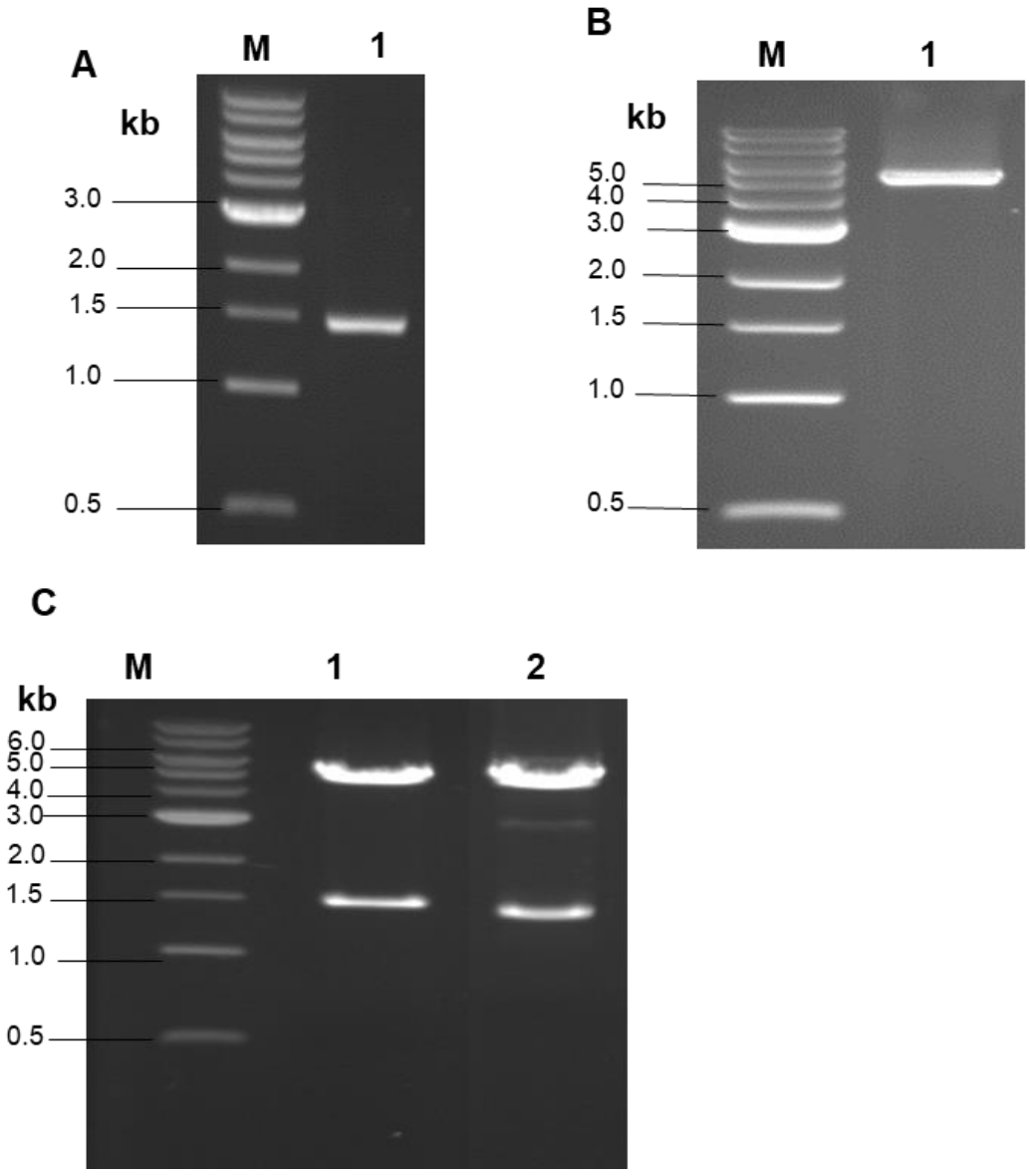

Figure 4.4. Generation of pGEX-KGSPLmxPK3. **A)** DNA fragment from pJCBMPKTEVLmxPK3. Lane 1, 1470 bp HindIII/EcoRI DNA fragment from pJCBMPKTEVLmxPK3. **B)** Linearised pGEX-KGSP. Lane 1, 4971 bp HindIII/EcoRI DNA fragment from pGEX-KGSP after SAP treatment. **C)** Restriction analysis. Lane 1, HindIII and EcoRI resulting in 1470 bp and 4971 bp DNA fragments; lane 2, PstI resulting in 1416 bp, 5025 bp DNA fragments. M, DNA size marker.

Figure 4 5. Alignment of partial DNA sequence of mutated *LmxPK3* (Sbjct) with the sequence of *LmxPK3* from TriTrypDB (Query). The yellow and green highlighted part is repetitive. The EcoRI site present in the database sequence has been disrupted by introduction of a silent mutation of the codon AGA to CGC, both coding for arginine.

LmxPK3 was corrected by cleaving pGEX-KGSPLmxPK3mut with MfeI and BglII, resulting in 5558 bp and 883 bp fragments (Figure 4.6 A). The 5558 bp DNA fragment from pGEX-KGSPLmxPK3 was isolated and dephosphorylated. pBX19lmkin24-30, containing the insert of a phage derived from a genomic DNA library carrying *LmxPK3* (originally called lmkin24-30), was cleaved with MfeI and BglII to generate 874 bp and 8078 bp DNA fragments (Figure 4.6 B). The 874 bp DNA fragments from pBX19lmkin24-30 DNA fragment was isolated. The 874 bp DNA fragments from pBX19lmkin24-30 were ligated with the 5558 bp fragments from pGEX-KGSPLmxPK3 and were transformed into *E. coli* DH5α to generate a corrected pGEX-KGSPLmxPK3, which was confirmed by DNA sequencing.

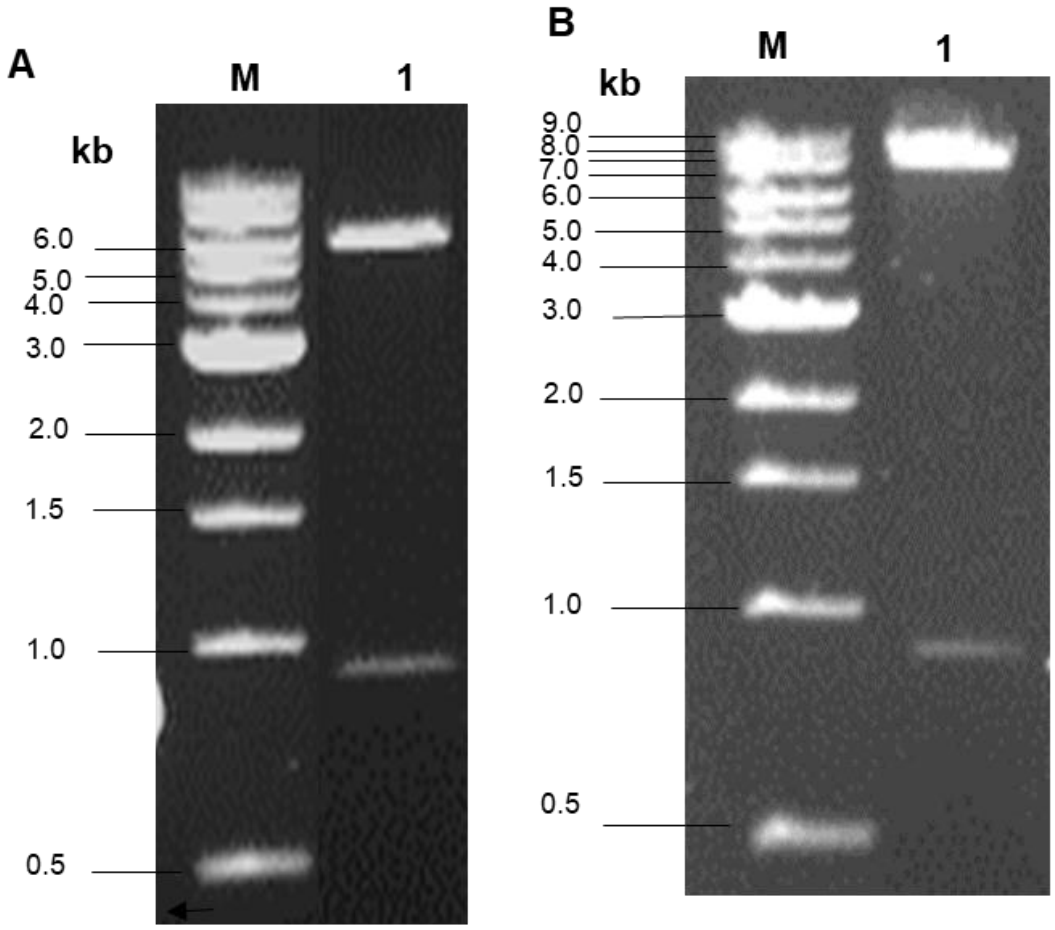

Figure 4.6. Generation of correct pGEX-KGSPLmxPK3. A) Preparative cleavage of pGEX-KGSPLmxPK3mut. Lane 1, pGEX-KGSPLmxPK3mut cleaved with MfeI and BglII resulting in 5558 bp and 883 bp DNA fragments. **B)** Preparative cleavage of pBX19lmkin24-30. Lane 1, pBX19lmkin24-30 cleaved with MfeI and BglII resulting in 874 bp and 8078 bp DNA fragments. M, DNA size marker.

4.2.3. Purification of recombinant LmxPK3

4.2.3.1 Protein purification of recombinant LmxPK3

As the mutated version of LmxPK3 with the duplication of an RLV sequence was available, it was decided to test whether there is any difference in activity between a mutated protein and the wild type protein expressed as GST-fusions in *E. coli*. The pGEX-KGSPLmxPK3mut and pGEX-KGSPLmxPK3 were used for protein

expression. Proteins were purified via their N-terminal GST-tags on glutathione sepharose. GST-tagged proteins were eluted using reduced glutathione and were analysed by 14% SDS-PAGE. Recombinant GST-LmxPK3 was expected at a size of 80 kDa made up of 52.6 kDa for LmxPK3, and 27.4 kDa for GST (Figure 4.7). A protein of this size was hardly visible on the gel. The main bands were for proteins of around 70 kDa, 32 kDa and 28 kDa. The presence of the GST band at around 28 kDa suggests that most of the protein was cleaved, resulting in the band for GST and the band around 70 kDa, which is still bigger than the expected size for LmxPK3. It is not unheard of that proteins do not move at their expected size in SDS-PAGE.

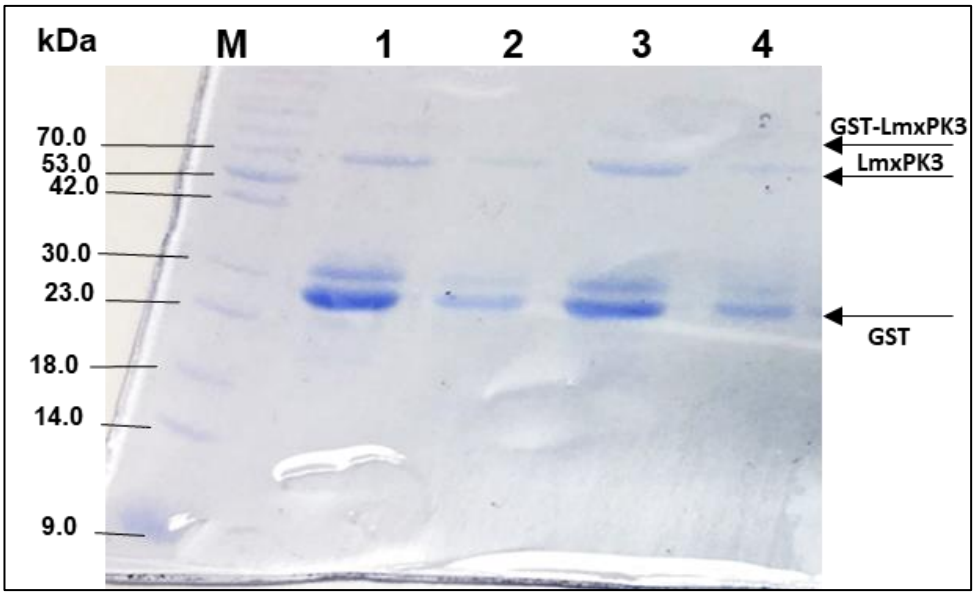

Figure 4.7. SDS-PAGE analysis of four eluted GST-tagged versions of LmxPK3 on Coomassie-stained 14% SDS-PAGE. Lane 1, elution 1 of mutated GST-LmxPK3; lane 2, elution 2 of mutated GST-LmxPK3; lane 3, elution 1 of GST-LmxPK3; lane 4, elution 2 of GST-LmxPK3. M, protein size marker.

4.2.3.2 Kinase assay of LmxPK3

To test whether the GST-LmxPK3 fusion proteins were catalytically active a kinase assay was performed using GSTLmxPK3 and GSTLmxPK3(mut). They were subjected to kinase assays with MBP as an artificial substrate in the presence of $Mg^{2+}$and Mn^{2+} at 34 °C incubation for 1 h. Each reaction was separated by 14% SDS-PAGE. The gel was stained with Coomassie Brilliant Blue, dried and analysed by phosphorimaging for the phosphorylation of MBP. Both versions of LmxPK3 (wild type and RLV duplication) showed phosphorylation of MBP. This indicates that LmxPK3 is a functional protein kinase and that the duplicated sequence had no effect on its catalytic activity (Figure 4.8 A and B).

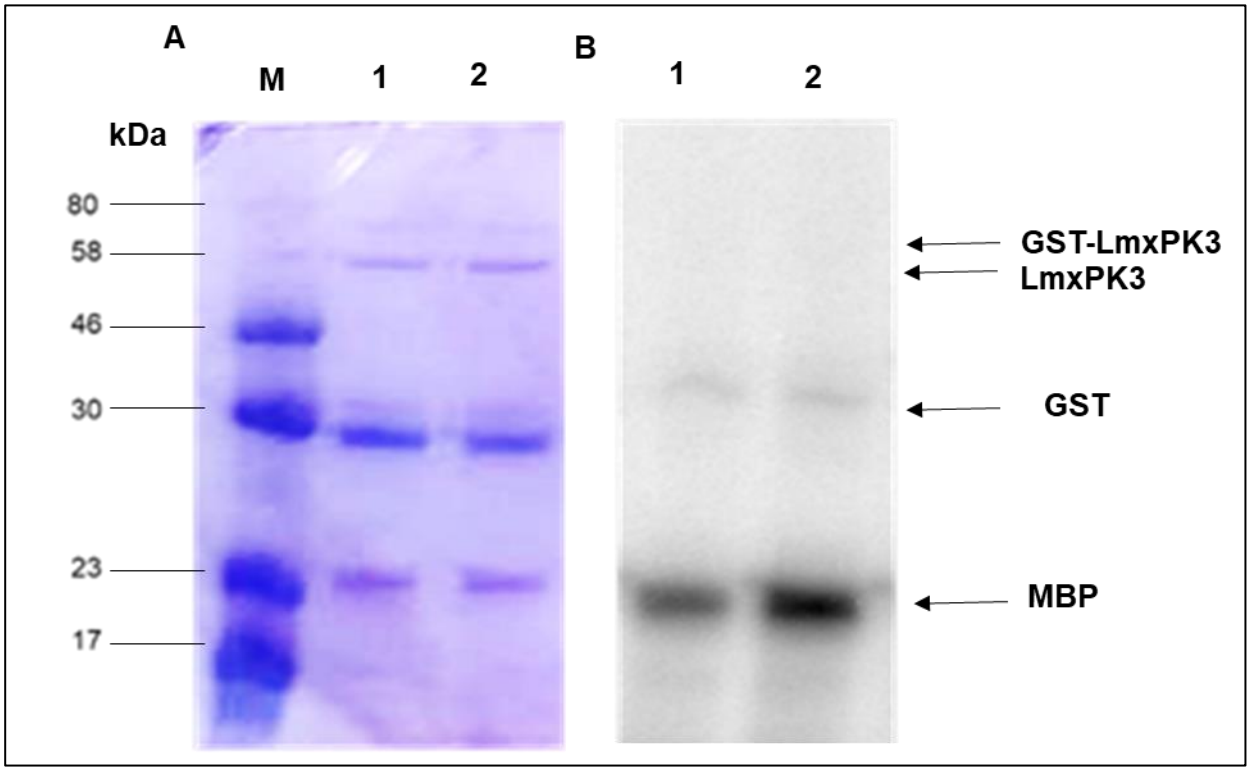

Figure 4.8. Kinase assay of different versions of LmxPK3 resolved on 14% SDS-PAGE. Lane 1, LmxPK3; lane 2, LmxPK3(mut) with repetitive sequences. **A)** Coomassie-stained gel; **B)** Phosphorimaging exposed for 72 h. Both kinases showed phosphorylation of MBP at the expected size of 18.5 kDa; however, LmxPK3 did not show autophosphorylation.

4.2.4 Knockout of *LmxPK3* in *L. mexicana*

A single allele deletion mutant for *LmxPK3* was already available in which one of the two alleles of the gene had been replaced by the gene encoding *hygromycin B phosphotransferase*. These cells were used to attempt to delete the second allele of *LmxPK3*, using genes coding for *neomycin phosphotransferase* and phleomycin binding protein, flanked by the upstream and downstream regions of LmxPK3. No recombinant parasites were obtained after using each construct three times. Hence, an alternative construct (pB1BALmxPK3updsDelMPK12neo), which was already available in the group but had never been tested in deletion analysis, was used (Schlabe, 2007). pB1BALmxPK3updsDelMPK12neo contains the LmxPK3 flanking regions, surrounding the upstream region of LmxMPK12 followed by the resistance marker neomycin phosphotransferase and the downstream region of *LmxMPK12*. The upstream and downstream regions of LmxMPK12 were chosen because this gene had been successfully deleted from *L. mexicana*. As a result, the expression of the resistance marker was now dependent on the LmxMPK12 regulatory regions and not those of LmxPK3 (Figure 4.9).

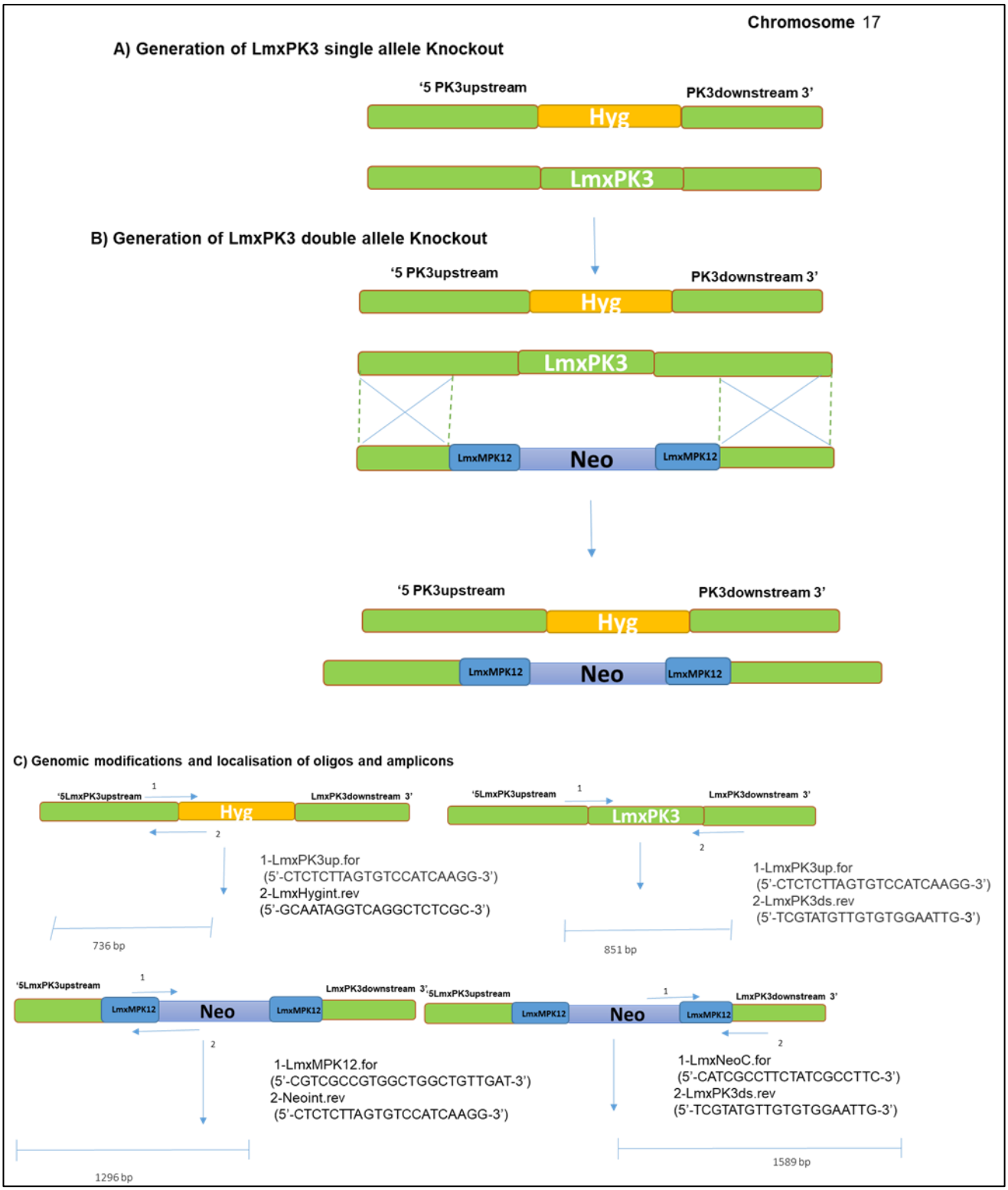

Figure 4.9. Knockout strategy for the generation of a null mutant for *LmxPK3*. A) Single allele knockout with *hygromycin B phosphotransferase gene* (*Hyg*). **B)** Generation of double allele deletion of LmxPK3 with neomycin phosphotransferase gene (Neo). **C)** PCR analysis of knockout strategy for LmxPK3.

4.2.4.1 Generation of null mutant for LmxPK3 in *L. mexicana*

To obtain a genomic null mutant for *LmxPK3*, the pB1BALmxPK3updsDelMPK12neo construct was used (Figure 4.10 A). First, pB1BALmxPK3updsDelMPK12neo was cleaved with KpnI, XbaI and ScaI, generating 1092 bp, 1795 bp and 3242 bp DNA fragments (Figure 4.10 B). The 3242 bp KpnI/XbaI DNA fragment from pB1BALmxPK3updsDelMPK12neo carried the following sequences in a given order; LmxPK3 upstream, LmxMPK12 upstream, resistance marker neomycin phosphotransferase, LmxMPK12 downstream and LmxPK3 downstream were isolated under sterile conditions (Figure 4.10 C). Fragment ws used for transfection into single allele deletion mutants of LmxPK3 promastigotes.

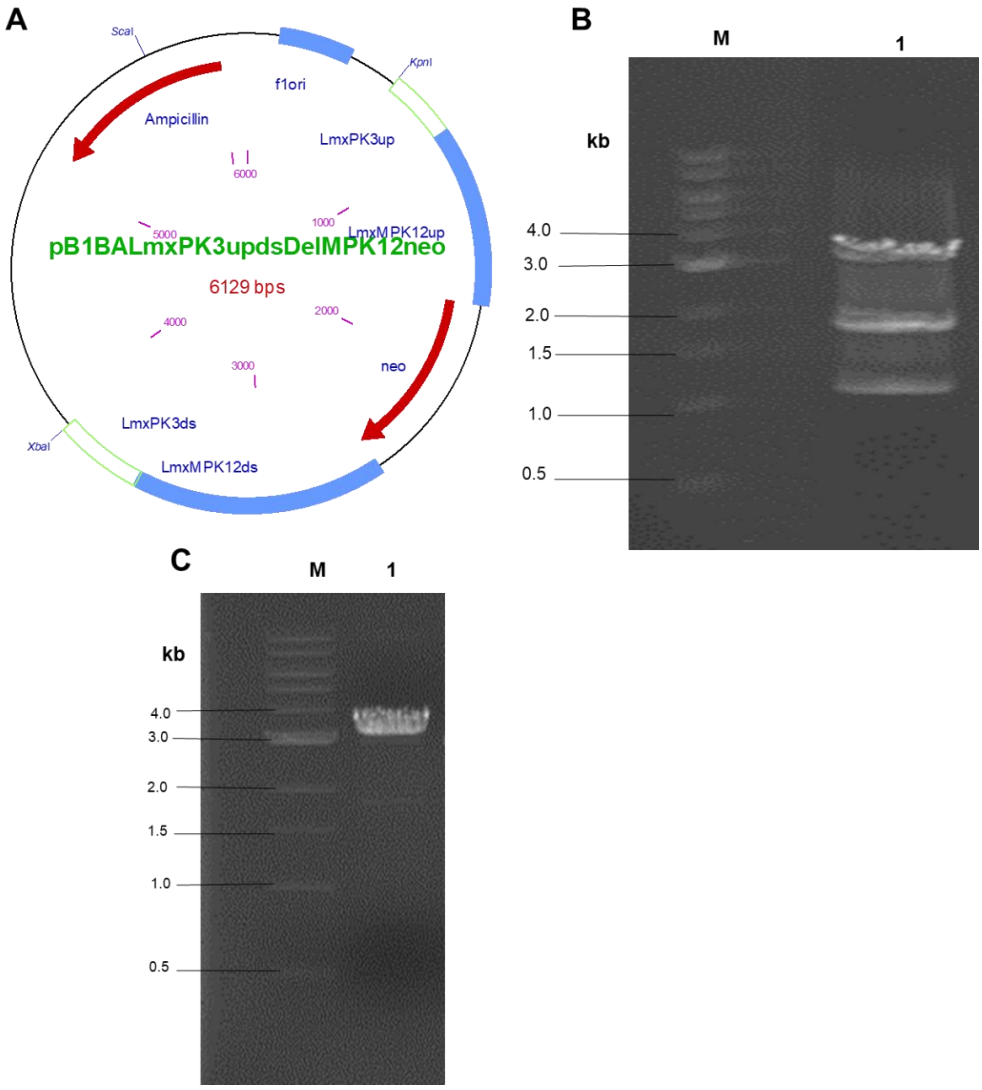

Figure 4.10. Generation of construct to obtain null mutant LmxPK3 in *L. mexicana*. A) MAP of pB1BALmxPK3updsDelMPK12neo, which contains LmxMPK12 flanking regions, flanking the resistance marker neomycin phosphotransferase, was cloned between the upstream and downstream regions of LmxPK3. **B)** Preparative cleavage of pB1BALmxPK3updsDelMPK12neo. Lane 1, pB1BALmxPK3updsDelMPK12neo was cleaved with KpnI, XbaI, and ScaI, resulting in 1092 bp, 1795 bp and 3242 bp DNA fragments. **C)** Isolated DNA fragment from pB1BALmxPK3updsDelMPK12neo. Lane 1, 3242 bp KpnI/XbaI DNA fragment of pB1BALmxPK3updsDelMPK12neo. M, DNA size marker.

4.2.4.2 Transfection of single allele deletion mutants of *LmxPK3* promastigotes to generate a null mutant in *L. mexicana*

The 3242 bp KpnI/XbaI pB1BALmxPK3updsDelMPK12neo fragment was used for transfection into two single allele deletion mutant clones of *LmxPK3* (ΔLmxPK3/K1+/-

H, ∆LmxPK3/K3+/-H) carrying the hygromycin B phosphotransferase resistance marker gene. Electroporation and selection using both antibiotics should lead to double allele deletion mutants, containing both resistance markers (*neomycin* and *hygromycin B*). Two attempts at electroporation were performed to transfect the *L. mexicana* cell lines. Promastigotes were incubated at 26°C for 10–15 days. 96 wells showed growth of parasites for the 1:2 dilutions of ∆LmxPK3/K1-/-H/N and ∆LmxPK3/K3-/-H/N. 55 and 77 wells were positive for the 1:40 dilution of ∆LmxPK3/K1-/-H/N and ∆LmxPK3/K3-/-H/N, respectively. One clone each was selected from the 1:40 dilution of both cell lines, ∆LmxPK3/K1-/-H/N D8 and ∆LmxPK3/K3-/-H/N F2. They were transferred to 12 well plates for scaling up. Subsequently, the putative positive clones were transferred into 10 mL culture. The null mutants were tested by PCR analysis.

4.2.4.2.1 PCR analysis of null mutant *LmxPK3* in *L. mexicana*

PCR analysis was done to confirm that both genomic alleles of *LmxPK3*, were replaced by a selective marker gene conferring *hygromycin B* and *neomycin* resistance. The absence of *LmxPK3* in the double allele deletion mutants ∆LmxPK3/K1-/-H/N D8 and ∆LmxPK3/K3-/-H/N F2 was also tested by PCR analysis. PCR analysis was performed with the oligos specific for *L. mexicana* LmxPK3, (LmxPK3int.rev and LmxPK3up.for). *L. mexicana* wild type and the single allele LmxPK3 mutants used as a control showed the presence of the LmxPK3 gene by a 851 bp band. This band was clearly absent in the putative null mutant clone ∆LmxPK3/K1-/-H/N D8, but present in ∆LmxPK3/K3-/-H/N F2 (Figure 4.11 A). PCR analysis with the oligos (LmxNeoC.for and LmxPK3ds.rev) were performed to prove the correct integration of the neo-construct expecting a band of 1589 bp and therefore the generation of an LmxPK3 null mutant. Again only ∆LmxPK3/K1-/-H/N D8 showed the expected band; no band was visible for ∆LmxPK3/K3-/-H/N F2 (Figure 4.11B).

The presence of the hygromycin B gene was proved by PCR analysis with the oligos (LmxHygint.rev and LmxPK3up.for) to amplify a 736 bp DNA fragment. All analysed clones showed the hygromycin DNA fragment (Figure 4.11 C). To further investigate why the PCR on ∆LmxPK3/K3-/-H/N F2 did not result in an amplification of a DNA fragment in the PCR with the oligos (LmxNeoC.for and LmxPK3ds.rev). A PCR analysis with the oligos (LmxMPK12.for and Neoint.rev) were done to test for integration of the construct into the *LmxMPK12* gene locus instead of the LmxPK3 gene locus. Indeed, this led to an amplicon of 1269 bp, indicating that the *LmxMPK12* gene locus was targeted rather than the *LmxPK3* one (Figure 4.12). To summarise, the clone ∆LmxPK3/K1-/-H/N D8 is a null mutant for *LmxPK3*.

A

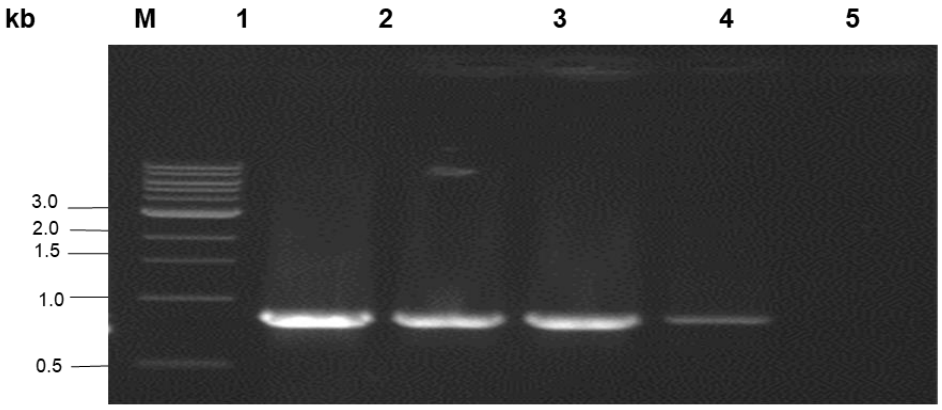

Lanes	Clones	Expected DNA fragment size
1	*L. mexicana* wild type	851 bp
2	ΔLmxPK3/K3+/-H	851 bp
3	ΔLmxPK3/K1+/-H	851 bp
4	ΔLmxPK3/K3-/-H/N F2	-
5	ΔLmxPK3/K1-/-H/N D8	-

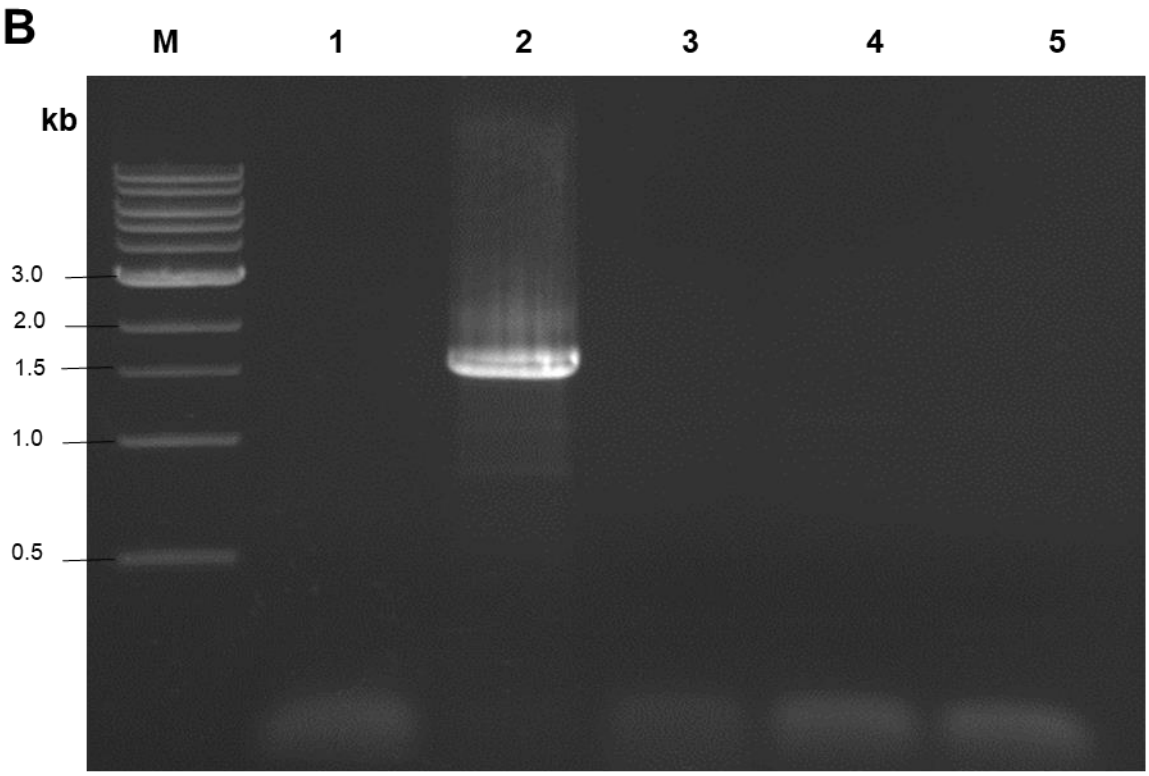

Lanes	Clones	Expected DNA fragment size
1	ΔLmxPK3/K3-/-H/N F2	-
2	ΔLmxPK3/K1-/-H/N D8	1589 bp
3	ΔLmxPK3/K1+/-H	-
4	ΔLmxPK3/K3+/-H	-
5	*L. mexicana* wild type	-

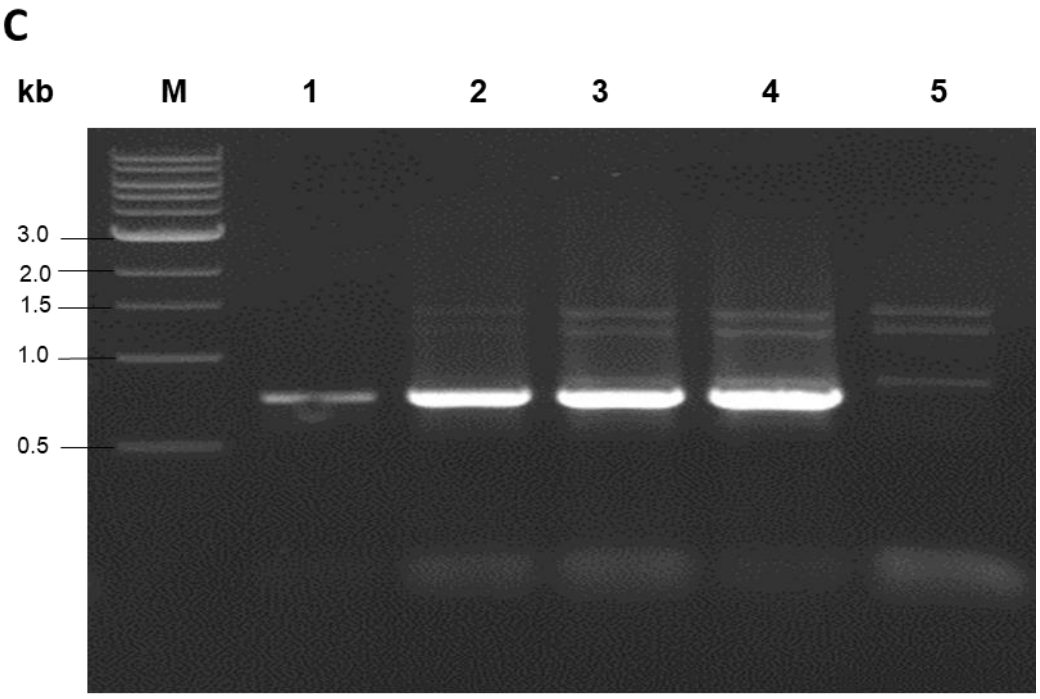

Lane	Clones	Expected DNA fragment size
1	ΔLmxPK3/K3-/-H/N F2	736 bp
2	ΔLmxPK3/K1-/-H/N D8	736 bp
3	ΔLmxPK3/K1+/-H	736 bp
4	ΔLmxPK3/K3+/-H	736 bp
5	*L. mexicana* wild type	-

Figure 4.11. Generation of *LmxPK3* null mutant. **A)** Confirmation of absence of *LmxPK3* in double allele deletion mutants by PCR. Lane 1, *L. mexicana* wild type; lane 2, ΔLmxPK3/K3+/-H; lane 3, ΔLmxPK3/K1+/-H; lane 4, ΔLmxPK3/K3-/-H/N F2; and lane 5. ΔLmxPK3/K1-/-H/N D8The expected size 851 bp. **B)** PCR analysis to detect the correct integration of the *neomycin* construct in the putative *LmPK3* null mutant by PCR analysis. Lane 1, ΔLmxPK3/K3-/-H/N F2; lane 2, ΔLmxPK3/K1-/-H/N D8; lane 3, ΔLmxPK3/K1+/-H; lane 4, Δ LmxPK3/K3+/-H; and lane 5, *L. mexicana* wild type. The expected size was 1589 bp. **C)** Confirmation of the presence of the *hygromycin B phosphotransferase* gene by PCR analysis. Lane 1, ΔLmxPK3/K3-/-H/N F2; lane 2, ΔLmxPK3/K1-/-H/N D8; lane 3, ΔLmxPK3/K1+/-H; lane 4, ΔLmxPK3/K3+/-H; lane 5, *L. mexicana* wild type. The expected size was 736 bp. M, DNA size marker.

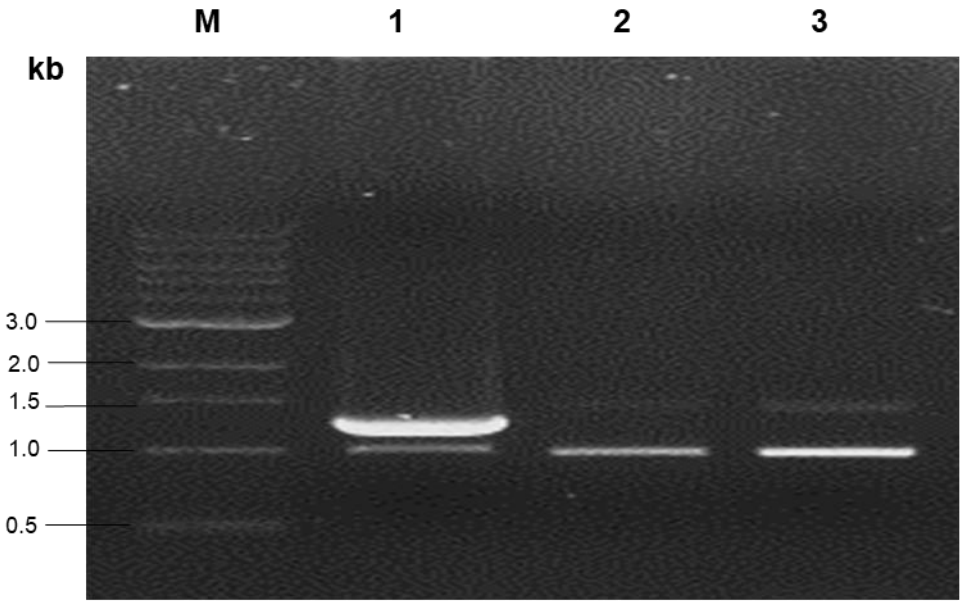

Lanes	Clones	Expected DNA fragment size
1	ΔLmxPK3/K3-/-H/N F2	1269 bp
2	ΔLmxPK3/K1-/-H/N D8	-
3	*L. mexicana* wild type	-

Figure 4.12. Confirmation of integration of the *neomycin phosphotransferase* construct into the *LmxMPK12* gene locus by PCR analysis. Lane 1, ΔLmxPK3/K3-/-H/N F2; lane 2, ΔLmxPK3/K1-/-H/N D8; lane 3, *L. mexicana* wild type. The expected size was 1296 bp. M, DNA size marker.

4.2.5 Importance of LmxPK3 in *L. mexicana*

Animal infection was carried out with late stationary growth phase promastigotes of *L. mexicana* wild type, the ΔLmxPK3/K1+/-H single allele mutant and the ΔLmxPK3/K1-/-H/N D8 null mutant. Additionally, phenotype analysis of LmxPK3 null mutant

promastigotes was performed to determine whether LmxPK3 is important for the survival of the amastigote stage of the parasite.

4.2.5.1. Animal infection using LmxPK3 null mutant promastigotes

A single animal experiment was performed to find out, whether LmxPK3 is essential for the infectivity of *L. mexicana*. *L. mexicana* wild type, ∆LmxPK3/K1+/-H and ∆LmxPK3/K1-/-H/N D8, 1×10^7 late log-phase promastigotes were used to inject five female BALB/c mice per cell line in the right footpad. Every week for up to twelve weeks, the diameter of both footpads was measured for each mouse. The measurements of the control left footpad was subtracted from those of the infected right footpad; the average change was calculated for the five mice per experiment and plotted in a graph. Pearson's two-tailed, non-paired student's T-test. was used for statistical analysis. Figure 4.13 shows that there was no significant difference in lesion development between the null mutant and the wild type (P value = 0.3133). Likewise, no significant difference was found between the single allele deletion mutant and the wild type (P value = 0.7306). After eight weeks, the mice infected with *L. mexicana* wild type and ∆LmxPK3/K1-/-H/N D8 had to be euthanised, because the lesion diameter reached the maximum allowed under the animal licence (licence number PPLPF669CAE8). However, onset of lesion development was delayed by four weeks in the mice infected with the single allele deletion mutant (∆LmxPK3/K1+/-H) (Figure 4.13; see appendice 9.2). It was decided to leave the mice infected with the single allele deletion mutant for another four weeks to monitor the progress of lesion development before the experiment was terminated. Figure 4.14 shows that the progress of lesion development (footpad swelling), shown by the slopes of the trendlines, of the single allele deletion mutant (∆LmxPK3/K1+/-H) is almost identical to that of *L. mexicana* wild type and that of the null mutant once the lesions started to show (week 2 for wild type and null mutant, week 6 for single allele deletion mutant).

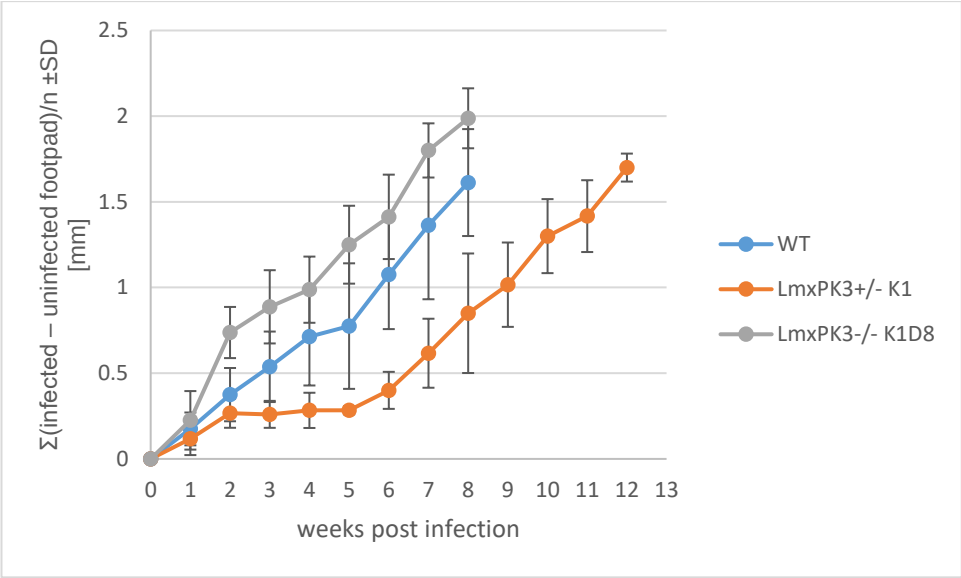

Figure 4.13. Footpad lesion development in female Balb/c mice caused by promastigotes of *L. mexicana* wild type, LmxPK3 single allele deletion mutant and null mutant. On week zero all mice were infected with 1 × 10^7 late log phase promastigotes of *L. mexicana* wild type (4 mice), LmxPK3 single allele deletion mutant (ΔLmxPK3/K1+/-H; 3 mice), and null mutant (ΔLmxPK3/K1-/-H/N D8; 4 mice) by subcutaneous injection into the footpad. Lesion development was determined by measuring the thickness of the infected footpad relative to the uninfected footpad over the course of infection. The experiment was terminated on weeks 8 post-infection for null mutant (ΔLmxPK3/K1-/-H/N D8) and *L. mexicana* wild type (P value = 0.3133) but ΔLmxPK3/K1+/-H was terminated on week 12 post-infection. ΔLmxPK3/K1+/-H was showed no significant difference compare to *L. mexicana* wild type and mutants (P value = 0.7306).

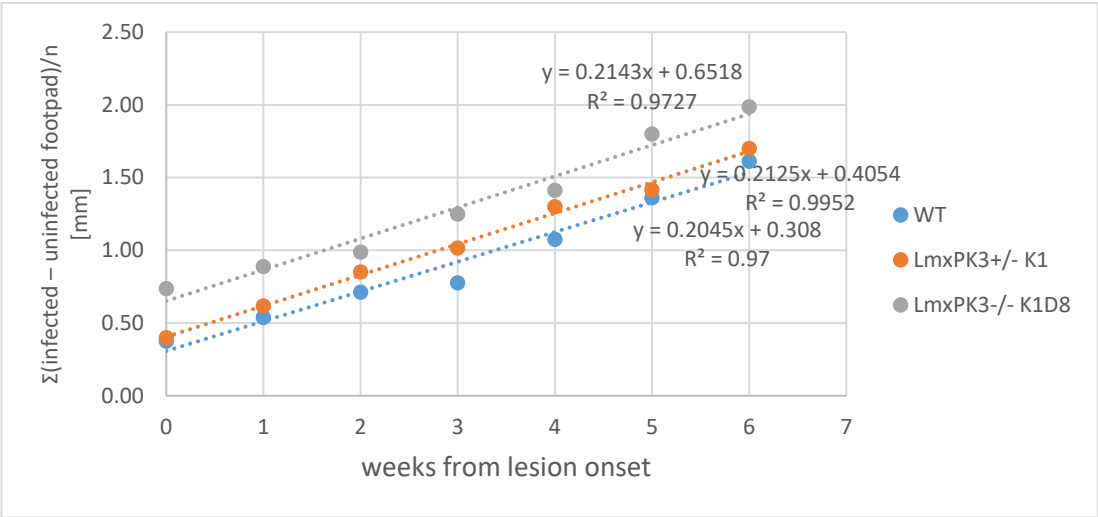

Figure 4.14. Onset of footpad lesions in infected female BALB/c mice. LmxPK3 single mutants (ΔLmxPK3/K1+/-H; 3 mice; week 6 to week 12 post-infection), null mutant (ΔLmxPK3/K1-/-H/N D8; 4 mice; week 2 to week 8 post-infection) and *L. mexicana* wild type (WT, 4 mice from week 2 to week 8 post-infection). Thickness of infected footpad was measured weekly.

4.2.5.2 Phenotypic analysis of *LmxPK3* null mutant promastigotes

4.2.5.2.1 Is LmxPK3 required for the differentiation of amastigotes to promastigotes?

Amastigotes were isolated from the lesions of the mice infected with *L. mexicana* wild type, *LmxPK3* single allele deletion mutant and null mutant and were incubated in SDM-79 medium. *L. mexicana* cells were successfully isolated from every footpad lesion. The identity of the *LmxPK3* single allele deletion mutant and the null mutant was confirmed by PCR using specific oligos to amplify LmxPK3, Hyg, or Neo. The expected amplicons of 851 bp for LmxPK3, 736 bp for Hyg and 1589 bp for Neo could be confirmed (Figure 4.15). This indicated that LmxPK3 is not required in the differentiation process.

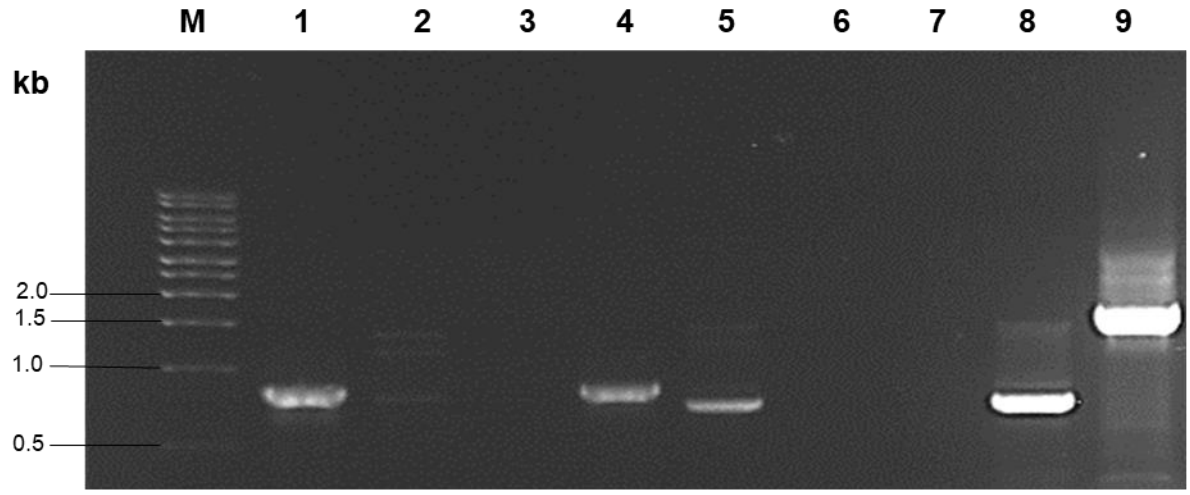

Lanes	Clones
1-3	*L. mexicana* wild type
4-6	ΔLmxPK3/K1+/- H
7-9	ΔLmxPK3/K1-/-H/N D8

Figure 4.15. PCR analysis to test identity of promastigotes derived from lesion amastigotes (12 weeks in the mouse). Lanes 1–3, *L. mexicana* wild type promastigotes; lanes 4–6, ΔLmxPK3/K1+/-H; lanes 7-9, ΔLmxPK3/K1-/-H/N D8. Lanes 1, 4, and 7, PCR with oligos to detect LmxPK3; lanes 2, 5, and 8, PCR with oligos to detect replacement of LmxPK3 by Hyg; lanes 3, 6, and 9, PCR with oligos to detect replacement of LmxPK3 with Neo. Samples were separated on a 0.8% agarose gel. The expected amplicons of 851 bp for LmxPK3, 736 bp for Hyg and 1589 bp for Neo. M, DNA size marker.

4.2.5.2.2 Does LmxPK3 deletion affect the morphology of promastigotes?

The effect of the absence of LmxPK3 on promastigote flagellum length, cell body length and cell body width was determined by taking measurements for 200 promastigotes of *L. mexicana* wild type, ΔLmxPK3/K1+/-H and ΔLmxPK3/K1-/-H/N D8 live cells (section 2.5.3) (Figure 4.16). The promastigotes were those that were derived from amastigotes after isolation from mice; all cultures were in logarithmic growth phase, with cell densities as displayed in Table 4.1.

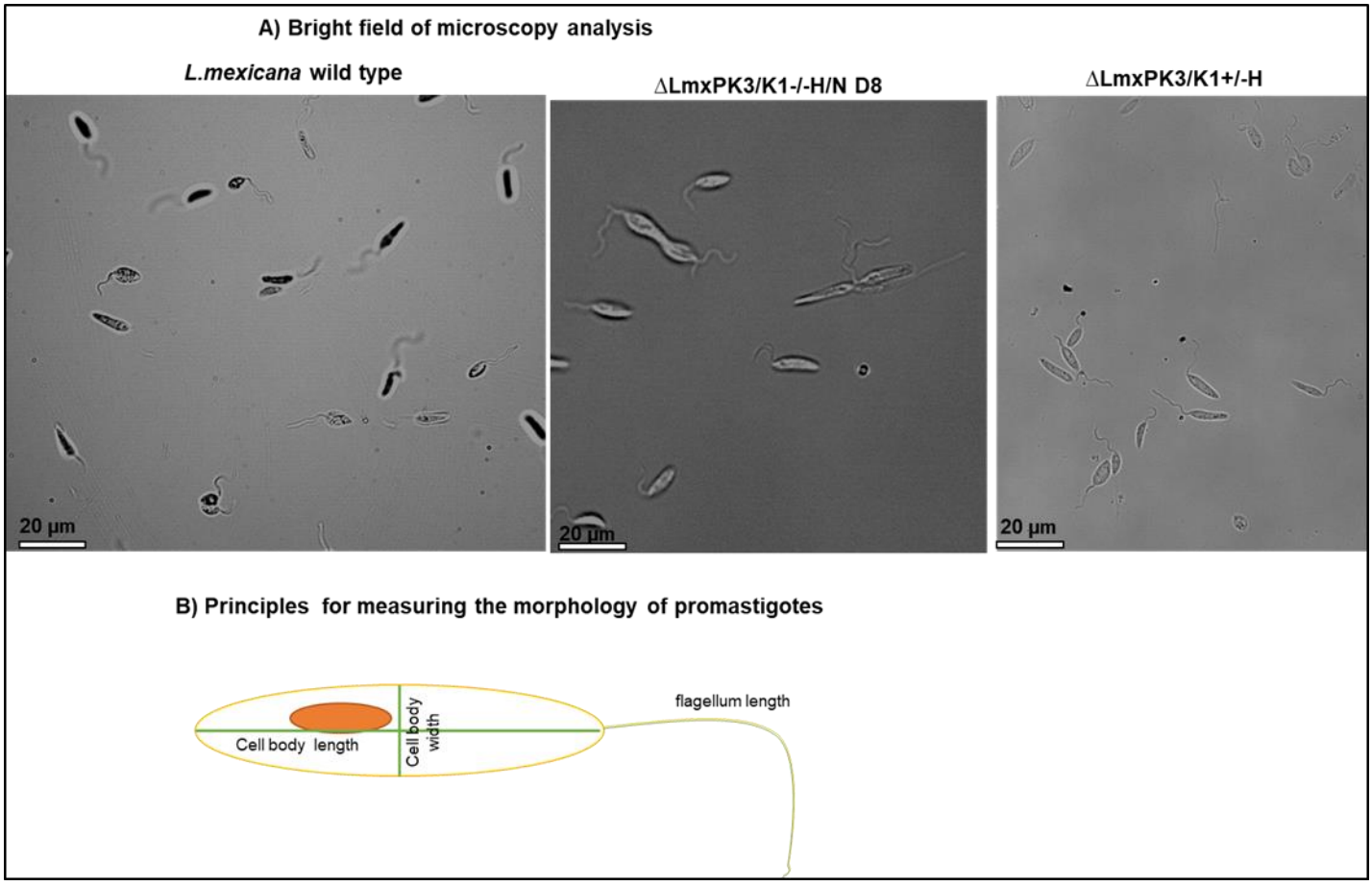

Figure 4.16. Cell body length, cell body width and flagellum length. A) Bright field microscopy of *L. mexicana* wild type and LmxPK3 mutants. Images were processed using ImageJ (NIH, USA). Size bar, 20 µm. **B)** Principle of measuring cell body length, cell body width and flagellum length in *L. mexicana* promastigotes. The green line indicates how the three parameters were measured using a freehand line in ImageJ.

Clones	Density cells/ ml
L. mexicana wild type	$3.9x10^7$
ΔLmxPK3/K1-/-H/N D8	$4.3\ x10^7$
ΔLmxPK3/K1+/-H	$3.8x10^7$

Table 4. 1.Cell density for *L. mexicana* wild type and LmxPK3 mutants at the time of measurement.

The data for cell body length, cell body width and flagellum length of the promastigote single allele and null mutant of LmxPK3 were compared to those taken from the *L. mexicana* wild type and were analysed using a Pearson's two-tailed, non-paired student's T-test. The measurements showed differences in cell body length, cell body width and flagellum length between single allele, null mutant of LmxPK3 and the *L. mexicana* wild type.

The cell body length analysis of ΔLmxPK3/K1+/-H showed no difference compared to the *L. mexicana* wild type, but ΔLmxPK3/K1-/-H/N D8 showed a significant increase in cell body length compared to the *L. mexicana* wild type and the single allele deletion mutant of LmxPK3 ($p \leq 0.0001$) (Figure 4.17).

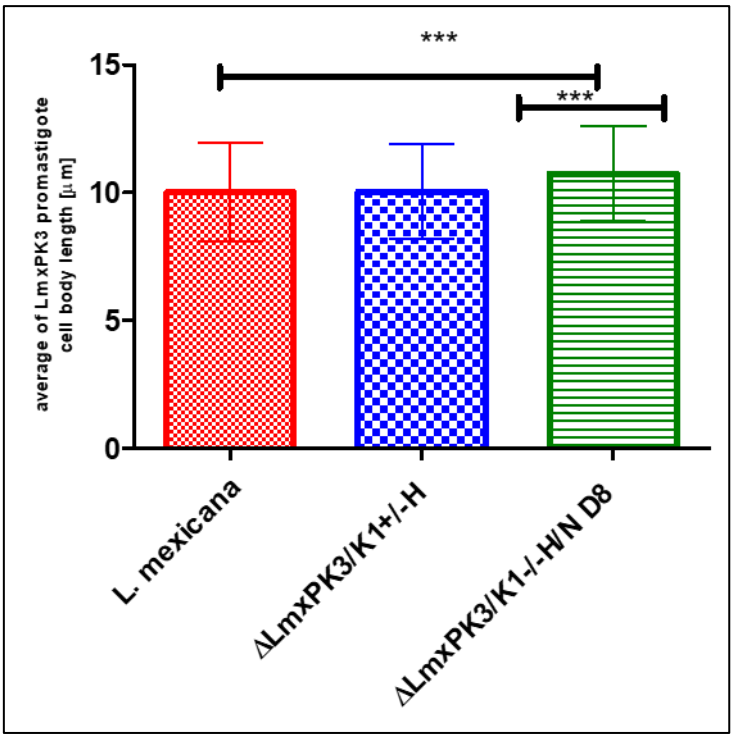

Figure 4.17. Morphological analysis for cell body length of LmxPK3 single and double allele deletion mutant compared to *L. mexicana* wild type promastigotes. The cell body length analysis of ΔLmxPK3/K1+/-H showed no difference compared to the *L. mexicana* wild type. Null mutant of LmPK3(ΔLmxPK3/K1-/-H/N D8) showed a significant increase in cell body length with an average of 10.7 ± 1.9 compared to the *L. mexicana* wild type, with an average of 10.0 ± 1.9 ($p \leq 0.0001$) and the single allele deletion mutant of LmxPK3 with an average of 10.0 ± 1.9. ***$p \leq 0.0001$.

On other hand, the cell body width analysis of ΔLmxPK3/K1+/-H and ΔLmxPK3/K1-/-H/N D8 showed a significant decrease compared to the *L. mexicana* wild type ($p \leq 0.0001$). However, ΔLmxPK3/K1+/-H showed a slight increase compared to ΔLmxPK3/K1-/-H/N D8 ($p \leq 0.05$) (Figure 4.18).

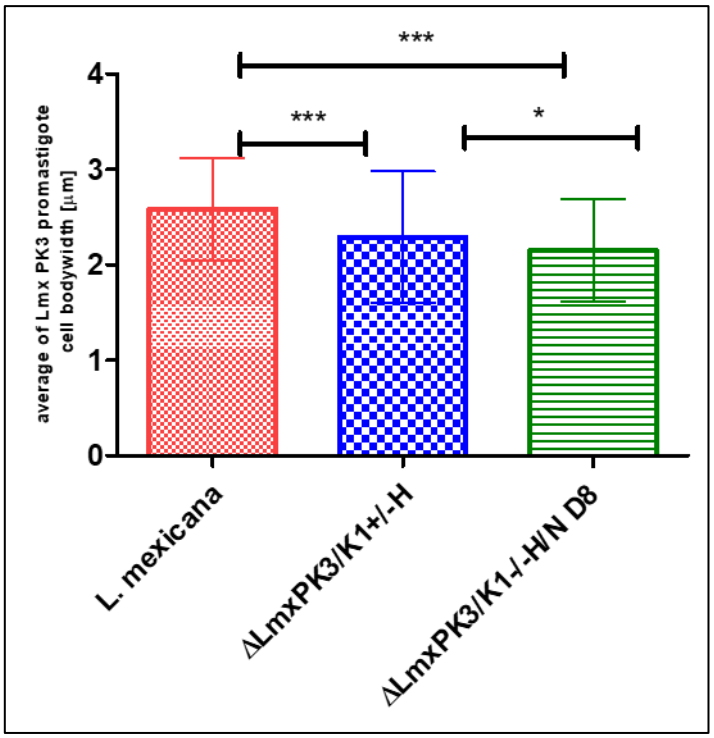

Figure 4.18. Morphological analysis for cell body width of LmxPK3 single and double allele deletion mutant compared to *L. mexicana* wild type promastigotes. The cell body width of ΔLmxPK3/K1+/-H showed an average of 2.3 ± 0.7, which is a significant decrease compared to the *L. mexicana* wild type with an average of 2.6 ± 0.5. ΔLmxPK3/K1-/-H/N D8 had an average of 2.2 ± 0.5, which is a significant decrease compared to the *L. mexicana* wild type and also a significant decrease compared to the single allele deletion mutant for LmxPK3. *p≤0.05 and ***p≤0.0001.

Additionally, the flagellum length analysis showed that the single allele deletion mutant ΔLmxPK3/K1+/-H showed no significance difference in flagellar length compared to the *L. mexicana* wild type (P value = 0.0895). However, ΔLmxPK3/K1-/-H/N D8 showed a significant decrease compared to the wild type of *L. mexicana* and the single allele deletion mutant for LmxPK3 (p≤0.0001) (Figure 4.19).

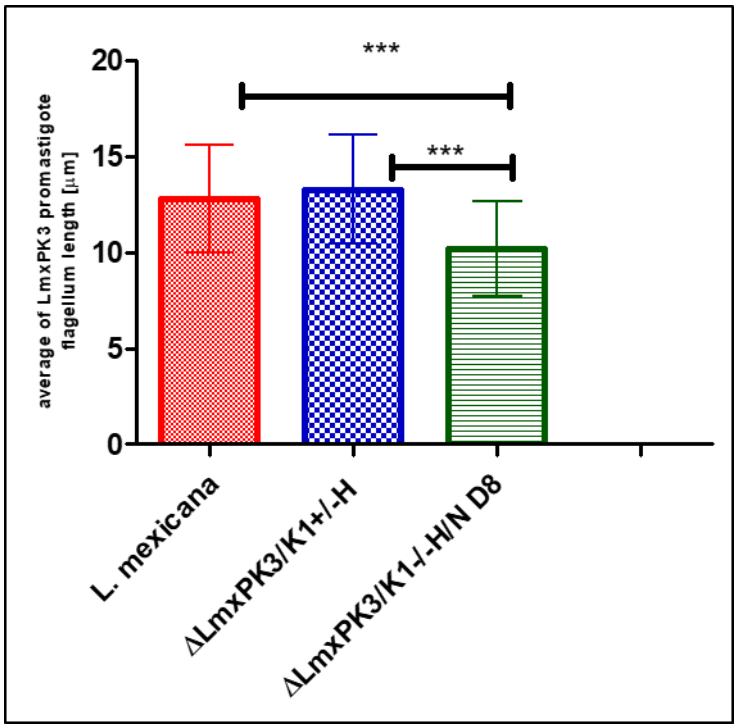

Figure 4.19. Morphological analysis of flagellum length for LmxPK3 single and double allele deletion mutant compared to *L. mexicana* wild type promastigotes. The flagellum length analysis showed that the single allele deletion mutant ΔLmxPK3/K1+/-H showed no significant difference in flagellar length compared to the *L. mexicana* wild type (P value = 0.0895). ΔLmxPK3/K1-/-H/N D8 showed a significant decrease, with an average of 10.2 ± 2.5 compared to the wild type of *L. mexicana,* with an average of 12.8 ± 2.8 and the single allele deletion mutant for LmxPK3, with an average of 13.3 ± 2.9. ***p≤0.0001.

4.2.6 Localisation of LmxPK3 in *L. mexicana*

GFP has been used in different species, including *Leishmania* and *Trypanosoma*, to analyse the localisation of a target protein (Docampo, 2011). GFP is a 27 kDa protein (238 amino acids) (Lodish et al., 2013) and contains a beta barrel structure of eleven β-strands, with an α-helix in the centre (Pakhomov and Martynov, 2008). Different add-back constructs carrying GFP-tagged LmxPK3 were generated and transfected into the null mutant background ΔLmxPK3/K1H/N D8 to find the localisation of LmxPK3 (Figure 4.20).

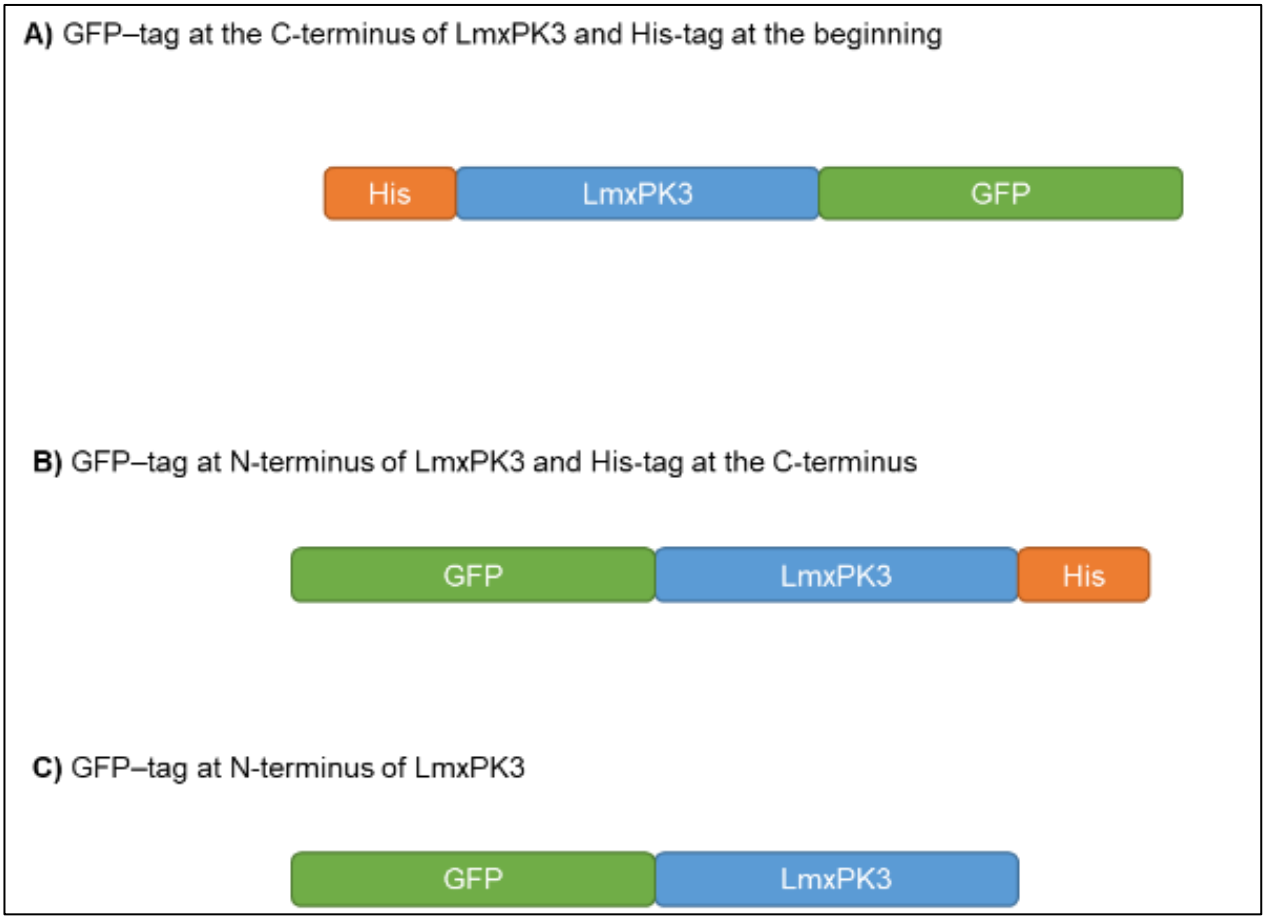

Figure 4.20. Different GFP-tagged versions of LmxPK3. Different GFP-tagged versions of LmxPK3.transfected into the null mutant background ΔLmxPK3/K1H/N D8 to determine the localisation of LmxPK3.A) GFP tag at the C-terminus of LmxPK3 and His-tag at the N-terminus. B) GFP tag at the N-terminus of LmxPK3 and His-tag at the C-terminus. C) GFP tag at the N-terminus of LmxPK3.

4.2.6.1 Generation of pTHBsdGFPTEVLmxPK3His, pTHBsdGFPTEVLmxPK3 and pTHBsdHisTEVLmxPK3GFP

To investigate the localisation of LmxPK3 in *L. mexicana* promastigotes, three plasmids, pTHBsdGFPTEVLmxPK3His (GFP-LmxPK3-His), pTHBsdGFPTEVLmxPK3 (GFP-LmxPK3) and pTHBsdHisTEVLmxPK3GFP (HisLmxPK3-GFP) were used. These were already available but carried the same nucleotide duplication as described for the GST-fusion constructs (see section

4.2.2.2). In order to correct these constructs, pTHBsdTEVGFPLmxPK3 was cleaved with EcoRV and BglII to generate 7852 bp and 688 bp DNA fragments; pTHBsd GFPTEVLmxPK3His was cleaved with EcoRV and BglII to produce 7837 bp and 688 bp DNA fragments; and pTHBsdHisTEVLmxPK3GFP was cleaved with EcoRV and BglII to generate 7839 bp and 688 bp DNA fragments (Figure 4.21 A). The 7852 bp DNA fragment from pTHBsdTEVGFPLmxPK3, the 7837 bp DNA fragment from pTHBsdGFPTEVLmxPK3His and the 7839 bp DNA fragment from pTHBsdHisTEVLmxPK3GFP were isolated and dephosphorylated. pBX19lmkin24-30, carrying the genomic copy of LmxPK3, was cleaved with EcoRV and BglII to generate 8030 bp, 3500 bp and 679 bp DNA fragments (Figure 4.21 B). The 679 bp DNA fragment from pBX19lmkin24-30 was isolated and ligated with the 7852 bp DNA fragment from pTHBsdTEVGFPLmxPK3, the 7837 bp DNA fragment from pTHBsdTEVLmxPK3His and the 7839 bp DNA fragment from pTHBsdHisTEVLmxPK3GFP in order to generate the corrected versions of the plasmids. The sequence of these plasmids were confirmed by DNA sequence analysis. pTHBsdTEVGFPLmxPK3, pTHBsdGFPTEVLmxPK3His and pTHBsdHisTEVLmxPK3GFP were subsequently used for transfection into null mutant LmxPK3 (∆LmxPK3/K1-/-N/H D8) promastigotes.

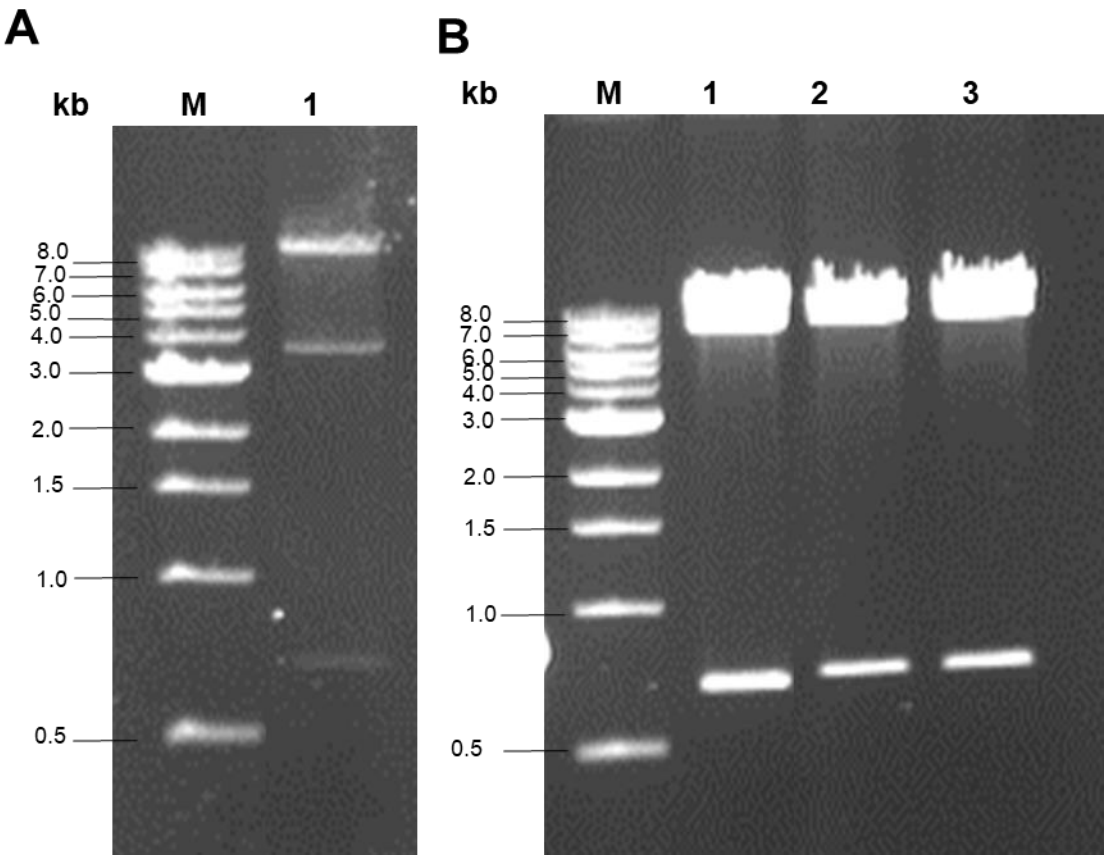

Figure 4.21. Generation of pTHBsdGFPTEVLmxPK3His, pTHBsdGFPTEVLmxPK3 and pTHBsdHisTEVLmxPK3GFP. A) Preparative cleavage of pBX19lmkin24-30 with EcoRV and BglII. Lane 1, pBX19lmkin24-30 generated 8030 bp, 3500 bp and 679 bp DNA fragments. **B)** Preparative cleavage of pTHBsdGFPTEVLmxPK3, pTHBsdGFPTEVLmxPK3His and pTHBsdHisTEVLmxPK3GFP cleaved with EcoRV and BglII. Lane 1, pTHBsdGFPTEVLmxPK3 generated 7852 bp and 688 bp DNA fragments; lane 2, pTHBsdGFPTEVLmxPK3His produced 7837 bp and 688 bp DNA fragments; lane 3, pTHBsdHisTEVLmxPK3GFP generated 7839 bp and 688 bp DNA fragments. M, DNA size marker.

4.2.6.2 Transfection of pTHBsdTEVGFPLmxPK3, pTHBsdGFPTEVLmxPK3His and pTHBsdHisTEVLmxPK3GFP into LmxPK3/K1-/-H/N D8 null mutant promastigotes

pTHBsdTEVGFPLmxPK3, pTHBsdGFPTEVLmxPK3His and pTHBsdHisTEVLmxPK3GFP were introduced into LmxPK3/K1-/-H/N D8 null mutant promastigotes to study the subcellular localisation of different versions of LmxPK3. One clone for each plasmid, ΔLmxPK3/K1-/-N/H D8 carrying

pTHBsdTEVGFPLmxPK3 (J12), ΔLmxPK3/K1-/-N/H D8 carrying pTHBsdGFPTEVLmxPK3His (A3) and ΔLmxPK3/K1-/-N/H D8 carrying pTHBsdHisTEVLmxPK3GFP (E5) was propagated from the 1:40 dilution plated on a 96-well plate after electroporation and was grown in 10 mL culture for fluorescence analysis.

4.2.6.3 Fluorescence analysis for the localisation of LmxPK3

The fixed promastigote *Leishmania* cells were inspected by fluorescence microscopy at an excitation wavelength of 488 nm (Figure 4.22). LmxPK3 was localised in the cytosol of the cells and some cells showed localisation in the flagellum. There was no difference in localisation between LmxPK3 with GFP at the N-terminus or C-terminus. Nor did the presence of the hexahistidine-tag affect the localisation. To confirm the identity of the protein as a GFP-fusion protein an immunoblot with an anti-GFP antibody could be performed.

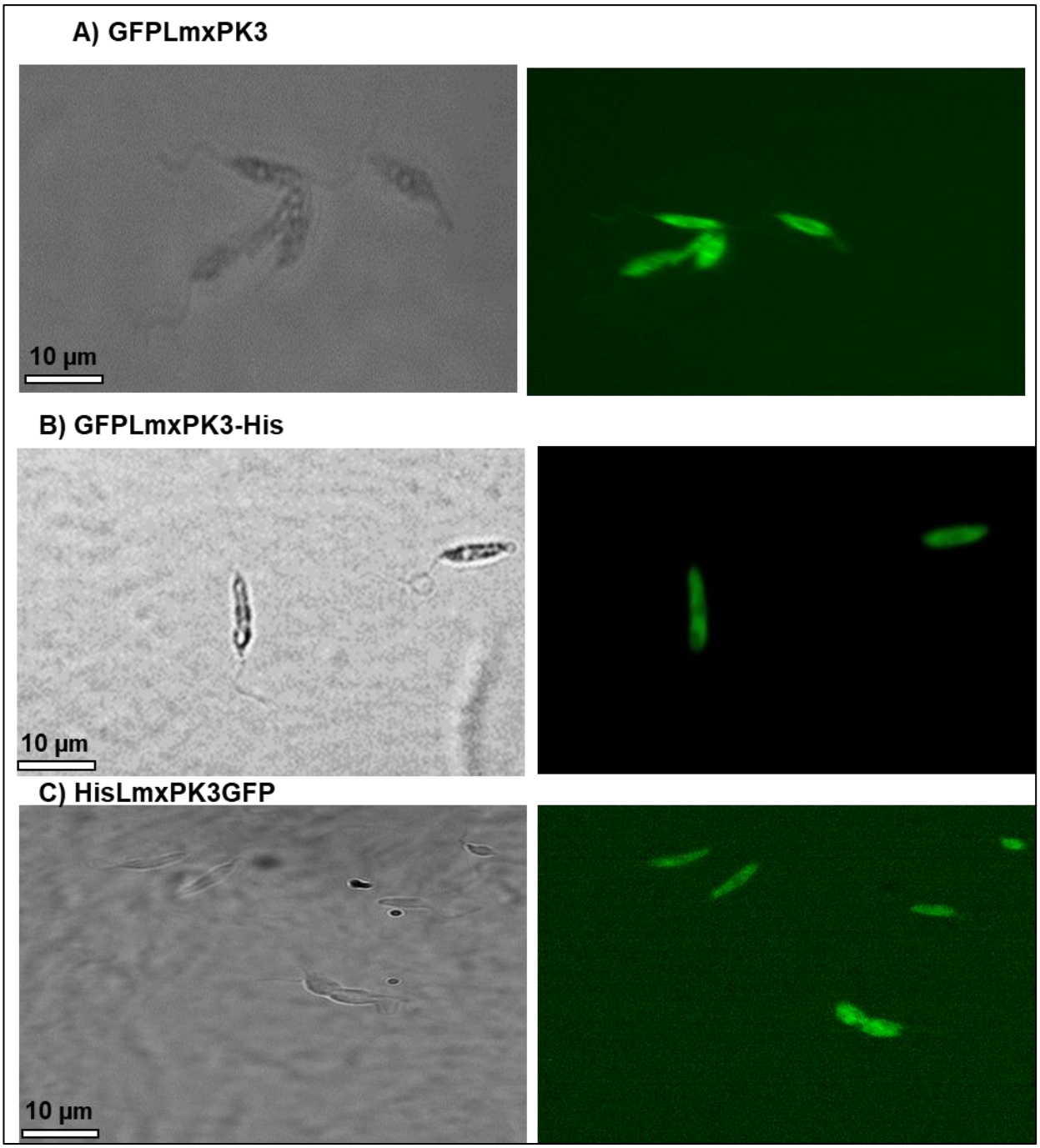

Figure 4.22. Subcellular localisation of different GFP-tagged versions of LmxPK3 in fixed promastigotes using fluorescence microscopy. A) GFPLmxPK3. **B)** GFPLmxPK3-His. **C)** HisLmxPK3GFP. Promastigotes were analysed at logarithmic growth phase (2-4 × 10^7 cells/mL). Images were processed using ImageJ (NIH, USA). Left, bright field; right, fluorescence using 488 nm excitation and FITC filter. Size bar, 10 µm. This indicated that LmxPK3 was localised in the cytosol in *the L. mexicana* promastigote cells.

4.3 Discussion

This study describes the molecular characterisation of the MAP kinase kinase homologue LmxPK3 (LmxM.17.0060). The full-length amino sequence of LmxPK3 shares 95% homology across *Leishmania* species and 50% and 45% homology with *T. cruzi* and *T. brucei*, respectively. The molecular characterisation of LmxPK3 shows that it is also related to CAMK. It was also shown by sequencing of mRNA that LmxPK3 transcripts are present in all life cycle stages, with highest abundance in lesion-derived amastigotes (Fiebig et al., 2015). Whether this reflects the level of protein in the different life cycle stages remains to be determined (also see discussion for LmxPK6).

LmxPK3 and its homologues in other kinetoplastids contain putative regulatory phosphorylation sites in the activation loop (SVFAGNKQCLTTCCGT), which are part of a sequence similar to the consensus sequence S/TXXXXXS/T found in plant MAP2Ks. There are additional threonine residues in LmxPK3, which could be putative phosphorylation sites in the activation loop between the DFG and APE motifs (Figure 4.1). However, only T185 of LmxPK3 is highly conserved between MAP kinase kinases from different species. LmxPK3 shares 57/199 (29% amino acid identity) and 103/199 (51% amino acid similarities) with *Xenopus laevis* dual-specificity MEK1 (NP_001080299). MEK1 is phosphorylated by Raf1 on S218 and S222 (Alessi et al., 1994; Zheng and Guan, 1993). LmxPK3 has four putative D-sites. Similarly, most eukaryotic MAP2Ks contain D-sites (Grewal et al., 2006).

Additionally, recombinant LmxPK3 was expressed as a GST-fusion protein. However, only low levels of protein could be obtained (Figure 4.7). There are several possible

explanations for this finding. First, this was most likely due to the relatively low final cell density obtained when expressing the protein in *E. coli*. LmxPK3 might be toxic to *E. coli* by phosphorylating proteins in the bacteria, affecting the homeostasis of the cell. In addition, codon bias can occur when the frequency of the occurrence of codons is different between *Leishmania* and *E. coli*. Low abundance of relevant tRNAs affects the efficiency of translation and ultimately leads to low protein production. Despite the fact that low levels of protein obtained from recombinant expression, eluted recombinant GST-LmxPK3 was found to have a distinct phosphotransferase activity towards MBP but no autophosphorylation activity in radiometric kinase assays (Figure 4.8). This is the first time that LmxPK3 was shown to have kinase activity. However, a control using a kinase-dead version of LmxPK3 purified from *E. coli* would need to be employed. This would be proving that the phosphorylation of MBP is indeed caused by LmxPK3 and not by a co-purified kinase from *E. coli*.

Despite the fact that homologous recombination allowed to generate a single allele deletion mutant using a resistance marker gene flanked by the LmxPK3 upstream and downstream regions, it turned out to be difficult to generate a LmxPK3 null mutant through homologous recombination. This suggested that the flanking regions of LmxPK3 might not allow production of sufficient amounts of the second resistance marker to result in viable, drug resistant parasites. Therefore, it was necessary to use an alternative strategy to obtain a null mutant of LmxPK3. pB1BALmxPK3updsDelMPK12neo (Figure 4.10) was generated containing the flanking regions of LmxMPK12 to drive expression of the neomycin phosphotransferase gene. This allowed the generation of the null mutant clone LmxPK3/K1-/-H/N D8 (Figure 4.11) . However, a second clone named LmxPK3/K3-/-H/N F2 showed integration of the deletion construct into the LmxMPK12 gene locus and therefore maintained a copy of LmxPK3. This was an unexpected result as

normally homologous recombination occurs using the end-regions of a targeting construct. In this case the LmxMPK12 regions, which are surrounded by the LmxPK3 flanking regions, led to replacement of one allele of LmxMPK12(Figure 4.12).

Moreover, this study has focussed on whether LmxPK3 is important for infectivity of *Leishmania* in the mammalian host. Most mice infected with LmxPK3 null mutant parasites showed no significant difference in lesion development compared to the wild type (Figure 4.13 and Figure 4.14). However, the onset of lesion development in mice infected with the single allele deletion mutant (ΔLmxPK3/K1+/-H) was delayed by four weeks compared to those infected with *L. mexicana* wild type or *LmxPK3* null mutant promastigotes. After the four weeks' lesion development occurred with the same kinetics as in the other two cell lines. The difference in onset of lesion development could be due to a variation in the number of parasites used for injection. Two wash steps are involved in the preparation of the inoculum and both could have led to loosing some parasites. Moreover, some of the inoculum could have been lost during the injection. In fact, two out of five mice never showed any lesion development suggesting that the quality of the inoculum (number and fitness of the promastigotes) was low. On the contrary, for the other two cell lines all five mice showed lesion development, however, always one out of the group of five showed slower increase in footpad size and was therefore excluded from the graphs. This suggests also variability in the injection procedure. Alternatively, it is still possible that the single allele deletion mutant promastigotes lacked fitness because of the absence of the gene, however as the null mutant is directly derived from this single allele deletion mutant clone and is as infective as the wild type an intrinsic lack of fitness is extremely unlikely. All recombinant promastigotes were kept under the appropriate antibiotic pressure. This means that the null mutant was exposed to the same concentration as the single allele deletion mutant excluding an effect that the presence of the antibiotic

could have on the expression of genes flanking the LmxPK3 gene locus. This result is similar to the null mutant of LmxMPK9, which also showed lesion development in BALB/c mice (Bengs et al., 2005). These results differ from other MAP2K null mutants (LmxPK4 and LmxMKK), for which the proteins could only be detected in promastigotes and which showed delayed onset of lesion development in animal experiments, which was thought to occur because of an unknown mechanism of compensation (Kuhn and Wiese, 2005; Wiese et al., 2003b). The ability of the LmxPK3 null mutant to differentiate into amastigotes, cause lesions and differentiate back into promastigotes after isolation of amastigotes from the lesion demonstrates that LmxPK3 was not required for *Leishmania* differentiation (Figure 4.15).

A further finding is that morphological changes occurred in *L. mexicana LmxPK3* null mutant promastigotes. The morphology of the promastigotes can be defined as cell body length and width, and flagellum length (section 4.2.5.2.2). LmxPK3K1H/N D8-/- promastigotes showed a significant increase in body length and a significant decrease in cell body width to wild type *L. mexicana* promastigotes. In addition, *LmxPK3* null mutants displayed reduced flagella lengths compared to flagella of the wild type (Figures 4.17, 4.18 and 4.19). The small differences in culture densities between LmxPK3 null mutant and wild type promastigotes (Table 4.1) might be responsible for the morphological differences observed. Logarithmic growth phase *L. mexicana* wild type promastigotes at cell densities between 3×10^6 and 1.3×10^7 cells/mL show a reduced cell body width at higher cell densities and, on average, longer flagella (Wheeler et al., 2011). However, all cultures were analysed in the late logarithmic growth phase at around 4×10^7 cells/mL. Hence, it is unlikely that cell density differences played a significant role. Taken together, the morphological changes were deemed too small and no measurements were undertaken for LmxPK3 add-back cells expressing N- or C-terminally GFP-tagged protein. Therefore, the relatively small

changes in promastigote morphology do not allow to assign a distinct function to LmxPK3 affecting the three parameters, body length, body width and flagellum length.

In addtion, the localisation analysis of LmxPK3 using fluorescence microscopy of parasites expressing GFP-tagged LmxPK3 confirmed the expression of different GFP-fusion proteins (GFP-LmxPK3His, GFP-LmxPK3 and HisLmxPK3-GFP; Figure 4.20) in the deletion background (ΔLmxPK3/K1-/-H/N D8). The fluorescence analyses revealed varying expression levels of these GFP-fusion proteins. LmxPK3, with a GFP-tag at either the N-terminus or C-terminus, was distributed throughout the cytosol and some cells showed localisation in the flagellum of recombinant promastigotes (Figure 4.22). These results match with results obtained for the *T. brucei* homologue of LmxPK3 (Tb927.7.6220) on TrypTag, a protein localisation database for *T. brucei* (Figure 4.23) (Dean et al., 2017).

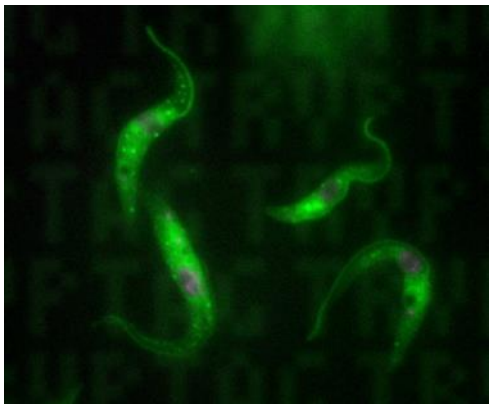

Figure 4.23. Localision of the LmxPK3 homologue in *T. brucei* (Tb927.7.6220) as shown on TrypTag. It localised in the cytosol and the flagellum. Adapted from (Dean et al., 2017).

Moreover, this result is similar to those reported for other MAP2K (LmxPK4, LmxMKK) (Erdmann et al., 2006; Kuhn and Wiese, 2005) and the MKKs, MEK1 and MEK2 in mammals, which contain N-terminal nuclear export signals and are located in the

cytosol of mammalian cells (Schaeffer and Weber., 1999). As the function of LmxPK3 is not known, it is not possible to determine whether a GFP-tagged version of the protein is functional.

In conclusion, LmxPK3 is a homologue of MAP2K, which is not required for the viability of *L. mexicana* promastigotes in culture nor for the infection of mammalian hosts. Hence, LmxPK3 is not suitable as a target for leishmanicidal drugs. However, it still might be important for the survival of promastigotes in the sand fly, a more challenging environment for the parasite than the culture flask.

Chapter 5: Interaction between the protein kinases LmxMPK3 and LmxPK4

Abstract

During their life cycle *Leishmania* undergo many changes in cell morphology such as various flagellar lengths in different life cycle stages. MAPK pathways were shown to play a role in flagellar length. The interactions between a MAP2K (LmxPK4) and a MAPK (LmxMPK3) was investigated *in vitro* and *in vivo*. Kinase assays showed phosphorylation of MBP as a result of co-expression of LmxMPK3 with LmxPK4. Tandem mass spectrometry of LmxMPK3 co-expressed with LmxPK4 identified 15 phosphorylated residues, three of which are likely phosphorylated by LmxMPK3 autophosphorylation. Like LmxMKK, LmxPK4 can phosphorylate LmxMPK3 at the TDY motif to activate the kinase. When comparing phosphorylation of LmxMPK3 by LmxMKK with that conferred by LmxPK4, the latter phosphorylated LmxMPK3 on additional phosphorylation sites (THR169, SER183, SER298), which might be relevant to distinguish activation of LmxMPK3 by LmxPK4 from activation by LmxMKK.

Additionally, the interaction between LmxMPK3 and LmxPK4 was confirmed *in vivo* by using a split-GFP approach. GFP was split between the tenth and the eleventh β-strand and the two segments were attached to the proteins of interest, generating LmxPK4GFP1-10 and LmxMPK3-GFP11. When LmxPK4-GFP1-10 and LmxMPK3-GFP11 interact, the two segments of GFP re-join, resulting in a fluorescent signal. Expression of the fusion proteins in the LmxMPK3 null mutant led to green fluorescence in distinct regions of the cytosol. The short flagellum of the LmxMPK3 null mutant parent cell line was rescued to a normal length indicating expression of a fully functional LmxMPK3 from the di-GFP construct.

5.1 Introduction

Metabolic networks are different types of biological networks in cells. These networks give information about the characteristics of an organism, particularly for protein–protein interactions. Protein phosphorylation plays an important role in the formation and function of flagella. Eighty flagellar proteins have been found to be phosphorylated in *C. reinhardtii* (Piperno and Luck, 1976). Like *Chlamydomonas, Leishmania* is a suitable model organism for studying the regulation of flagellar length, because *Leishmania* flagella maintain many structurally conserved elements (Bengs et al., 2005; Wiese et al., 2003b). Flagellar length could be regulated using LmxMPK3 (LmxM.10.0490), a MAP kinase homologue of *L. mexicana* (Wiese et al., 2003a). The LmxMPK3 gene is a single copy gene in the haploid set of chromosomes and has an open reading frame of 1164 base pairs which encode 388 amino acids. LmxMPK3 protein has a molecular mass of 43.7 kDa (Erdmann et al., 2006). The typical twelve kinase subdomains and amino acid residues conserved in MAPK are found in LmxMPK3. LmxMPK3 carries a common docking domain (LHDEEDEPACP) at the C-terminus. A constitutively activated version of LmxMKK phosphorylated and activated LmxMPK3 *in vitro* (Erdmann et al., 2006). The LmxMPK3 null mutant promastigotes exhibit shorter flagella compared to *L. mexicana* wild type, while the re-expression of LmxMPK3 in the deletion mutant leads to the regeneration of *L. mexicana* wild type length flagella (Erdmann et al., 2006). Similar to the deletion mutant for LmxMPK3, the null mutant for LmxMKK demonstrated reduced flagellar length. Hence, both LmxMPK3 and LmxMKK are involved in flagellar length regulation in *L. mexicana* (Wiese et al., 2003b).

LmxPK4 (LmxM.24.2320) is a MAP2K homologue of *L. mexicana* composed of 350 amino acids and a calculated molecular mass of 39 kDa. The amino acid sequence

of LmxPK4 revealed a typical protein kinase domain (L73-I331) with twelve highly conserved subdomains. A putative D-site (KRPQALEKLHV) could be identified close to the N-terminus. The deletion of LmxPK4 from the *L. mexicana* genome resulted in elongated flagella in promastigotes. It has been suggested that LmxPK4 plays a role in the differentiation from promastigotes to amastigotes (Kuhn and Wiese, 2005). LmxPK4 has been found to phosphorylate LmxMPK13 and LmxMPK9, indicating crosstalk between the pathways (Scholz, 2008).

To conclude, *L. mexicana* null mutants for LmxMKK or LmxMPK3 were identified to have shortened flagella in promastigotes. However, null mutants for LmxPK4, LmxMPK9 or LmxMPK13 demonstrated elongated flagella. It had been shown that LmxPK4 was able to phosphorylate LmxMPK3 *in vitro*. These experiments needed confirmation and inclusion of appropriate controls in form of a kinase-dead version of LmxMPK3. Following on from this analysis the interaction of the two kinases was planned to be analysed *in vivo* using the split-GFP system.

5.2 Results

5.2.1 Activation of LmxMPK3 by LmxPK4 *in vitro*

The potential interactions between LmxMPK3 and LmxPK4 (Figure 5.1) *in vitro was* investigated. A number of different already available expression constructs were used containing the following genes; LmxMPK3 for single expression (pJCLmxMPK3), a kinase-dead LmxMPK3K62M (pJCLmxMPK3KM), LmxMPK3 and LmxPK4 for simultaneous expression (pJCLmxMPK3LmxPK4), LmxMPK3 and LmxMKK for the co-expression (pJCLmxMPK3LmxMKK), LmxMPK3KM together with activated LmxMKK (pJCLmxMPK3KMLmxMKKmut2). pJCLmxMPK3KMLmxPK4, which allowed co-expression of LmxMPK3KMLmxPK4, was generated new.

A) Amino acid sequence LmxMPK3(LmxM.10.0490)

MHKSNQELSVPKVVGDFKVYNVSGSPFEVPSKYTLLKILGMGAYGIACSCLDGDTGEKVSIKKCRDVFRDVEDGK
RVLREIDMMRFFHHENLLNVVNILPPLKCEYHSFEDVYVVTPLMDVDMNVVLRSRQVLEESHMQYFVYQILRGLK
YLHSANVAHRDLKPANLVTNISCELKIIDFGLSRSVDVPYSELTDYVITRWYRPPELLLENTNYSTAVDIWSVGC
IFAEMYNRKPVFPGRNTMDQLRMIAQHIGKPPASIVEHREALEKLNELPGGSLNIPKLVPGLAGNTEGIDFLSKM
WTLDPSKRPTAADMLAHPYLAHLHDEEDEPACPCPFLWAHESTPMGVSELRRAFWADIVDYNPSLEHATPPATTA
GGSSSKNGSGHH

CD domain

B) Amino acid sequence LmxPK4(LmxM.24.2320)

D-site

MPPKRPQALEKLHVEPHDKGVSITDTMTLVVKGEGGVEMRVKQTGIAQGPGSSSAGGQPK
SDAVMNKIKFEDLRIGSELGKGSQGKVRVAQHKLTGEKYAMKYIAFDGDSDDMRSALEAE
LRQVAAVKHHNVVSSYEAFFRDGRLYIVLEYMDCGTMNNLIDRHPEGFSEDMLAYIAREL
FKGLEFLHHLNMIHRDIKPANVLANTKGEIKISDFGVAKTLSGGDLQTLSAQGSVPYMSP
ERIQSKPYSFNSDIWSAGLTIAECAFREYPFASLKPKLFELCQAIASGTAKINWDDRETK
FSDEFKEFIELCLRPEATRPSATEMLSHSLIQKASNVNPLEAGRWMSRK

C) Activation of LmxMPK3 by LmxPK4

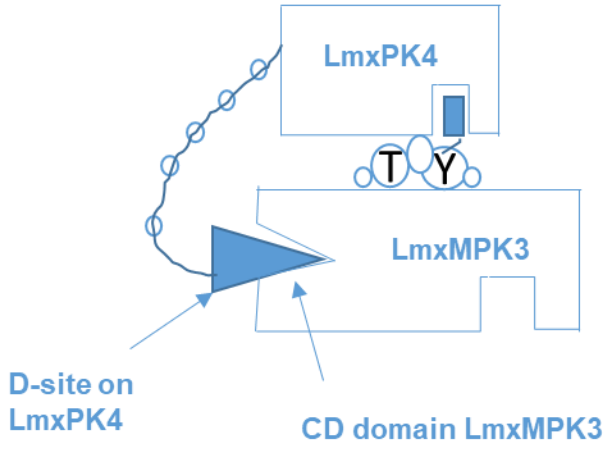

Figure 5.1. Activation of LmxMPK3 by LmxPK4. A) amino acid sequence of LmxMPK3. **B)** Amino acid sequence of LmxPK4. **C)** Predicted interaction between LmxMPK3 and LmxPK4. Yellow, kinase domain; green, CD domain; red, phosphorylation sites; pink, CD domain.

5.2.1.1 Generation of co-expression constructs of *L. mexicana* LmxMPK3KM and LmxPK4 *in vitro*

pJCLmxMPK3, pJCLmxMPK3KM, pJCLmxMPK3LmxPK4, pJCLmxMPK3LmxMKK and pJCLmxMPK3KMLmxMKKmut2 were used to generate a new construct, which allowed co-expression of LmxMPK3KM and LmxPK4. The cloning history to generate pJCLmxMPK3KMLmxPK4 is illustrated in Figure 5.2. The plasmid pJCLmxMPK3LmxPK4 was cleaved using the restriction enzymes EcoRI and EcoRV to obtain 1954 bp and 3520 bp DNA fragments. The 3520 bp EcoRI/EcoRV DNA fragment carrying LmxPK4 was isolated and subjected to SAP treatment. pJCLmxMPK3KMLmxMKKmut2 was cleaved using the restriction enzymes EcoRI and EcoRV, resulting in 1954 bp and 3507 bp DNA fragments, followed by isolation of 1955 bp EcoRI/EcoRV DNA fragment containing LmxMPK3KM (Figure 5.3). Both fregments were ligated and transformed into *E. coli* DH5α to generate pJCLmxMPK3KMLmxPK4. A putative positive clone was isolated and sequenced. This revealed that a frameshift separated the hexahistidine-tag from the open reading frame of LmxMPK3KM. This plasmid is further on called pJCLmxMPK3KMLmxPK4F.

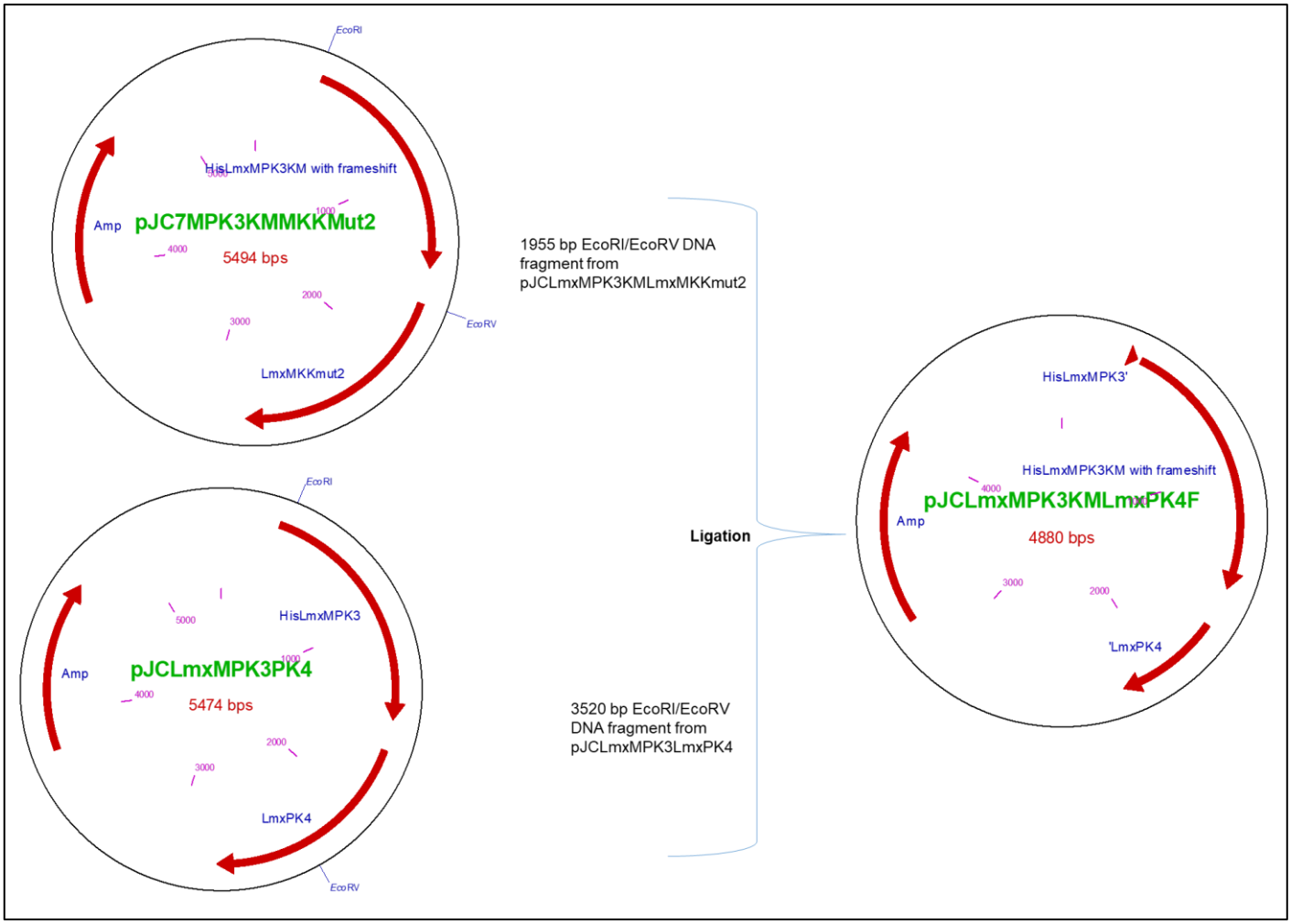

Figure 5.2. Cloning history for the generation of pJCLmxMPK3KMLmxPK4 carrying a frameshift. A 1955 bp EcoRI/EcoRV DNA fragment from pJCLmxMPK3KMLmxMKKmut2 was ligated with a 3520 bp EcoRI/EcoRV DNA fragment from pJCLmxMPK3LmxPK4 to generate pJCLmxMPK3KMLmxPK4. Amp, ampicillin selectable marker.

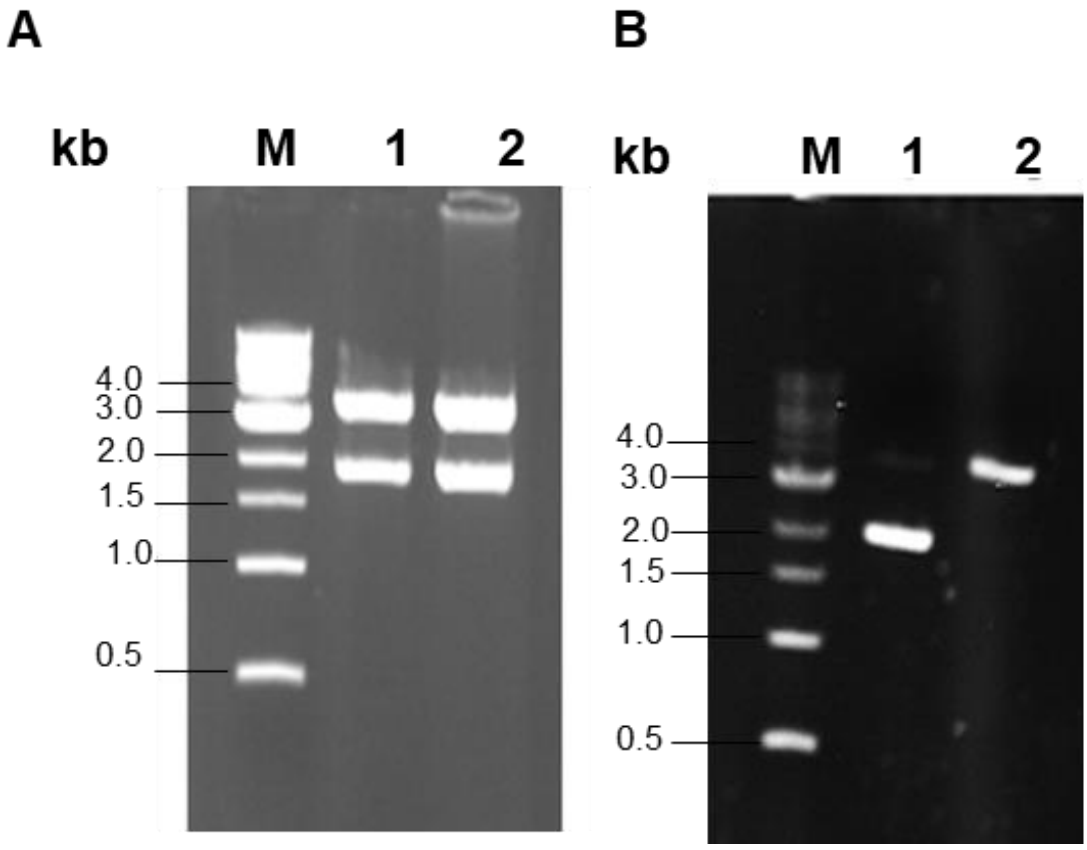

Figure 5.3. Preparative cleavage of pJCLmxMPK3KMLmxMKKmut2 and pJCLmxMPK3LmxPK4 and isolated DNA fragments. A) Restriction enzyme cleavage with EcoRI and EcoRV. Lane 1, pJCLmxMPK3KMLmxMKKmut2, resulting in 1955 bp and 3507 bp DNA fragments; lane 2, pJCLmxMPK3LmxPK4, resulting in 1954 bp and 3520 bp DNA fragments. **B)** Isolated DNA fragments. Lane 1, 1955 bp EcoRI/EcoRV DNA fragment from pJCLmxMPK3KMLmxMKKmut2; lane 2, 3520 bp EcoRI/EcoRV DNA fragment from pJCLmxMPK3LmxK4. M, DNA size marker.

As the frameshift was not present in pJCLmxMPK3LmxPK4 a 353 bp PciI-DNA fragment from pJCLmxMPK3LmxPK4 was used to replace the corresponding 353 bp PciI-DNA fragment from pJCLmxMPK3KMLmxPK4F, which carried the frameshift (Figure 5.2). The cloning history to generate the corrected plasmid pJCLmxMPK3KMLmxPK4 is illustrated in Figure 5.4. pJCLmxMPK3KMLmxPK4F cleaved with PciI resulting in 353 bp and 5121 bp DNA fragments. The 5121 bp DNA fragment was isolated and dephosphorylated. pJCLmxMPK3LmxPK4 was also cleaved with PciI resulting in 353 bp and 5121 bp DNA fragments, followed by

isolation of the 353 bp PciI-DNA fragment. This fragment was ligated with the 5121 bp PciI-DNA fragment from pJCLmxMPK3KMKLmxPK4F (Figure 5.5) and transformed into *E. coli* DH5α to generate the corrected pJCLmxMPK3KMLmxPK4. The identity of pJCLmxMPK3KMLmxPK4 was confirmed by DNA sequencing.

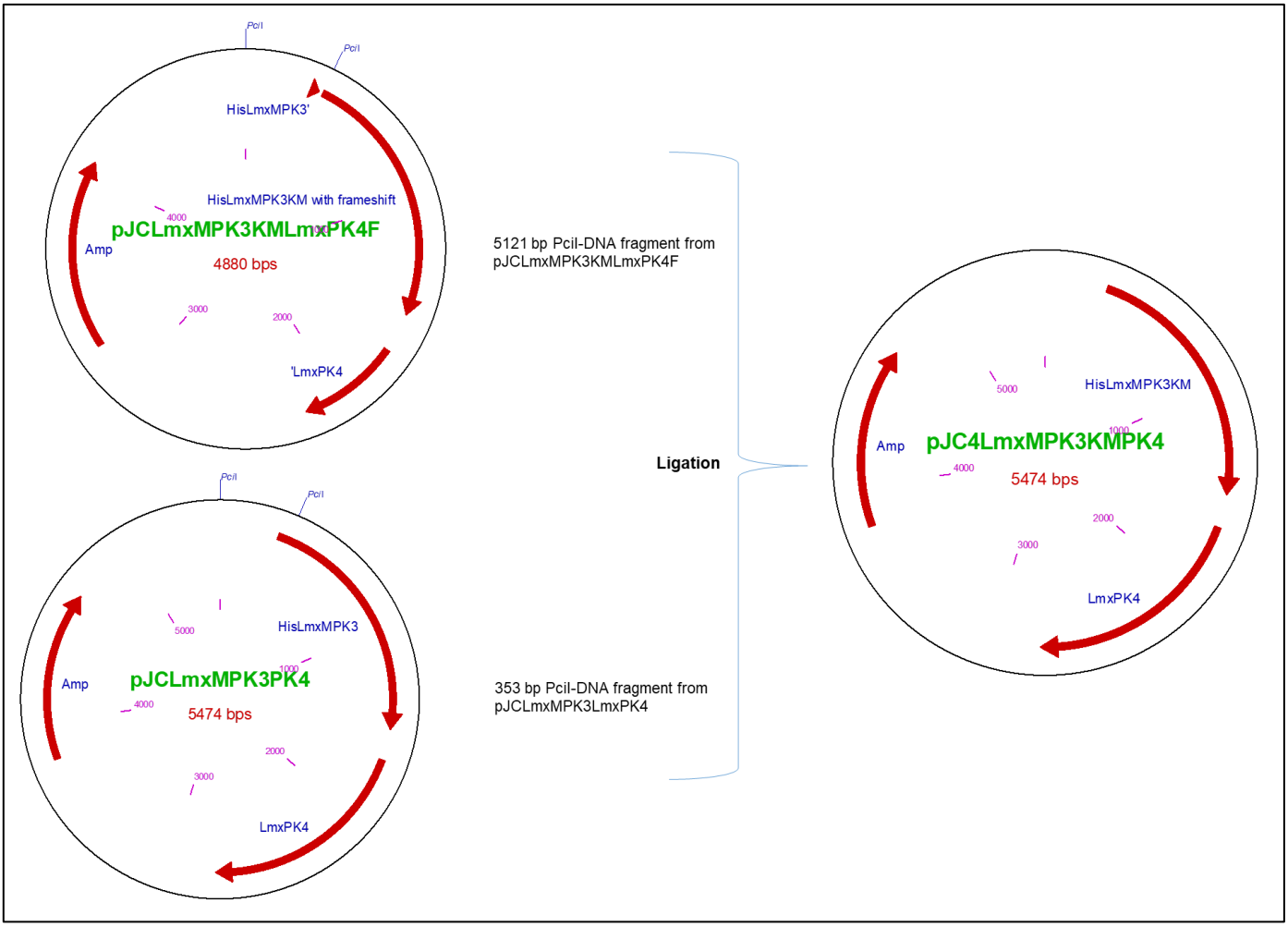

Figure 5.4 Cloning history for the generation of the corrected pJCLmxMPK3KMLmxPK4. The 5121 bp PciI-DNA fragment from pJCLmxMPK3KMLmxPK4F was ligated with the 353 bp PciI-DNA fragment from pJCLmxMPK3LmxPK4 to generate the corrected pJCLmxMPK3KMLmxPK4. Amp, ampicillin selectable marker.

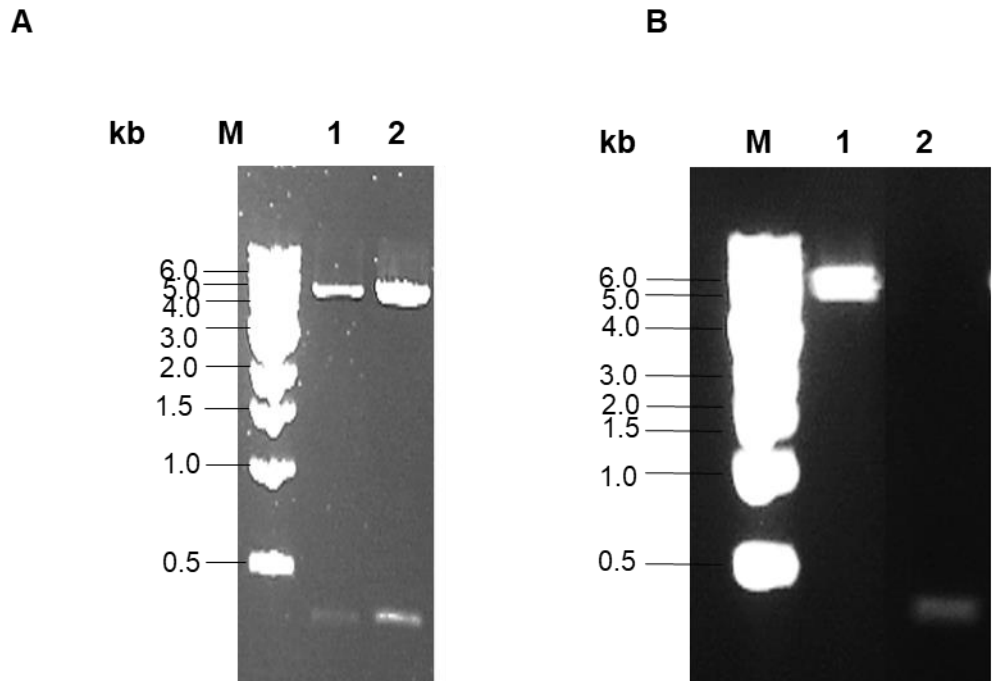

Figure 5.5. Preparative cleavage of plasmids pJCLmxMPK3LmxPK4, pJCLmxMPK3KMLmxPK4F and DNA fragment isolation. A) Restriction cleavage with PciI. Lane 1, pJCLmxMPK3LmxPK4, resulting in 353 bp and 5121 bp DNA fragments; lane 2, pJCLmxMPK3KMLmxPK4, resulting in 353 bp and 5121 bp DNA fragments**; B)** Isolated DNA fragments from pJCLmxMPK3LmxPK4 and pJCLmxMPK3KMLmxPK4F. Lane 1, 5121 bp PciI-DNA fragment from pJCLmxMPK3KMKLmxPK4F; lane 2, 353 bp PciI-DNA fragment from pJCLmxMPK3LmxPK4. M, DNA size marker.

Additionally, sequencing of the parent plasmid pJCLmxMPK3KMLmxMKKmut2 and single-gene expression plasmid pJCLmxMPK3KM revealed a similar frameshift. Subsequently, pJCLmxMPK3KMLmxPK4 carrying the correct open reading frame of LmxMPK3KM was used to generate pJCLmxMPK3KM and pJCLmxMPK3KMLmxMKKmut2 with the correct open reading frame of LmxMPK3KM (Figures 5.6 and 5.7). For this purpose, pJCLmxMPK3KMLmxPK4 was cleaved with NcoI and NotI resulting in 4241 bp and 1233 bp DNA fragments, followed by isolation of the 1233 bp NcoI/NotI DNA fragment. pJCLmxMPK3KMLmxMKKmut2 and pJCduetLinker were also cleaved with NcoI/NotI, resulting in 1243 bp and 4260 bp DNA fragments from pJCLmxMPK3KMLmxMKKmut2 and a 3165 bp DNA fragment

from pJCduetLinker (Fiugure 5.8 A). The 4260 bp NcoI/NotI DNA fragment derived from pJCLmxMPK3KMLmxMKKmut2 and the 3165 bp NcoI/NotI DNA fragment derived from pJCduetLinker were isolated and dephosphorylated. Both fragments were ligated with the 1233 bp NcoI/NotI DNA fragment from pJCLmxMPK3KMLmxPK4 and transformed into *E. coli* DH5α (Figure 5.8 B). Furthermore, restriction analysis was performed; i) pJCLmxMPK3KMLmxMKKmut2 with BamHI and HindIII (801 bp, 1189 bp, and 3503 bp), BglII (1493 bp and 4021 bp), and NdeI (665 bp and 4828 bp), which resulted in the expected fragments (Figure 5.8 C); ii) pJCLmxMPK3KM with BamHI and HindIII (1189 bp and 3209 bp), KpnI, (771 bp and 3627 bp) and NdeI (665 bp and 3733 bp), which also resulted in the correct fragments (Figure 5.8 D). This confirmed the successful generation of the corrected plasmids for pJCLmxMPK3KMLmxMKKmut2 and pJCLmxMPK3KM.

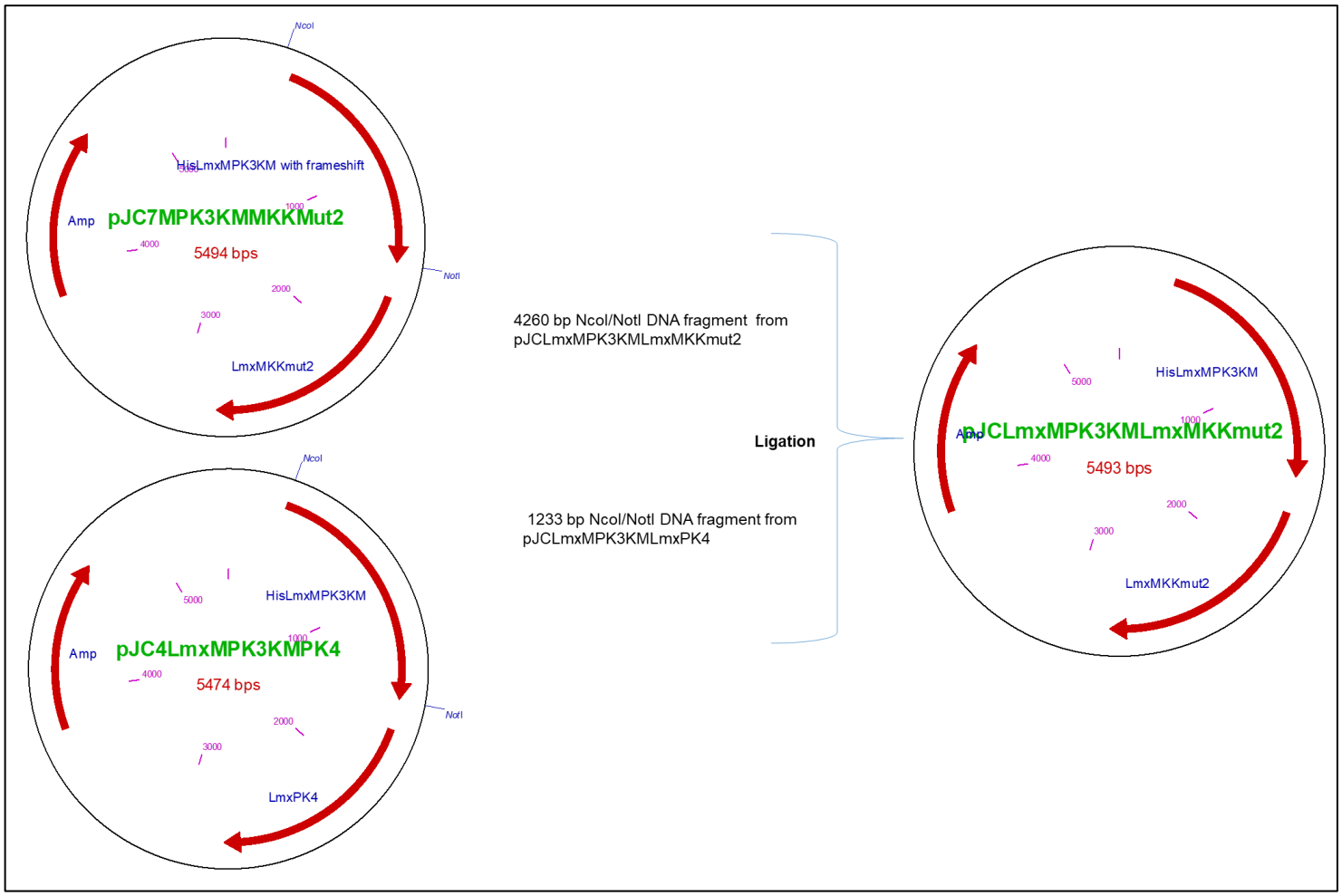

Figure 5.6. Cloning history of pJCLmxMPK3KMLmxMKKmut2 carrying correct open reading frame of LmxMPK3KM. The 4260 bp NcoI/NotI DNA fragment from pJCLmxMPK3KMLmxMKKmut2 was ligated with the 1233 bp NcoI/NotI DNA fragment from pJCLmxMPK3KMLmxPK4 to generate pJCLmxMPK3KMLmxMKKmut2 carrying correct open reading frame of LmxMPK3KM. Amp, ampicillin selectable marker.

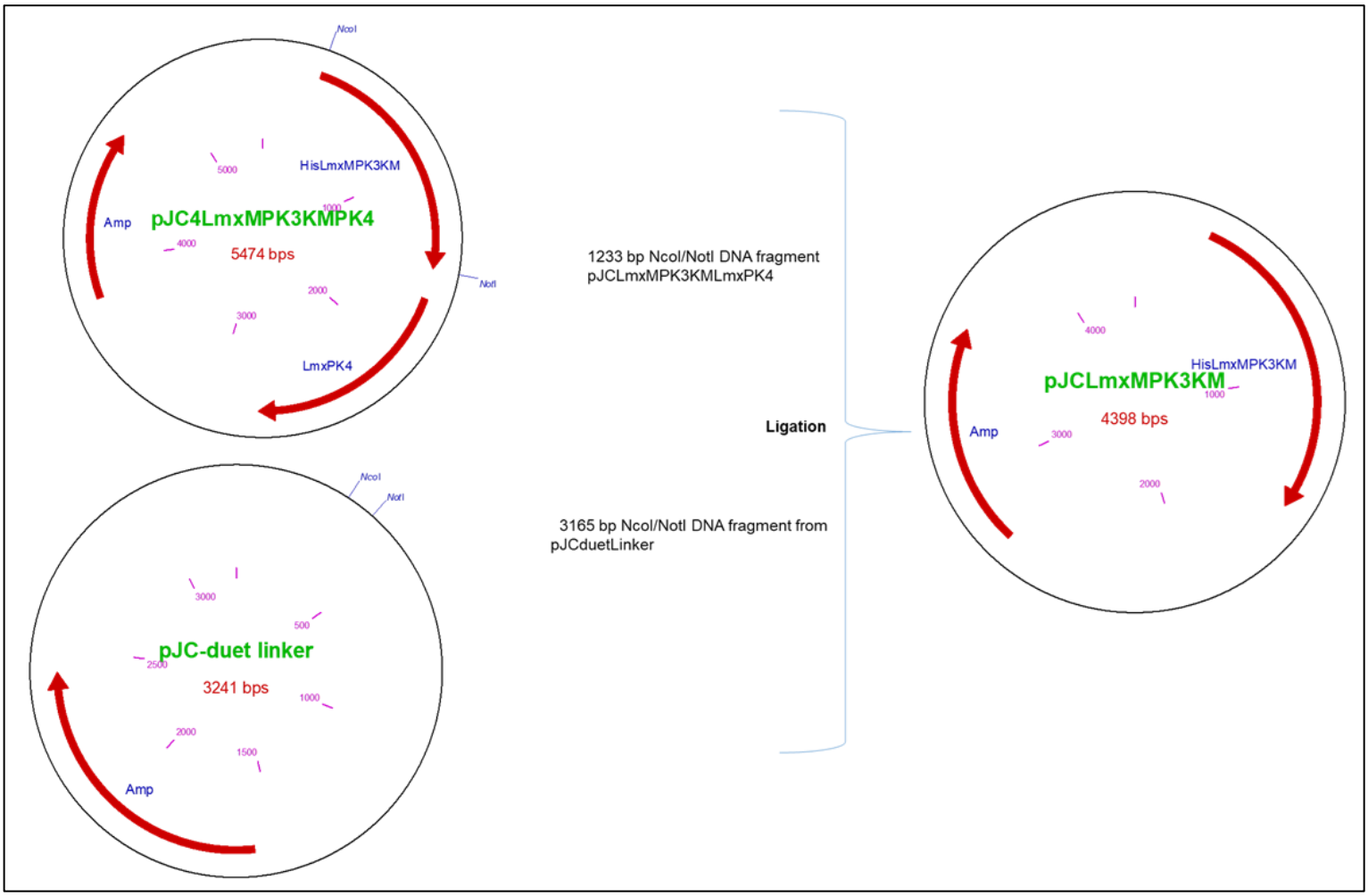

Figure 5.7. Cloning history of pJCLmxMPK3KM carrying correct open reading frame of LmxMPK3KM. The 1233 bp NcoI/NotI DNA fragment from pJCLmxMPK3KMLmxPK4 was ligated with the 3165 bp NcoI/NotI DNA fragment from pJCduetLinker to generate pJCLmxMPK3KM carrying correct open reading frame of LmxMPK3KM. Amp, ampicillin selectable marker.

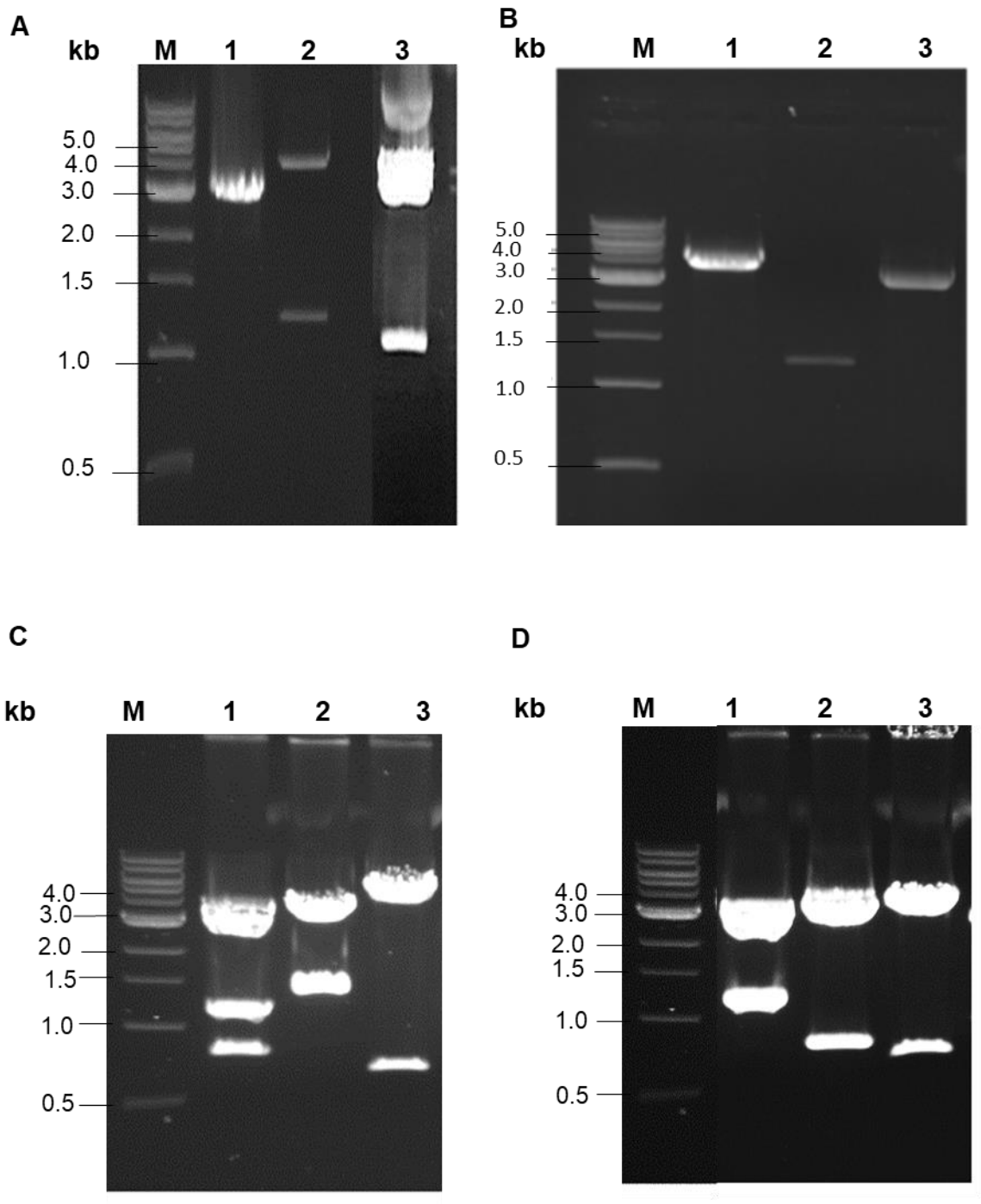

Figure 5.8. Generation of pJCLmxMPK3KMLmxMKKmut2 and pJCLmxMPK3KM carrying correct open reading frame of LmxMPK3KM. Preparative cleavage of pJCduetLinker, pJCLmxMPK3KMLmxPK4 and pJCLmxMPK3KMLmxMKKmut2 cleaved with NcoI and NotI. **A)** Lane 1, pJCduetLinker, resulting in 3165 bp DNA fragment; lane 2, pJCLmxMPK3KMLmxPK4, resulting in 4241 bp and 1233 bp DNA fragments; lane 3, pJCLmxMPK3KMLmxMKKmut2, resulting in1243 bp and 4260 bp DNA fragments. **B)** Isolated NcoI/NotI DNA fragments from pJCLmxMPK3KMLmxMKKmut2, pJCLmxMPK3KMLmxPK4 and pJCduetLinker**.** Lane 1, 4260 bp NcoI/NotI DNA fragment from pJCLmxMPK3KMMKKmut2; lane 2, 1233 bp NcoI/NotI DNA fragment from

pJCLmxMPK3KLmxMPK4; lane 3, 3165 bp NcoI/NotI DNA fragment from pJCduetLinker; **C)** Restriction analysis of pJCLmxMPK3KMLmxMKKmut2. Lane 1, cleavage with BamHI and HindIII, resulting in 801bp,1189 bp and 3503 bp DNA fragments; lane 2, cleavage with BglII, generating 1493 bp and 4021 bp DNA fragments; lane 3, cleavage with NdeI, resulting in 665 bp and 4828 bp DNA fragments and **D)** Restriction analysis of pJCLmxMPK3KM. Lane 1, cleavage with BamHI and HindIII, resulting in 1189 bp and 3209 bp DNA fragments; lane 2, cleavage with KpnI, generating 771 bp and 3627 bp DNA fragments; lane 3, cleavage with NdeI, resulting in 665 bp and 3733 bp DNA fragments. M, DNA size marker.

5.2.2 Protein purification of recombinant versions of LmxMPK3

The following plasmids were used for protein expression in *E. coli* [paPlaclQ]: His-LmxMPK3 was expressed using pJCLmxMPK3, His-LmxMPK3KM was expressed using pJCLmxMPK3KM, His-LmxMPK3KM phosphorylated by LmxPK4 was expressed using pJCLmxMPK3KMLmxPK4, His-LmxMPK3 phosphorylated by LmxPK4 was expressed by pJCLmxMPK3LmxPK4, His-LmxMPK3KM phosphorylated by LmxMKK was expressed by pJCLmxMPK3KMLmxMKKmut2, and His-LmxMPK3 phosphorylated by LmxMKK was expressed by pJC3LmxMPK3LmxMKK.

Plasmids	Insert 1	Insert 2
pJCLmxMPK3	His-LmxMPK3	
pJCLmxMPK3KM	His-LmxMPK3KM	
pJCLmxMPK3KMLmxPK4	His-LmxMPK3KM	LmxPK4
pJCLmxMPK3LmxPK4	His-LmxMPK3	LmxPK4
pJCLmxMPK3KMLmxMKK mut2	His-LmxMPK3KM	LmxMKK
pJC3LmxMPK3LmxMKK	His-LmxMPK3	LmxMKK

Table 5. 1.Summary of different constructs for LmxMPK3. plasmids were used for protein expression in *E. coli* [paPlaclQ].

The different forms of LmxMPK3 resulting from the various plasmids were purified via their N-terminal hexahistidine tag using cobalt-sepharose. The His-tagged proteins were kept bound to beads in washing buffer. The bead suspensions carrying the non-eluted proteins were also analysed using 14% SDS-PAGE, in which ~0.1 µg of different proteins were loaded for each lane. For samples with very low protein amounts, a maximum amount of protein bound to a 20 µL bead volume was loaded.

The proteins LmxMPK3KMLmxPK4, LmxMPK3LmxPK4, LmxMPK3KMLmxMKK, LmxMPK3LmxMKK, LmxMPK3 and LmxMPK3KM showed the expected size of 43.7 kDa on 14% SDS-PAGE (Figure 5.9).

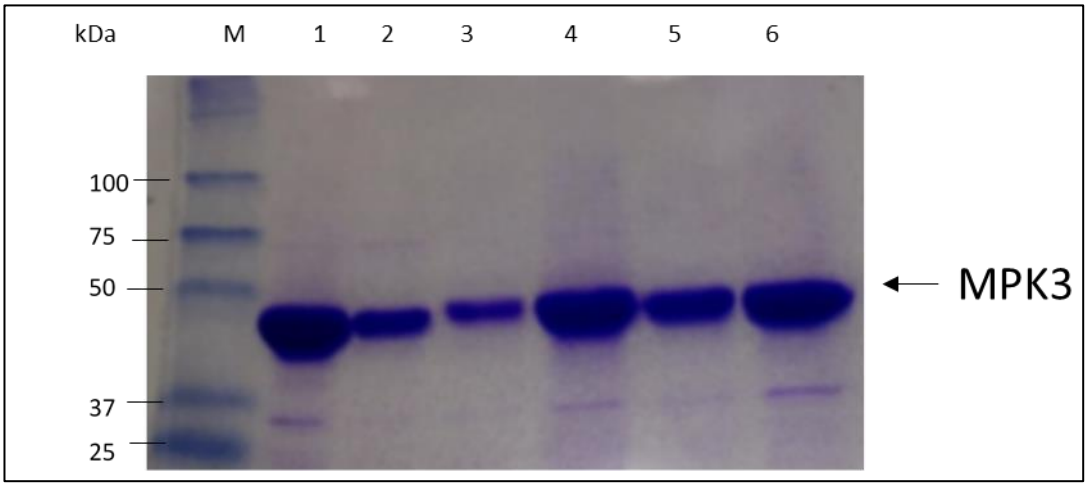

Figure 5.9. Six purified hexahistidine-tagged versions of LmxMPK3 analysed by 14% SDS-PAGE. Lane 1, LmxMPK3; lane 2, LmxMPK3KM; lane 3, LmxMPK3LmxPK4; lane 4, LmxMPK3KMLmxPK4; lane 5, LmxMPK3LmxMKK; lane 6, LmxMPK3KMLmxMKKmut2. Recombinant proteins were isolated from *E. coli*. The expected size of 43.7 kDa .M, protein size marker.

5.2.3 Activation of LmxMPK3 by LmxMKK and LmxPK4

His-LmxMPK3 or His-LmxMPK3KM bound to sepharose beads from the different expression constructs were tested using kinase assays with MBP as a generic substrate at 27°C and for different lengths of incubation. Each reaction was terminated by boiling after the addition of 5× SSB/DTT. The samples were separated using 14% SDS-PAGE. The gel was stained with Coomassie Brilliant Blue and dried. It showed bands of the expected size of His-LmxMPK3 (43.7 kDa). The activity of the different versions of His-LmxMPK3 were determined using a radiometric kinase activity assay, autoradiography and phosphorimaging.

His-LmxMPK3 was used as a positive control to show the basic activity of the kinase. Figure 5.10 did not show autophosphorylation of His-LmxMPK3 at 5 and 10 min incubation time at different exposure times (30 min, 1 h, 3 h and 24 h). However, His-LmxMPK3 showed autophosphorylation when it was incubated for 15 min and exposed for 24 h. This autophosphorylation was present as a single band.

On other hand, His-LmxMPK3KM is a kinase-dead version and was expected to show no activity, as a negative control. However, it showed clearly visible substrate phosphorylation at 15 minutes of incubation and 3 h exposure (Figure 5.10; 4C).

Moreover, His-LmxMPK3 co-expressed with LmxMKK was used as a positive control for an activation of a MAPK by a co-expressed MAP2K. His-LmxMPK3 co-expressed with LmxMKK or LmxPK4 showed substrate phosphorylation activity (MBP) after a 5 min assay followed by 30 min exposure of the autoradiograph. This reaction increased for the different times of exposure and incubation times. His-LmxMPK3 co-expressed with LmxPK4 or LmxMKK showed two bands for autophosphorylation when it was incubated for 5, 10 or 15 min at 1 h exposure time. Longer exposure increased the intensity of the bands, leading to less resolution on the autoradiograph (Figure 5.10)

Additionally, His-LmxMPK3KM co-expressed with LmxPK4 or LmxMKK did not show substrate phosphorylation activity (MBP) at 5 min when exposing the gel to a film for 30 min and 1 h. However, His-LmxMPK3KM co-expressed with LmxMKK showed phosphorylation of MBP in a 15 min assay followed by 1 h exposure of the gel to a film. Longer exposure times revealed substrate phosphorylation of LmxMPK3KM co-expressed with LmxPK4 or LmxMKK. Moreover, the double band for autophosphorylation was clearly visible in the 24 h exposure in all samples containing LmxMPK3KM co-expressed with a MAP2K (Figure 5.10).

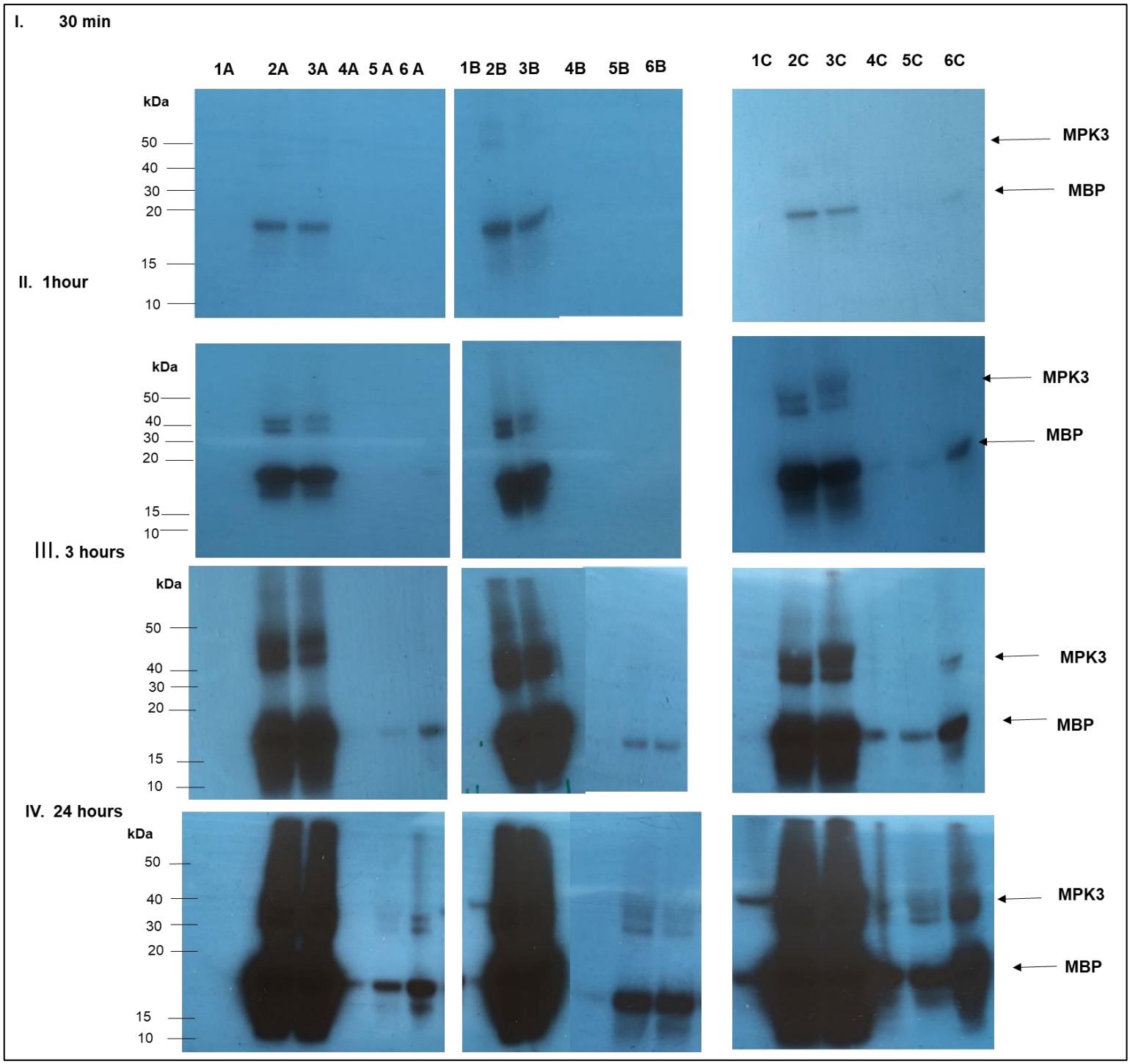

Figure 5.10. Autoradiographs of LmxMPK3 kinase assays exposed for different lengths of time; incubation of assay for 5 min (A), 10 min (B), and 15 min (C). Lane 1 (A, B, C), His-LmxMPK3; lane 2 (A, B, C), His-LmxMPK3LmxPK4; lane 3 (A, B, C), His-LmxMPK3LmxMKK; lane 4 (A, B, C), His-LmxMPK3KM; lane 5 (A, B, C), His-LmxMPK3KMLmxPK4; lane 6 (A, B, C), His-LmxMPK3KMLmxMKKmut2. Autoradiography at different time points of X-ray exposure; (I) 30 min, (II) 1 h, (III) 3 h, and (IV) 24 h.

For phosphorimaging (Figure 5.11), an exposure of the gel for 24 h was chosen. The different versions of His-LmxMPK3 showed an increase in kinase activity over time. His-LmxMPK3 co-expressed with LmxPK4 or LmxMKK showed strong MBP phosphorylation. Interestingly, His-LmxMPK3KM showed very weak MBP phosphorylation co-expressed with LmxPK4 or LmxMKK. His-LmxMPK3 and His-LmxMPK3KM showed no MBP phosphorylation but showed some autophosphorylation for His-LmxMPK3.

Quantitative phosphorylation analysis was used to study the activity of the different versions of His-LmxMPK3 by phosphorimaging. In figure 5.12 showed that His-LmxMPK3 and His-LmxMPK3KM showed no MBP phosphorylation. His-LmxMPK3 co-expressed with LmxPK4 or LmxMKK showed increasing substrate phosphorylation activity with an increase in incubation time from 2 min to 10 min. Surprisingly, His-LmxMPK3KM co-expressed with any of the MAP2Ks led to some increase of MBP phosphorylation over time, albeit by far not as pronounced as for His-LmxMPK3. His-LmxMPK3 was significantly more active when co-expressed with LmxPK4 than with LmxMKK.

On other hand, relative autophosphorylation analysis was used to study autophosphorylation of the different versions of His-LmxMPK3 by phosphorimaging. Autophosphorylation of His-LmxMPK3 and of His-LmxMPK3 co-expressed with LmxMKK increased during the time between 2 min and 5 min (Figure 5.13). A decrease was noted after 10 min incubation. His-LmxMPK3 co-expressed with LmxPK4 showed a gradual increase of band intensity over time. However, His-LmxMPK3KM and His-LmxMPK3KM co-expressed with LmxMKK showed no autophosphorylation in this assay. His-LmxMPK3KM co-expressed with LmxPK4

showed a minor increase of autophosphorylation over time.

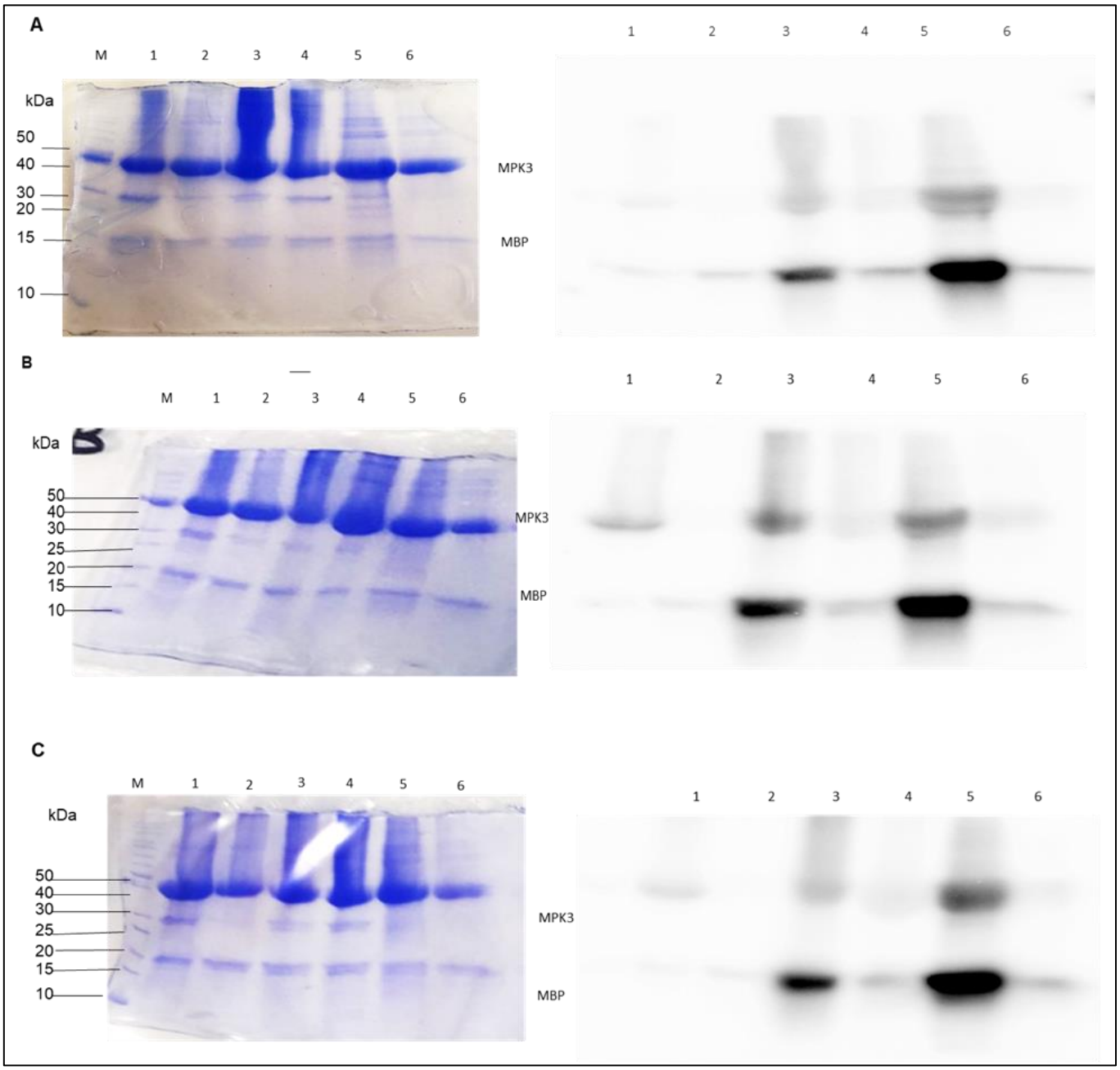

Figure 5.11. Kinase activity of different versions of His-LmxMPK3. Duration of kinase assay (A) 2 min, (B) 5 min, and (C) 10 min. Left, 14% SDS-PAGE after Coomassie-staining. Right, image taken with phosphorimager using the same settings. Lane 1, His-LmxMPK3 showing no phosphorylation of MBP; lane 2, His-LmxMPK3KM showing no phosphorylation of MBP; lane 3, His-LmxMPK3LmxMKK shows strong phosphorylation of MBP; lane 4, His-LmxMPK3KMLmxMKKmut2 shows weak phosphorylation of MBP; lane 5, His-LmxMPK3LmxPK4 shows strong phosphorylation of MBP; lane 6, His-LmxMPK3KMLmxPK4 shows weak phosphorylation of MBP. Visualised using a Typhoon 9200 phosphorimager after exposure for 24 h (Piscataway, NJ).

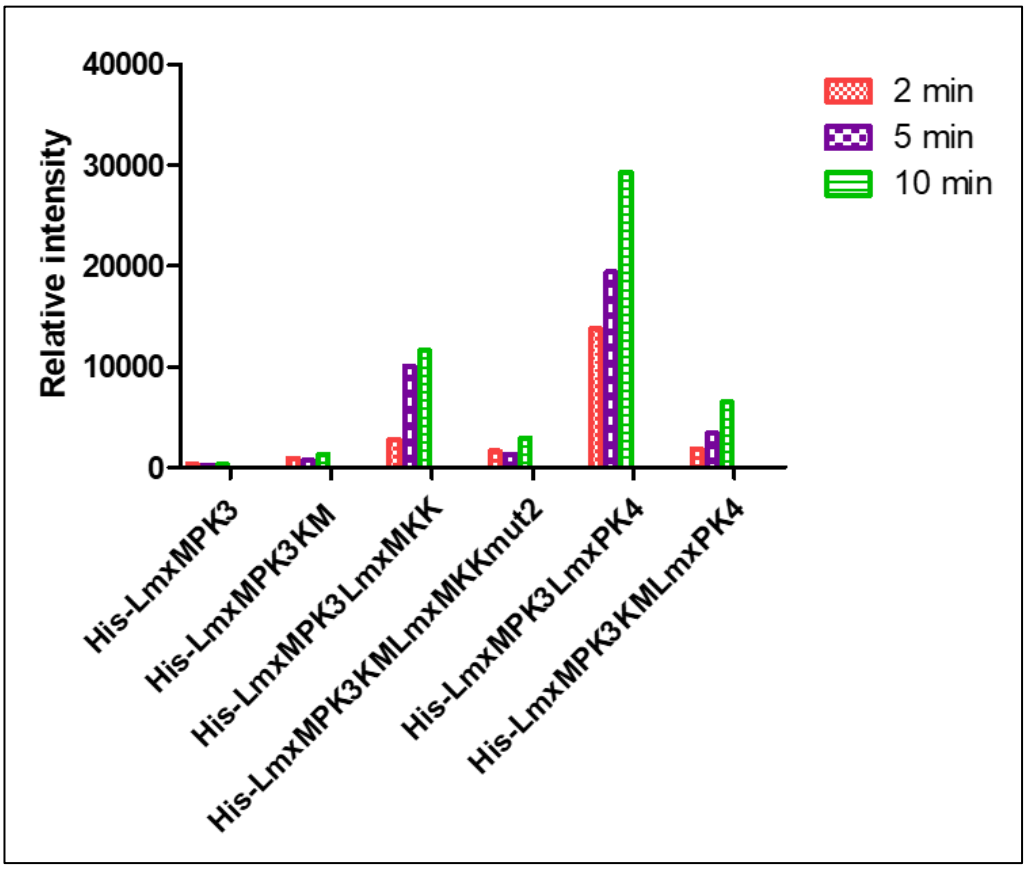

Figure 5.12. Relative quantitative phosphorylation of MBP by different versions of LmxMPK3. The histogram was plotted from the results in Figure 5.11. Relative phosphorylation intensity of MBP for different versions of His-LmxMPK3 after different times of incubation (2 min, 5 min, and 10 min) and normalisation according to the amounts of kinase present in the assay.

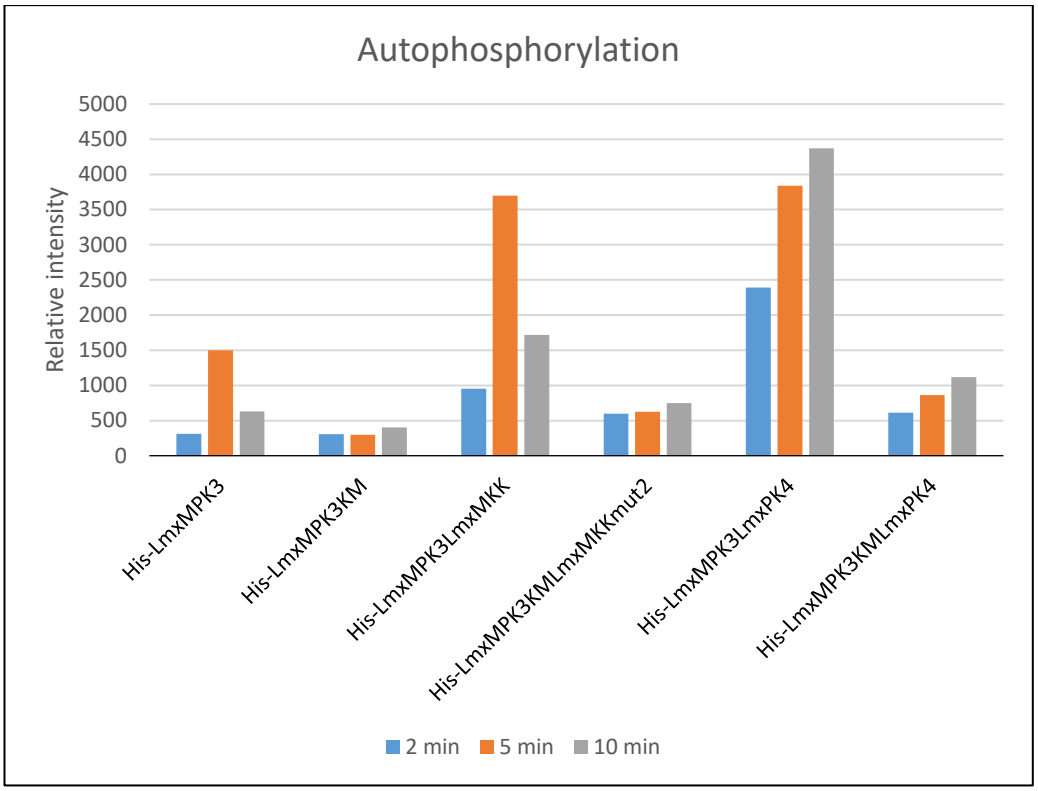

Figure 5.13. Relative quantitative autophosphorylation of different versions of LmxMPK3. The histogram was plotted from the results in figure 5.11. Relative autophosphorylation intensity for the different versions of His-LmxMPK3 after different times of incubation (2 min, 5 min, and 10 min) and normalisation according to the amounts of kinase present in the assay.

5.2.4 Phosphorylation analysis of LmxMPK3 co-expressed with LmxPK4

Phosphopeptide identification was performed by tandem mass spectrometry (MS/MS) to identify phosphorylated residues in His-LmxMPK3/His-LmxMPK3KM after co-expression with LmxPK4 (Table 5.2) or LmxMKK (Table 5.3), followed by purification from *E. coli*. Phosphorylated peptides present in both LmxMPK3 and His-LmxMPK3KM co-expressed with LmxPK4 are shown in yellow in table 5.2 and indicate phosphorylation by LmxPK4. Orange is for peptides with missed tryptic cleavage. Blue is for unique phosphopeptides for kinase-dead LmxMPK3KM, indicating phosphorylation by LmxPK4. The white peptides which are unique in the His-LmxMPK3 sample indicate autophosphorylation. Table 5.3 shows the results for

co-expression with His-LmxMKK; blue is for phosphorylated peptides present in both His-LmxMPK3 and His-LmxMPK3KM, which indicates phosphorylation by His-LmxMKK. Light yellow shows unique phosphopeptides for kinase-dead His-LmxMPK3KM, indicating phosphorylation by His-LmxMKK. White is for unique phosphopeptides for His-LmxMPK3, indicating autophosphorylation. A Mascot score of >20 indicates a reliable identification.

LmxMPK3PK4	Mascot score	LmxMPK3KMPK4	Mascot score	interpretaion
LVPGLAGNTEGIDFLSK	84	LVPGLAGNTEGIDFLSK	78	phosphorylated by LmxPK4
LVPGLAGNTEGIDFLSK	64	LVPGLAGNTEGIDFLSK	72	phosphorylated by LmxPK4
SVDVPYSELTDYVITR	70	SVDVPYSELTDYVITR	64	phosphorylated by LmxPK4
LVPGLAGNTEGIDFLSK	50	LVPGLAGNTEGIDFLSK	54	phosphorylated by LmxPK4
LNELPGGSLNIPK	48	LNELPGGSLNIPK	49	phosphorylated by LmxPK4
MWTLDPSK	42	MWTLDPSK	47	phosphorylated by LmxPK4
IIDFGLSR	39	IIDFGLSR	40	phosphorylated by LmxPK4
SNQELSVPK	41	SNQELSVPK	31	phosphorylated by LmxPK4
MIAQHIGKPPASMEHR	45	MIAQHIGKPPASMEHR	27	phosphorylated by LmxPK4
DLKPANLVTNSCELK	44	DLKPANLVTNSCELK	53	phosphorylated by LmxPK4
		LNELPGGSLNIPKLVPGLAGNTEGIDFLSK	53	phosphorylated by LmxPK4
		SNQELSVPKVVGDFK	23	phosphorylated by LmxPK4
		SVDVPYSELTDYVITR	81	phosphorylated by LmxPK4
		SVDVPYSELTDYVITR	41	phosphorylated by LmxPK4
		DLKPANLVTNISCELK	23	phosphorylated by LmxPK4
		ILGMGAYGIACSCLDGDTGEKVSIMK	40	phosphorylated by LmxPK4
ILGMGAYGIACSCLDGDTGEKVSKK	45			LmxMPK3 autophosphorylation
VYNVSGSPFEVPSK	55			LmxMPK3 autophosphorylation
VYNVSGSPFEVPSK	43			LmxMPK3 autophosphorylation

Table 5.2. Phosphoproteomics analysis of His-LmxMPK3 and His-LmxMPK3KM co-expressed with LmxPK4 in *E. coli.* Phosphorylated serine, threonine and tyrosine residues are shown in red.

LmxMPK3MKK	Macot result	LmxMPK3KMMKK	Macot Score	Interpretation
SVDVPYSELTDYVITR	70	SVDVPYSELTDYVITR	84	Phosphorylated by LmxMKK
LVPGLAGNTEGIDFLSK	59	LVPGLAGNTEGIDFLSK	51	Phosphorylated by LmxMKK
MIAQHIGKPPASIVEHR	30	MIAQHIGKPPASIVEHR	30	Phosphorylated byLmxMKK
SVDVPYSELTDYVITR	56	SVDVPYSELTDYVITR	67	Phosphorylated by LmxMKK
SNQELSVPK	28	LNELPGGSLNIPK	38	Phosphorylated by LmxMKK
		SNQELSVPK	26	Phosphorylated by LmxMKK
LVPGLAGNTEGIDFLSK	50			LmxMPK3 autophosphorylation
QVLEESHMQYFVYQILR	33			LmxMPK3 autophosphorylation
SNQELSVPK	26			LmxMPK3 autophosphorylation

Table 5.3. Phosphoproteomics analysis of His-LmxMPK3 and His-LmxMPK3KM co-expressed with LmxMKK in *E. coli.* Phosphorylated serine, threonine and tyrosine residues are shown in red.

When using the SWISS-Model (https://swissmodel.expasy.org/) to attempt to model the structure of LmxMPK3, the program identified the already available crystal structure of the *L. donovani* homologue, which has 98.89% amino acid sequence identity with LmxMPK3. The crystal structure of LdoMPK3 from *L. donovani* (PDB 4O2Z) was obtained in the presence of NVP-BBT594 at 2.7Å resolution.

The localisation of the identified phosphorylation sites is shown in Figure 5.14. Phosphorylated THR194, TYR196 and SER259 residues were present in both His-LmxMPK3 and His-LmxMPK3KM co-expressed with LmxMKK or LmxPK4. Phosphopeptides containing SER9 and SER277 were also present in both His-LmxMPK3 and His-LmxMPK3KM co-expressed with LmxPK4. Surprisingly, SER277 residues were also phosphorylated in kinase-dead LmxMPK3KM co-expressed with LmxMKK. THR169, SER183 and SER298 were found to be phosphorylated in His-LmxMPK3 and kinase-dead His-LmxMPK3KM co-expressed with LmxPK4. Interestingly, phosphorylated SER172, THR55 and THR199 residues were found only in kinase-dead LmxMPK3KM co-expressed with LmxPK4. SER23, SER25, SER60 and SER136 were present as autophosphorylation residues in His-LmxMPK3 co-expressed with LmxMKK or LmxPK4.

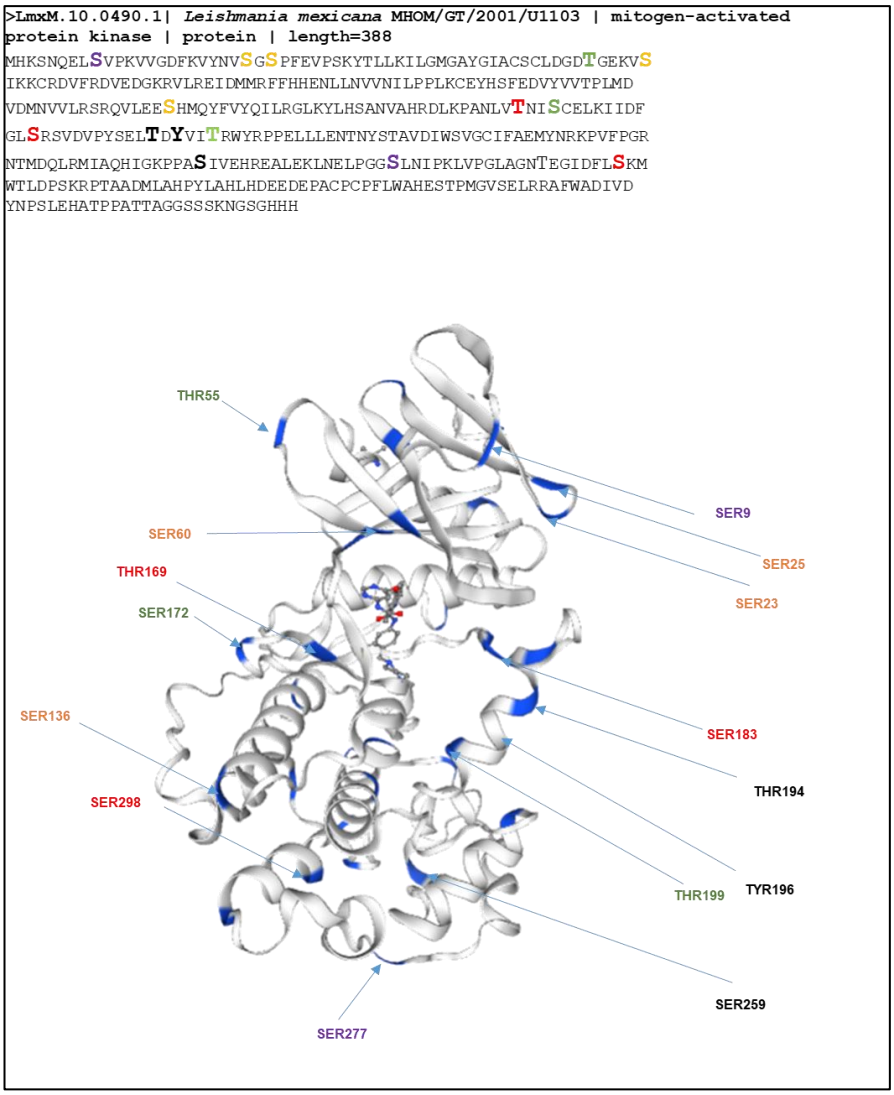

Figure 5.14. Localisation of LmxMPK3 phosphorylation sites mapped on *L. donovani* MPK3 (PDB 4O2Z). All serine and threonine residues in the structure are highlighted. Amino acid names in different colours indicate phosphorylation site identification in different co-expression samples. Black, phosphorylation sites identified in LmxMPK3 and LmxMPK3KM after co-expression with LmxPK4 or LmxMKK; purple, phosphorylation sites in LmxMPK3KM co-expressed with LmxPK4 or LmxMKK and LmxMPK3 co-expressed with LmxPK4 but not LmxMKK; red, phosphorylation sites of LmxMPK3 and LmxMPK3KM co-expressed with LmxPK4; green, phosphorylation sites of LmxMPK3KM co-expressed with LmxPK4; orange, autophosphorylation sites residues in His-LmxMPK3 co-expressed with LmxMKK or LmxPK4.

5.2.5 Interaction between LmxMPK3 and LmxPK4 *in vivo*

In MAPK pathways MAP2Ks (LmxPK4) activate MPKs (LmxMPK3) by phosphorylation. *In vitro* studies showed that LmxPK4 activated LmxMPK3 by

phosphorylation in the TXY motif. However, it is not known whether this interaction occurs in living cell of *L. mexicana* promastigotes. Here, the split-GFP system is used to attempt to observe the interaction between LmxMPK3 and LmxPK4 *in vivo*.

5.2.5.1 Protein–protein interaction of LmxPK4 with LmxMPK3 in *L. mexicana* using tripartite split GFP

In the tripartite split-GFP complementation assay, the β-strand 10β (GFP10) of GFP was fused to one interaction partner, the β-strand 11β (GFP11) of GFP was fused to a second interaction partner and β-strands 1–9 of GFP form the detector molecule. When the two interaction partners GFP10LmxPK4 and LmxMPK3GFP11 bind to each other, they cause β-strands 10 and 11 to align, which in turn can then interact with β-strands 1–9 to form a functional GFP molecule detectable by fluorescence (Figure 5.15).

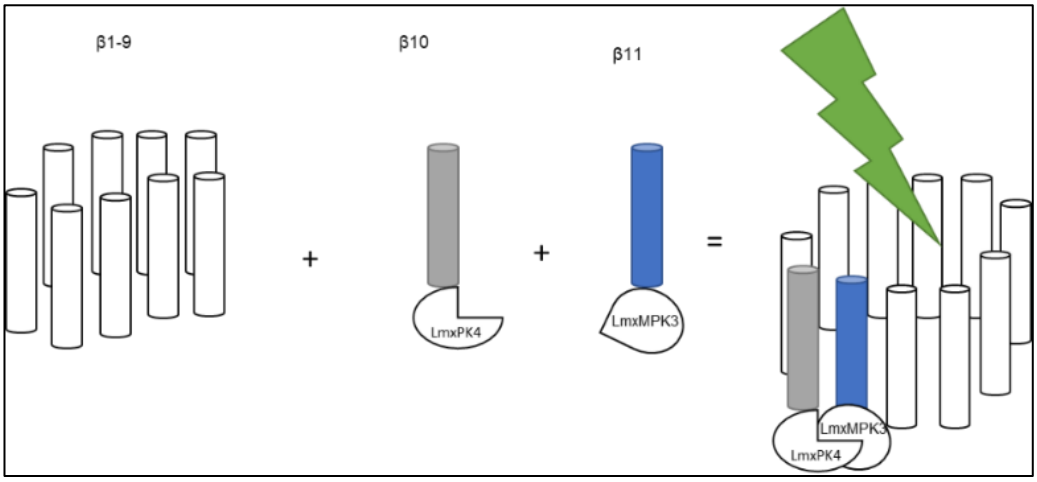

Figure 5.15. Principle of tripartite split GFP. It is composed of the beta-strands GFP1-9 (β1-9) as a detector molecule, the beta-strand GFP10 (β10) fused to the C-terminus of LmxPK4 and the beta-strand GFP11 (β11) fused to the N-terminus of LmxMPK3**.** Fluorescence can only occur when LmxPK4 and LmxMPK3 interact, leading to the assembly of all β-strands of GFP to from a functional fluorescent protein.

5.2.5.1.1 Generation of a tri-GFP construct to test LmxPK4–LmxMPK3 protein interaction

The potential interactions between LmxMPK3 and LmxPK4 *in vivo* was investigated by split tri-GFP. To this end, the pSSUPacTriGFP10LmxPK4LmxMPK3GFP11 construct was generated, which allows integration into the ribosomal RNA gene locus to achieve homogeneous expression of all three components, GFP1-9, GFP10-*LmxPK4*, and *LmxMPK3GFP11*. The cloning history started by generating pSSUPacTriGFP10LmxPK4 (Figure 5.16). pB-LmxPK4-3 was cleaved with BamHI to generate 1072 bp and 2964 bp DNA fragments, and the 1072 bp BamHI-DNA fragment carrying LmxPK4 from pB-LmxPK4-3 was isolated. pSSUPacTriGFP was linearised with BamHI, resulting in 10983 bp BamHI-DNA fragment, which contains GFP1-9, GFP10 and GFP11, followed by isolation and dephosphorylation (Figure 5.17 A). The 1072 bp BamHI-DNA fragment from pB-LmxPK4-3 and 10983 bp BamHI-DNA fragment from pSSUPacTriGFP were ligated and transformed into *E. coli* DH5α to generate pSSUPacTriGFP10LmxPK4 (Figure 5.17 B). The identity of the plasmid was verified by restriction analysis with XbaI (2657 bp, 9398 bp), MfeI (2987 bp, 9068 bp) and BamHI (1072 bp, 10983 bp) (Figure 5.17 C).

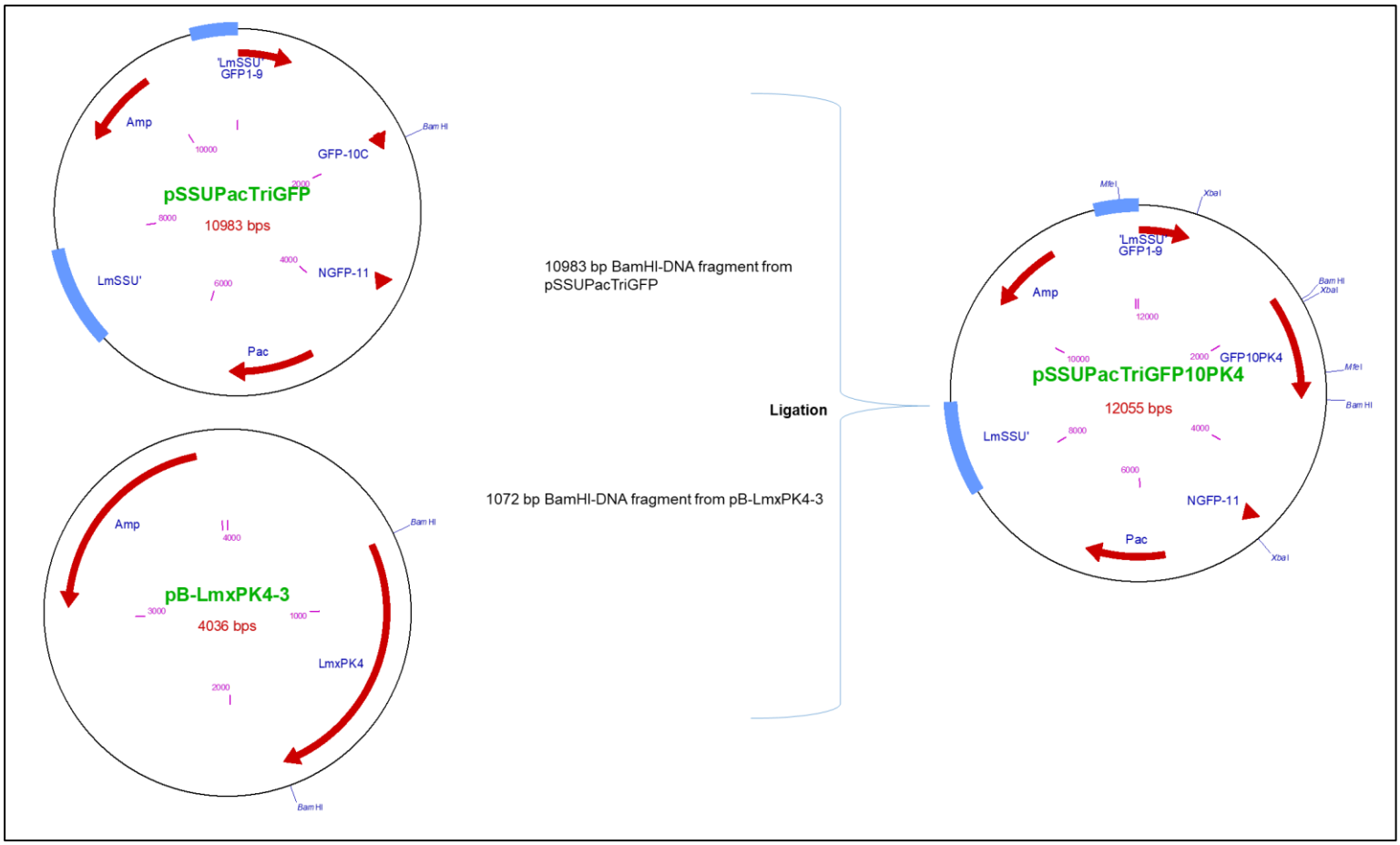

Figure 5.16. Cloning history for the generation of pSSUPacTriGFP10LmxPK4. The 10983 bp BamHI-DNA fragment from pSSUPacTriGFP was ligated with the 1072 BamHI-DNA fragment from pB-LmxPK4-3 to generate pSSUPacTriGFP10LmxPK4. Amp, ampicillin selectable marker. Lmssu (18S rRNA); Pac, purmycin antibiotic resistance gene, and Amp, ampicillin selectable marker.

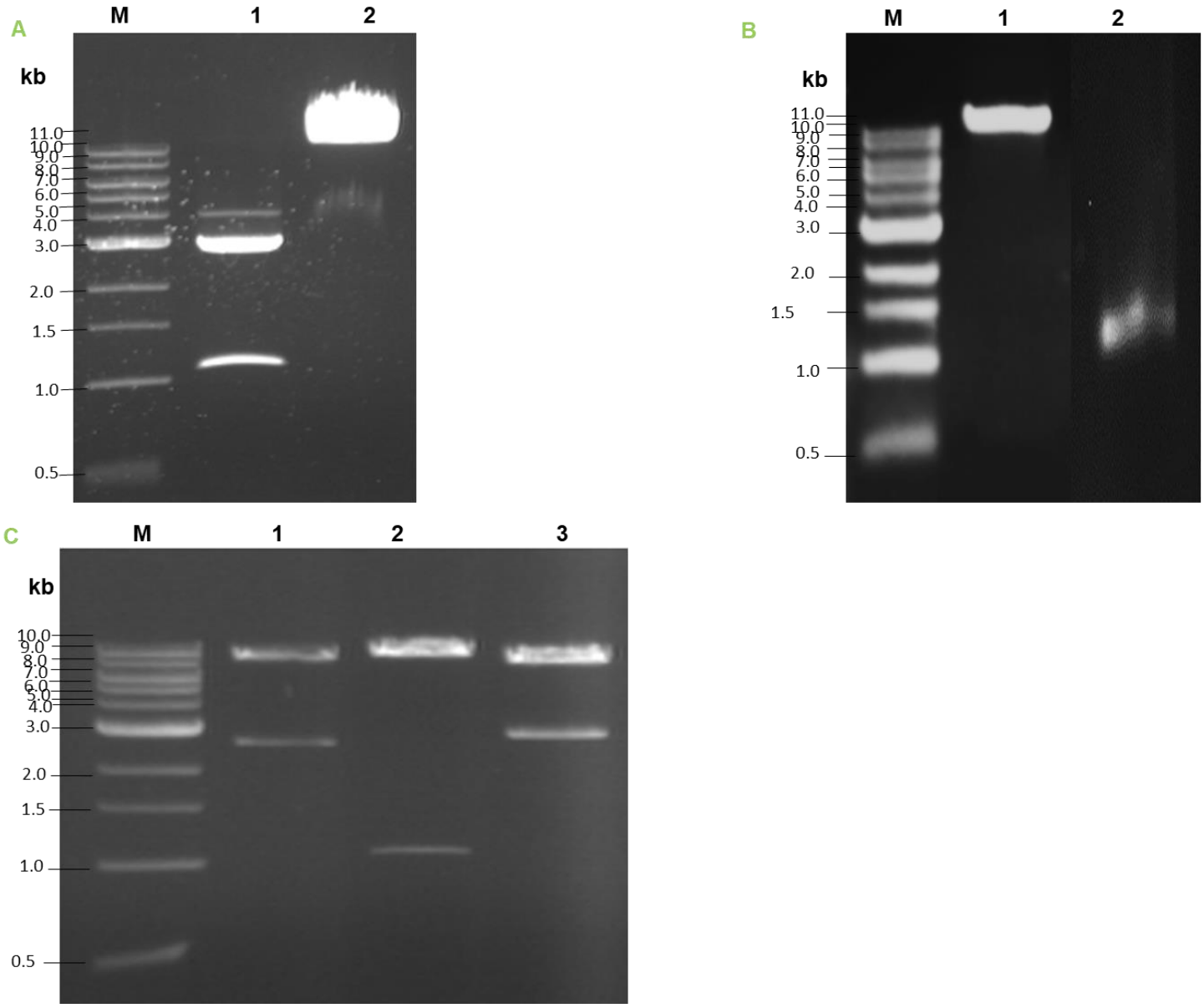

Figure 5.17. Generation of pSSUPacTriGFP10LmxPK4. A) Preparative cleavage of pB-LmxPK4-3 and pSSUPacTriGFP with BamHI**.** Lane 1, pB-LmxPK4-3, 1072 bp and 2964 bp DNA fragments; lane 2, pSSUPacTriGFP, 10983 DNA fragment. **B)** Isolated DNA fragments from pB-LmxPK4-3 and pSSUPacTriGFP. Lane 1, 10983 bp BamHI-DNA fragment from pSSUPacTriGFP; lane 2, 1072 bp BamHI-DNA fragment from pB-LmxPK4-3. **C)** Restriction analysis of pSSUPacTriGFP10LmxPK4. Lane 1, XbaI, generating 2657 bp and 9398 bp DNA fragments; lane 2, BamHI, resulting in 1072 bp and 10983 bp DNA fragments; and lane 3, MfeI, generating 2987 bp and 9068 bp DNA fragments. M, DNA size marker.

Subsequently, to generate pSSUPacTriGFP10LmxPK4LmxMPK3GFP11 (Figure 5.18), pSSUPacTriGFP10LmxPK4 was cleaved with NsiI, PmeI and BglII to generate 1390 bp, 4416 bp and 6249 bp DNA fragments, followed by isolation of the 6249 bp DNA fragment carrying GFP1-9 and GFP10-LmxPK4. The pSSUPacTriGFP10LmxMKKLmxMPK3GFP11 was cleaved with NsiI, PmeI and XhoI to generate 269 bp, 6964 bp, 3103 bp, and 2912 bp DNA fragments followed by the isolation of the 6964 bp DNA fragment carrying LmxMPK3-GFP11. The 6249 bp NsiI/PmeI DNA fragment from pSSUPacTriGFP10LmxPK4 and 6964 bp NsiI/PmeI DNA fragment from pSSUPacTriGFP10LmxMKKLmxMPK3GFP11 were ligated and transformed into *E. coli* to generate pSSUPacTriGFP10LmxPK4LmxMPK3GFP11 (Figures 5.19 A and B). The plasmid was verified by DNA sequencing to confirm the successful generation of pSSUPacTriGFP10LmxPK4LmxMPK3GFP11.

Finally, pSSUPacTriGFP10LmxPK4LmxMPK3GFP11 was cleaved with PmeI and PacI to generate 10555 bp and 2658 bp DNA fragments (not shown). The 10555 bp PmeI/PacI DNA fragment, which carried GFP1-9, GFP10-LmxPK4 and LmxMPK3-GFP11 was isolated under sterile conditions for transfection into promastigotes of LmxMPK3 null mutants (ΔLmxMPK3-/- HN6) and *L. mexicana* wild type (Figures 5.19 C and D).

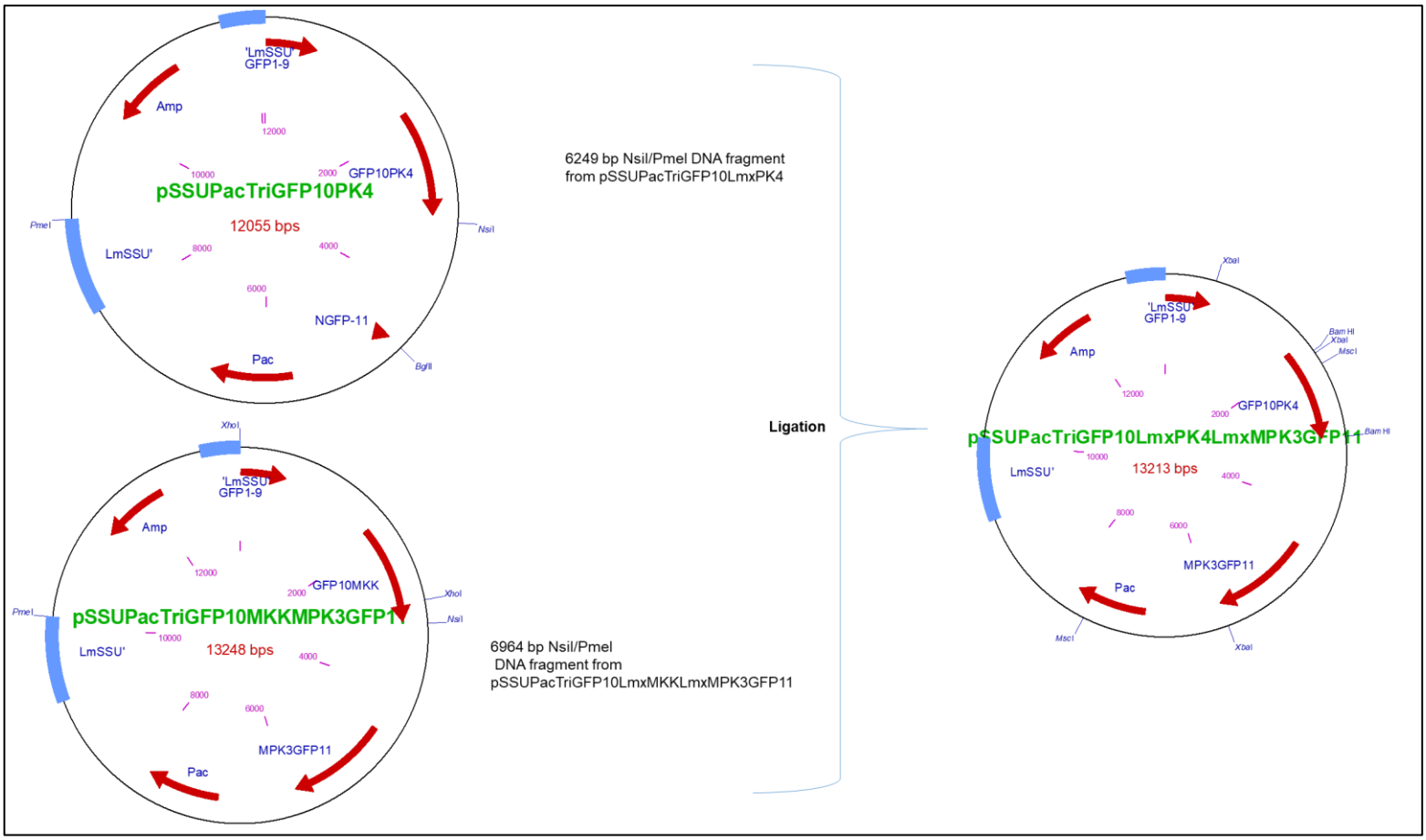

Figure 5.18. Cloning history for the generation of pSSUPacTriGFP10LmxPK4 LmxMPK3GFP11. The 6249 bp NsiI/PmeI DNA fragment from pSSUPacTriGFP10LmxPK4 was ligated with the 6964 bp NsiI/PmeI DNA fragment from pSSUPacTriGFP10LmxMKKLmxMPK3GFP11 to generate pSSUPacTriGFP10LmxPK4 LmxMPK3GFP11. Lmssu (18S rRNA); Pac, puromycin antibiotic resistance gene; and Amp, ampicillin selectable marker.

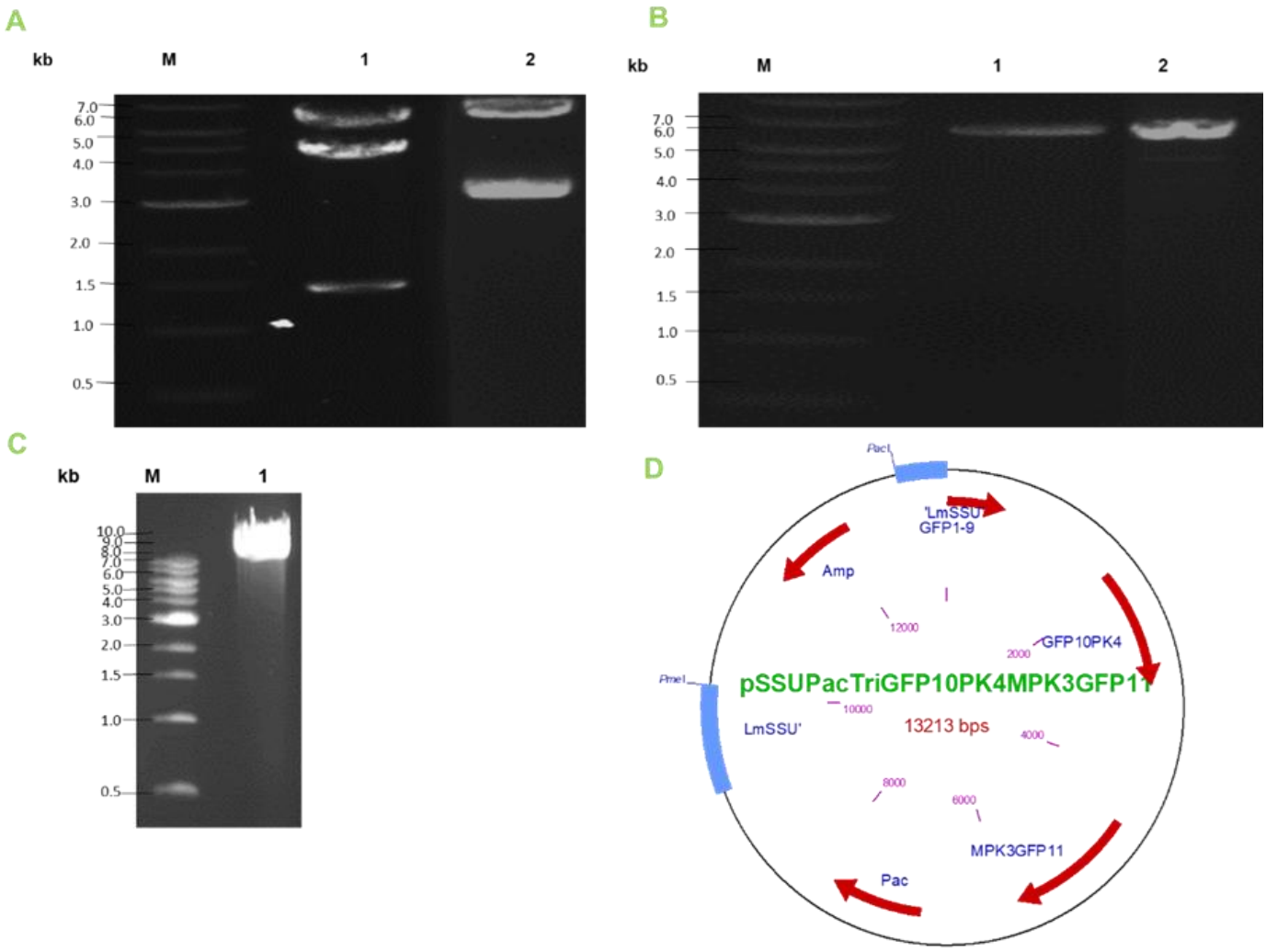

Figure 5.19. Generation of pSSUPacTriGFP10LmxMKKLmxMPK3GFP11. A) Preparative cleavage of pSSUPacTriGFP10LmxPK4 and pSSUPacTriGFP10LmxMKK LmxMPK3GFP11. Lane 1, pSSUPacTriGFP10LmxPK4 cleaved simultaneously with NsiI, PmeI and BglII to generate 1390 bp, 4416 bp and 6249 bp DNA fragments; lane 2, pSSUPacTriGFP10LmxMKKLmxMPK3GFP11 cleaved with NsiI, PmeI and XhoI to obtain 269 bp, 6964 bp, 3103 bp and 2912 bp DNA fragments**. B)** Isolated DNA fragments from pSSUPacTriGFP10LmxMKK LmxMPK3GFP11 and pSSUPacTriGFP10LmxPK4. Lane 1, 6964 bp NsiI/PmeI DNA fragment form pSSUPacTriGFP10LmxMKK; lane 2, 6249 bp NsiI/PmeI DNA fragment from pSSUPacTriGFP10LmxPK4. **C)** Isolated DNA fragment from pSSUPacTriGFP10 LmxPK4LmxMPK3GFP11. Lane 1, 10555 bp PmeI/PacI DNA fragment. **D)** Plasmid map of pSSUPacTriGFP10LmxPK4LmxMPK3GFP11.

5.2.5.1.2 Integration of the split tri-GFP construct into the rRNA gene locus of *L. mexicana* to test LmxPK4-LmxMPK3 protein interaction

The 10555 bp PmeI/PacI DNA fragment from pSSUPacTriGFP10LmxPK4LmxMPK3GFP11 carrying *GFP1-9*, *GFP10-LmxPK4* and *GFP11LmxMPK3* was introduced into promastigotes of LmxMPK3 null mutants (∆LmxMPK3-/- HN6) and *L. mexicana* wild type. These two cell types were chosen for the following reasons. Previous attempts to re-express LmxMPK3 in the null mutant had shown that not all parasites expressing LmxMPK3 also showed wild type length flagella. This suggests that a certain amount of LmxMPK3 is required to generate these flagella. For the protein-protein interaction it was desirable to work with protein levels guaranteeing wild type function. Therefore, the LmxMPK3 null mutant was used and cells swimming normally were analysed. For re-expression of LmxPK4 in the LmxPK4 null mutants, which show longer than wild type flagella, a similar effect was never observed. It is much easier to see the change from short flagella to normal length flagella than to see the difference from elongated flagella back to normal length. Hence, only the LmxMPK3 null mutant and not the LmxPK4 null mutant was employed. *L. mexicana* wild type was used to express LmxPK4 and LmxMPK3 in case that no swimming promastigotes could be obtained from the experiment using the LmxMPK3 null mutant.

Cell proliferation was observed after 15 days of incubation at 27°C in 96-well plates. 96 wells showed growth for transfected ∆LmxMPK3-/-N/H6 in the 1:2 dilutions and 89 wells for transfected *L. mexicana* wild type. The 1:40 dilution resulted in cell growth in 55 wells for ∆LmxMPK3-/-, and 46 wells for *L. mexicana* wild type. Four putative positive cell lines of the 1:40 dilution for each cell type were selected and expanded for further analysis.

5.2.5.1.3 Fluorescence analysis of protein–protein interactions between LmxPK4 and LmxMPK3 using tripartite split GFP

The 10555 bp PmeI/PacI DNA fragment carrying GFP1-9, GFP10-LmxPK4 and GFP11LmxMPK3 derived from pSSUPacTriGFP10LmxPK4LmxMPK3GFP11, was integrated into one ribosomal RNA gene locus of ∆LmxMPK3-/- HN6. Bright field microscopy of live promastigotes showed normal length flagella in the null mutant background, indicating expression of a functional LmxMPK3 fused to GFP11 (Figure 5.20). Fluorescence microscopy did not show green fluorescence indicating no formation of a functional GFP, therefore, no images were taken. Images taken of live cells during their logarithmic (2-4 × 10^7 cells/mL) growth phase were processed using ImageJ (NIH, USA).

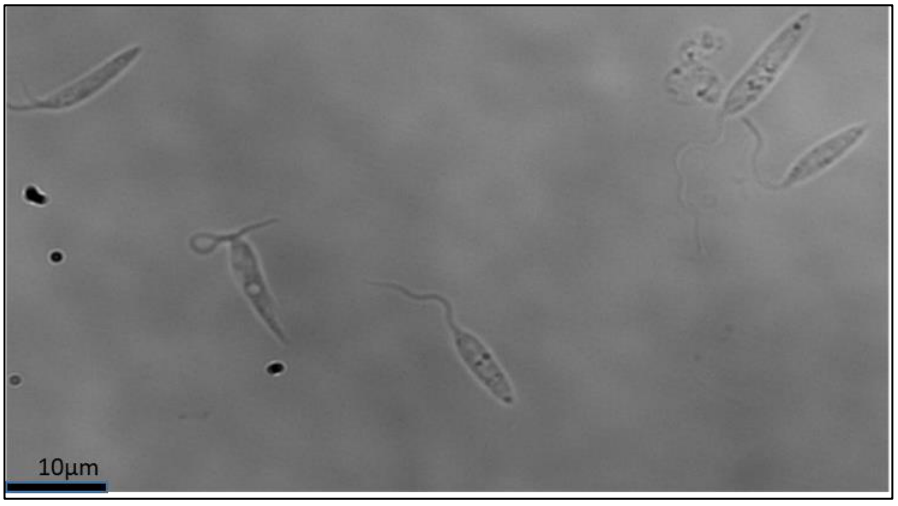

Figure 5.20. Bright field microscopy of live LmxMPK3 (∆LmxMPK3-/- HN6) null mutant promastigotes carrying the tri-GFP construct in the rRNA gene locus. The promastigotes showed normal length flagella in LmxMPK3 null mutant background. Size bar, 10 µm.

5.2.5.2 Analysis of protein–protein interaction between LmxPK4 and LmxMPK3 *in vivo* using split di-GFP

The split di-GFP system was attempted as an alternative approach because an interaction between LmxPK4 and LmxMPK3 could not be shown by the split tri-GFP

approach. For the split di-GFP system only to proteins have to join up to form a functional GFP and not three as in the split tri-GFP system. LmxPK4 was directly fused to the N-terminus of a partial GFP composed β-strands 1–10. The construct also codes for LmxMPK3 fused to β-strand GFP11, no separate detector molecule was present (GFP1-9). The expectation was that when LmxPK4 interacted with LmxMPK3, GFP11 could complement GFP1-10 to form a complete green fluorescent GFP (Figure 5.21).

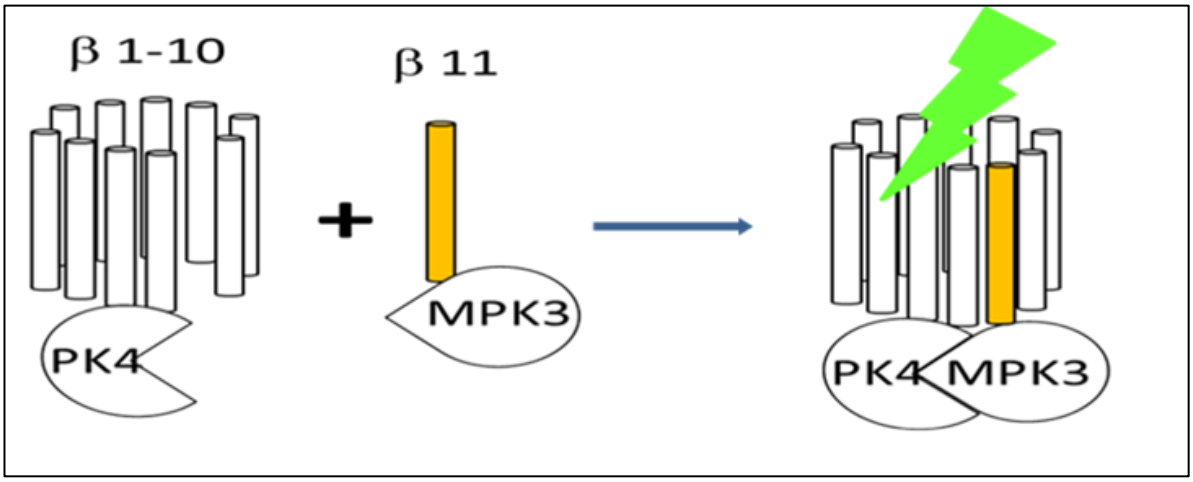

Figure 5.21. Principle of split di-GFP system. GFP1–10 (β1-10) fused to the N-terminus of LmxPK4, and GFP11 (β11) fused to the N-terminus of LmxMPK3. Fluorescence can only occur when LmxPK4 and LmxMPK3 interact, leading to the assembly of the β-sheets of GFP to from a functional fluorescent protein.

5.5.5.2.1 Generation of pSSUPacDiLmxPK4triHAGFP1-10MPK3GFP11 for testing LmxPK4-LmxMPK3 protein interaction

The potential interactions between LmxMPK3 and LmxPK4 in vivo was investigated by using split di-GFP. The generation of pSSUPacDiLmxPK4triHAGFP1-10MPK3GFP11 was started by the generation of pSSUPacDiCtriHAGFP (Figure

5.22). The pSSUPacTriGFP was cleaved with SpeI and HpaI to generate 189 bp, 1834 bp and 8960 bp DNA fragments, followed by the isolation and dephosphorylation of the 8960 bp HpaI/SpeI DNA fragment carrying GFP11 and Lmssu (18S rRNA) from pSSUPacTriGFP. pBXtHAGFP1-10tmyc was cleaved with SpeI and PmeI to generate 211bp, 771 bp, and 2910 bp DNA fragments (not shown), followed by the isolation of the 771 bp SpeI/PmeI DNA fragment, which contains GFP1-10 from pBXtHAGFP1-10tmyc.The 8960 bp HpaI/SpeI DNA fragment from pSSUPacTriGFP and the 771 bp SpeI/PmeI DNA fragment form pBXtHAGFP1-10tmyc were ligated and and transformed into *E. coli* to generate pSSUPacDiCtriHAGFP (Figure 5.23 A). The successful generation of pSSUPacDiCtriHAGFP was tested by cleavage with SacII (2075 bp, 7656 bp), BglII (9731 bp), and BamHI + EcoRV (1954 bp, 2795 bp, 4982 bp) (Figure 5.23 B). The identity of pSSUPacDiCtriHAGFP was also confirmed by DNA sequencing.

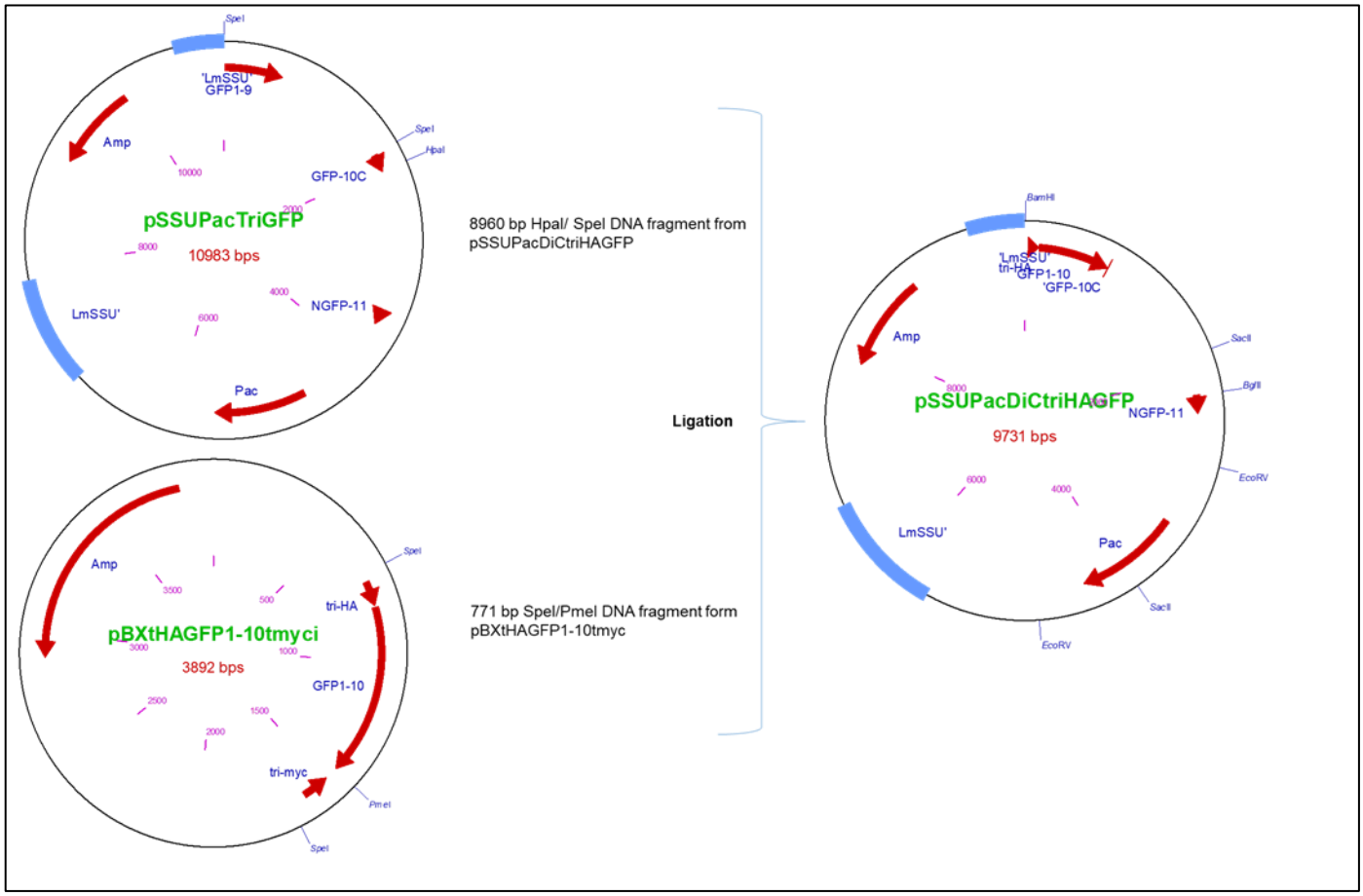

Figure 5.22. Cloning history for the generation of pSSUPacDiCtriHAGFP. The 8960 bp HpaI/SpeI DNA fragment from pSSUPacDiCtriHAGFP was ligated with the 771 bpSpeI/PmeI DNA fragment from pBXtHAGFP1-10tmyc. Lmssu (18S rRNA); Pac, purmycin antibiotic resistance gene; and Amp, ampicillin selectable marker.

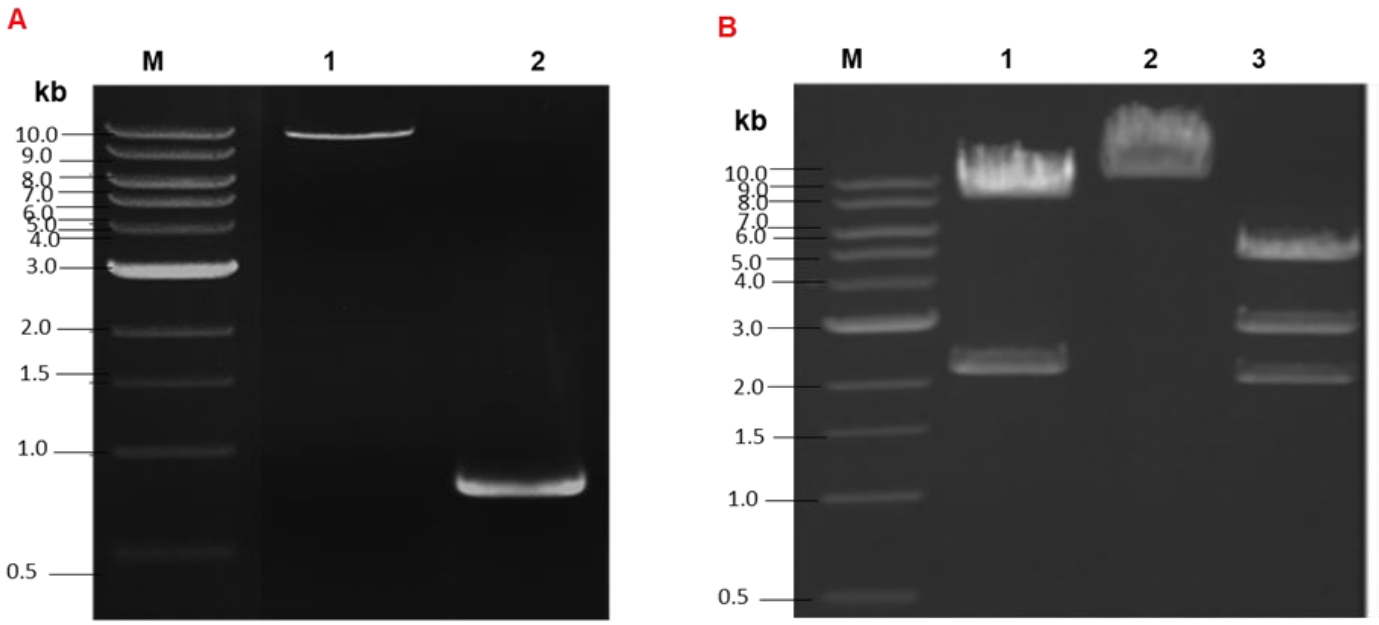

Figure 5. 23. Generation of pSSUPacDiCtriHAGFP. A) Isolated DNA fragments from pSSUPacTriGFP and pBXtHAGFP1-10tmyc. Lane 1, 8960 bp HpaI/ SpeI DNA fragment from pSSUPacDiCtriHAGFP; lane 2, 771 bpSpeI/PmeI DNA fragment form pBXtHAGFP1-10tmyc. **B)** Restriction analysis of pSSUPacDiCtriHAGFP. Lane 1, SacII resulting in 2075 bp and 7656 bp DNA fragments; lane 2, BglII resulting in 9731 bp DNA fragment; lane 3, BamHI and EcoRV resulting in1954 bp, 2795 bp and 4982 bp DNA fragments. M, DNA size marker.

The second step was to generate pSSUPacDiLmxPK4triHAGFP1-10 as shown in figure 5.24. pBLmxPK4NheI was cleaved by BamHI and NheI to generate 1062 bp and 2934 bp fragments (Figure 5.25 A), followed by the isolation of the 1062 bp BamHI/NheI DNA fragment carrying LmxPK4. The pSSUPacDiCtriHAGFP1-10 was cleaved with BamHI and AvrII to generate 9 bp and 9722 bp DNA fragments (Figure 5.25 B; the small band of 9 bp is not visible on the gel) and the 9722 bp BamHI/AvrII DNA fragment carrying GFP1-10, GFP11 and Lmssu (18S rRNA) was isolated followed by dephosphorylation. The 9722 bp BamHI/AvrII DNA fragment from pSSUPacDiCtriHAGFP was ligated with the 1062 bp BamHI/NheI DNA fragment from pBLmxPK4NheI and transformed into *E. coli* to generate

pSSUPacDiCPK4triHAGFP1-10. The identity of pSSUPacDiCPK4triHAGFP1-10 it was confirmed by cleavage MfeI (9794 bp and 990 bp), XbaI (3383 bp and 7401 bp) and XhoI (10211 bp and 573 bp) (Figure 5.25 C).

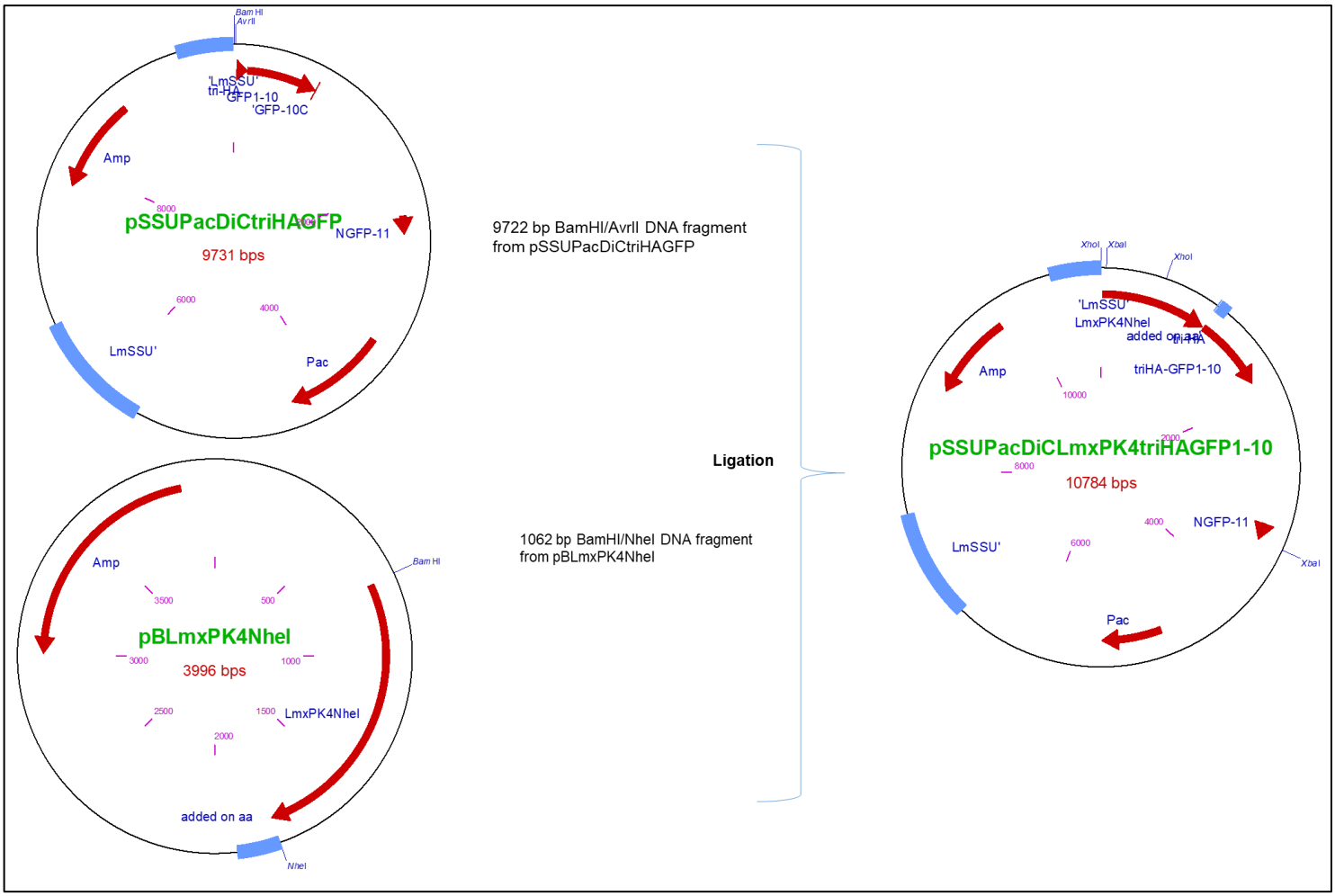

Figure 5.24. Cloning history for the generation of pSSUPacDiLmxPK4triHAGFP1-10. The 9722 bp BamHI/AvrII DNA fragment from pSSUPacDiCtriHAGFP was ligated with 1062 bp BamHI/NheI DNA fragment from pBLmxPK4NheI to generate pSSUPacDiCPK4triHAGFP1-10. Lmssu (18S rRNA); Pac, purmycin antibiotic resistance gene; and Amp, ampicillin selectable marker.

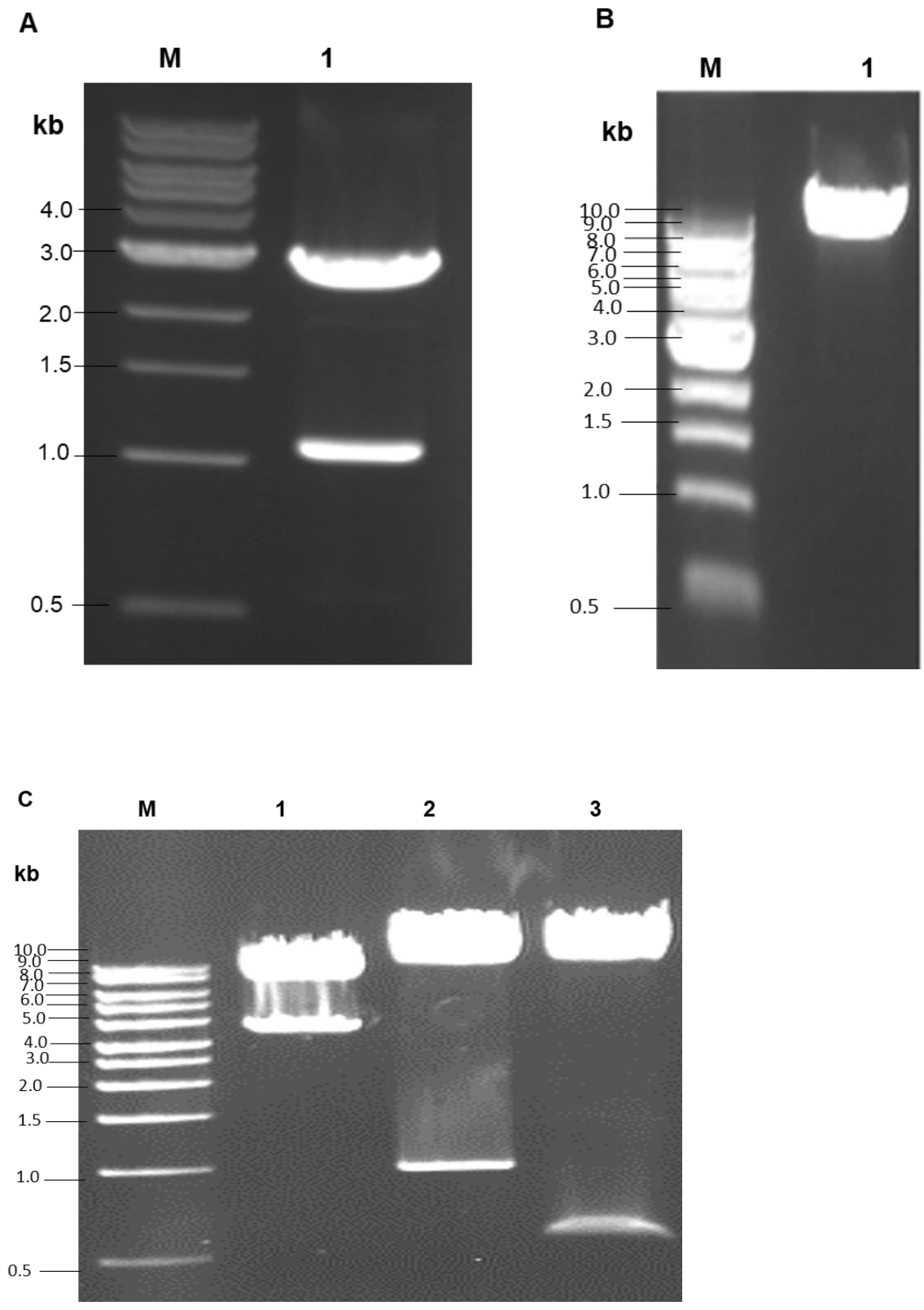

Figure 5. 25.Generation of pSSUPacDiLmxPK4triHAGFP1-10. A) Preparative cleavage of pBLmxPK4NheI. Lane 1, pBLmxPK4NheI cleaved with BamHI and NheI to generate 1062 bp and 2934 bp DNA fragments. **B)** Preparative cleavage of pSSUPacDiCtriHAGFP. Lane 1, pSSUPacDiCtriHAGFP cleaved with BamHI and AvrII to generate 9 bp (not visible on the gel)

and 9722 bp DNA fragments. **C)** Restriction analysis of pSSUPacDiCLmxPK4triHAGFP1-10. Lane 1, cleavage with XbaI to generate 3383 bp and 7401 bp DNA fragments; lane 2, cleavage with MfeI to generate 9794 bp and 990 bp DNA fragments; lane 3, cleavage with XhoI to generate 10211 bp and 573 bp DNA fragments. M, DNA size marker.

The third step was the generation of pSSUPacDiLmxPK4triHAGFP1-10MPK3GFP11 (Figure 5.26). The pSSUPacDiCLmxPK4triHAGFP1-10 was cleaved with NsiI, PmeI and SacII to generate 4978 bp, 2682 bp, 2075 bp and 1049 bp DNA fragments. The 4978 bp NsiI/PmeI DNA fragment carrying LmxPK4-triHAGFP1-10 from pSSUPacDiCLmxPK4triHAGFP1-10 was isolated. pSSUPacTriGFP10LmxPK4LmxMPK3GFP11 was cleaved with NsiI, PmeI and XhoI to generate 576 bp, 6964 bp, 3103 bp and 2570 bp DNA fragments. The 6964 bp NsiI/PmeI DNA fragment, which has *LmxMPK3-GFP11* from pSSUPacTriGFP10LmxPK4MPK3GFP11, was isolated and dephosphorylated (Figure 5.27 A, B). The 4978 bp NsiI/PmeI DNA fragment from pSSUPacDiCLmxPK4triHAGFP1-10 was ligated with the 6964 bp NsiI/PmeI DNA fragment from pSSUPacTriGFP10LmxPK4MPK3GFP11 and transformed into *E. coli* to generate pSSUPacDiLmxPK4triHAGFP1-10LmxMPK3GFP11. The identity of pSSUPacDiLmxPK4triHAGFP1-10LmxMPK3GFP11 was confirmed by cleavage with NdeI (7343 bp and 4599 bp), XbaI (7401 bp and 4541 bp) and XhoI (11369 bp and 573 bp) (Figure 5.27 C).

Finally, pSSUPacDiLmxPK4triHAGFP1-10LmxMPK3GFP11 was cleaved with PacI and PmeI to generate 2658 bp and 9284 bp fragments. The 9284 bp PmeI/PacI DNA fragment carrying LmxPK4-triHAGFP1-10 and LmxMPK3-GFP11 from pSSUPacDiLmxPK4triHAGFP1-10LmxMPK3GFP11 was isolated under sterile conditions (Figure 5.28) and was used for transfection into *L. mexicana* wild type and the ∆LmxMPK3-/- HN6 null mutant.

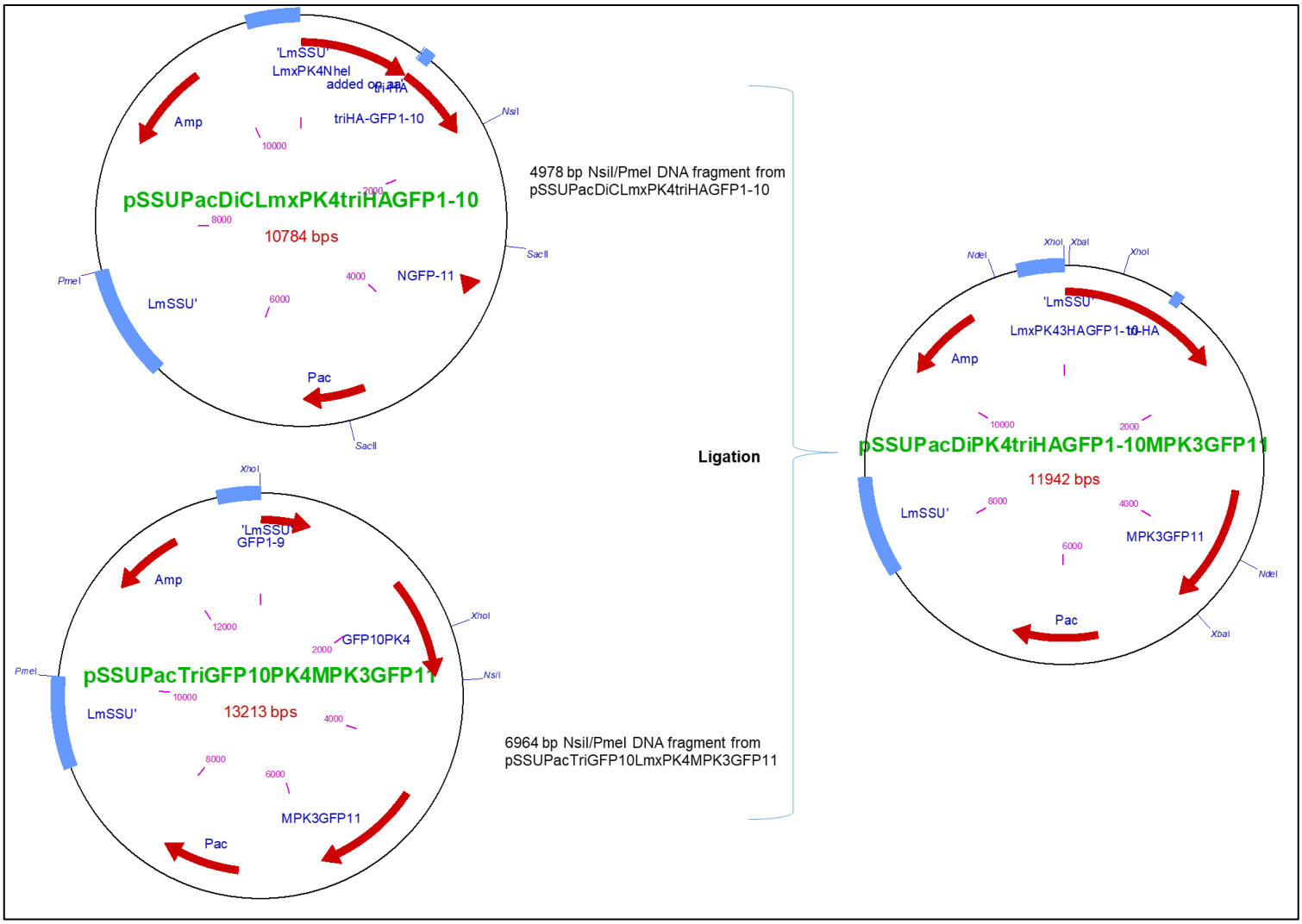

Figure 5.26. Cloning history for the generation of pSSUPacDiLmxPK4triHAGFP1-10MPK3GFP11. The 4978 bp NsiI/PmeI DNA fragment from pSSUPacDiCLmxPK4triHAGFP1-10 was ligated with 6964 bp NsiI/PmeI DNA fragment from pSSUPacTriGFP10LmxPK4MPK3GFP11 to generate pSSUPacDiLmxPK4triHAGFP1-10MPK3GFP11. Lmssu (18S rRNA), Pac, purmycin antibiotic resistance gene; and Amp, ampicillin selectable marker.

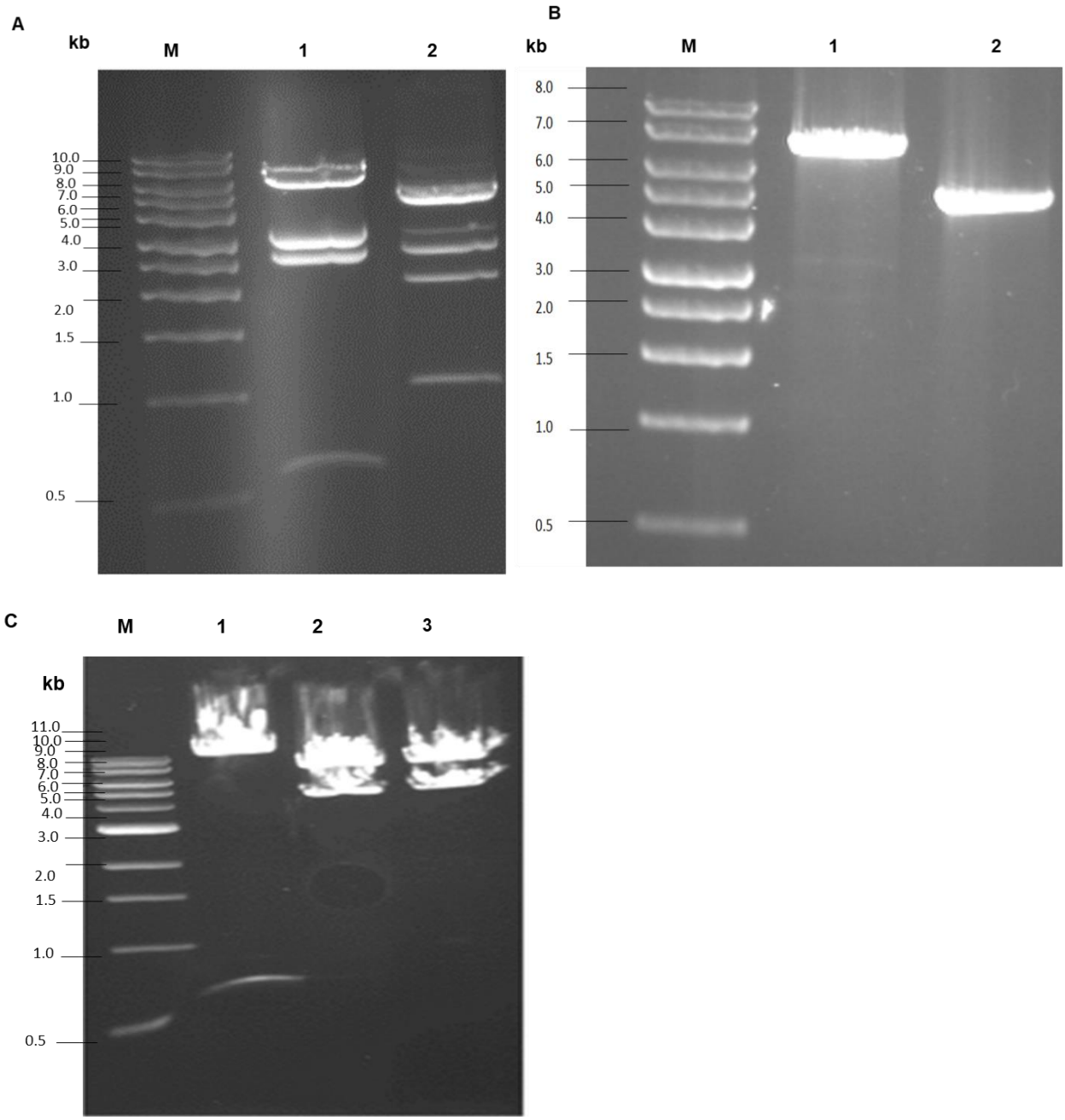

Figure 5.27. Generation of pSSUPacDiLmxPK4triHAGFP1-10MPK3GFP11. A) Preparative cleavage of pSSUPacTriGFP10LmxPK4LmxMPK3GFP11 and pSSUPacDiCLmxPK4triHAGFP1-10. Lane 1, pSSUPacTriGFP10LmxPK4LmxMPK3GFP11 cleaved with NsiI, PmeI and XhoI, resulting in 576 bp, 6964 bp, 3103 bp and 2570 bp DNA fragments; lane 2, pSSUPacDiCLmxPK4triHAGFP1-10 cleaved with NsiI, PmeI and SacII, resulting in 4978 bp, 2682 bp, 2075 bp and 1049 bp DNA fragments; **B)** Isolated DNA fragments from pSSUPacTriGFP10LmxPK4LmxMPK3GFP11 and pSSUPacDiCLmxPK4triHAGFP1-10. Lane 1, 6964 bp NsiI/PmeI DNA fragment from pSSUPacTriGFP10LmxPK4MPK3GFP11; lane 2, 4978 bp NsiI/PmeI DNA fragment from pSSUPacDiCLmxPK4triHAGFP1-10 **C)** Restriction analysis of pSSUPacDiLmxPK4triHAGFP1-10LmxMPK3GFP11. Lane 1, XhoI (11369 bp and 573 bp); lane 2, XbaI (7401 bp and 4541 bp); lane 3, NdeI (7343 bp and 4599 bp). M, DNA size marker.

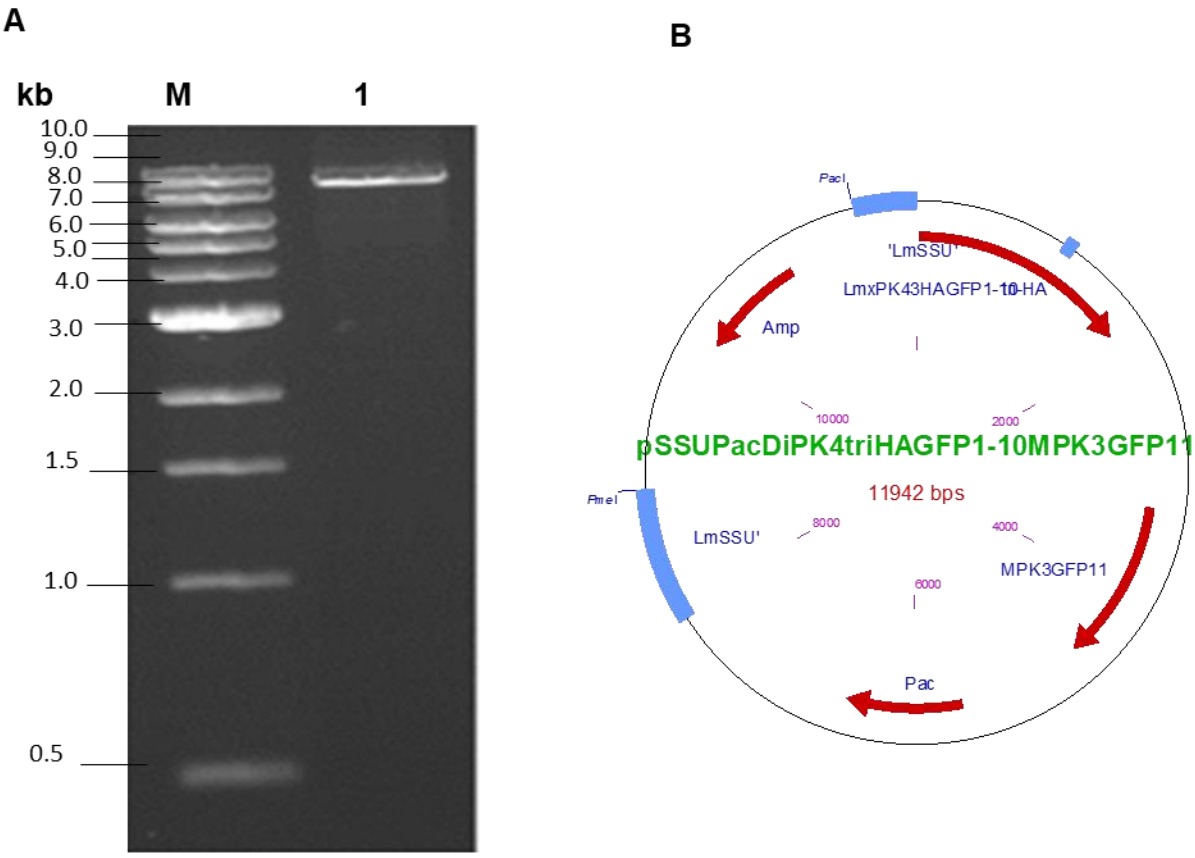

Figure 5.28. Isolated DNA fragment from pSSUPacDiLmxPK4triHAGFP1-10LmxMPK3GFP11 for transfection. A) Lane 1, 9284 bp PmeI/PacI DNA fragment from pSSUPacDiLmxPK4triHAGFP1-10LmxMPK3GFP11; and **B)** Plasmid map of pSSUPacDiLmxPK4triHAGFP1-10LmxMPK3GFP11. M, DNA size marker.

5.2.5.2.2 Transfection of *LmxPK4-GFP1-10LmxMPK3-GFP11* construct into *L. mexicana*

The 9284 bp PmeI/PacI DNA fragment from pSSUPacDiLmxPK4triHAGFP1-10LmxMPK3GFP11 was integrated into promastigotes of two different *Leishmania* cell lines by electroporation; the null mutant for LmxMPK3 (ΔLmxMPK3-/- HN6) and wild type *L. mexicana.* After two weeks of incubation at 27°C in 96-well plates in media containing 10 µg/µL puromycin, cell growth was observed in 90 wells for transfected ΔLmxMPK3-/- HN6 and in 95 wells for wild type *L. mexicana* in the 1:2 dilutions of

electroporated cells. The 1:40 dilution resulted in 55 wells for ∆LmxMPK3-/- HN6 and 60 wells for wild type *L. mexicana,* showing growth. Four putative positive clones from the 1:40 dilution for each cell type, ∆LmxMPK3-/- HN6 and wild type *L. mexicana* were expanded for further analysis.

5.2.5.2.3 Fluorescence analysis for protein–protein interactions of LmxPK4 with LmxMPK3 using split di-GFP

A split di-GFP approach was used to test interactions between LmxPK4 and LmxMPK3 in promastigotes of null mutant ∆LmxMPK3-/- HN6 (used as a control) and wild type *L. mexicana*. *LmxPK4GFP1-10* and *LmxMPK3GFP11*. split di-GFP approach (LmxPK4GFP1-10, LmxMPK3GFP11) was expressed from the ribosomal RNA gene locus of promastigotes of *L. mexicana* wild type and LmxMPK3 null mutant (∆LmxMPK3-/- HN6). Promastigotes in the logarithmic (2-4 × 10^7 cells/mL) growth phase showed green fluorescence using 488 nm excitation, indicating protein-protein interaction. Bright field microscopy of live promastigotes of ∆LmxMPK3-/- HN6 containing the split di-GFP (LmxPK4GFP1-10 and LmxMPK3GFP11) construct showed normal length flagella, indicating that a functional LmxMPK3 was expressed in the null mutant background (Figure 5.29).

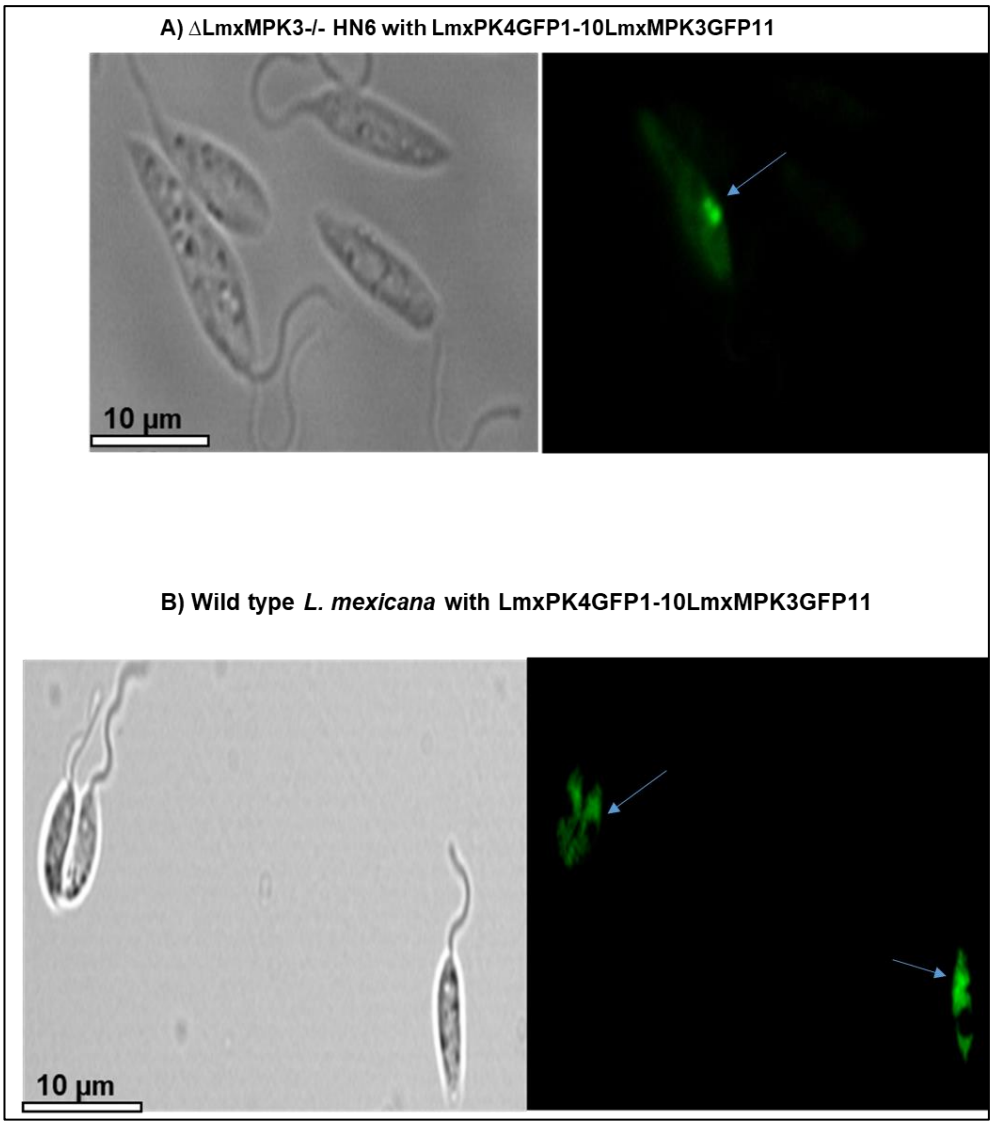

Figure 5.29. Fluorescence microscopy of live *L. mexicana* promastigotes to test the interaction between LmxPK4GFP1-10 and LmxMPK3GFP11. A) Bright field microscopy showed formation of normal length flagella in the null mutant background (∆LmxMPK3-/- HN6), and green fluorescence visualised the interaction of LmxPK4GFP1-10 and LmxMPK3GFP11 (100× magnification). **B)** Localisation of the interaction of LmxPK4GFP1-10 with LmxMPK3GFP11 in *L. mexicana* wild type background showed green fluorescence at 40× magnification. Images were processed using ImageJ (NIH, USA). Left, bright field; right, fluorescence using 488 nm excitation and FITC filter. Size bar 10 µm. Arrows indicate localisation of the interaction between LmxPK4GFP1-10 and LmxMPK3GFP11.

5.3 Discussion

MAPKs play important roles in the cell biology of *L. mexicana.* The TXY motif, a typical MAPK motif, is present in all 15 *Leishmania* MAPKs and is most likely phosphorylated during activation. The docking interaction between MAPK and MAP2K contributes to the determination of MAP2K substrates in yeast (Bardwell and Thorner, 1996). This study investigated the interactions between LmxPK4 (LmxM.24.2320) and LmxMPK3 (LmxM.10.0490) involved in flagellar length regulation. The most common site for the docking interaction of MAP2K with their activator is the CD domain in MAPK (Tanoue and Nishida, 2003). LmxMPK3 showed a putative CD domain L-H-D-E-E-D-E-P-A-C-P, which contains DEEDE, an accumulation of negatively charged residues likely to be involved in protein interactions (Erdmann et al., 2006). LmxPK4 (LmxM.24.2320) has a putative D-site K-R-P-Q-A-L-E-K-L-H-V. MAP2K D-sites can bind with CD sites (CD domains) of downstream MAPKs, which can regulate the phosphorylation reaction and specificity (Tanoue and Nishida, 2003). The activation of MAPK by phosphorylation of the TXY motif in the phosphorylation loop increased its catalytic activity 5000-fold (Bardwell, 2006). MAPKs can be co-expressed with MAP2Ks in a bacterial expression system which uses pJCduet plasmids. An N-terminal hexahistidine tag fused to the MAPK allows its purification (John von Freyend et al., 2010). This system was used to study the interaction between LmxMPK3 and LmxPK4. The generation of different plasmid constructs allowed for the purification of different versions of His-LmxMPK3 from *E. coli*. The clear band visible at approximately 44 kDa using Coomassie-stained SDS-PAGE corresponds to His-tagged LmxMPK3, the expected molecular mass of which is 43.7 kDa.

The enzymatic activities of different purified versions of the His-LmxMPK3 proteins were analysed. His-LmxMPK3 alone was used to test its autophosphorylation as a positive control. The results of the autoradiography assay showed an autophosphorylation one band of His-LmxMPK3 after 15 min incubation length with 24 h exposure (Figure 5.10; lane 1). Phosphorimaging showed that autophosphorylation of His-LmxMPK3 increased between 2 and 5 min of incubation in the kinase assay (Figure 5.11; lane 1, Figure 5.13) and then decreased after 10 min. This result may be attributed to the higher amount of protein in lane 1B than in lane 1C (Figure 5.11 and Figure 5.13).

The radiometric assay of His-LmxMPK3 or kinase-dead His-LmxMPK3KM co-expressed with LmxMKK (Figure 5.10; lane 3) or LmxPK4 (Figure 5.10; lane 2) showed two bands for autophosphorylation after 5 min incubation length with 1 h exposure, increasing with longer assay time. On other hand, the phosphorimaging of His-LmxMPK3 co-expressed with LmxMKK showed that autophosphorylation increased between the 2 and 5 min incubations and then decreased after 10 min. This result may be attributed to the higher amount of protein in lane 3B than in lane 3C (Figures 5.11 and Figure 5.12). His-LmxMPK3 co-expressed with LmxPK4 showed an increase of autophosphorylation over time at 24 h exposure (Figures 5.11 and Figure 5.13). One autophosphorylation band is caused by His-LmxMPK3 alone and two autophosphorylation bands were observed when His-LmxMPK3 was co-expressed with either LmxPK4 or LmxMKK. This suggests that the MAP2Ks phosphorylate additional residues compared to His-LmxMPK3 alone.

The kinase-dead version of His-LmxMPK3KM was also used as a negative control to ensure that the phosphorylation was the result of co-expression with a MAP2K (LmxPK4 or LmxMKK) and was not due to autophosphorylation or phosphorylation by

a kinase from the bacterial expression system (see section 5.2.2). As expected, His-LmxMPK3KM showed no MBP phosphorylation (Figures 5.11 and 5.12 and Figure 5.13), because lysine 62 (K62), which is highly conserved in subdomain II and is required for the proper orientation of ATP to allow phosphotransfer, was replaced by methionine. This lysine forms ionic bonds with the glutamate residue of the αC-helix (Carrera, 1993). Unexpectedly, LmxMPK3KM showed MBP phosphorylation when co-expressed with LmxMKK or LmxPK4. Its activity was significantly weaker than the activity of wild type LmxMPK3. It might be possible that the lysine residue at position 63 (Figure 5.1) can form the required salt bridge and leads to a less active conformation of the kinase, allowing the K62M mutant to be partially active after phosphorylation with either LmxMKK or LmxPK4.

Moreover, His-LmxMPK3 and His-LmxMPK3KM co-expressed with LmxPK4 or LmxMKK phosphorylated MBP, showing an increase with longer incubation and exposure times in both the autoradiography and the phosphorimaging (Figures 5.10, Figure 5.11 and Figure 5.12). LmxMKK has been found to phosphorylate LmxMPK3 (Erdmann et al., 2006). This result indicates that His-LmxMPK3 underwent a phosphorylation-induced conformational change when co-expressed with LmxPK4, which led to increased catalytic kinase activity and therefore to strong MBP phosphorylation. Similar results have been found for the phosphorylation of MBP, resulting from LmxMPK4 co-expressed with LmxMKK5 (John von Freyend et al., 2010). Interestingly, His-LmxMPK3 co-expressed with LmxPK4 showed greater MBP phosphorylation compared to His-LmxMPK3 co-expressed with LmxMKK.

Additionally, the MS/MS experiments identified 15 phosphorylated residues associated with the activation of His-LmxMPK3 or His-LmxMPK3KM by LmxPK4 or LmxMKK, and 3 phosphorylated residues resulted from the autophosphorylation of

LmxMPK3 (Tables 5.2 and 5.2). His-LmxMPK3 and His-LmxMPK3KM were activated by LmxPK4 or LmxMKK by phosphorylation on threonine (THR194) and tyrosine (TYR196) residues (Table 5.2 and Figure 5.14). This is similar to LmxMKK5, which activated LmxMPK4 on THR190 and TYR192 (John von Freyend et al., 2010). The MS/MS result of His-LmxMPK3 or His-LmxMKP3KM co-expressed with LmxPK4 or LmxMKK displayed additional phosphorylated serine and threonine residues located at the N-terminus and C-terminus of LmxMPK3 (Figure 5.14).

LmxMKK activated LmxMPK3 *in vitro,* and both deletion mutants for LmxMPK3 and LmxMKK have similar short flagellum length phenotypes. However, *in vivo*, only a very weak phosphorylation of LmxMPK3 could be detected when LmxMKK was deleted from the *L. mexicana* genome (Erdmann et al., 2006). As a result, the activation of LmxMPK3 by LmxPK4 *in vitro* does not necessarily mean that an *in vivo* interaction takes place. Therefore, a split-GFP system was used to resolve this issue conclusively. The purpose of splitting GFP is studying protein interaction in live cells. The split-GFP system was used to localise and visualise the protein interactions involving the MAP2K (LmxPK4) and MAPK (LmxMPK3) *in vivo*. Two proteins expressed *in vivo* can be used to localise their interaction when a complete GFP is reformed and becomes fluorescent (Ghosh et al., 2000). The split GFP reveals the interaction between proteins and the fluorescent protein (GFP) intrinsically produces a fluorescent signal proportional to the number of correctly assembled GFP with mature chromophores (Romei et al., 2019). The two parts of the split GFP were genetically fused to separated leucine zipper domains, which were subsequently coexpressed in *E. coli* and led to formation of the antiparallel leucine zipper bringing together the two parts of the GFP, which formed the active chromophore leading to green fluorescence (Ghosh et al., 2000). The advantage of splitting GFP is the stability of GFP, once re-assembled, caused by the robust β-barrel structure, where

conserving the fluorescent protein leads to visualisation of protein-protein interactions (Romei et al., 2019).

The tri-GFP system was used as a biosensor to detect localised protein-protein interactions in promastigote cells. The protein-protein interactions were monitored by engineering a GFP split into three parts; the short peptides, beta-strand GFP10 and beta-strand GFP11, were linked to the interaction partners, LmxPK4 and LmxMPK3, and GFP1-9 was used as a detector molecule (Figures 5.15). These components did not show any fluorescence in fluorescence microscopy analysis of live cells used at a cell density of 2–4 × 10^7 cells/mL. The construct had been integrated into the ribosomal RNA gene locus of *L. mexicana* wild type and an LmxMPK3 null mutant. The presence of untagged LmxMKK and LmxPK4 in these cells to compete with GFP10LmxPK4 for interaction with LmxMPK3GFP11 might explain why no signal was observed. Ideally, the experiment should be repeated in a cell line that is devoid of both LmxPK4 and LmxMPK3 to exclude competition between GFP10LmxPK4 and its wild type version. Moreover, an analysis in a LmxMKK and LmxMPK3 null mutant might lead to a positive result as well. Importantly, the bright field microscopy revealed normal length flagella, which indicated the expression of a LmxMPK3GFP11 in the null mutant background that is as functional as the wild type LmxMPK3 (Figure 5.20). It might be that this result is still a false negative result for the interaction between GFP10LmxPK4 and LmxMPK3GFP11 in fluorescence analysis because the superfold split tri-GFP requires three molecules (GFP1–9, GFP10, and GFP11) to join together in the appropriate way (Romei et al., 2019). If the GFP10 and GFP11 are too far apart from each other when LmxPK4 and LmxMPK3 interact the assembly of a functional GFP would be impossible. Swapping the position of the GFP10 and GFP11 might resolve this issue.

For this work, it was fundamental to demonstrate the ability to detect the protein interaction between LmxPK4 and LmxMAPK3 via the reconstitution of split GFP fragments. Therefore, the alternative di-GFP split-GFP system was used. The di-GFP construct consisted of two fragments, namely LmxPK4GFP1-10 and LmxMPK3GFP11, which were generated using the superfoder tri-GFP as a starting construct. No assistance of a complementary detector (GFP1-9) was required (Figure 5.21). It had been shown that the split di-GFP between GFP1-10 (β-strands1-10) and GFP11 (β-strand 11) led to great improvement in solubility and complementation efficiency (Cabantous and Waldo, 2006). In this work, the di-GFP experiment was performed with both a null mutant for LmxMPK3 and wild type *L. mexicana*. In fact, both cell lines expressing the di-GFP construct generated a positive result. The protein complexes could be visualised based on the localised fluorescence of the reassembled GFP based on the interaction of LmxPK4GFP1-10 and LmMPK3GFP11. Moreover, the expression of LmxMPK3GFP11 led to flagella of normal length (Figure 5.29). It has been shown in other systems that expression of GFP1-10 only and GFP11-only did not lead to any detectable fluorescence (Avilov et al. el, 2018). Fluorescence analysis of LmxMPK3GFP in LmxMPK3 null mutant background and LmxPK4GFP in a genomic null mutant of LmxPK4 showed fluorescence in the flagellum and the cytosol of *L. mexicana* promastigotes (Kuhn and Wiese, 2005; Erdmann., 2009; Figure 5.30). However, using the di-GFP system to co-express LmxPK4GFP1-10 and LmxMPK3GFP11 in a null mutant for LmxMPK3 showed a localisation of the fluorescent signal in a distinct area of the cytosol in fluorescence microscopy analysis (Figure 5.29). This localisation was not as clear when the co-expression was done in *L. mexicana* wild type promastigotes. In these cells a fluorescent signal with a higher intensity was found in the same area as in the null mutant background, however other areas of the cytosol were flurescent as well,

but no signal could be detected in the flagellum. This finding provides evidence for the interaction between LmxMPK3 and LmxPK4 *in vivo*.

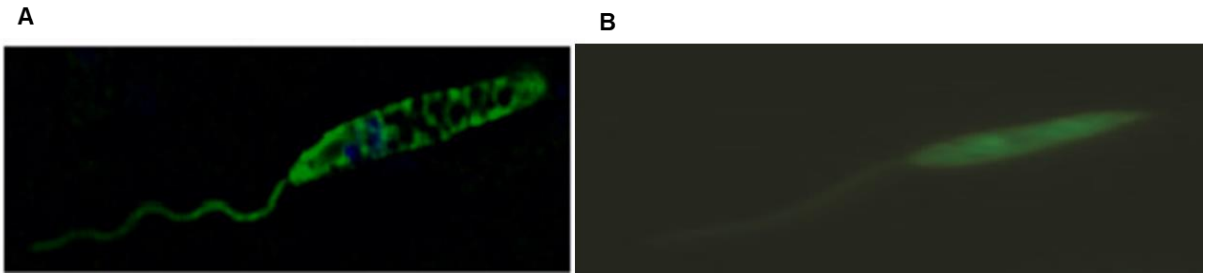

Figure 5.30. Fluorescence analysis of LmxMPK3 and LmxPK4 tagged with GFP. A) LmxMPK3-GFP in null mutant background of LmxMPK3. B) LmxPK4-GFP in null mutant background of LmxPK4. Both showed fluorescence in the cytosol and the flagellum of recombinant promastigotes (adapted from Kuhn and Wiese, 2005; Erdmann, 2009).

To summarise, the above analyses demonstrate that the MAP2K LmxPK4 could phosphorylate and activate MAPK LmxMPK3 at the threonine and tyrosine residues of the TXY motif *in vitro* and that they colocalise *in vivo* making a phosphorylation likely as well.

Chapter 6: General Discussion

6.1 General discussion

The second-largest parasitic disease in the world, leishmaniasis affects approximately 2 million new patients yearly and roughly 350 million people in endemic areas. The major obstacles for anti-*Leishmania* treatments are poor therapeutic interventions, resistance development, low cost effectiveness, drug toxicity and a lack of vaccines. In short, all accounts indicate an urgent need to develop new and improved drugs to combat the parasites responsible for leishmaniasis (Ramu et al., 2019).

Protein kinases are key regulators of cellular molecules, forming a complex network, which can activate and silence cellular molecules, and as such, they constitute promising drug targets for numerous diseases (Cheng et al., 2011). Many protein kinases have been used for inhibitor screening, for instance p38 MAPK, followed by development of identified inhibitors in clinical trials for cardiovascular disease, cancer and inflammatory diseases (Hammaker and Firestein, 2010).

Additionally, it was found that 2% of the trypanosomatid genome codes for protein kinases. This is 33% more compared to *Saccharomyces cerevisiae* and 50% more than *Plasmodium falciparum* (Parsons et al., 2005). A prioritisation analysis for *T. brucei* confirmed eight out of 33 highly expressed protein kinases as drug targets (Borba et al., 2019). These were the previously genetically validated drug targets, Polo-like kinase (PLK) (Hammarton et al., 2007), WEE-1-like kinase (Boynaket et al., 2013), Casein kinase 1 (CK1) (Urbaniak, 2009), glycogen synthase kinase 3 (GSK3) (Ojo et al., 2008), cdc2-related kinase1 and 3 (CRK1 and CRK3) (Tu and Wang, 2005), and Aurora kinase (AIRK) (Tu et al., 2006). They have also been investigated in *Leishmania* species. Amongst them, CK1 is an exokinase (Rachidi et al., 2014). CK1 has emerged as a suitable drug target for leishmaniasis given its necessity for

intracellular parasite survival and infection; however, the identity between CK1 in *Leishmania* and humans is approximately 71% for the kinase domain, generates a challenge with identifying specific parasite kinase inhibitors (Allocco et al., 2006; Rachidi et al., 2014). At the same time, CRK1 and CRK3 have proven to be essential proteins in *L. mexicana* and to play important roles during cell cycle progression in *L. major* and *L. donovani* (Mottram et al., 1996; Hassan et al, 2001). Moreover, GSK3 caused defects in the cell cycle and apoptosis in *Leishmania* (Xingi et al., 2009*).* The crystal structure of LmajGSK3 has been identified, and 11 protein kinase inhibitors have been tested against LinfGSK3, HsapGSK3 and TbGSK3 in order to identify the structure activity relationship as a way to predict inhibitors with selective binding modes that could be effective against *Leishmania* GSK3 (Ojo et al., 2011). In addition, LdAIRK was found to be involved in cell cycle progression in *L. donovani* and showed an effect similar to that of AIRK in *T. brucei* in chemical validation studies *(*Chhajer et al., 2016).

Members of the MAPK family have also been investigated. MAPKs are important players in signal transduction pathways, and their signalling pathway is vital in nearly all eukaryotes, as it plays a key role in regulating the differentiation, proliferation and apoptosis of cells (Wiese et al., 2007). Therefore, the MAPK pathway has attracted considerable attention as a potential target for the treatment of various diseases, including leishmaniasis (Erdmann et al., 2006). To date, the following MAPKs have been proposed as suitable drug targets for leishmaniasis, LmxMPK1, LmxMPK2 and LmxMPK4 (Ashutosh et al., 2012; Brumlik et al., 2011; Mandal et al., 2012; John von Freyend et al., 2010; Wang et al., 2005; Wiese, 1998, Wiese et al., 2007). Moreover, LdMPK1 was found to phosphorylate and activate the heat shock proteins HSP70 and HSP90, which proved to be essential in cell cycle progression of *Leishmania* (Ommen et al., 2010; Kaur et al., 2017; Hombach-Barrigah et al., 2019). Added to that,

LmajMPK2 was confirmed to be phosphorylated and able to activate LmajAQP1, which increased Sb(III) uptake and sensitivity (Mandal et al., 2012).

MAP2Ks are components of MAPK cascades, which are the upstream regulators of MAPKs. MAP2K inhibitors are used to treat lung cancer, colorectal cancer, melanoma and anaplastic thyroid cancer as a single therapy or in combination with other therapies. All of those inhibitors have been approved by the FDA (Cheng and Tian, 2017). Moreover, the MAP2K inhibitor, known as Trametinib targets human MKK1 and MKK2 and is used to treat anaplastic thyroid cancer. Trametinib showed a 50% decrease of intracellular amastigotes at 15 µM for *L. braziliensis* and at 30 µM for *L. infantum.* Therefore, it was predicted to target MKKs in *Leishmania (*Borba et al., 2019; Infante et al., 2012).

Knowledge about MAP2K in trypanosomatids remains limited. LmxMKK, LmxPK4 and LmxPK5, out of seven putative MAP2Ks, have been studied in *Leishmania* (Erdmann et al., 2006; Kuhn and Wiese, 2005; John von Freyend et al., 2010). This project develops knowledge about other MAP2Ks in *L. mexicana,* identified as LmxPK3 and LmxPK6. It also investigated the interaction between MAP2K (LmxPK4) and MAPK (LmxMPK3) *in vivo* and *in vitro*.

This study represents the first molecular characterisation of LmxPK3 and LmxPK6 through bioinformatics. Both proteins show a homology to MAP2Ks and contain 12 highly conserved kinase subdomains (Figure 3.1 and Figure 4.1). LmxPK3 also shows some similarity to calcium/calmodulin-regulated kinases (CAMK), while LmxPK6 is closely related to serine/threonine-protein kinase 7 (STE7) (Parsons et al., 2005). The mRNAs of LmxPK6 and *LmxPK3* are present in all life cycle stages (Fiebig et al., 2015). However, for other MAP2K, such as LmxPK4 and LmxMKK the mRNAs were also found in amastigotes but proteins were both found to be absent in lesion-derived

amastigotes using immunoblot analysis (Erdmann et al., 2006; Kuhn and Wiese, 2005). Therefore, the mRNA analysis provides no information about whether the protein is actually present throughout the life cycle.

Moreover, a bacterial expression system designed to express and purify recombinant Glutathione-S-transferase fusion proteins of LmxPK3 and LmxPK6 was used in order to test their activity *in vitro*. However, GST-LmxPK6 expression was unsuccessful whereas expression of GST-LmxPK3 only led to low amounts of protein (Figure 3.9 and 4.7). It is important to highlight the fact that *Leishmania* has a higher amount of G-C rich tRNAs, which are rare in *E. coli*; this could limit the expression of *Leishmania* proteins (Beverley et al., 1991). However, kinase assays of eluted recombinant GST-LmxPK3 was conducted as the first experimental validation of LmxPK3, proving its function as a phosphotransferase of MBP but showing no autophosphorylation activity (Figure 4.8). In contrast, LmxPK4 was readily expressed, purified and can autophosphorylate and phosphorylate MBP *in vitro* (Kuhn and Wiese, 2005). It has been shown that phosphorylation can modulate binding properties, protein stability, enzyme activity and changes in the subcellular localisation of proteins (Cheng et al., 2011).

Several studies have performed gene deletions by homologous recombination in *Leishmania* as a powerful and efficient way to study the physiological function of proteins and to understand their biology (Duncan et al., 2017; Jones et al., 2018). *LmxPK3* is located on chromosome 17 and *LmxPK6* is located on chromosome 31 in *L. mexicana*. Both chromosomes are diploid in this *Leishmania* species (Rogers et al., 2011; TriTrypDB, https://tritrypdb.org/tritrypdb/). Two rounds of transfection would be necessary to replace LmxPK3 or LmxPK6 by resistance marker genes. A single allele knockout mutant, which carried a wild type LmxPK6 gene or LmxPK3 gene on one

allele and a deletion cassette conferring resistance on the other, had been generated without problems. However, the generation of a double allele knockout was unsuccessful. The inability to generate double allele knockout mutants in *LmxPK6* using resistance markers suggested that the LmxPK6 gene locus is difficult to target (section 3.2.3). Therefore, a plasmid which encodes an extrachromosomal copy of wild type *LmxPK6* was introduced into *L. mexicana* promastigotes first, before attempting to delete the genomic alleles (Section 3.2.4). Nevertheless, all attempts failed to generate a null mutant by replacing the two alleles of LmxPK6 with resistance conferring genes using homologous recombination and an extrachromosomal copy of wild type *LmxPK6*. It was impossible to generate null mutants for LmxMPK4 by homologous recombination and only the introduction of an episomal copy of *LmxMPK4* into *L. mexicana* promastigotes allowed the replacement of both genomic alleles of LmxMPK4 (Wang et al., 2005). This finding suggested that LmxPK6 might require a very accurate control of protein expression. pXpolNcoIPacLmxPK6ds contains the entire intergenic region between LmxPK6 and the downstream septum formation protein MAF gene. However, the upstream region of LmxPK6 is not present. Instead the intergenic region of DHFR-TS is present (Figure 3.19). This might not allow appropriate regulation of LmxPK6 protein expression. Both, absence of protein (null mutant) and expression of LmxPK6 from a plasmid using the DHFR-TS expression control region might have been detrimental to the parasites and hence no recombinant promastigotes lacking *LmxPK6* in the genome could be obtained. This aspect of the research strongly suggested that LmxPK6 is essential in *L. mexicana* promastigotes. LmxPK6 could be a drug target, provided that the kinase is also required in amastigotes. This claim should be further tested in the future. Once LmxPK6 is approved as a drug target, the problem of low yield of recombinant protein

obtained from *E. coli* needs to be solved, as the low yield prevents any direct inhibitor studies using a recombinant protein kinase.

In contrast, a LmxPK3 null mutant (LmxPK3K1H/N D8-/-) was successfully generated. The expression of the neomycin phosphotransferase resistance marker gene in the null mutant of LmxPK3 relied on the LmxMPK12 regulatory regions. Using the LmxPK3 flanking regions did not lead to any parasites growing in several deletion attempts. The LmxPK3 null mutant was able to develop lesions in mouse infections (section 4.2.5) and differentiated from lesion-derived amastigotes to promastigotes. This suggested that LmxPK3 is not essential in *L. mexicana* (section 4.2.4). Similarly, LmxMPK9 and LmxMPK3 were found to be dispensable in the amastigote stage of the parasite and hence are not suitable as drug targets for *Leishmania* (Bengs et al., 2005; Erdmann et al., 2006). This clearly rules out LmxPK3 as a drug target against leishmaniasis. However, null mutants for LmxPK4 and LmxMKK have been shown to cause delayed development of lesions in infected mice (Kuhn and Wiese, 2005; Wiese et al., 2003b).

LmxPK3 mutants showed effects on the cell body length and width and flagellar length, with significant differences compared to *L. mexicana* wild type promastigotes (section 4.2.5.2.2). These findings are similar with research showing reduced flagella length in the LmxMPK3 and LmxMKK mutants. However, the null mutants of LmxPK4, LmxMPK13 and LmxMPK9 showed elongated flagella (Erdmann, 2009; Kuhn and Wiese, 2005; Wiese et al., 2007). Additionally, mechanisms for control of cell shape and size are important for biological processes in the cells of both unicellular and multicellular organisms (Picone et al., 2010). This aspect of the results demonstrates that LmxPK3 is likely to be involved in processes of *L. mexicana* promastigotes, which could be important in the insect vector. Regarding possible effects of cell culture

density on parasite shape, it could be argued that the experiment could be repeated using different cell densities (log-phase, late log-phase), ensuring that the density and growth conditions for all cell lines are identical.

Successful expression of GFP has been reported in *Plasmodium*, *Entamoeba, Trypanosoma* and *Leishmania* (Docampo, 2011). LmxPK3 fused to GFP was found to be localised in the cytosol and in the flagellum of recombinant promastigotes. Several strategies have been successfully applied to complement the LmxPK3 deletion cell line with GFPLmxPK3-His, GFPLmxPK3 and His-LmxPK3-GFP. Fluorescence microscopy analyses revealed that the localisation of LmxPK3 was independent from a GFP-tag on the N- or C-terminal end expressed in the LmxPK3 null mutant (Figure 4.2.6.3). When comparing our results to those of previous studies, other MAP2Ks (LmxMKK and LmxPK4) were also localised in the cytosol (Erdmann et al., 2006; Kuhn and Wiese, 2005). This experiment adds to a growing corpus of research showing that MAP2Ks could be localised in the cytosol. This provides a good starting point for further research into the function of MAP2Ks.

The most remarkable result to emerge from this research is the interaction between MAPK and MAP2K. In *Leishmania,* the MAP2K LmxMKK can phosphorylate the MAPK LmxMPK3 *in vitro* on tyrosine and threonine within the TXY motif (Erdmann et al., 2006; Erdmann, 2009). The deletion of LmxMPK3 or LmxMKK led to a dramatic reduction in flagellar length; however, mouse infection experiments showed that LmxMPK3 is not required for the development of lesions. Other examples of MAP2Ks phosphorylating MAPKs are LmxMKK5, which can activate recombinant LmxMPK4 (John von Freyend et al., 2010), and LmxPK4, which can phosphorylate and activate LmxMPK13 (Scholz, 2008). Both LmxPK4 and LmxMPK13 deletion mutants showed elongated flagella, indicating that LmxMPK13 can also be activated by LmxPK4 *in*

vivo (Scholz, 2008). A possible interaction between LmxMPK3 and LmxPK4 was evaluated by co-expression of His-LmxMPK3 and His-LmxMPK3K62M with LmxPK4 or LmxMKK followed by kinase activity assays. The phosphotransferase activity of LmxMPK3 towards MBP could be clearly demonstrated *in vitro* (section 5.2.2.2). Moreover, phosphorylation activity required the presence of an activated LmxMPK3. LmxMPK3 alone was unable to phosphorylate MBP (Figure 5.10, Figure 5.11 and Figure 12).

The kinase-dead mutant, LmxMPK3K62M, was expected to not correctly bind and orientate ATP, due to the mutation of the highly conserved lysine residue (K62) of subdomain II, which is essential for the kinase activity, to a methionine residue (Carrera et al., 1993). However, there is another lysine residue following on from K62 (Figure 5.1), which may be able to form the crucial salt bridge, resulting in a less active conformation of the kinase, making the K62M mutant partially active after phosphorylation by LmxMKK or LmxPK4 as observed in figure 5.11 and figure 5.13.

Additionally, the most conspicuous observation from comparison of quantitative analyses of the kinase assays (Figure 5.11 and Figure 5.12) is that LmxMPK3 co-expressed with LmxPK4 resulted in significantly increased MBP phosphorylation compared to LmxMPK3 co-expressed with LmxMKK. This concurs well with the phosphorylation of LmxMPK3 by LmxPK4 occurred *in vitro* as shown by MS/MS analysis. It not only showed phosphorylation of the TDY motif in the activation loop but also phosphorylation of additional amino acid residues (THR169, SER183 and SER298). These were not found in the co-expression with LmxMKK and were not a result of autophosphorylation of LmxMPK3 as they were present in the LmxPK4 co-expression with the LmxMPK3K62M mutant. As SER183 is localised on the activation

loop it is likely to effect the substrate binding specificity (Table 5.2; Table 5.3 and Figure 5.14).

The interaction between LmxPK4 and LmxMPK3 *in vivo* was studied by using a new strategy of split GFP to monitor protein–protein interactions within intact living *L. mexicana* promastigotes. The split GFP was proved to be a useful tool to test protein-protein interaction. The split-tri-GFP system was successfully used *in vivo* in *S. cerevisiae* for protein interaction analysis (Finnigan et al., 2016). However, the split-tri-GFP system to detect the interaction between LmxPK4 and LmxMPK3 in *L. mexicana* did not show green fluorescence but the reduced flagellum length in the null mutant of LmxMPK3 could be restored to the normal length by the expression of LmxMPK3-GFP11. Therefore, the di-GFP system was used, composed of LmxPK4-GFP1-10 and LmxMPK3-GFP11 to examine kinase interaction in an LmxMPK3 null mutant background (see section 5.3.3.1). The interaction was successfully detected by the formation of an intact GFP from the two components of the spilt di-GFP using fluorescence microscopy, also revealing the subcellular localisation of the kinases (Figure 5.21 and Figure 5.29). The results of the LmxPK4GFP1-10LmxMPK3GFP11 interaction analysis demonstrated that the interaction between LmxMPK3 and LmxPK4 was localised in the cytosol, and a functional LmxMPK3 was expressed, which restored the flagella to normal lengths (section 5.3.5; Figure 5.29). Both, LmxPK4 and LmxMKK activate and phosphorylate LmxMPK3. This result ties well with previous studies where both, MKK7 and MKK4 activated and phosphorylated stress-activated protein kinase-1c JNK1 kinase at Thr–X–Tyr motif in humans (Lawler et al, 1998). Added to that, more than one MAP2K can activate and phosphorylate MAPKs in *Arabidopsis* (Lee et al., 2008).

In an enrichment of phosphorylated proteins from LmxMKK null mutant promastigotes LmxMPK3 was only present in a very low amount. Hence, LmxPK4 is most likely not the activator of LmxMPK3 in the dominant form of cultured promastigotes. This might be different for the various morphological stages of the parasite in the sand fly (section 1.4), which are not represented in great numbers in culture. This is also reflected by the small number of cells revealing LmxMPK3-LmxPK4 interaction by fluorescence microscopy. However, the fact that the activation of LmxMPK3 is involved in increasing or maintaining the length of the flagellum (absence leads to short flagella), whereas LmxPK4 is involved in shortening the flagellum (absence leads to longer flagella) appears to be contradictory. LmxMPK3 is phosphorylated at the TXY motif by both LmxMKK and LmxPK4, but LmxPK4 phosphorylates additional residues on LmxMPK3, which could result in a different substrate affinity or reduced kinase activity. This is supported by the MS/MS results, but the identified additional phosphorylation sites (THR169, SER183 and SER298) still need to be confirmed *in vivo*. Figure 6.1 shows a model of our current hypothesis how LmxPK4, LmxMPK3 and LmxMKK might be involved in flagellar length regulation. LmxMKK phosphorylates LmxMPK3, which most likely phosphorylates the OSM3-like kinesin LmxOSM3.1 (Emmerson, 2014) leading to flagellum elongation and maintenance. If LmxPK4 competes with LmxMKK for phosphorylation of LmxMPK3, the phosphorylation of LmxOSM3.1 will be reduced and the anterograde intraflagellar transport will decline leading to short flagella. On the other side, LmxPK4 has been found to phosphorylate and activate LmxMPK13 and phosphorylate LmxMPK9 (activation of LmxMPK9 still needs to be shown). Deletion of all three kinases, LmxPK4, LmxMPK9, and LmxMPK13, led to parasites with on average longer flagella than the wild type promastigotes. These kinases might therefore be involved in retrograde intraflagellar transport, which when reduced or shut down will cause

flagellum elongation. Why is phosphorylation of LmxMPK3 by LmxPK4 useful for promastigotes? The different forms of promastigotes in the sand fly display variations in flagellum length. This could be regulated by activation of LmxMKK and LmxPK4. However, phosphoproteomics on *L. mexicana* promastigotes did not provide any information on phosphopeptides derived from the activation loop of these kinases (Rosenqvist, 2011). If regulation is not by activation, it could be by protein presence and abundance. Both kinases are not expressed in amastigotes at all. In promastigotes however they are present all the time and could compete for their substrate LmxMPK3. This could be part of an intrinsic system for differentiation to the different promastigote stages.

This thesis presents knowledge about MAP2K in *Leishmania* as potential drug targets. LmxPK3 was not suitable for a drug target; however, LmxPK6 could be a potential drug target for *Leishmania*. Finally, the interaction between the MAP2K (LmxPK4) and the MAPK (LmxMPK3) furthers our understanding of MAPK pathways in *Leishmania,* and revealed that two MAP2Ks compete for the same substrate influencing flagellum length.

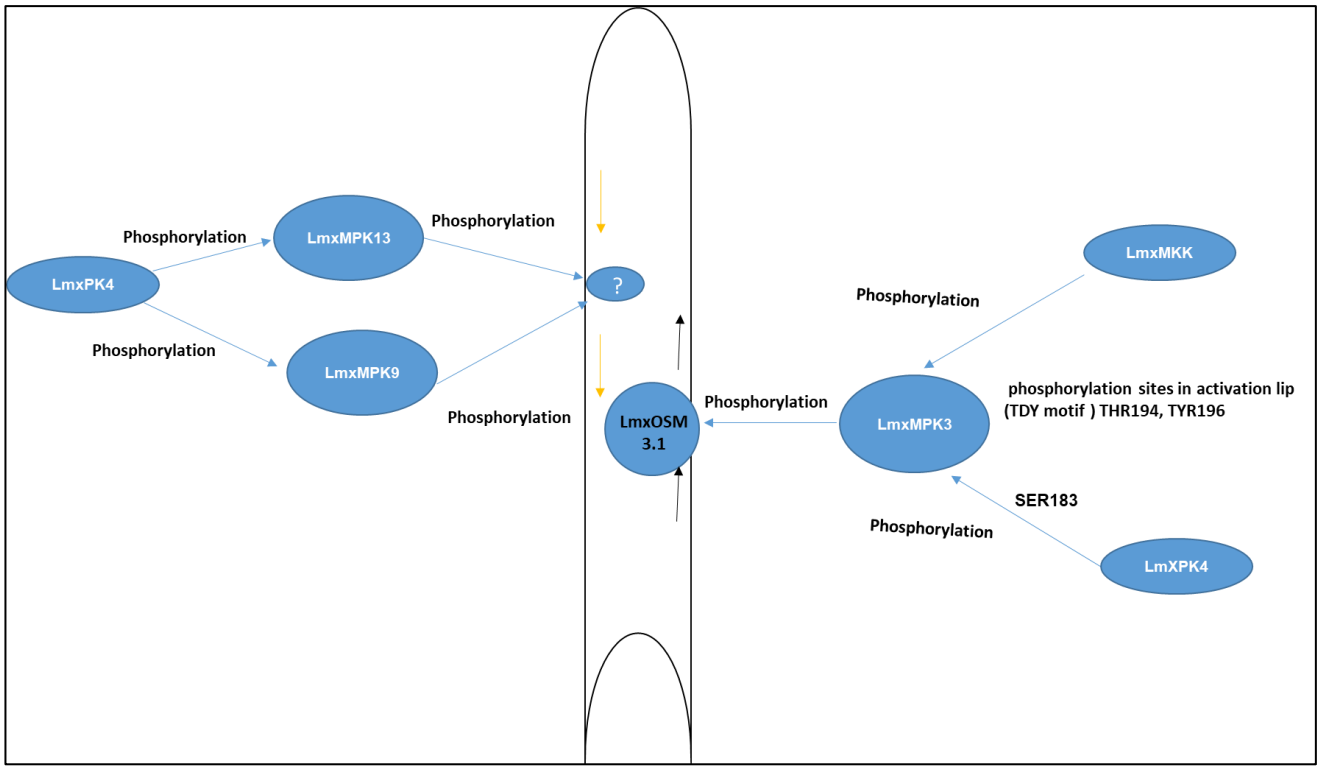

Figure 6.1. Model of current hypothesis for how LmxPK4, LmxMPK3 and LmxMKK might be involved in flagellar length regulation. Black arrows indicate anterograde IFT involving LmxOSM3.1 as a result of the activation of LmxMPK3 by LmxMKK or LmxPK4. Orange arrows indicate retrograde IFT regulated by LmxMPK13 and LmxMPK9, which are both phosphorylated by LmxPK4.

6.2 Conclusion and Future work

MAP2Ks play an important role during the *Leishmania* life cycle. This thesis was concerned with the analysis of the two MAP2K homologues, LmxPK3 and LmxPK6 in *L. mexicana.*

LmxPK6, with an unusually long N-terminus, was demonstrated to be a difficult to express recombinant protein, while LmxPK3 showed at least low amounts of recombinant protein, which was able to phosphorylate MBP *in vitro*. Future research should further develop and improve the expression of LmxPK6 and LmxPK3. Other

expression systems could be tested such as insect cells and yeast. Once sufficient amounts of protein can be generated the kinases can be further characterised with regard to temperature, ion concentrations and pH in *in vitro* kinase assays.

Several successive rounds of LmxPK6 transfection did not produce a double allele knockout mutant using standard homologous recombination methods relying on the flanking regions of LmxPK6, suggesting that this gene might be essential in *Leishmania*. Hence, further investigations are necessary to validate this conclusion such as using the CRISPR-Cas9 system to generate an LmxPK6 null mutant. On the other hand, the LmxPK3 knockout was successfully generated in this work and mouse infection studies using this mutant showed that LmxPK3 is not required in the two main life cycle stages, promastigotes and amastigotes. However, sand fly infection studies could reveal whether any of the sand fly stages require the activity of LmxPK3.

This study also investigated the interaction between LmxMPK3 and LmxPK4. LmxPK4 and LmxMPK3 were already known to play a role in flagellum length regulation, and the research presented in the thesis successfully identified the interaction between the MAP2K LmxPK4 and the MAPK LmxMPK3 *in vitro*. Recombinant co-expression of the two kinases, LmxMPK3 co-expressed with LmxPK4 in *E. coli,* led to the purification of a highly active LmxMPK3. LmxPK4 was shown to phosphorylate LmxMPK3 at TYR196, THR194 and SER183 in the activation loop of LmxMPK3. This provides a good starting point for further research to study the role of SER183 phosphorylation in *L. mexicana* using mutant versions of LmxMPK3, which cannot be phosphorylated (SER to ALA) or which mimic phosphorylation (SER to ASP). Moreover, this was also the first time using split di-GFP to study the interaction between a MAP2K and MAPK in *Leishmania in vivo.* Future investigations are necessary to examine the interaction between LmxMPK3

and LmxPK4 by using appropriate controls such as *Leishmania* promastigotes expressing GFP1-10 alone along with LmxMPK3GFP11.

Chapter 8: References

8 References

Aboagye-Kwarteng, T., Ole-MoiYoi, O. K.and Lonsdale-Eccles, J. D., 1991. Phosphorylation differences among proteins of bloodstream developmental stages of *Trypanosoma brucei*. *Biochem J, 275*, pp.7-14.

Absalon S, Blisnick T, Kohl L, Toutirais G, Doré G, Julkowska D, Tavenet A, Bastin P., 2008. Intraflagellar transport and functional analysis of genes required for flagellum formation in trypanosomes. *Mol Biol Cell, 19,* pp.929-44.

Al-Chalabi, K.A., Ziz, L.A. and Al-Khayat, B., 1989. Presence and properties of cAMP phosphodiesterase from promastigote forms of *Leishmania tropica* and *Leishmania donovani*. *Comparative Biochemistry and Physiology. B, Comparative Biochemistry, 93(4),* pp.789-792.

Adler-Moore, J.P. and Proffitt, R.T., 1993. Development, characterization, efficacy and mode of action of AmBisome, a unilamellar liposomal formulation of amphotericin B. *Journal of Liposome Research, 3(3),* pp.429-450.

Allocco, J.J., Donald, R., Zhong, T., Lee, A., Tang, Y.S., Hendrickson, R.C., Liberator, P. and Nare, B., 2006. Inhibitors of casein kinase 1 block the growth of *Leishmania major* promastigotes *in vitro*. *International Journal for Parasitology, 36(12),* pp.1249-1259.

Alvar, J., Vélez, I.D., Bern, C., Herrero, M., Desjeux, P., Cano, J., Jannin, J., den Boer, M. and WHO Leishmaniasis Control Team, 2012. Leishmaniasis worldwide and global estimates of its incidence. *PloS one, 7(5),* p. e35671.

Alessi, D.R., Saito, Y., Campbell, D.G., Cohen, P., Sithanandam, G., Rapp, U., Ashworth, A., Marshall, C.J. and Cowley, S., 1994. Identification of the sites in MAP kinase kinase-1 phosphorylated by p74raf-1. *The EMBO journal, 13(7),* pp.1610-1619.

Alexander, B. and Maroli, M., 2003. Control of phlebotomine sandflies. *Medical and Veterinary Entomology, 17(1),* pp.1-18.

Akopyants, N.S., Kimblin, N., Secundino, N., Patrick, R., Peters, N., Lawyer, P., Dobson, D.E., Beverley, S.M. and Sacks, D.L., 2009. Demonstration of genetic exchange during cyclical development of *Leishmania* in the sand fly vector. *Science, 324(5924),* pp.265-268.

Afrin, F., Rajesh, R., Anam, K., Gopinath, M., Pal, S. and Ali, N., 2002. Characterization of *Leishmania donovani* antigens encapsulated in liposomes that induce protective immunity in BALB/c mice. *Infection and Immunity, 70(12),* pp.6697-6706.

Avilov, S.V. and Aleksandrova, N., 2018. Fluorescence protein complementation in microscopy: applications beyond detecting bi-molecular interactions. *Methods and Applications in Fluorescence, 7(1),* p.012001.

Ashutosh, Garg, M., Sundar, S., Duncan, R., Nakhasi, H. L. and Goyal, N., 2012. Downregulation of mitogenactivated protein kinase 1 of *Leishmania donovani* field isolates is associated with antimony resistance. *Antimicrobial Agents and Chemotherapy, 56(1),* 518-525.

Bandyopadhyay, G., Sajan, M.P., Kanoh, Y., Standaert, M. L., Burke, T. R. Jr., Quon, M. J., Reed, B. C., Dikic, I., Noel, L. E., Newgard, C. B. and Farese, R., 2000. Glucose activates mitogen-activated protein kinase (extracellular signal-regulated kinase) through proline-rich tyrosine kinase-2 and the Glut1 glucose transporter. *J Biol Chem, 275*, 40817-40822.

Banuls, A. L., Hide, M. and Tibayrenc, M., 2002. Evolutionary genetics and molecular diagnosis of *Leishmania* species. *Transactions of the Royal Society of Tropical Medicine and Hygiene, 96 (Suppl 1)*, S9-S13.

Barcinski, M.A., Schechtman, D., Quintao, L.G., de A Costa, D., Soares, L.R., Moreira, M.E. and Charlab, R., 1992. Granulocyte-macrophage colony-stimulating factor increases the infectivity of Leishmania amazonensis by protecting promastigotes from heat-induced death. *Infection and Immunity*, *60*(9), pp.3523-3527.

Bardwell, L., 2006. Mechanisms of MAPK signalling specificity. *Journal of Biological Chemistry*, *34(5),* pp.837-841.

Bardwell, A.J., Flatauer, L.J., Matsukuma, K., Thorner, J. and Bardwell, L., 2001. A conserved docking site in MEKs mediates high-affinity binding to MAP kinases and cooperates with a scaffold protein to enhance signal transmission. *Journal of Biological Chemistry, 276(13),* pp.10374-10386.

Bardwell, L. and Thorner, J., 1996. A conserved motif at the amino termini of MEKs might mediate high-affinity interaction with the cognate MAPKs. *Trends in Biochemical Sciences, 21(10),* pp.373-374.

Bari, A.U., 2012. Clinical spectrum of cutaneous leishmaniasis: an overview from Pakistan. *Dermatology Online Journal*, *18*(2), pp.4-4.

Bao, Y., Weiss, L.M., Braunstein, V.L. and Huang, H., 2008. Role of protein kinase A in *Trypanosoma cruzi*. *Infection and Immunity, 76(10)*, pp.4757-4763.

Baneyx, F., 1999. Recombinant protein expression in *Escherichia coli*. *Current Opinion in Biotechnology, 10(5)*, pp.411-421.

Bastin, P., Pullen, T. J., Moreira-Leite, F. F. and Gull, K., 2000. Inside and outside of the trypanosome flagellum: a multifunctional organelle. *Microbes Infect, 2*, pp.1865-1874.

Bastin, P., Ellis, K., Kohl, L. and Gull, K., 2000. Flagellum ontogeny in trypanosomes studied via an inherited and regulated RNA interference system. *Journal of Cell Science*, *113*(18), pp.3321-3328.

Bates, P.A. and Rogers, M.E., 2004. New insights into the developmental biology and transmission mechanisms of *Leishmania*. *Current Molecular Medicine*, *4*(6), pp.601-609.

Bates, P. A., 2007. Transmission of *Leishmania* metacyclic promastigotes by phlebotomine sand flies. *International Journal for Parasitology*, 37, pp.1097-1110.

Bengs, F., Scholz, A., Kuhn, D. and Wiese, M., 2005. LmxMPK9, a mitogen-activated protein kinase homologue affects flagellar length in *Leishmania mexicana. Molecular Microbiology*, *55*(5), pp.1606-1615.

Berman, S. A., Wilson, N. F., Haas, N. A. and Lefebvre, P. A., 2003. A novel MAP kinase regulates flagellar length in *Chlamydomonas*. *Curr Biol*, *13*, pp.1145-1149.

Beverley, S. M., 1991. Gene amplification in *Leishmania*. *Annual Review of Microbiology*, *45*(1), pp.417-444.

Bleicher, N.M., 2019. Characterization of the MAP kinase LmxMPK7 and the glycogen synthase kinases GSK3α and GSK3β of the human pathogenic parasite *Leishmania mexicana*. Doctoral Dissertation, *University of Hamburg,* Hamburg, Germany.

Borba, J.V., Silva, A.C., Ramos, P.I., Grazzia, N., Miguel, D.C., Muratov, E.N., Furnham, N. and Andrade, C.H., 2019. Unveiling the Kinomes of *Leishmania infantum* and *Leishmania braziliensis* Empowers the Discovery of New Kinase Targets and Antileishmanial Compounds.*Computational and Structural Biotechnology Journal*,*17*, pp.352-361.

Boynak, N.Y., Rojas, F., D'Alessio, C., Larrea, S.C.V., Rodriguez, V., Ghiringhelli, P.D. and Tellez-Inon, M.T., 2013. Identification of a Wee1–Like Kinase Gene Essential for Procyclic *Trypanosoma brucei* Survival. *PloS one*, *8*(11), p. e79364.

Bird, L.E., 2011. High throughput construction and small scale expression screening of multi-tag vectors in *Escherichia coli*. *Methods*, *55*(1), pp.29-37.

Bradley, B. A. and Quarmby, L. M., 2005.A NIMA-related kinase, Cnk2p, regulates both flagellar length and cell size in *Chlamydomonas*. *J Cell Sci*, *118*, 3317-3326.

Brandau, S., Dresel, A. and Clos, J., 1995. High constitutive levels of heat-shock proteins in human pathogenic parasites of the genus *Leishmania*. *Biochem J*, *310*, 225-232.

Branche, C., Kohl, L., Toutirais, G., Buisson, J., Cosson, J. and Bastin, P., 2006. Conserved and specific functions of axoneme components in trypanosome motility. *Journal of Cell Science*, *119*(16), pp.3443-3455.

Brotherton, M.C., Bourassa, S., Legare, D., Poirier, G.G., Droit, A. and Ouellette, M., 2014. Quantitative proteomic analysis of amphotericin B resistance in *Leishmania infantum*. International Journal for Parasitology: *Drugs and Drug Resistance*, *4*(2), pp.126-132.

Bringaud, F., Vedrenne, C., Cuvillier, A., Parzy, D., Baltz, D., Tetaud, E., Pays, E., Venegas, J., Merlin, G. and Baltz, T. 1998. Conserved organization of genes in trypanosomatids. *Mol Biochem Parasitol*, *94*, pp.249-264.

Britto, C., Ravel, C., Bastien, P., Blaineau, C., Pages, M., Dedet, J.P. and Wincker, P., 1998. Conserved linkage groups associated with large-scale chromosomal rearrangements between Old World and New World *Leishmania* genomes. *Gene*, *222*(1), pp.107-117.

Brumlik, M.J., Pandeswara, S., Ludwig, S.M., Murthy, K. and Curiel, T.J., 2011. Parasite mitogen-activated protein kinases as drug discovery targets to treat human protozoan pathogens. *Journal of Signal Transduction*, *2011*.

Brun, R., 1979. Cultivation and in vitro cloning or procyclic culture forms of *Trypanosoma brucei* in a semi-defined medium. Short communication. *Acta Tropica*, *36*(3), pp.289-292.

Burghoorn, J., Dekkers, M.P., Rademakers, S., de Jong, T., Willemsen, R. and Jansen, G., 2007. Mutation of the MAP kinase DYF-5 affects docking and undocking of kinesin-2

motors and reduces their speed in the cilia of *Caenorhabditis elegans*. *Proceedings of the National Academy of Sciences*, *104*(17), pp.7157-7162.

Cabantous, S. and Waldo, G.S., 2006. *In vivo* and *in vitro* protein solubility assays using split GFP. *Nature Methods*, *3*(10), p.845.

Calvert, P.D., Klenchin, V.A. and Bownds, M.D., 1995. Rhodopsin Kinase Inhibition by Recoverin Funcion of Recoverin Myristoylation. *Journal of Biological Chemistry*, *270*(41), pp.24127-24129.

Canagarajah, B.J., Khokhlatchev, A., Cobb, M.H. and Goldsmith, E.J., 1997. Activation mechanism of the MAP kinase ERK2 by dual phosphorylation. *Cell*, *90*(5), pp.859-869.

Cargnello, M. and Roux, P.P., 2011. Activation and function of the MAPKs and their substrates, the MAPK-activated protein kinases. *Microbiol. Mol. Biol. Rev.*, *75*(1), pp.50-83.

Carrera, A.C., Alexandrov, K. and Roberts, T.M., 1993. The conserved lysine of the catalytic domain of protein kinases is actively involved in the phosphotransfer reaction and not required for anchoring ATP. *Proceedings of the National Academy of Sciences*, *90*(2), pp.442-446.

Cayla, M., Rachidi, N., Leclercq, O., Schmidt-Arras, D., Rosenqvist, H., Wiese, M. and Spath, G.F., 2014. Transgenic analysis of the *Leishmania* MAP kinase MPK10 reveals an auto-inhibitory mechanism crucial for stage-regulated activity and parasite viability. *PLoS pathogens*, *10*(9), p. e1004347.

Cayla, M., Rachidi, N., Leclercq, O., Schmidt-Arras, D., Rosenqvist, H., Wiese, M. and Späth, G.F., 2014. Transgenic analysis of the *Leishmania* MAP kinase MPK10 reveals an auto-inhibitory mechanism crucial for stage-regulated activity and parasite viability. *PLoS pathogens*, *10*(9), p. e1004347.

Chhajer, R., Bhattacharyya, A., Didwania, N., Shadab, M., Das, N., Palit, P., Vaidya, T. and Ali, N., 2016. *Leishmania donovani* Aurora kinase: a promising therapeutic target against visceral leishmaniasis. *Biochimica et Biophysica Acta (BBA)-General Subjects*, *1860*(9), pp.1973-1988.

Chen, Q., Luo, H., Zhang, C. and Chen, Y.P.P., 2015. Bioinformatics in protein kinases regulatory network and drug discovery. *Mathematical Biosciences*, *262*, pp.147-156.

Cheng, H. C., Qi, R. Z., Paudel, H. and Zhu, H. J., 2011. Regulation and function of protein kinases and phosphatases. *Enzyme Research*.*EMBO J*, *21*, pp.1881-1888.

Cheng, Y. and Tian, H., 2017. Current development status of MEK inhibitors. *Molecules*, *22*(10), p.1551.

Clayton, C.E., 2002. Life without transcriptional control? From fly to man and back again. *The EMBO journal*, *21*(8), pp.1881-1888.

Croft, S.L. and Coombs, G.H., 2003. Leishmaniasis–current chemotherapy and recent advances in the search for novel drugs. *Trends in parasitology*, *19*(11), pp.502-508.

Croft, S.L., Sundar, S. and Fairlamb, A.H., 2006. Drug resistance in leishmaniasis. Clinical Microbiology Reviews, *19*(1), pp.111-126.

Cruz, A.K., Titus, R. and Beverley, S.M., 1993. Plasticity in chromosome number and testing of essential genes in *Leishmania* by targeting. *Proceedings of the National Academy of Sciences*, *90*(4), pp.1599-1603.

Cruz, A., Coburn, C.M. and Beverley, S.M., 1991. Double targeted gene replacement for creating null mutants. *Proceedings of the National Academy of Sciences*, *88*(16), pp.7170-7174.

Dean, S., Sunter, J.D. and Wheeler, R.J., 2017. TrypTag.org: a trypanosome genome-wide protein localisation resource. *Trends in Parasitology*, *33*(2), pp.80-82.

Castro, S.L.D. and Luz, M.R., 1993. The second messenger cyclic 3′, 5′-adenosine monophosphate in pathogenic microorganisms with special reference to protozoa. *Canadian journal of Microbiology*, *39*(5), pp.473-479.

De Moura, T.R., Santos, M.L.B., Braz, J.M., Santos, L.F.V., Aragão, M.T., de Oliveira, F.A., Santos, P.L., da Silva, A.M., de Jesus, A.R. and de Almeida, R.P., 2016. Cross-resistance of *Leishmania infantum* isolates to nitric oxide from patients' refractory to antimony treatment, and greater tolerance to antileishmanial responses by macrophages. *Parasitology Research*, *115*(2), pp.713-721.

Dell, K.R. and Engel, J.N., 1994. Stage-specific regulation of protein phosphorylation in *Leishmania major*. *Molecular and Biochemical Parasitology*, *64*(2), pp.283-292.

Docampo, R., 2011. Molecular parasitology in the 21st century. *Essays in Biochemistry*, *51*, pp.1-13.

Docampo, R. and Moreno, S.N.J., 1999. Acidocalcisome: a novel Ca^{2+} storage compartment in trypanosomatids and apicomplexan parasites. *Parasitology Today*, *15*(11), pp.443-448.

Dorlo, T.P., Balasegaram, M., Beijnen, J.H. and de Vries, P.J., 2012. Miltefosine: a review of its pharmacology and therapeutic efficacy in the treatment of leishmaniasis. *Journal of Antimicrobial Chemotherapy*, *67*(11), pp.2576-2597.

Dostalova, A. and Volf, P., 2012. *Leishmania* development in sand flies: parasite-vector interactions overview. *Parasites & Vectors*, *5*(1), p.276.

Duncan, S.M., Jones, N.G. and Mottram, J.C., 2017. Recent advances in *Leishmania* reverse genetics: Manipulating a manipulative parasite. *Molecular and Biochemical Parasitology*, *216*, pp.30-38.

Dumetz, F., Imamura, H., Sanders, M., Seblova, V., Myskova, J., Pescher, P., Vanaerschot, M., Meehan, C.J., Cuypers, B., De Muylder, G. and Spath, G.F., 2017. Modulation of aneuploidy in *Leishmania donovani* during adaptation to different in vitro and in vivo environments and its impact on gene expression. *MBio*, *8*(3), pp. e00599-17.

Ellis, J., Sarkar, M., Hendriks, E. and Matthews, K., 2004. A novel ERK-like, CRK-like protein kinase that modulates growth in *Trypanosoma brucei* via an autoregulatory C-terminal extension. *Molecular Microbiology*, *53*(5), pp.1487-1499.

Endicott, J.A., Noble, M.E. and Johnson, L.N., 2012. The structural basis for control of eukaryotic protein kinases. *Annual Review of Biochemistry*, *81*, pp.587-613.

Engman, D.M., Krause, K.H., Blumin, J.H., Kim, K.S., Kirchhoff, L.V. and Donelson, J.E., 1989. A novel flagellar Ca^{2+}-binding protein in trypanosomes. *Journal of Biological Chemistry*, *264*(31), pp.18627-18631.

Erdmann, M., 2009. LmxMPK3, a mitogen-activated protein kinase involved in length control of a eukaryotic flagellum. Doctoral Dissertation, *University of Hamburg, Hamburg, Germany.*

Erdmann, M., Scholz, A., Melzer, I.M., Schmetz, C. and Wiese, M., 2006. Interacting protein kinases involved in the regulation of flagellar length. *Molecular Biology of The cell, 17*(4), *pp.2035-2045.*

Emmerson, J., 2014. Determining the substrates for MAP kinases in *Leishmania mexicana. MReS Dissertation, University of Hamburg*.

Ersfeld, K., Barraclough, H. and Gull, K., 2005. Evolutionary relationships and protein domain architecture in an expanded calpain superfamily in kinetoplastid parasites. *Journal of Molecular Evolution*, *61*(6), pp.742-757.

Fiebig, M., Kelly, S. and Gluenz, E., 2015. Comparative life cycle transcriptomics revises *Leishmania mexicana* genome annotation and links a chromosome duplication with parasitism of vertebrates. *PLoS pathogens*, *11*(10), p. e1005186.

Finnigan, G.C., Duvalyan, A., Liao, E.N., Sargsyan, A. and Thorner, J., 2016. Detection of protein–protein interactions at the septin collar in *Saccharomyces cerevisiae* using a tripartite split-GFP system. *Molecular Biology of The cell*, *27*(17), pp.2708-2725.

Fisch, C. and Dupuis-Williams, P., 2011. Ultrastructure of cilia and flagella–back to the future! *Biology of The Cell,* 103(6), pp.249-270.

Ghorbani, M. and Farhoudi, R., 2018. Leishmaniasis in humans: drug or vaccine therapy? Drug design, *Development and Therapy*, 12, p.25.

Ghosh, I., Hamilton, A.D. and Regan, L., 2000. Antiparallel leucine zipper-directed protein reassembly: application to the green fluorescent protein. *Journal of the American Chemical Society*, *122*(23), pp.5658-5659.

Gibbs, C.S. and Zoller, M.J., 1991. Rational scanning mutagenesis of a protein kinase identifies functional regions involved in catalysis and substrate interactions. *Journal of Biological Chemistry*, *266*(14), pp.8923-8931.

Goldsmith, E.J., Akella, R., Min, X., Zhou, T. and Humphreys, J.M., 2007. Substrate and docking interactions in serine/threonine protein kinases. *Chemical Reviews*, *107*(11), pp.5065-5081.

Sela, D., Milman, N., Kapeller, I., Zick, A., Bezalel, R., Yaffe, N. and Shlomai, J., 2008. Unique characteristics of the kinetoplast DNA replication machinery provide potential drug targets in trypanosomatids. In *Drug Targets in Kinetoplastid Parasites*. Springer, New York, NY. pp.9-21.

Gueiros-Filho, F.J. and Beverley, S.M., 1996. Selection against the dihydrofolate reductase-thymidylate synthase (DHFR-TS) locus as a probe of genetic alterations in *Leishmania major*. *Molecular and Cellular Biology*, *16*(10), pp.5655-5663.

Guttinger, A., Schwab, C., Morand, S., Roditi, I. and Vassella, E., 2007. A mitogen-activated protein kinase of *Trypanosoma brucei* confers resistance to temperature stress. *Molecular and Biochemical Parasitology*, *153*(2), pp.203-206.

Grewal, S., Molina, D.M. and Bardwell, L., 2006. Mitogen-activated protein kinase (MAPK)-docking sites in MAPK kinases function as tethers that are crucial for MAPK regulation in vivo. *Cellular Signalling*, *18*(1), pp.123-134.

Hanahan, D., 1983. Studies on transformation of *Escherichia coli* with plasmids. *Journal of Molecular Biology*, *166*(4), pp.557-580.

Hammaker, D. and Firestein, G.S., 2010. Go upstream, young man: lessons learned from the p38 saga. *Annals of The Rheumatic Diseases*, *69*(Suppl 1), pp. i77-i82.

Hammarstrom, M., Woestenenk, E.A., Hellgren, N., Hard, T. and Berglund, H., 2006. Effect of N-terminal solubility enhancing fusion proteins on yield of purified target protein. *Journal of Structural and Functional Genomics*, *7*(1), pp.1-14.

Hammarton, T.C., Kramer, S., Tetley, L., Boshart, M. and Mottram, J.C., 2007. *Trypanosoma brucei* Polo-like kinase is essential for basal body duplication, kDNA segregation and cytokinesis. *Molecular Microbiology*, *65*(5), pp.1229-1248.

Hassan, P., Fergusson, D., Grant, K.M. and Mottram, J.C., 2001. The CRK3 protein kinase is essential for cell cycle progression of *Leishmania mexicana.* Molecular and Biochemical Parasitology, *113*(2), pp.189-198.

Hanks, S.K. and Hunter, T., 1995. Protein kinases 6. The eukaryotic protein kinase superfamily: kinase (catalytic) domain structure and classification. *The FASEB journal*, *9*(8), pp.576-596.

Henriquez, F.L., Campbell, S.A., Roberts, C.W., Mullen, A.B., Burchmore, R. and Carter, K.C., 2010. Vaccination with recombinant *Leishmania donovani* gamma-glutamylcysteine synthetase fusion protein protects against L. donovani infection. *Journal of Parasitology*, *96*(5), pp.929-937.

Hombach-Barrigah, A., Bartsch, K., Smirlis, D., Rosenqvist, H., MacDonald, A., Dingli, F., Loew, D., Spath, G.F., Rachidi, N., Wiese, M. and Clos, J., 2019. *Leishmania donovani* 90 kD Heat Shock Protein–Impact of Phosphosites on Parasite Fitness, Infectivity and Casein Kinase Affinity. *Scientific Reports*, *9*(1), p.5074.

Hombach, A., Ommen, G., Chrobak, M. and Clos, J., 2013. The Hsp 90–Sti 1 interaction is critical for *Leishmania donovani* proliferation in both life cycle stages. *Cellular Microbiology*, *15*(4), pp.585-600.

Hanks, S.K. and Hunter, T., 1995. Protein kinases 6. The eukaryotic protein kinase superfamily: kinase (catalytic) domain structure and classification. *The FASEB journal*, *9*(8), pp.576-596.

Hua, S.B. and Wang, C.C., 1997. Interferon-γ activation of a mitogen-activated protein kinase, KFR1, in the bloodstream form of *Trypanosoma brucei*. *Journal of Biological Chemistry*, *272*(16), pp.10797-10803.

Hubbard, M.J. and Cohen, P., 1993. On target with a new mechanism for the regulation of protein phosphorylation. *Trends in Biochemical Sciences*, *18*(5), pp.172-177.

Hubel, A., Brandau, S., Dresel, A. and Clos, J., 1995. A member of the ClpB family of stress proteins is expressed during heat shock in *Leishmania* spp. *Molecular and Biochemical Parasitology*, *70*(1-2), pp.107-118.

Hussain, H., Al-Harrasi, A., Al-Rawahi, A., Green, I.R. and Gibbons, S., 2014. Fruitful decade for antileishmanial compounds from 2002 to late 2011. *Chemical Reviews*, *114*(20), pp.10369-10428.

Hide, G., Gray, A., Harrison, C.M. and Tait, A., 1989. Identification of an epidermal growth factor receptor homologue in trypanosomes. *Molecular and Biochemical Parasitology*, *36*(1), pp.51-59.

Infante, J.R., Fecher, L.A., Falchook, G.S., Nallapareddy, S., Gordon, M.S., Becerra, C., DeMarini, D.J., Cox, D.S., Xu, Y., Morris, S.R. and Peddareddigari, V.G., 2012. Safety, pharmacokinetic, pharmacodynamic, and efficacy data for the oral MEK inhibitor trametinib: a phase 1 dose-escalation trial. *The lancet Oncology*, *13*(8), pp.773-781.

Ivens, A.C. and Blackwell, J.M., 1999. The *Leishmania* genome comes of age. *Parasitology Today*, *15*(6), pp.225-231.

Ivens, A.C., Peacock, C.S., Worthey, E.A., Murphy, L., Aggarwal, G., Berriman, M., Sisk, E., Rajandream, M.A., Adlem, E., Aert, R. and Anupama, A., 2005. The genome of the kinetoplastid parasite, *Leishmania major*. *Science*, *309*(5733), pp.436-442.

Jeffrey, K.L., Camps, M., Rommel, C. and Mackay, C.R., 2007. Targeting dual-specificity phosphatases: manipulating MAP kinase signalling and immune responses. *Nature Reviews Drug Discovery*, *6*(5), p.391.

Johnson, L.N. and Lewis, R.J., 2001. Structural basis for control by phosphorylation. *Chemical Reviews*, *101*(8), pp.2209-2242.

Johnson, S.A. and Hunter, T., 2005. Kinomics: methods for deciphering the kinome. *Nature Methods*, *2*(1), p.17.

John von Freyend, S., Rosenqvist, H., Fink, A., Melzer, I.M., Clos, J., Jensen, O.N. and Wiese, M., 2010. LmxMPK4, an essential mitogen-activated protein kinase of *Leishmania mexicana* is phosphorylated and activated by the STE7-like protein kinase LmxMKK5.*International Journal for Parasitology*,*40*(8), pp.969-978.

Jones, N.G., Catta-Preta, C.M., Lima, A.P.C. and Mottram, J.C., 2018. Genetically validated drug targets in *Leishmania*: current knowledge and future prospects. *ACS Infectious Diseases*, *4*(4), pp.467-477.

Kamhawi, S., 2006. Phlebotomine sand flies and *Leishmania* parasites: friends or foes? *Trends in Parasitology*, *22*(9), pp.439-445.

Kassi, M., Kassi, M., Afghan, A.K., Rehman, R. and Kasi, P.M., 2008. Marring leishmaniasis: the stigmatization and the impact of cutaneous leishmaniasis in Pakistan and Afghanistan. *PLoS Neglected Tropical Diseases*, *2*(10), p. e259.

Kaur, P., Garg, M., Hombach-Barrigah, A., Clos, J. and Goyal, N., 2017. MAPK1 of *Leishmania donovani* interacts and phosphorylates HSP70 and HSP90 subunits of foldosome complex. *Scientific Reports*, *7*(1), p.10202.

Kohl, L., Robinson, D. and Bastin, P., 2003. Novel roles for the flagellum in cell morphogenesis and cytokinesis of trypanosomes. *The EMBO journal*, *22*(20), pp.5336-5346.

Krupa, A., Preethi, G. and Srinivasan, N., 2004. Structural modes of stabilization of permissive phosphorylation sites in protein kinases: distinct strategies in Ser/Thr and Tyr kinases. *Journal of Molecular Biology*, *339*(5), pp.1025-1039.

Kuhn, D. and Wiese, M., 2005. LmxPK4, a mitogen-activated protein kinase kinase homologue of *Leishmania mexicana* with a potential role in parasite differentiation. *Molecular Microbiology*, *56*(5), pp.1169-1182.

Kultz, D., 1998. Phylogenetic and functional classification of mitogen-and stress-activated protein kinases. *Journal of Molecular Evolution*, *46*(5), pp.571-588.

Landfear, S.M. and Ignatushchenko, M., 2001. The flagellum and flagellar pocket of trypanosomatids. *Molecular and Biochemical Parasitology*, *115*(1), pp.1-17.

Lane, R.P., 1993. Sand flies (Phlebotominae). In *Medical insects and arachnids*. Springer, Dordrecht.pp. 78-119.

Laxman, S. and Beavo, J.A., 2007. Cyclic nucleotide signaling mechanisms in trypanosomes: possible targets for therapeutic agents. *Molecular Interventions*, *7*(4), p.203.

Lawler, S., Fleming, Y., Goedert, M. and Cohen, P., 1998. Synergistic activation of SAPK1/JNK1 by two MAP kinase kinases in vitro. *Current Biology*, *8*(25), pp.1387-1391.

Lee, J.S., Huh, K.W., Bhargava, A. and Ellis, B.E., 2008. Comprehensive analysis of protein-protein interactions between *Arabidopsis* MAPKs and MAPK kinases helps define potential MAPK signalling modules. *Plant Signaling & Behavior*, *3*(12), pp.1037-1041.

Lodish, H. F., Berk, A., Kaiser, C. A., Krieger, M., Bretsche, A., Ploegh, H., Amon, A. & Scott, M. P. 2013. *Molecular cell Biology*, USA, New York: W.H. Freeman and Co.

Luhovy, A.Y., Jaberi, A., Papillon, J., Guillemette, J. and Cybulsky, A.V., 2012. Regulation of the Ste20-like Kinase, Slk Involvement of Activation Segment Phosphorylation. *Journal of Biological Chemistry*, *287*(8), pp.5446-5458.

Lukes, J., Hashimi, H. and Zikova, A., 2005. Unexplained complexity of the mitochondrial genome and transcriptome in kinetoplastid flagellates. *Current Genetics*, *48*(5), pp.277-299.

Manning, G., Whyte, D.B., Martinez, R., Hunter, T. and Sudarsanam, S., 2002a. The protein kinase complement of the human genome. *Science*, *298*(5600), pp.1912-1934.

Manning, G., Plowman, G.D., Hunter, T. and Sudarsanam, S., 2002b. Evolution of protein kinase signaling from yeast to man. *Trends in Biochemical Sciences*, *27*(10), pp.514-520.

Mandal, G., Sharma, M., Kruse, M., Sander-Juelch, C., Munro, L.A., Wang, Y., Vilg, J.V., Tamás, M.J., Bhattacharjee, H., Wiese, M. and Mukhopadhyay, R., 2012. Modulation of *Leishmania major* aquaglyceroporin activity by a mitogen-activated protein kinase. *Molecular Microbiology*, *85*(6), pp.1204-1218.

Maran, N., Gomes, P.S., Freire-de-Lima, L., Freitas, E.O., Freire-de-Lima, C.G. and Morrot, A., 2016. Host resistance to visceral leishmaniasis: prevalence and prevention. *Expert review of Anti-Infective Therapy*, *14*(4), pp.435-442.

Martinez-Calvillo, S., Stuart, K. and Myler, P.J., 2005. Ploidy changes associated with disruption of two adjacent genes on *Leishmania major* chromosome 1. *International Journal for Parasitology*, *35*(4), pp.419-429.

Manzano, J.I., Perea, A., León-Guerrero, D., Campos-Salinas, J., Piacenza, L., Castanys, S. and Gamarro, F., 2017. *Leishmania* LABCG1 and LABCG2 transporters are involved in virulence and oxidative stress: functional linkage with autophagy. *Parasites & Vectors*, *10*(1), p.267.

McMichael, A.J. and Koff, W.C., 2014. Vaccines that stimulate T cell immunity to HIV-1: the next step. *Nature Immunology*, *15*(4), p.319.

Melzer, I. M., 2007. Biochemische Charakterisierung von LmxMPK1, einer essentiellen MAP Kinase aus *Leishmania mexicana*. Doctoral dissertation, *University of Hamburg,* Hamburg, Germany.

Mottram, J.C., McCready, B.P., Brown, K.G. and Grant, K.M., 1996. Gene disruptions indicate an essential function for the LmmCRK1 cdc2-related kinase of *Leishmania mexicana*. *Molecular Microbiology*, *22*(3), pp.573-582.

Michaeli, S., 2011. Trans-splicing in trypanosomes: machinery and its impact on the parasite transcriptome. *Future Microbiology*, *6*(4), pp.459-474.

Miller, C.J. and Turk, B.E., 2018. Homing in: mechanisms of substrate targeting by protein kinases. *Trends in Biochemical Sciences*, *43*(5), pp.380-394.

Min, X., Akella, R., He, H., Humphreys, J.M., Tsutakawa, S.E., Lee, S.J., Tainer, J.A., Cobb, M.H. and Goldsmith, E.J., 2009. The structure of the MAP2K MEK6 reveals an autoinhibitory dimer. *Structure*, *17*(1), pp.96-104.

Minodier, P. and Parola, P., 2007. Cutaneous leishmaniasis treatment. *Travel Medicine and Infectious disease*, *5*(3), pp.150-158.

Miroux, B. and Walker, J.E., 1996. Over-production of proteins in Escherichia coli: mutant hosts that allow synthesis of some membrane proteins and globular proteins at high levels. *Journal of Molecular Biology*, *260*(3), pp.289-298.

Moreno, S.N., Vercesi, A.E., Pignataro, O.P. and Docampo, R., 1992. Calcium homeostasis in *Trypanosoma cruzi* amastigotes: presence of inositol phosphates and lack of an inositol 1, 4, 5-trisphosphate-sensitive calcium pool. *Molecular and Biochemical Parasitology*, *52*(2), pp.251-261.

Murray, H.W., Berman, J.D., Davies, C.R. and Saravia, N.G., 2005. Advances in leishmaniasis. *The Lancet*, *366*(9496), pp.1561-1577.

Myler, P.J., Audleman, L., DeVos, T., Hixson, G., Kiser, P., Lemley, C., Magness, C., Rickel, E., Sisk, E., Sunkin, S. and Swartzell, S., 1999. *Leishmania major* Friedlin chromosome 1 has an unusual distribution of protein-coding genes. *Proceedings of the National Academy of Sciences*, *96*(6), pp.2902-2906.

Nare, B., Garraway, L.A., Vickers, T.J. and Beverley, S.M., 2009. PTR1-dependent synthesis of tetrahydrobiopterin contributes to oxidant susceptibility in the trypanosomatid protozoan

parasite *Leishmania major*. *Current Genetics*, *55*(3), pp.287-299.

Nishi, H., Hashimoto, K. and Panchenko, A.R., 2011. Phosphorylation in protein-protein binding: effect on stability and function. *Structure*, *19*(12), pp.1807-1815.

Nolan, D.P., Reverlard, P. and Pays, E., 1994. Overexpression and characterization of a gene for a Ca^{2+}-ATPase of the endoplasmic reticulum in *Trypanosoma brucei*. *Journal of Biological Chemistry*, *269*(42), pp.26045-26051.

Noazin, S., Modabber, F., Khamesipour, A., Smith, P.G., Moulton, L.H., Nasseri, K., Sharifi, I., Khalil, E.A., Bernal, I.D.V., Antunes, C.M. and Kieny, M.P., 2008. First generation leishmaniasis vaccines: A review of Field Efficacy Trials. Vaccine, *26*(52), pp.6759-6767.

Nozaki, T., Toh-e, A., Fujii, M., Yagisawa, H., Nakazawa, M. and Takeuchi, T., 1999. Cloning and characterization of a gene encoding phosphatidyl inositol-specific phospholipase C from *Trypanosoma cruzi*. *Molecular and Biochemical Parasitology*, *102*(2), pp.283-295.

Oberholzer, M., Marti, G., Baresic, M., Kunz, S., Hemphill, A. and Seebeck, T., 2007. The *Trypanosoma brucei* cAMP phosphodiesterases TbrPDEB1 and TbrPDEB2: flagellar enzymes that are essential for parasite virulence. *The FASEB Journal*, *21*(3), pp.720-731.

Ojo, K.K., Gillespie, J.R., Riechers, A.J., Napuli, A.J., Verlinde, C.L., Buckner, F.S., Gelb, M.H., Domostoj, M.M., Wells, S.J., Scheer, A. and Wells, T.N., 2008. Glycogen synthase kinase 3 is a potential drug target for African trypanosomiasis therapy. *Antimicrobial Agents and Chemotherapy*, *52*(10), pp.3710-3717.

Ojo, K.K., Arakaki, T.L., Napuli, A.J., Inampudi, K.K., Keyloun, K.R., Zhang, L., Hol, W.G., Verlinde, C.L., Merritt, E.A. and Van Voorhis, W.C., 2011. Structure determination of glycogen synthase kinase-3 from *Leishmania major* and comparative inhibitor structure–activity relationships with Trypanosoma brucei GSK-3. *Molecular and Biochemical Parasitology*, *176*(2), pp.98-108.

Ommen, G., Chrobak, M. and Clos, J., 2010. The co-chaperone SGT of *Leishmania donovani* is essential for the parasite's viability. *Cell Stress and Chaperones*, *15*(4), pp.443-455.

Ozcan, S., Dover, J., Rosenwald, A.G., Wolfl, S. and Johnston, M., 1996. Two glucose transporters in *Saccharomyces cerevisiae* are glucose sensors that generate a signal for induction of gene expression. *Proceedings of the National Academy of Sciences*, *93*(22), pp.12428-12432.

Pakhomov, A.A. and Martynov, V.I., 2008. GFP family: structural insights into spectral tuning. *Chemistry & Biology*, *15*(8), pp.755-764.

Palatnik-de-Sousa, C.B., 2008. Vaccines for leishmaniasis in the fore coming 25 years. *Vaccine*, *26*(14), pp.1709-1724.

Pan, J., Wang, Q. and Snell, W.J., 2004. An aurora kinase is essential for flagellar disassembly in *Chlamydomonas*. *Developmental cell*, *6*(3), pp.445-451.

Paindavoine, P., Rolin, S., Van Assel, S., Geuskens, M., Jauniaux, J.C., Dinsart, C., Huet, G. and Pays, E., 1992. A gene from the variant surface glycoprotein expression site encodes one of several transmembrane adenylate cyclases located on the flagellum of *Trypanosoma brucei*. *Molecular and Cellular Biology*, *12*(3), pp.1218-1225.

Parsons, M. and Ruben, L., 2000. Pathways involved in environmental sensing in trypanosomatids. *Parasitology Today*, *16*(2), pp.56-62.

Parsons, M., Worthey, E.A., Ward, P.N. and Mottram, J.C., 2005. Comparative analysis of the kinomes of three pathogenic trypanosomatids: *Leishmania major*, *Trypanosoma brucei* and *Trypanosoma cruzi*. *BMC genomics*, *6*(1), p.127.

Papadopoulou, B., Huang, X.F., Boucher, N. and McNicoll, F., 2003. Stage-specific regulation of gene expression in *Leishmania*. *ASM News-American Society for Microbiology*, *69*(6), pp.282-288.

Payne, D.M., Rossomando, A.J., Martino, P., Erickson, A.K., Her, J.H., Shabanowitz, J., Hunt, D.F., Weber, M.J. and Sturgill, T.W., 1991. Identification of the regulatory phosphorylation sites in pp42/mitogen-activated protein kinase (MAP kinase). *The EMBO journal*, *10*(4), pp.885-892.

Peacock, C.S., Seeger, K., Harris, D., Murphy, L., Ruiz, J.C., Quail, M.A., Peters, N., Adlem, E., Tivey, A., Aslett, M. and Kerhornou, A., 2007. Comparative genomic analysis of three *Leishmania* species that cause diverse human disease. *Nature Genetics*, *39*(7), p.839.

Pearson, G., Robinson, F., Beers Gibson, T., Xu, B.E., Karandikar, M., Berman, K. and Cobb, M.H., 2001. Mitogen-activated protein (MAP) kinase pathways: regulation and physiological functions. *Endocrine Reviews*, *22*(2), pp.153-183.

Pfister, D.D., Burkard, G., Morand, S., Renggli, C.K., Roditi, I. and Vassella, E., 2006. A mitogen-activated protein kinase controls differentiation of bloodstream forms of *Trypanosoma brucei*. *Eukaryotic Cell*, *5*(7), pp.1126-1135.

Perez-Victoria, F.J., Gamarro, F., Ouellette, M. and Castanys, S., 2003. Functional cloning of the miltefosine transporter A Novel P-type phospholipid translocase from *Leishmania* involved in drug resistance. Journal of Biological Chemistry, *278*(50), pp.49965-49971.

Picone, R., Ren, X., Ivanovitch, K.D., Clarke, J.D., McKendry, R.A. and Baum, B., 2010. A polarised population of dynamic microtubules mediates homeostatic length control in animal cells. *PLoS biology*, *8*(11), p. e1000542.

Pike, A.C., Rellos, P., Niesen, F.H., Turnbull, A., Oliver, A.W., Parker, S.A., Turk, B.E., Pearl, L.H. and Knapp, S., 2008. Activation segment dimerization: a mechanism for kinase autophosphorylation of non-consensus sites. *The EMBO Journal*, *27*(4), pp.704-714.

Pimenta, P.F.P., Modi, G.B., Pereira, S.T., Shahabuddin, M. and Sacks, D.L., 1997. A novel role for the peritrophic matrix in protecting *Leishmania* from the hydrolytic activities of the sand fly midgut. *Parasitology*, *115*(4), pp.359-369.

Pinto-Martinez, A.K., Rodriguez-Durán, J., Serrano-Martin, X., Hernandez-Rodriguez, V. and Benaim, G., 2018. Mechanism of action of miltefosine on *Leishmania donovani* involves the impairment of acidocalcisome function and the activation of the sphingosine-dependent plasma membrane Ca^{2+} channel. *Antimicrobial Agents and Chemotherapy*, *62*(1), pp.e01614-17.

Portman, N. and Gull, K., 2010. 'The paraflagellar rod of kinetoplastid parasites: from structure to components and function'. *International Journal for Parasitology,* 40(2), pp.135-148.

Piper, R.C., Xu, X., Russell, D.G., Little, B.M. and Landfear, S.M., 1995. Differential targeting of two glucose transporters from *Leishmania enriettii* is mediated by an NH2-terminal domain. *The Journal of Cell Biology*, *128*(4), pp.499-508.

Piperno, G.I.A.N.N.I. and Luck, D.J., 1976. Phosphorylation of axonemal proteins in *Chlamydomonas reinhardtii*. *Journal of Biological Chemistry*, *251*(7), pp.2161-2167.

Purkait, B., Kumar, A., Nandi, N., Sardar, A.H., Das, S., Kumar, S., Pandey, K., Ravidas, V., Kumar, M., De, T. and Singh, D., 2012. Mechanism of amphotericin B resistance in clinical isolates of *Leishmania donovani*. Antimicrobial Agents and Chemotherapy, 56(2), pp.1031-1041.

Rachidi, N., Taly, J.F., Durieu, E., Leclercq, O., Aulner, N., Prina, E., Pescher, P., Notredame, C., Meijer, L. and Spath, G.F., 2014. Pharmacological assessment defines *Leishmania*

donovani casein kinase 1 as a drug target and reveals important functions in parasite viability and intracellular infection. *Antimicrobial Agents and Chemotherapy*, *58*(3), pp.1501-1515.

Raman, M., Chen, W. and Cobb, M.H., 2007. Differential regulation and properties of MAPKs. *Oncogene*, *26*(22), p.3100.

Ramirez, C., Díaz-Toro, Y., Tellez, J., Castilho, T.M., Rojas, R., Ettinger, N.A., Tikhonova, I., Alexander, N.D., Valderrama, L., Hager, J. and Wilson, M.E., 2012. Human macrophage response to *L.(Viannia) panamensis*: microarray evidence for an early inflammatory response. *PLoS Neglected Tropical Diseases*, *6*(10), p. e1866.

Ramu, D., Jain, R., Kumar, RR, Sharma, V., Garg, S., Ayana, R., Luthra, T., Yadav, P., Sen, S. and Singh, S., 2019 Design and synthesis of imidazolidinone derivatives as potent anti-leishmanial agents by bioisosterism. *Pharmacy Archives*, *352* (4), p.1800290.

Remenyi, A., Good, M.C., Bhattacharyya, R.P. and Lim, W.A., 2005. The role of docking interactions in mediating signaling input, output, and discrimination in the yeast MAPK network. *Molecular cell*, *20*(6), pp.951-962.

Reithinger, R., Dujardin, J.C., Louzir, H., Pirmez, C., Alexander, B. and Brooker, S., 2007. Cutaneous leishmaniasis. *The Lancet infectious diseases*, *7*(9), pp.581-596.

Ridgley, E., Webster, P., Patton, C. and Ruben, L., 2000. Calmodulin-binding properties of the paraflagellar rod complex from *Trypanosoma brucei*. *Molecular and biochemical parasitology*, *109*(2), pp.195-201.

Rogers, M.B., Hilley, J.D., Dickens, N.J., Wilkes, J., Bates, P.A., Depledge, D.P., Harris, D., Her, Y., Herzyk, P., Imamura, H. and Otto, T.D., 2011. Chromosome and gene copy number variation allow major structural change between species and strains of *Leishmania*. *Genome research*, *21*(12), pp.2129-2142.

Rogers, M.E., Chance, M.L. and Bates, P.A., 2002. The role of promastigote secretory gel in the origin and transmission of the infective stage of *Leishmania mexicana* by the sandfly *Lutzomyia longipalpis*. *Parasitology*, *124*(5), pp.495-507.

Romei, M.G. and Boxer, S.G., 2019. Split green fluorescent proteins: scope, limitations, and outlook. *Annual Review of Biophysics*, *48*, pp.19-44.

Rosenqvist, H., 2011. *Leishmania mexicana* phosphoproteomics. Doctoral Dissertation, *University of Strathclyde, Glasgow, UK*.

Saraiva, E.M.B., Pimenta, P.F.P., Brodin, T.N., Rowton, E., Modi, G.B. and Sacks, D.L., 1995. Changes in lipophosphoglycan and gene expression associated with the development of *Leishmania major* in *Phlebotomus papatasi*. *Parasitology*, *111(3),* pp.275-287.

Schaeffer, H.J. and Weber, M.J., 1999. Mitogen-activated protein kinases: specific messages from ubiquitous messengers. *Molecular and Cellular Biology, 19(4),* pp.2435-2444.

Schlabe, S., 2007. Identification of activators of the mitogen-activated protein kinases of *Leishmania mexicana*. Diploma Dissertation, *University of Hamburg*, Hamburg, Germany.

Schlein, Y., Jacobson, R.L. and Shlomai, J., 1991. Chitinase secreted by *Leishmania* functions in the sandfly vector. *Proceedings of the Royal Society of London. Series B: Biological Sciences*, *245*(1313), pp.121-126.

Scholz, A., 2008. Interacting protein kinases in *Leishmania mexicana* which are involved in the regulation of flagellar length. Doctoral Dissertation *University of Hamburg*, Hamburg Germany.

Seebeck, T., Schaub, R. and Johner, A., 2004. cAMP signalling in the kinetoplastid protozoa. *Current Molecular Medicine*, *4*(6), pp.585-599.

Shadab, M. and Ali, N., 2011. Evasion of host defence by *Leishmania donovani*: subversion of signaling pathways. *Molecular Biology International*, *2011*.

Shaw, G., 1996. The pleckstrin homology domain: an intriguing multifunctional protein module. *Bioessays*, *18*(1), pp.35-46.

Soni, N., Jain, K., Gupta, U. and Jain, N.K., 2015. Controlled delivery of Gemcitabine Hydrochloride using mannosylated poly (propyleneimine) dendrimers. *Journal of Nanoparticle Research, 17(11)*, p.458.

Souza, C.F., Carneiro, A.B., Silveira, A.B., Laranja, G.A.T., Silva-Neto, M.A.C., da Costa, S.G. and Paes, M.C., 2009. Heme-induced *Trypanosoma cruzi* proliferation is mediated by CaM kinase II. *Biochemical and Biophysical Research Communications*, *390*(3), pp.541-546.

Sterkers, Y., Lachaud, L., Bourgeois, N., Crobu, L., Bastien, P. and Pagès, M., 2012. Novel insights into genome plasticity in Eukaryotes: mosaic aneuploidy in *Leishmania*. Molecular Microbiology, 86(1), pp.15-23.

Stojdl, D.F. and Clarke, M.W., 1996. *Trypanosoma brucei*: Analysis of Cytoplasmic Ca^{2+} during Differentiation of Bloodstream

Stages *in vitro*. *Experimental Parasitology*, *83*(1), pp.134-146.

Stiles, J.K., Hicock, P.I., Shah, P.H. and Meade, J.C., 1999. Genomic organization, transcription, splicing and gene regulation in *Leishmania*. *Annals of Tropical Medicine & Parasitology*, *93*(8), pp.781-807.

Takekawa, M., Tatebayashi, K. and Saito, H., 2005. Conserved docking site is essential for activation of mammalian MAP kinase kinases by specific MAP kinase kinase kinases. *Molecular Cell*, *18*(3), pp.295-306.

Tagoe, D.N.A., Kalejaiye, T.D. and De Koning, H.P., 2015. The ever unfolding story of cAMP signaling in trypanosomatids: vive la difference! *Frontiers in Pharmacology*, *6*, p.185.

Tanoue, T. and Nishida, E., 2003. Molecular recognitions in the MAP kinase cascades. *Cellular Signalling*, *15*(5), pp.455-462.

Tam, L.W., Wilson, N.F. and Lefebvre, P.A., 2007. A CDK-related kinase regulates the length and assembly of flagella in Chlamydomonas. *The Journal of Cell Biology*, *176*(6), pp.819-829.

Taylor, S.S. and Kornev, A.P., 2011. Protein kinases: evolution of dynamic regulatory proteins. *Trends in Biochemical Sciences*, *36*(2), pp.65-77.

Teixeira, D.E., Benchimol, M., Rodrigues, J.C., Crepaldi, P.H., Pimenta, P.F. and de Souza, W., 2013. The cell biology of *Leishmania*: how to teach using animations. *PLoS Pathogens*, *9*(10), p. e1003594.

Tirado-Duarte, D., Marín-Villa, M., Ochoa, R., Blandón-Fuentes, G., Soares, M.J., Robledo, S.M. and Varela-Miranda, R.E., 2018. The Akt-like kinase of *Leishmania panamensis:* As a new molecular target for drug discovery. *Acta Tropica*, *177*, pp.171-178.

Tu, X. and Wang, C.C., 2005. Pairwise knockdowns of cdc2-related kinases (CRKs) in *Trypanosoma brucei* identified the CRKs for G1/S and G2/M transitions and demonstrated distinctive cytokinetic regulations between two developmental stages of the organism. *Eukaryotic Cell*, *4*(4), pp.755-764.

Tu, X., Kumar, P., Li, Z. and Wang, C.C., 2006. An aurora kinase homologue is involved in regulating both mitosis and cytokinesis in *Trypanosoma brucei*. *Journal of Biological Chemistry*, *281*(14), pp.9677-9687.

Ullu, E., Matthews, K.R. and Tschudi, C., 1993. Temporal order of RNA-processing reactions in trypanosomes: rapid trans splicing precedes polyadenylation of newly synthesized tubulin transcripts. *Molecular and Cellular Biology*, *13*(1), pp.720-725.

Urbaniak, M.D., 2009. Casein kinase 1 isoform 2 is essential for bloodstream form *Trypanosoma brucei*. *Molecular and Biochemical Parasitology*, *166*(2), pp.183-185.

Velashjerdi Farahani, S., Reza Aghasadeghi, M., Memarnejadian, A., Faezi, S., Shahosseini, Z. and Mahdavi, M., 2016. Naloxone/alum mixture a potent adjuvant for HIV-1 vaccine: induction of cellular and poly-isotypic humoral immune responses. *Pathogens and Global Health*, *110*(2), pp.39-47.

Wanders, P., 2004.In vitro and in vivo characterization of an LmxMPK5 deletion mutant of *Leishmania mexicana.* Doctoral Dissertation, *University of Hamburg*, Hamburg, Germany.

Wang, Q., Melzer, I.M., Kruse, M., Sander-Juelch, C. and Wiese, M., 2005. LmxMPK4, a mitogen-activated protein (MAP) kinase homologue essential for promastigotes and amastigotes of *Leishmania mexicana*. *Kinetoplastid Biology and Disease*, *4*(1), p.6.

Wang, Y., Liu, Z., Cheng, H., Gao, T., Pan, Z., Yang, Q., Guo, A. and Xue, Y., 2013. EKPD: a hierarchical database of eukaryotic protein kinases and protein phosphatases. *Nucleic Acids Research*, *42*(D1), pp.D496-D502.

Wasan, E.K., Gershkovich, P., Zhao, J., Zhu, X., Werbovetz, K., Tidwell, R.R., Clement, J.G., Thornton, S.J. and Wasan, K.M., 2010. A novel tropically stable oral amphotericin B formulation (iCo-010) exhibits efficacy against visceral Leishmaniasis in a murine model. *PLoS Neglected Tropical Diseases*, *4*(12), p. e913.

Wheeler, R.J., Gluenz, E. and Gull, K., 2011. The cell cycle of *Leishmania*: morphogenetic events and their implications for parasite biology. *Molecular Microbiology*, *79*(3), pp.647-662.

World Health Organization, 2018. Control of leishmaniasis. World Health Organization. *Technical Report Series*, no. 949, p. xii.

Widmann, M. and Christen, P., 2000. Comparison of folding rates of homologous prokaryotic and eukaryotic proteins. *Journal of Biological Chemistry*, *275*(25), pp.18619-18622.

Wiese, M., 1998. A mitogen-activated protein (MAP) kinase homologue of *Leishmania mexicana* is essential for parasite survival in the infected host. *The EMBO Journal*, *17*(9), pp.2619-2628.

Wiese, M., Wang, Q. and Gorcke, I., 2003a. Identification of mitogen-activated protein kinase homologues from *Leishmania mexicana. International Journal for Parasitology*, *33*(14), pp.1577-1587.

Wiese, M., Kuhn, D. and Grunfelder, C.G., 2003. Protein kinase involved in flagellar-length control. *Eukaryotic Cell*, *2*(4), pp.769-777.

Wiese, M., 2007. *Leishmania* MAP kinases–familiar proteins in an unusual context. *International Journal for Parasitology*, *37*(10), pp.1053-1062.

Wilson, N.F. and Lefebvre, P.A., 2004. Regulation of flagellar assembly by glycogen synthase kinase 3 in Chlamydomonas reinhardtii. *Eukaryotic cell*, *3*(5), pp.1307-1319.

Windelberg, M. 2007. Molecular characterisation of the mitogen-activated protein kinases LmxMPK11 and LmxMPK12 from *Leishmania mexicana*. MD Dissertation, *University of Hamburg*.

Wu, J., Rossomando, A.J., Horng-Her, J., Weber, M.J. and Sturgill, T.W., 1992. Apparent sufficiency of a dual-specificity tyrosine/threonine kinase for activation of MAP kinase poses new questions for the dual-phosphorylation mechanism.

Xiong, Z.H. and Ruben, L., 1998. *Trypanosoma brucei*: the dynamics of calcium movement between the cytosol, nucleus, and mitochondrion of intact cells. *Experimental Parasitology*, *88*(3), pp.231-239.

Xingi, E., Smirlis, D., Myrianthopoulos, V., Magiatis, P., Grant, K.M., Meijer, L., Mikros, E., Skaltsounis, A.L. and Soteriadou, K., 2009. 6-Br-5methylindirubin-3′ oxime (5-Me-6-BIO) targeting the leishmanial glycogen synthase kinase-3 (GSK-3) short form affects cell-cycle progression and induces apoptosis-like death: exploitation of GSK-3 for treating leishmaniasis. *International Journal for Parasitology*, *39*(12), pp.1289-1303.

Yao, Z. and Seger, R., 2009. The ERK signaling cascade—views from different subcellular compartments. *Biofactors*, *35*(5), pp.407-416.

Zeke, A., Misheva, M., Reményi, A. and Bogoyevitch, M.A., 2016. JNK signaling: regulation and functions based on complex protein-protein partnerships. *Microbiol. Mol. Biol. Rev.*, *80*(3), pp.793-835.

Zheng, C.F. and Guan, K.L., 1993. Cloning and characterization of two distinct humans extracellular signal-regulated kinase activator kinases, MEK1 and MEK2. *Journal of Biological Chemistry, 268(15)*, pp.11435-11439.

Zhou, C., Yang, Y. and Jong, A.Y., 1990. Mini-prep in ten minutes. *Biotechniques*, *8*(2), p.172.

Zhou, T., Sun, L., Humphreys, J. and Goldsmith, E.J., 2006. Docking interactions induce exposure of activation loop in the MAP kinase ERK2. *Structure*, *14*(6), pp.1011-1019.

Zijlstra, E.E., 2016. The immunology of post-kala-azar dermal leishmaniasis (PKDL). *Parasites & vectors*, *9*(1), p.464.

Websites

Manual Report about Leishmaniasis situation and trends (www.who.int/leishmaniasis/en/), access date 23th of February 2019.

National Institute of Allergy and Infectious Diseases (NIAID).,2015. Available at https://www.niaid.nih.gov/about/Pages/default.aspx acceded 26/05/2018.

Appendices

Chapter 9: Appendices

9.1 Plasmids MAP

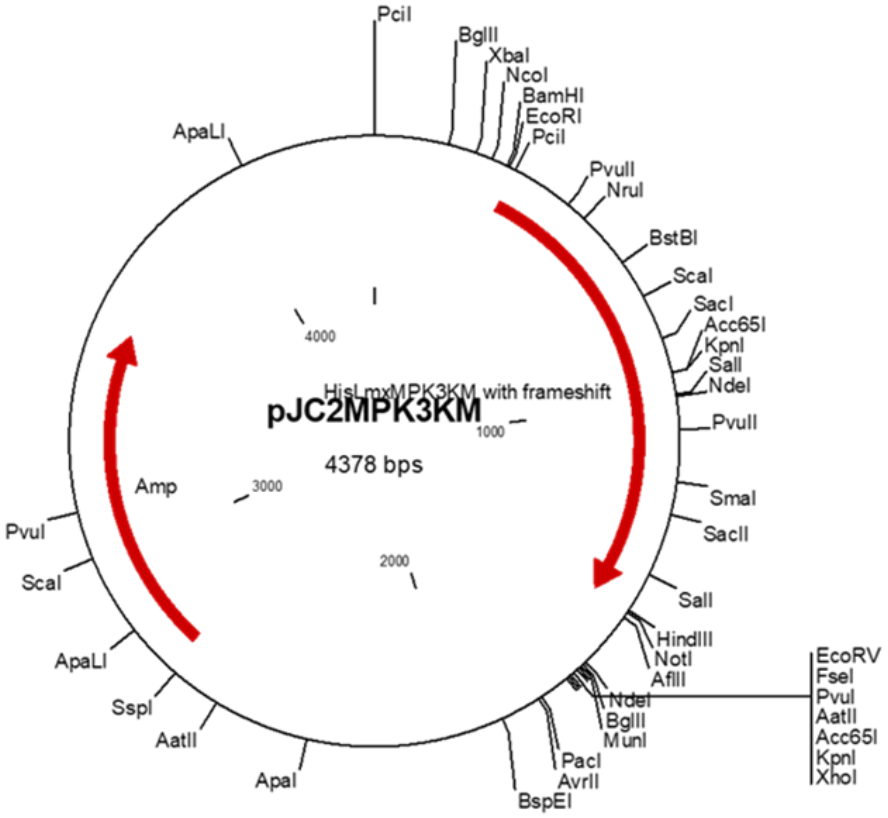

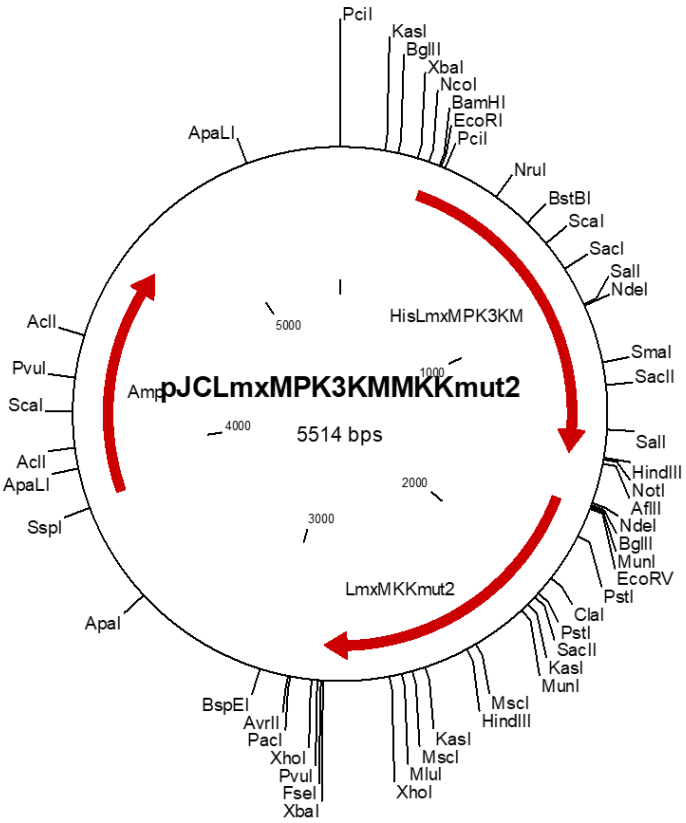
pJCLmxMPK3KMMKKmut2
5514 bps
HisLmxMPK3KM
LmxMKKmut2
Amp
5000
1000
2000
3000
4000
PciI
KasI
BglII
XbaI
NcoI
BamHI
EcoRI
PciI
NruI
BstBI
ScaI
SacI
SalI
NdeI
SmaI
SacII
SalI
HindIII
NotI
AflII
NdeI
BglII
MunI
EcoRV
PstI
ClaI
PstI
SacII
KasI
MunI
MscI
HindIII
KasI
MscI
MluI
XhoI
BspEI
AvrII
PacI
XhoI
PvuI
FseI
XbaI
ApaI
SspI
ApaLI
AclI
ScaI
PvuI
AclI
ApaLI

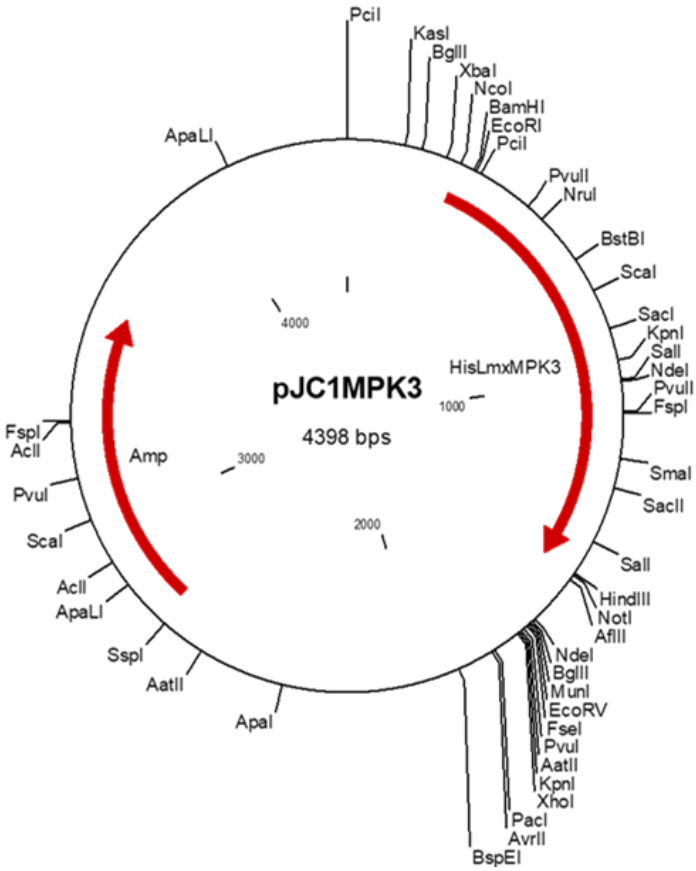
pJC1MPK3
4398 bps
HisLmxMPK3
Amp
1000
2000
3000
4000
PciI
KasI
BglII
XbaI
NcoI
BamHI
EcoRI
PciI
PvuII
NruI
BstBI
ScaI
SacI
KpnI
SalI
NdeI
PvuII
FspI
SmaI
SacII
SalI
HindIII
NotI
AflII
NdeI
BglII
MunI
EcoRV
FseI
PvuI
AatII
KpnI
XhoI
PacI
AvrII
BspEI
ApaI
AatII
SspI
ApaLI
AclI
ScaI
PvuI
FspI
AclI
ApaLI

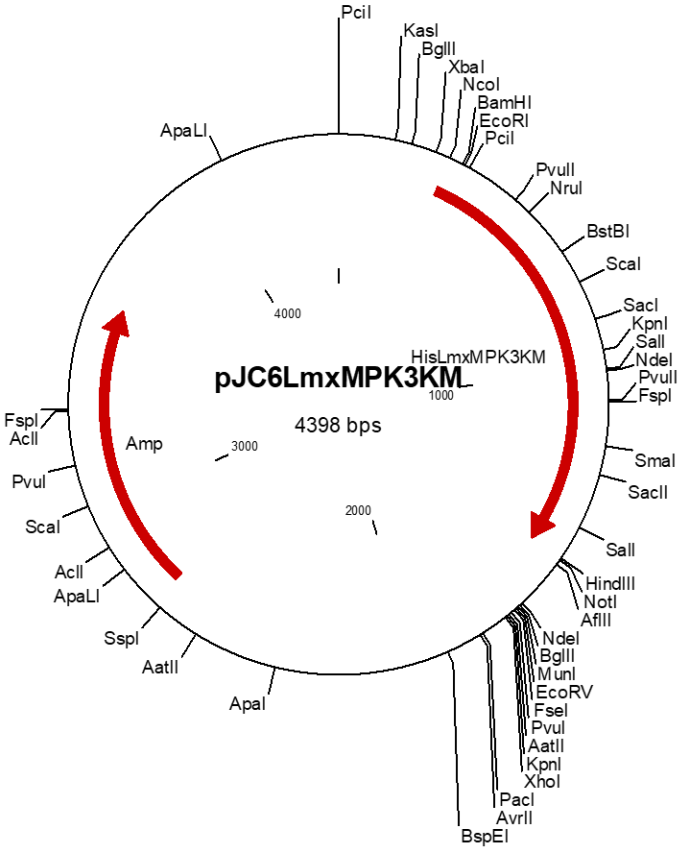
pJC6LmxMPK3KML
4398 bps
HisLmxMPK3KM
Amp
PciI
KasI
BglII
XbaI
NcoI
BamHI
EcoRI
PciI
PvuII
NruI
BstBI
ScaI
SacI
KpnI
SalI
NdeI
PvuII
FspI
SmaI
SacII
SalI
HindIII
NotI
AflII
NdeI
BglII
MunI
EcoRV
FseI
PvuI
AatII
KpnI
XhoI
PacI
AvrII
BspEI
ApaI
AatII
SspI
ApaLI
AclI
ScaI
PvuI
AclI
FspI
ApaLI
4000
1000
2000
3000

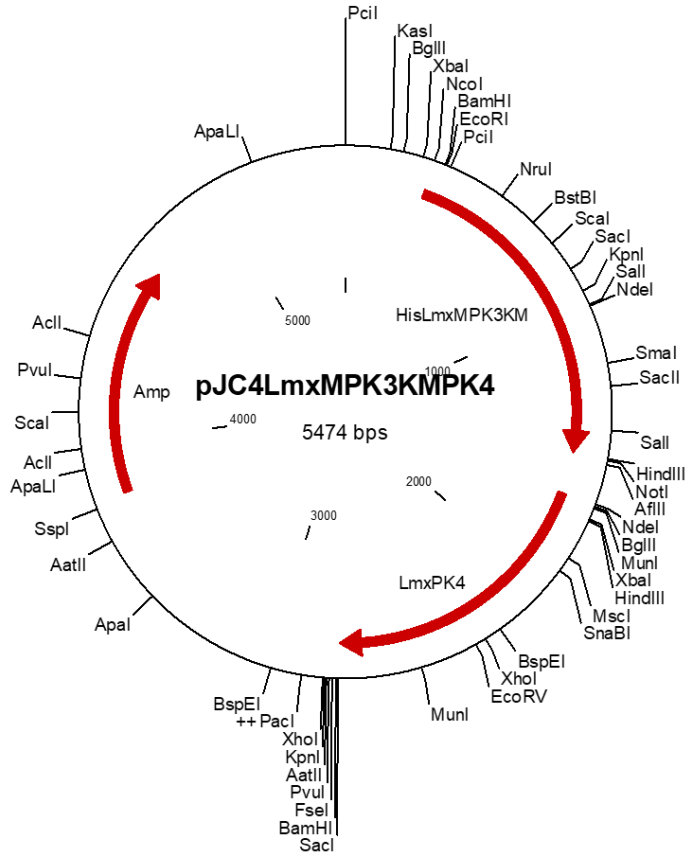
pJC4LmxMPK3KMPK4
5474 bps
HisLmxMPK3KM
LmxPK4
Amp
PciI
KasI
BglII
XbaI
NcoI
BamHI
EcoRI
PciI
NruI
BstBI
ScaI
SacI
KpnI
SalI
NdeI
SmaI
SacII
SalI
HindIII
NotI
AflII
NdeI
BglII
MunI
XbaI
HindIII
MscI
SnaBI
BspEI
XhoI
EcoRV
MunI
BspEI
++ PacI
XhoI
KpnI
AatII
PvuI
FseI
BamHI
SacI
ApaI
AatII
SspI
ApaLI
AclI
ScaI
PvuI
AclI
ApaLI
5000
1000
2000
3000
4000

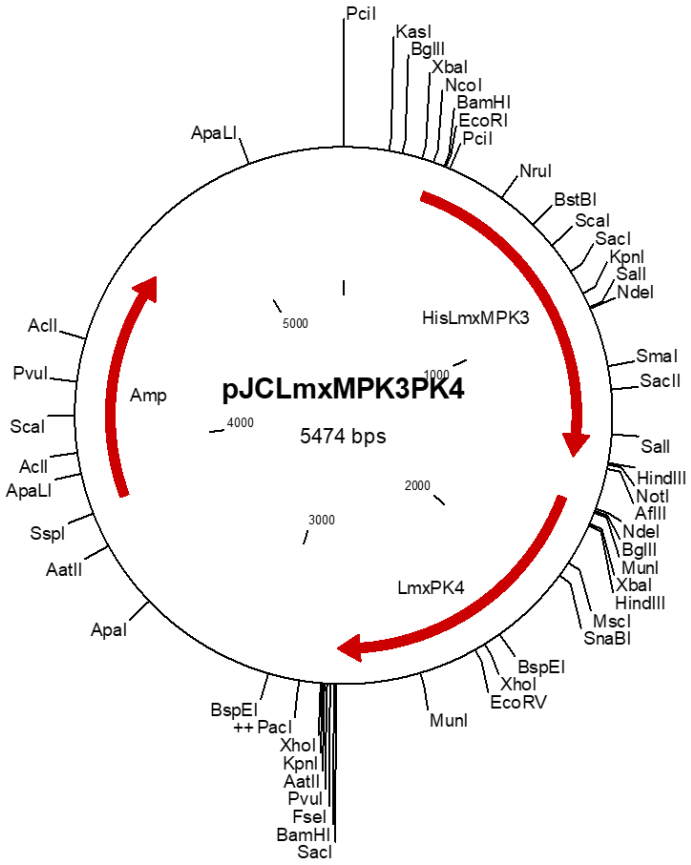
pJCLmxMPK3PK4
5474 bps
HisLmxMPK3
LmxPK4
Amp
5000
1000
2000
3000
4000
PciI
KasI
BglII
XbaI
NcoI
BamHI
EcoRI
PciI
NruI
BstBI
ScaI
SacI
KpnI
SalI
NdeI
SmaI
SacII
SalI
HindIII
NotI
AflII
NdeI
BglII
MunI
XbaI
HindIII
MscI
SnaBI
BspEI
XhoI
EcoRV
MunI
BspEI
++ PacI
XhoI
KpnI
AatII
PvuI
FseI
BamHI
SacI
ApaI
AatII
SspI
ApaLI
AclI
ScaI
PvuI
AclI
ApaLI

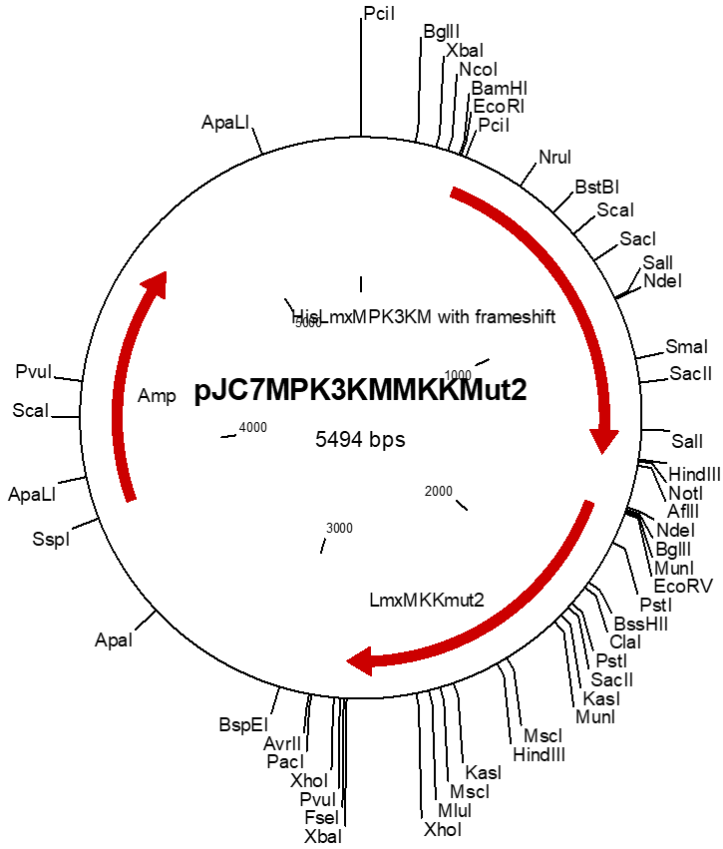
pJC7MPK3KMMKKMut2
5494 bps
HisLmxMPK3KM with frameshift
LmxMKKmut2
Amp
1000
2000
3000
4000
5000
PciI
BglII
XbaI
NcoI
BamHI
EcoRI
PciI
NruI
BstBI
ScaI
SacI
SalI
NdeI
SmaI
SacII
SalI
HindIII
NotI
AflII
NdeI
BglII
MunI
EcoRV
PstI
BssHII
ClaI
PstI
SacII
KasI
MunI
MscI
HindIII
KasI
MscI
MluI
XhoI
BspEI
AvrII
PacI
XhoI
PvuI
FseI
XbaI
ApaI
SspI
ApaLI
ScaI
PvuI
ApaLI

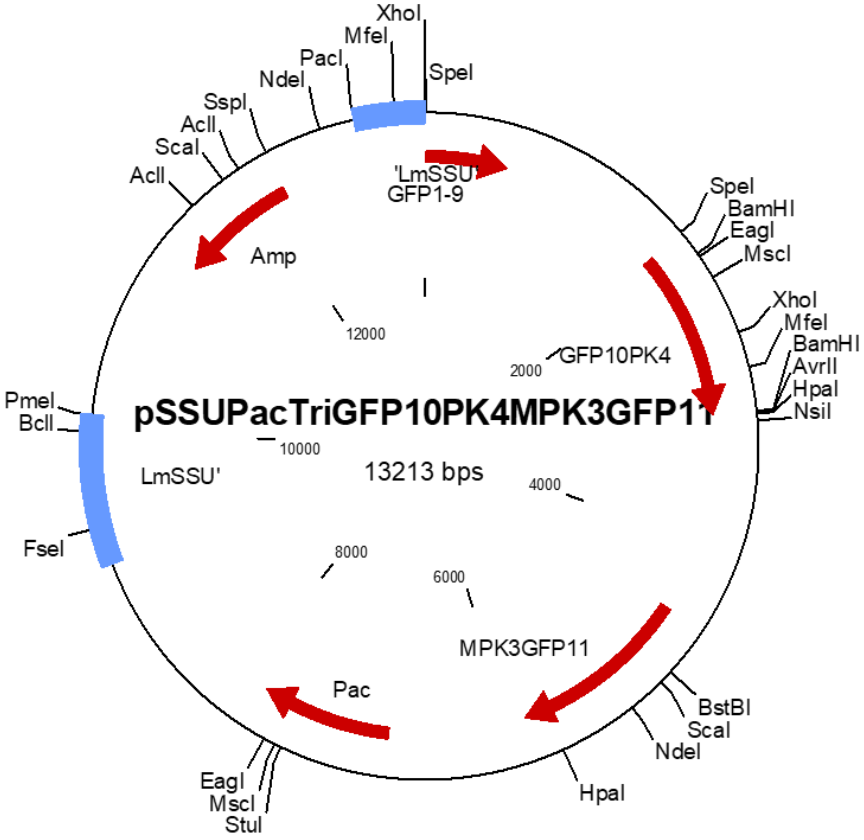
XhoI
MfeI
PacI
NdeI
SpeI
SspI
AclI
ScaI
AclI
'LmSSU'
GFP1-9
Amp
SpeI
BamHI
EagI
MscI
XhoI
MfeI
BamHI
AvrII
HpaI
NsiI
12000
2000
GFP10PK4
pSSUPacTriGFP10PK4MPK3GFP11
PmeI
BclI
10000
LmSSU'
13213 bps
4000
FseI
8000
6000
MPK3GFP11
Pac
BstBI
ScaI
NdeI
EagI
MscI
StuI
HpaI

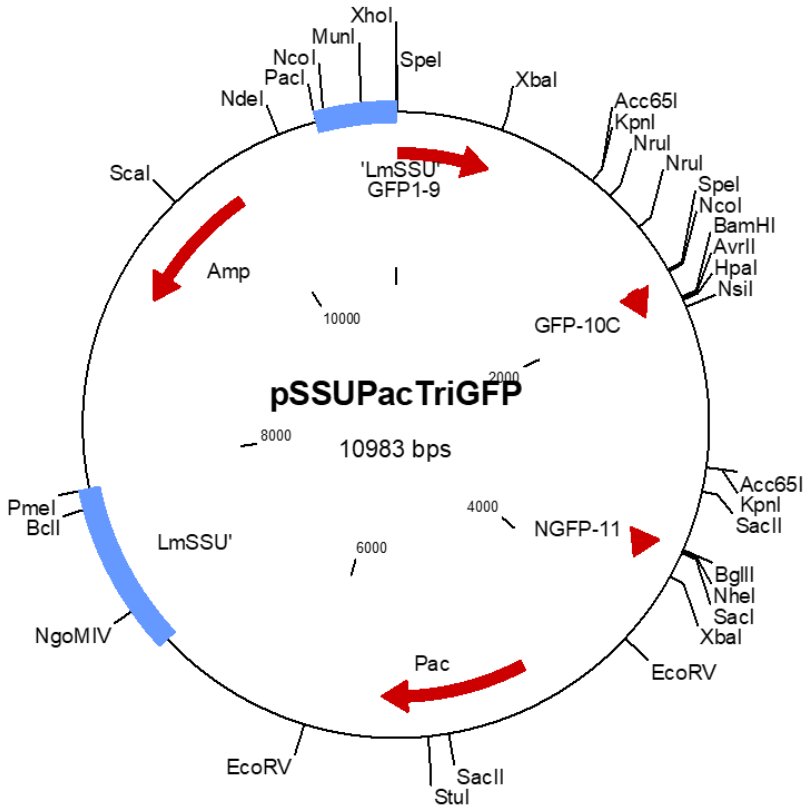
XhoI
MunI
NcoI
PacI
NdeI
SpeI
XbaI
Acc65I
KpnI
NruI
NruI
SpeI
NcoI
BamHI
AvrII
HpaI
NsiI
ScaI
'LmSSU'
GFP1-9
Amp
10000
GFP-10C
2000
pSSUPacTriGFP
8000
10983 bps
Acc65I
KpnI
SacII
PmeI
BclI
4000
NGFP-11
LmSSU'
6000
BglII
NheI
SacI
XbaI
NgoMIV
Pac
EcoRV
EcoRV
SacII
StuI

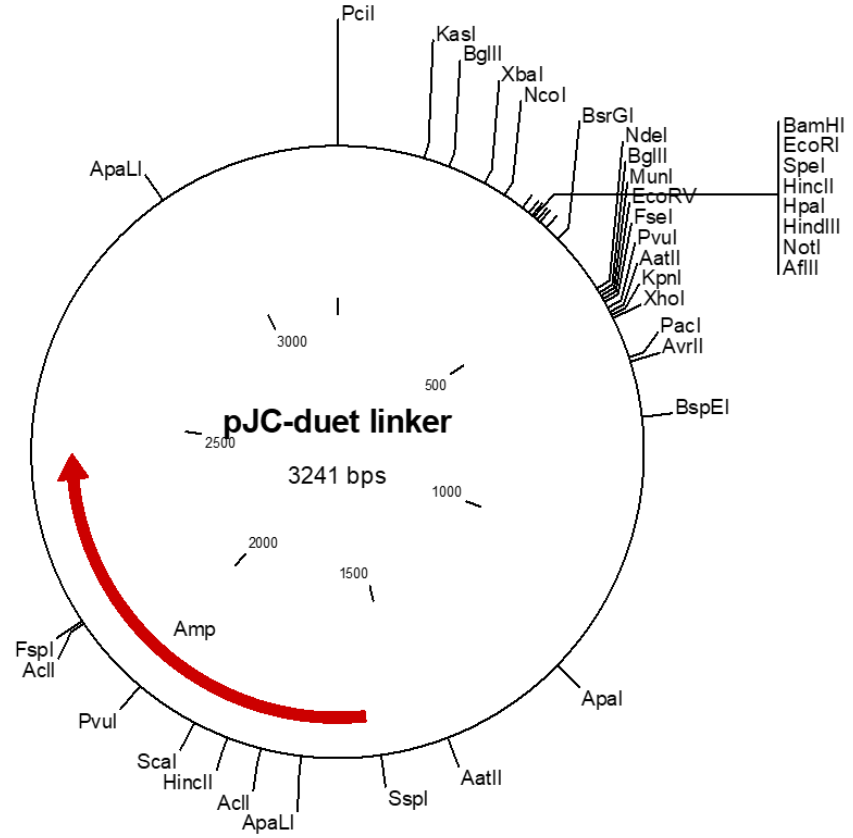
pJC-duet linker
3241 bps
I
3000
500
2500
1000
2000
1500
Amp
PciI
KasI
BglII
XbaI
NcoI
BsrGI
NdeI
BglII
MunI
EcoRV
FseI
PvuI
AatII
KpnI
XhoI
PacI
AvrII
BspEI
ApaI
AatII
SspI
ApaLI
AclI
HincII
ScaI
PvuI
AclI
FspI
ApaLI
BamHI
EcoRI
SpeI
HincII
HpaI
HindIII
NotI
AflII

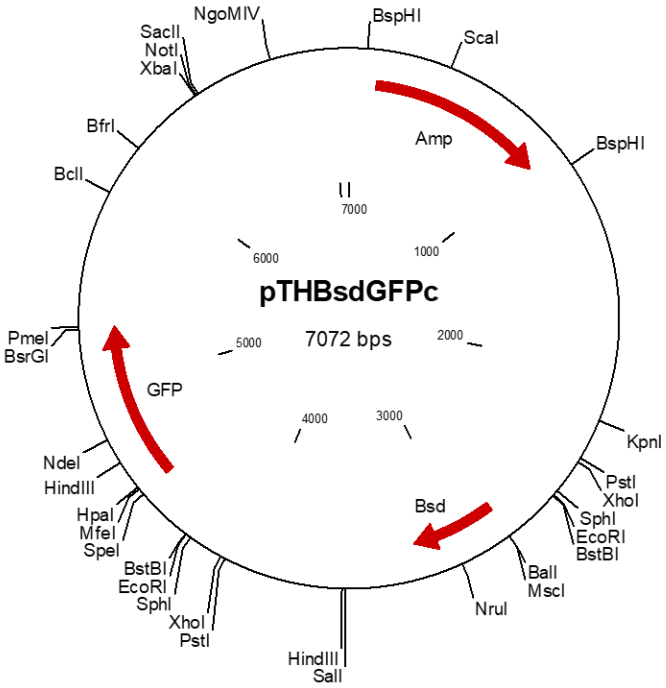
pTHBsdGFPc
7072 bps
II
7000
1000
2000
3000
4000
5000
6000
Amp
GFP
Bsd
NgoMIV
BspHI
ScaI
BspHI
KpnI
PstI
XhoI
SphI
EcoRI
BstBI
BalI
MscI
NruI
HindIII
SalI
XhoI
PstI
BstBI
EcoRI
SphI
HpaI
MfeI
SpeI
NdeI
HindIII
PmeI
BsrGI
BclI
BfrI
SacII
NotI
XbaI

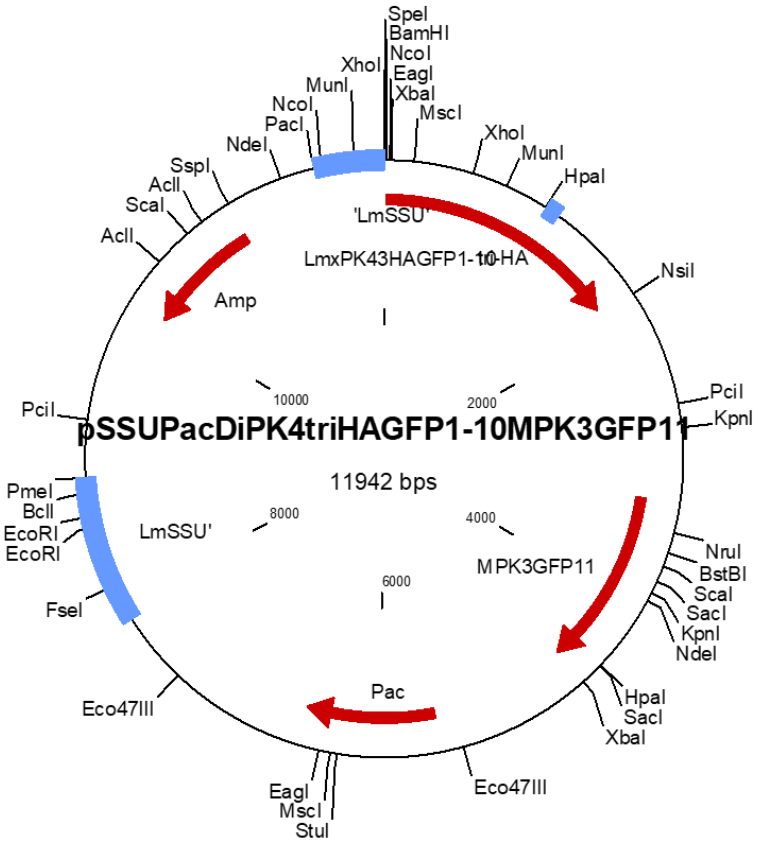
SpeI
BamHI
NcoI
EagI
XbaI
MscI
XhoI
MunI
HpaI
NsiI
PciI
KpnI
NdeI
SacI
ScaI
NruI
BstBI
MPK3GFP11
Pac
Eco47III
HpaI
SacI
XbaI
Eco47III
EagI
MscI
StuI
FseI
EcoRI
EcoRI
BclI
PmeI
LmSSU'
'LmSSU'
LmxPK43HAGFP1-10-HA
Amp
AclI
ScaI
AclI
SspI
NdeI
PacI
NcoI
MunI
XhoI
10000
2000
4000
6000
8000
pSSUPacDiPK4triHAGFP1-10MPK3GFP11
11942 bps

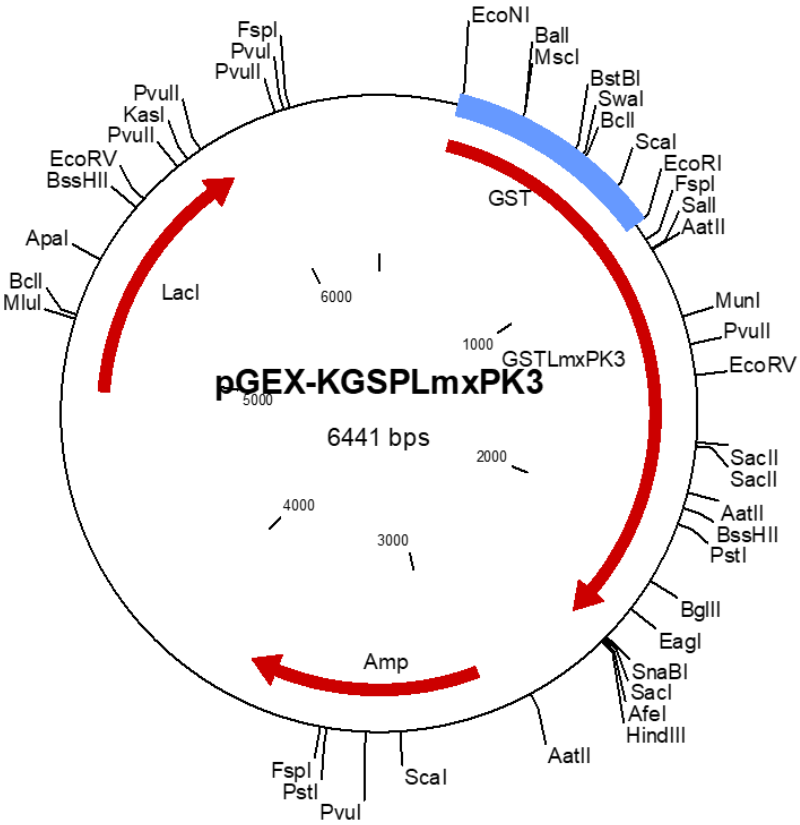
EcoNI
BalI
MscI
BstBI
SwaI
BclI
ScaI
EcoRI
FspI
SalI
AatII
MunI
PvuII
EcoRV
SacII
SacII
AatII
BssHII
PstI
BglII
EagI
SnaBI
SacI
AfeI
HindIII
AatII
ScaI
FspI
PstI
PvuI
Amp
LacI
BclI
MluI
ApaI
EcoRV
BssHII
PvuII
KasI
PvuII
FspI
PvuI
PvuII
GST
GSTLmxPK3
pGEX-KGSPLmxPK3
6441 bps
1000
2000
3000
4000
5000
6000

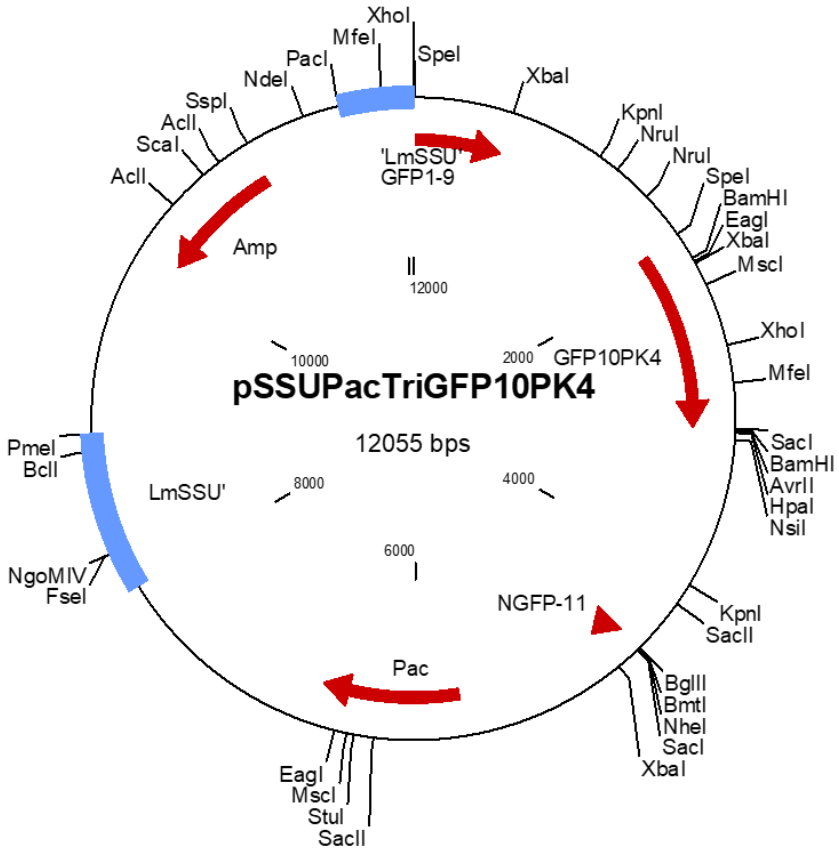
XhoI
MfeI
SpeI
PacI
NdeI
SspI
AclI
ScaI
AclI
XbaI
KpnI
NruI
NruI
SpeI
BamHI
EagI
XbaI
MscI
XhoI
MfeI
SacI
BamHI
AvrII
HpaI
NsiI
KpnI
SacII
BglII
BmtI
NheI
SacI
XbaI
EagI
MscI
StuI
SacII
NgoMIV
FseI
PmeI
BclI
'LmSSU'
GFP1-9
Amp
12000
10000
2000
GFP10PK4
pSSUPacTriGFP10PK4
12055 bps
LmSSU'
8000
4000
6000
NGFP-11
Pac

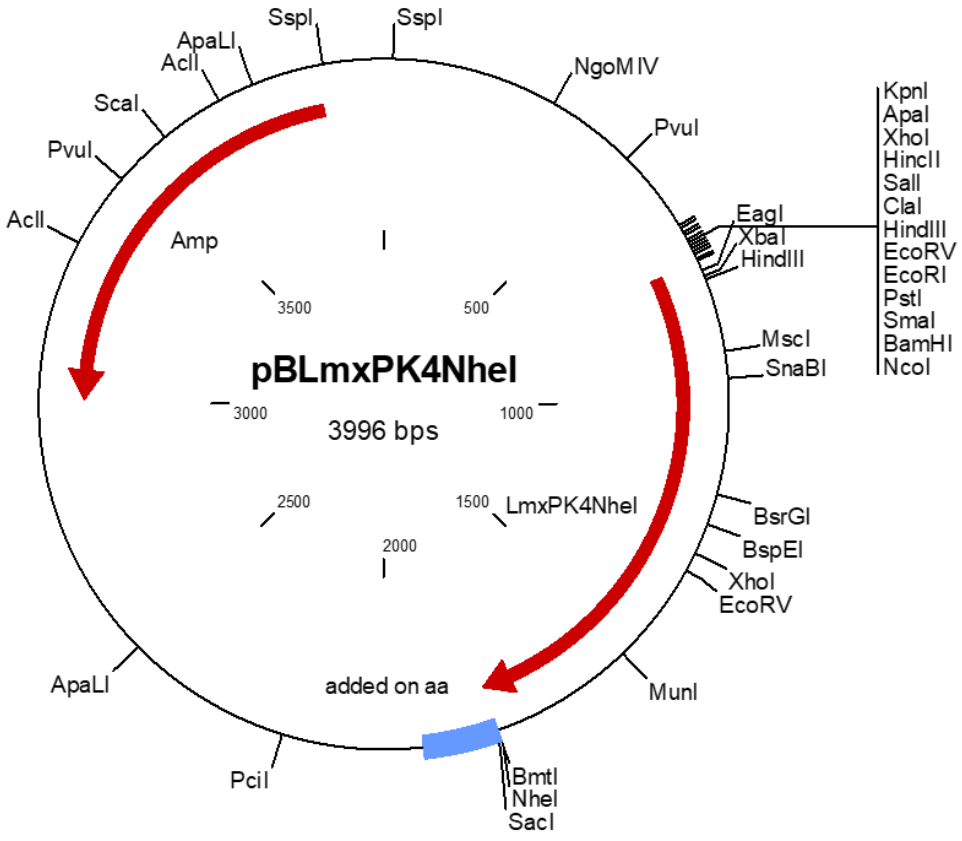
SspI
SspI
ApaLI
AclI
NgoMIV
ScaI
PvuI
PvuI
AclI
KpnI
ApaI
XhoI
HincII
SalI
ClaI
HindIII
EcoRV
EcoRI
PstI
SmaI
BamHI
NcoI
EagI
XbaI
HindIII
MscI
SnaBI
Amp
3500
500
pBLmxPK4NheI
3000
1000
3996 bps
2500
1500
LmxPK4NheI
2000
BsrGI
BspEI
XhoI
EcoRV
ApaLI
added on aa
MunI
PciI
BmtI
NheI
SacI

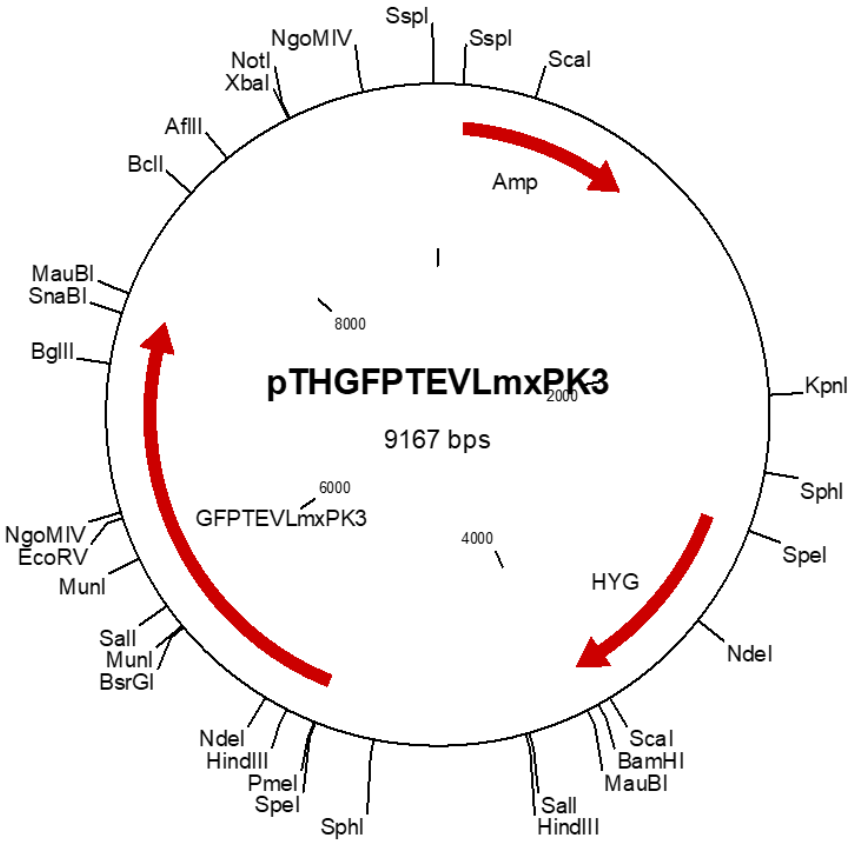
SspI
SspI
ScaI
NgoMIV
NotI
XbaI
AflII
BclI
MauBI
SnaBI
BglII
KpnI
SphI
SpeI
NdeI
ScaI
BamHI
MauBI
SalI
HindIII
SphI
SpeI
PmeI
NdeI
HindIII
SalI
MunI
BsrGI
NgoMIV
EcoRV
MunI
Amp
HYG
8000
2000
4000
6000
pTHGFPTEVLmxPK3
9167 bps
GFPTEVLmxPK3

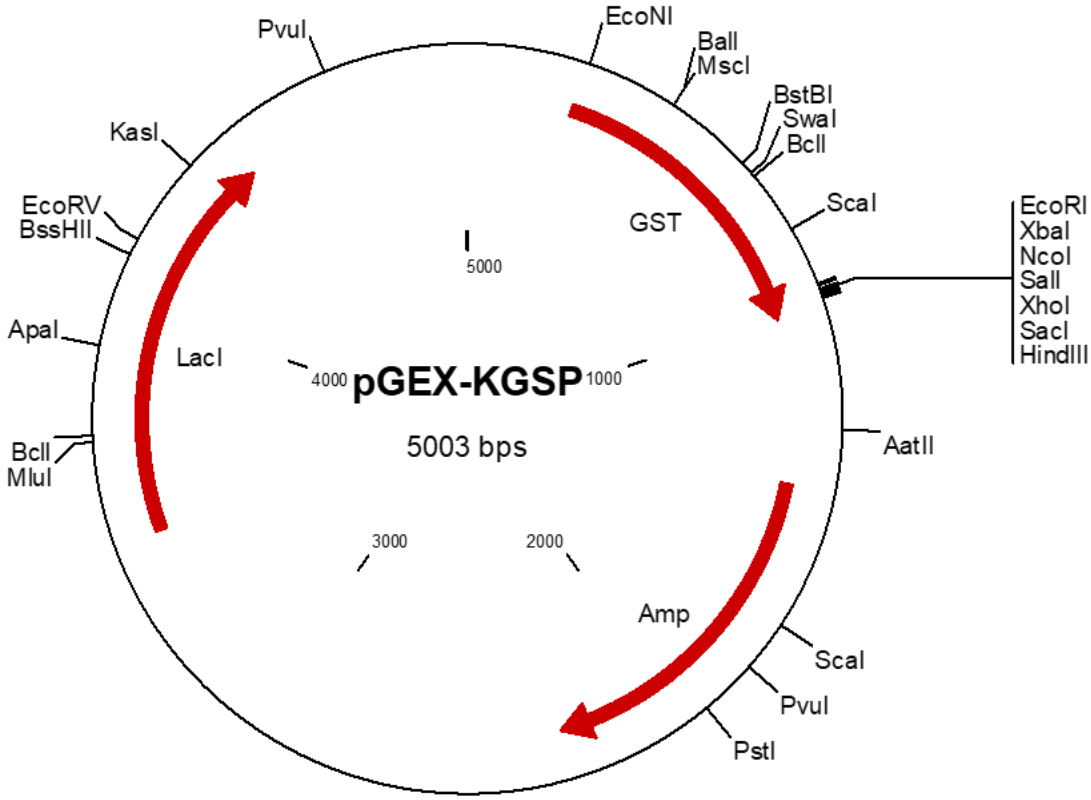
PvuI
EcoNI
BalI
MscI
BstBI
SwaI
BclI
ScaI
EcoRI
XbaI
NcoI
SalI
XhoI
SacI
HindIII
AatII
ScaI
PvuI
PstI
Amp
GST
LacI
KasI
EcoRV
BssHII
ApaI
BclI
MluI
5000
4000
1000
3000
2000
pGEX-KGSP
5003 bps

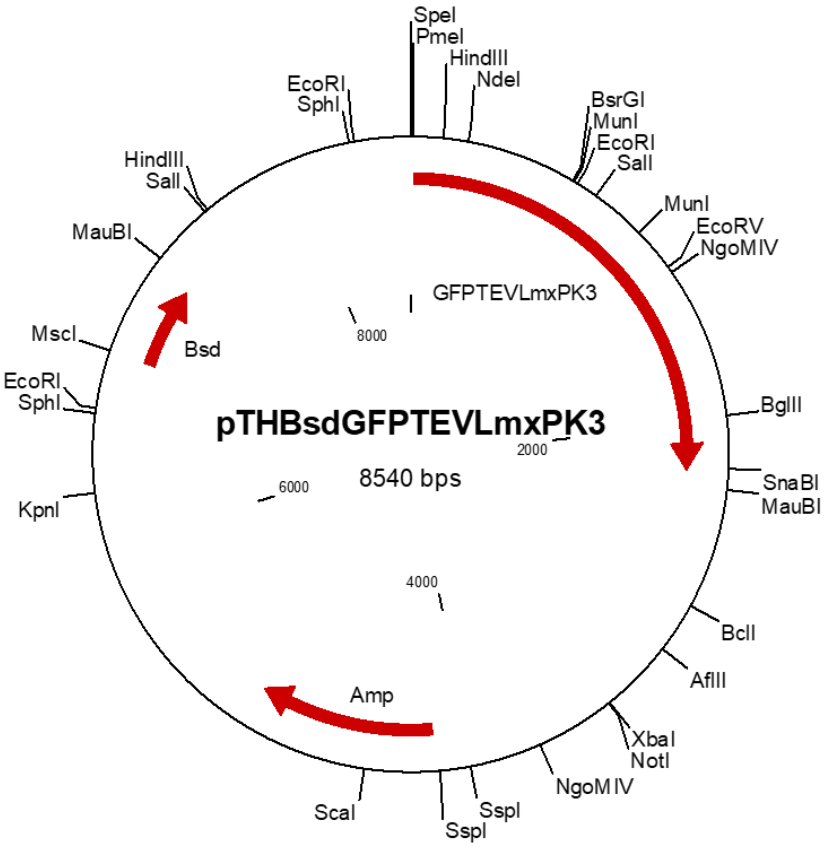
SpeI
PmeI
HindIII
NdeI
EcoRI
SphI
BsrGI
MunI
EcoRI
SalI
HindIII
SalI
MunI
EcoRV
NgoMIV
MauBI
GFPTEVLmxPK3
8000
MscI
Bsd
EcoRI
SphI
pTHBsdGFPTEVLmxPK3
2000
BglII
6000
8540 bps
SnaBI
MauBI
KpnI
4000
BclI
AflII
Amp
XbaI
NotI
NgoMIV
ScaI
SspI
SspI

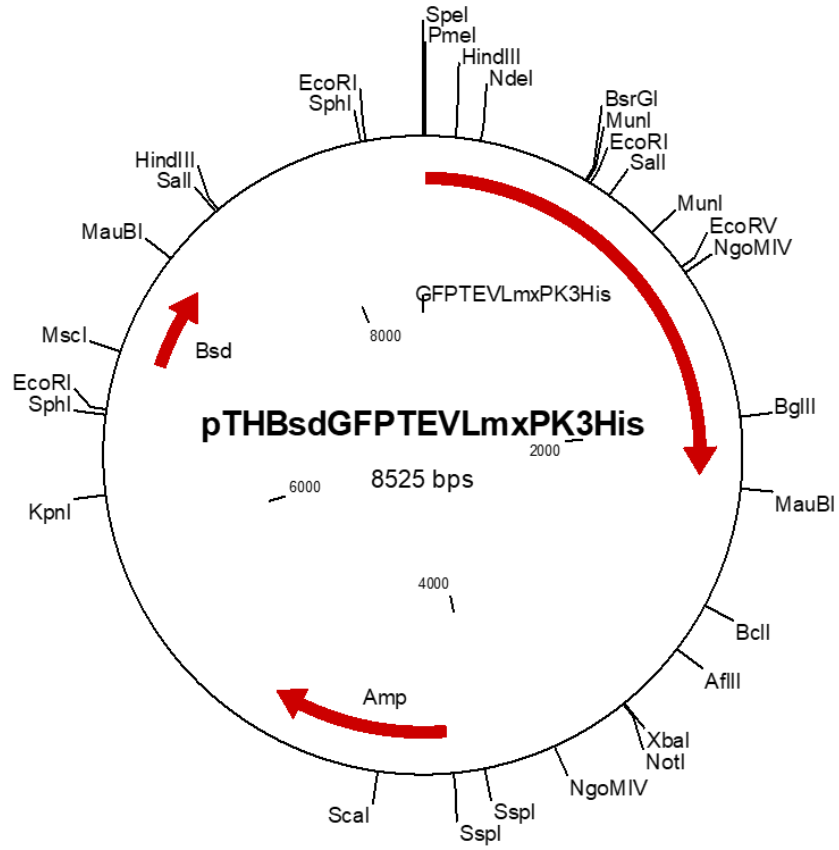
SpeI
PmeI
HindIII
NdeI
EcoRI
SphI
BsrGI
MunI
EcoRI
SalI
HindIII
SalI
MunI
EcoRV
NgoMIV
MauBI
GFPTEVLmxPK3His
8000
MscI
Bsd
EcoRI
SphI
pTHBsdGFPTEVLmxPK3His
2000
BglII
6000
8525 bps
MauBI
KpnI
4000
BclI
AflII
Amp
XbaI
NotI
NgoMIV
ScaI
SspI
SspI

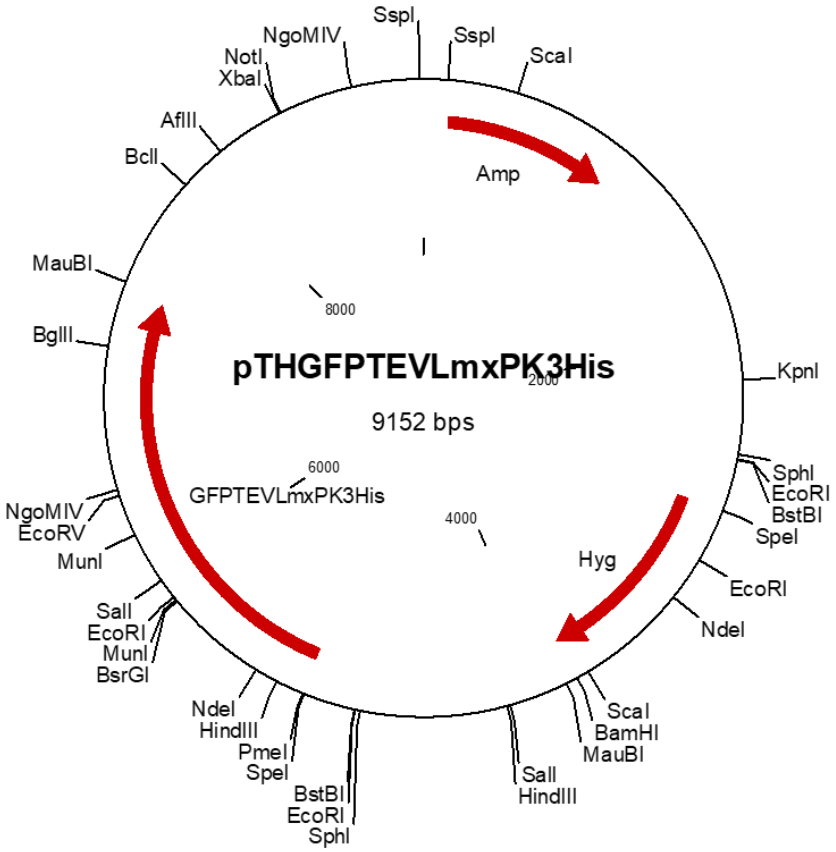
pTHGFPTEVLmxPK3His
9152 bps
GFPTEVLmxPK3His
Amp
Hyg
8000
2000
4000
6000
SspI
SspI
ScaI
NgoMIV
NotI
XbaI
AflII
BclI
MauBI
BglII
KpnI
SphI
EcoRI
BstBI
SpeI
EcoRI
NdeI
ScaI
BamHI
MauBI
SalI
HindIII
NdeI
HindIII
PmeI
SpeI
BstBI
EcoRI
SphI
NgoMIV
EcoRV
MunI
SalI
EcoRI
MunI
BsrGI

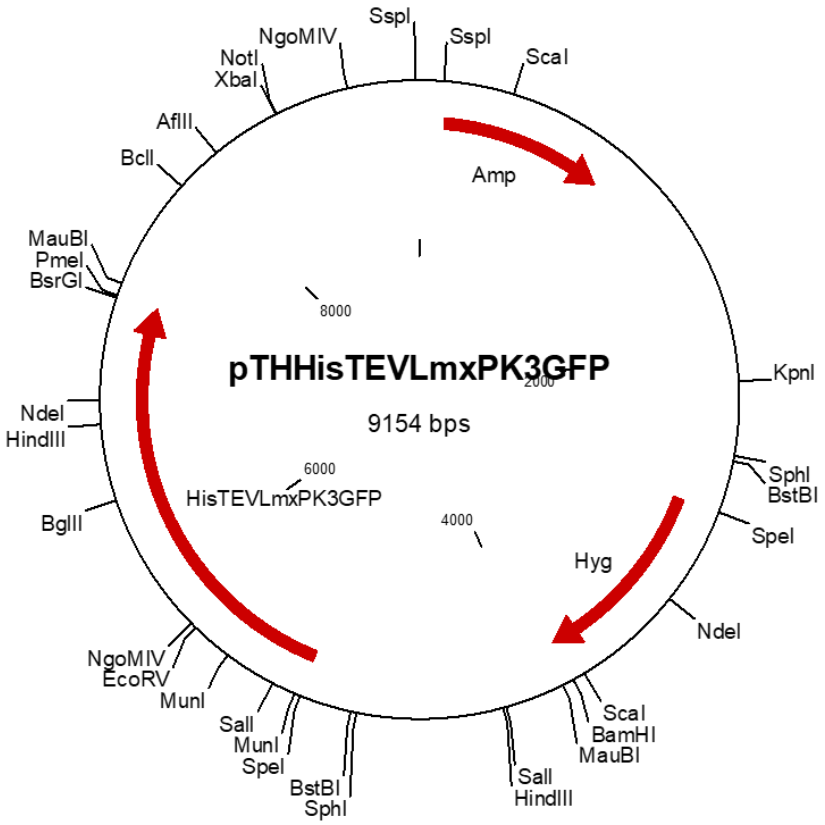
pTHHisTEVLmxPK3GFP
9154 bps
HisTEVLmxPK3GFP
Amp
Hyg
8000
2000
4000
6000
SspI
SspI
ScaI
NgoMIV
NotI
XbaI
AflII
BclI
MauBI
PmeI
BsrGI
KpnI
SphI
BstBI
SpeI
NdeI
ScaI
BamHI
MauBI
SalI
HindIII
NdeI
HindIII
BglII
NgoMIV
EcoRV
MunI
SalI
MunI
SpeI
BstBI
SphI

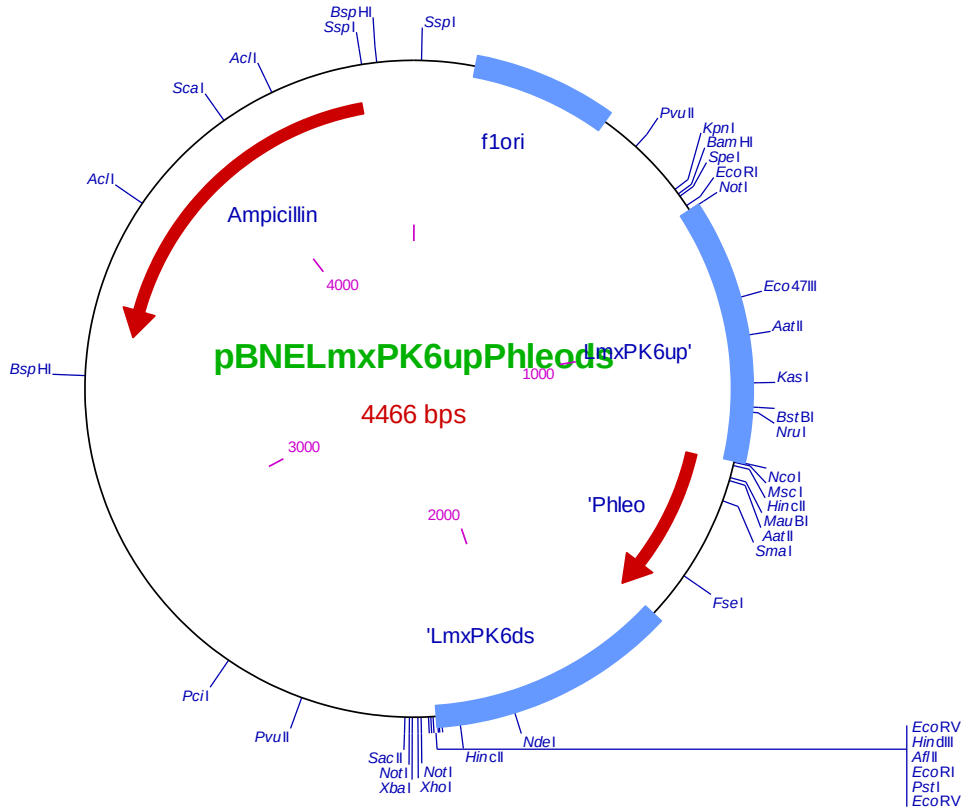
pBNELmxPK6upPhleods
4466 bps
f1ori
Ampicillin
'LmxPK6up'
'Phleo
'LmxPK6ds
1000
2000
3000
4000
BspHI
SspI
AclI
ScaI
PvuII
KpnI
BamHI
SpeI
EcoRI
NotI
Eco47III
AatII
KasI
BstBI
NruI
NcoI
MscI
HincII
MauBI
AatII
SmaI
FseI
EcoRV
HindIII
AflII
EcoRI
PstI
EcoRV
NdeI
HincII
SacII
NotI
XbaI
NotI
XhoI
PvuII
PciI

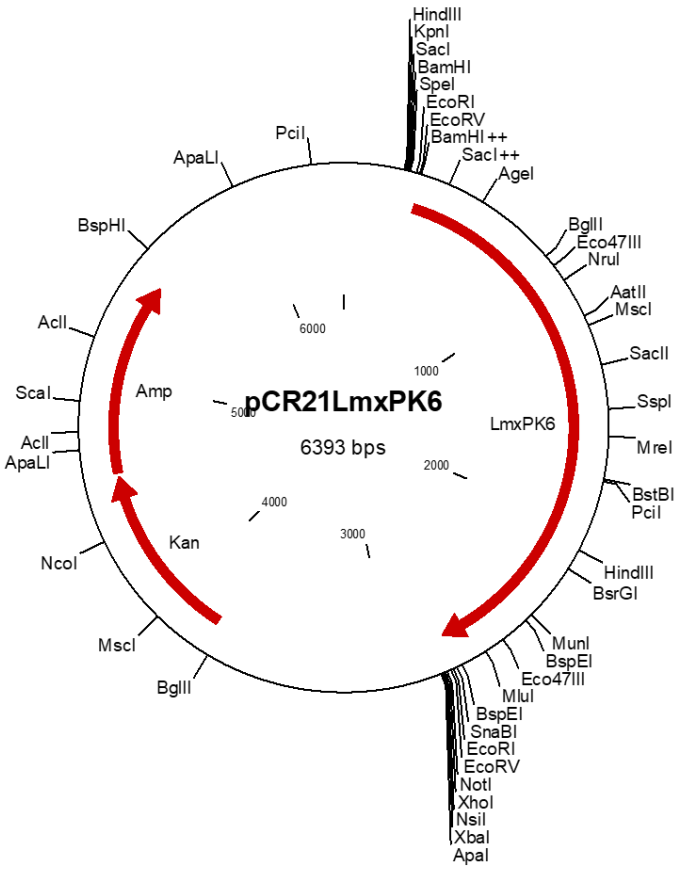
pCR21LmxPK6
6393 bps
Amp
Kan
LmxPK6
1000
2000
3000
4000
5000
6000
HindIII
KpnI
SacI
BamHI
SpeI
EcoRI
EcoRV
BamHI++
SacI++
AgeI
BglII
Eco47III
NruI
AatII
MscI
SacII
SspI
MreI
BstBI
PciI
HindIII
BsrGI
MunI
BspEI
Eco47III
MluI
BspEI
SnaBI
EcoRI
EcoRV
NotI
XhoI
NsiI
XbaI
ApaI
PciI
ApaLI
BspHI
AclI
ScaI
AclI
ApaLI
NcoI
MscI
BglII

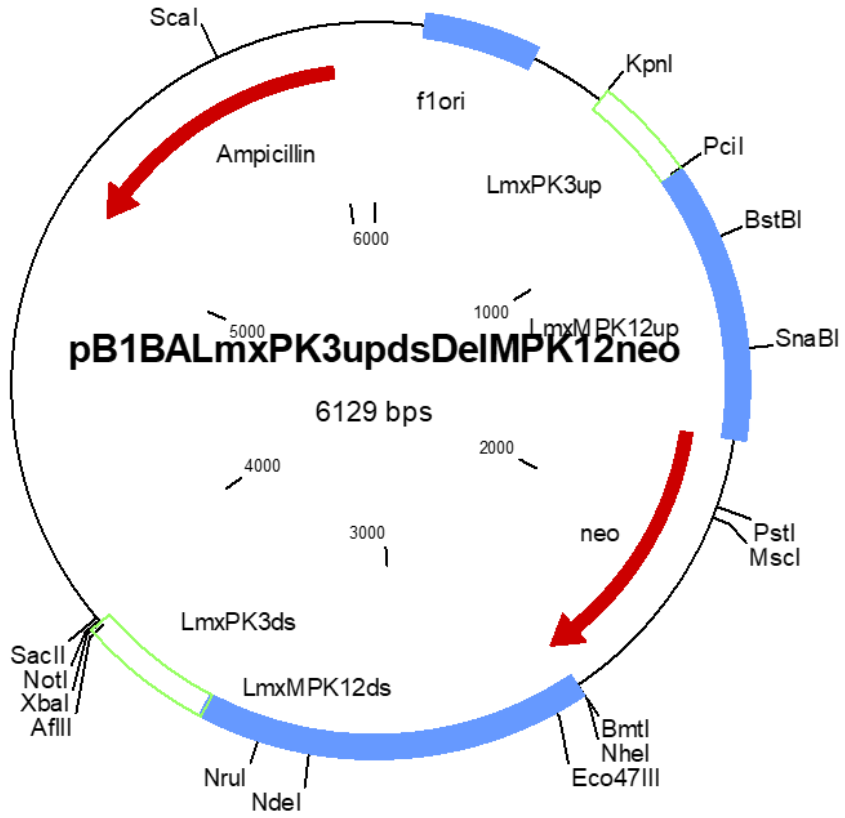
ScaI
KpnI
PciI
BstBI
SnaBI
PstI
MscI
BmtI
NheI
Eco47III
NdeI
NruI
XbaI
AflII
NotI
SacII
f1ori
Ampicillin
LmxPK3up
LmxMPK12up
LmxPK3ds
LmxMPK12ds
neo
pB1BALmxPK3updsDelMPK12neo
6129 bps
1000
2000
3000
4000
5000
6000

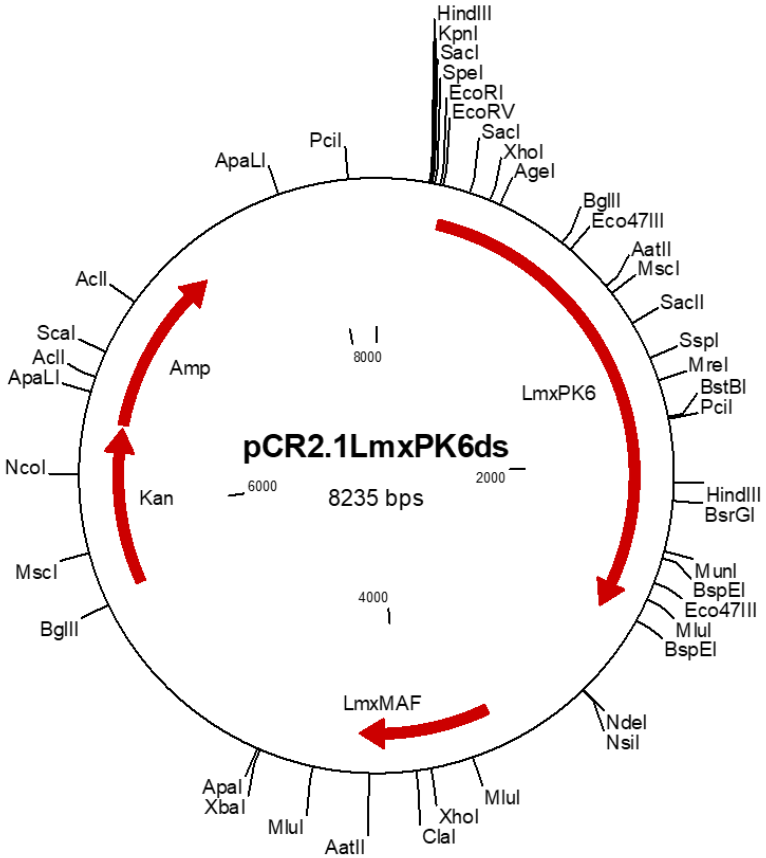
HindIII
KpnI
SacI
SpeI
EcoRI
EcoRV
SacI
XhoI
AgeI
BglII
Eco47III
AatII
MscI
SacII
SspI
MreI
BstBI
PciI
HindIII
BsrGI
MunI
BspEI
Eco47III
MluI
BspEI
NdeI
NsiI
MluI
ClaI
XhoI
AatII
MluI
XbaI
ApaI
BglII
MscI
NcoI
AclI
ScaI
AclI
ApaLI
PciI
ApaLI
Amp
Kan
LmxPK6
LmxMAF
pCR2.1LmxPK6ds
8235 bps
2000
4000
6000
8000

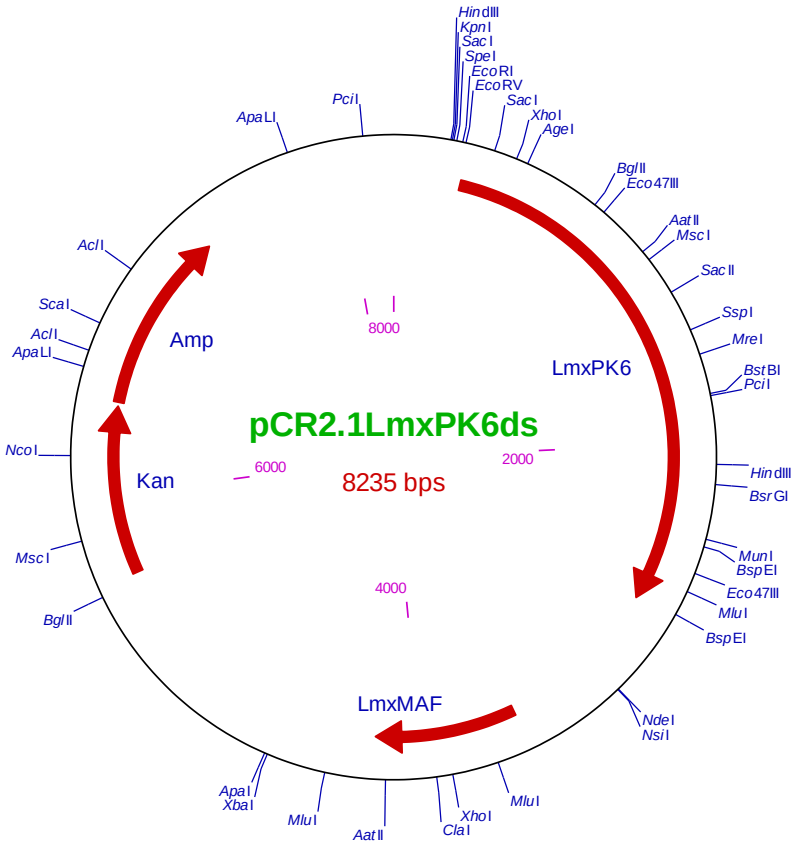
HindIII
KpnI
SacI
SpeI
EcoRI
EcoRV
SacI
XhoI
AgeI
BglII
Eco47III
AatII
MscI
SacII
SspI
MreI
BstBI
PciI
HindIII
BsrGI
MunI
BspEI
Eco47III
MluI
BspEI
NdeI
NsiI
MluI
XhoI
ClaI
AatII
MluI
ApaI
XbaI
NcoI
MscI
BglII
AclI
ScaI
AclI
ApaLI
ApaLI
PciI
8000
2000
4000
6000
Amp
Kan
LmxPK6
LmxMAF
pCR2.1LmxPK6ds
8235 bps

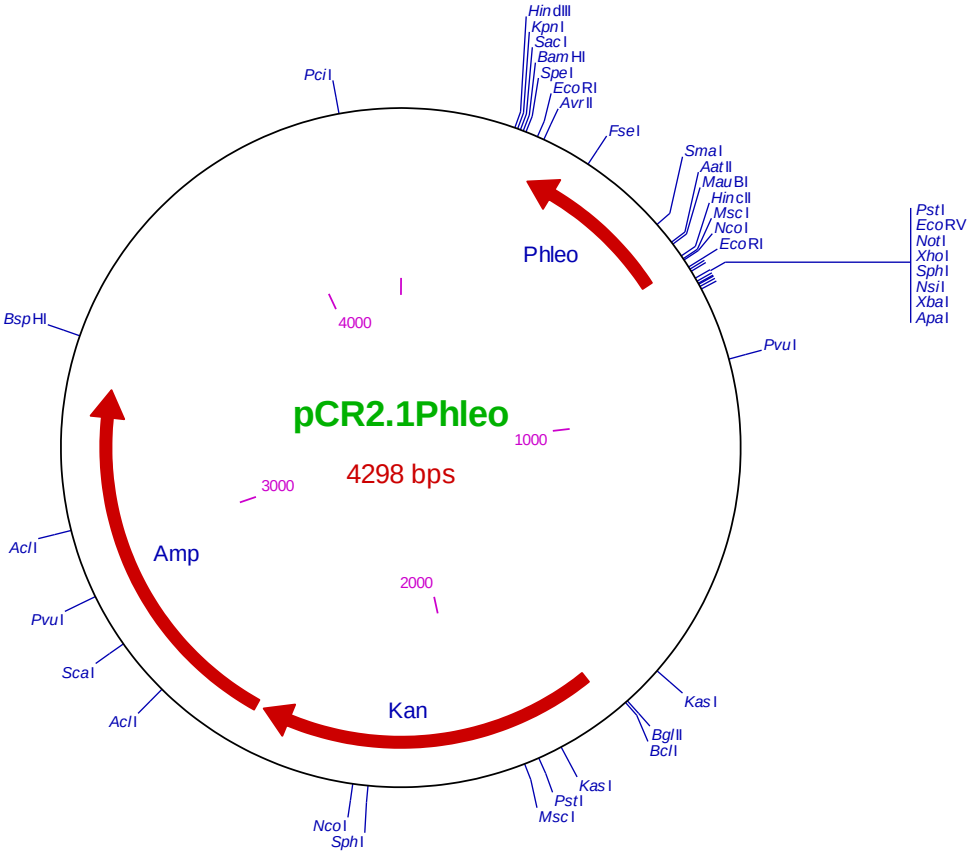
HindIII
KpnI
SacI
BamHI
SpeI
EcoRI
AvrII
FseI
SmaI
AatII
MauBI
HincII
MscI
NcoI
EcoRI
PstI
EcoRV
NotI
XhoI
SphI
NsiI
XbaI
ApaI
PvuI
KasI
BglII
BclI
KasI
PstI
MscI
NcoI
SphI
ScaI
AclI
PvuI
AclI
BspHI
PciI
1000
2000
3000
4000
Amp
Kan
Phleo
pCR2.1Phleo
4298 bps

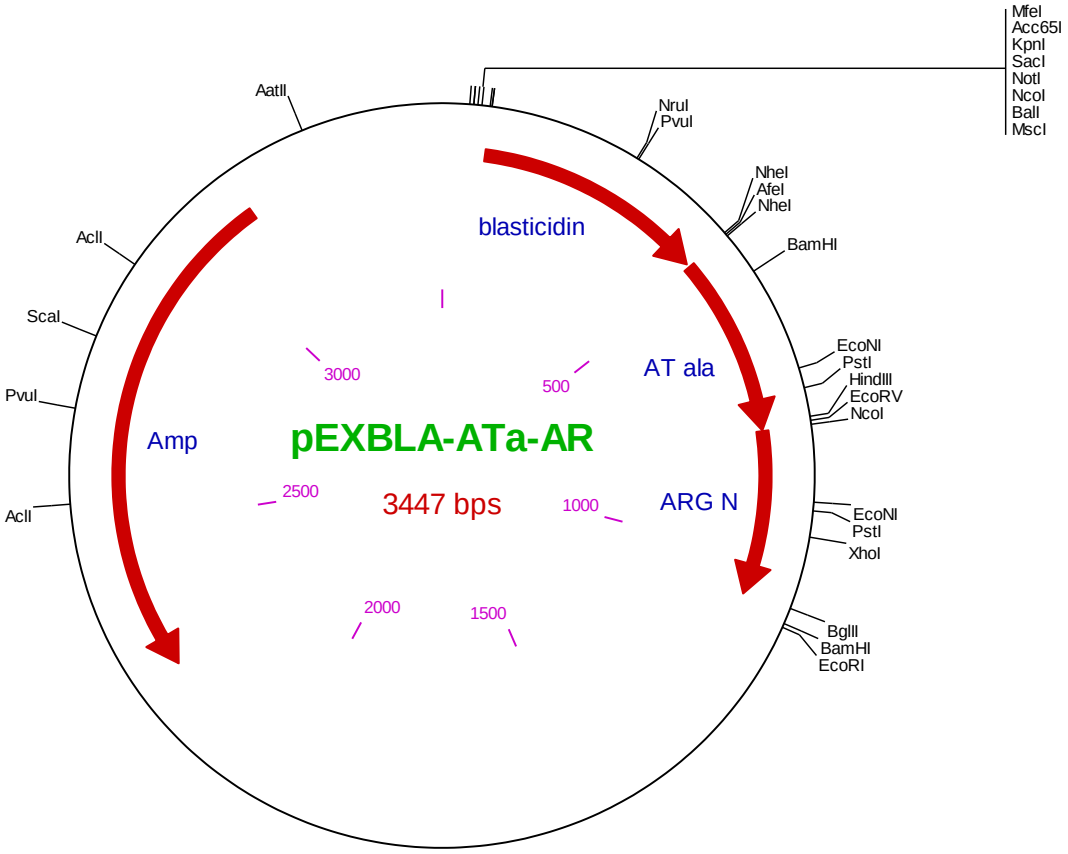
MfeI
Acc65I
KpnI
SacI
NotI
NcoI
BalI
MscI
AatII
NruI
PvuI
NheI
AfeI
NheI
BamHI
AclI
ScaI
PvuI
AclI
EcoNI
PstI
HindIII
EcoRV
NcoI
EcoNI
PstI
XhoI
BglII
BamHI
EcoRI
blasticidin
AT ala
ARG N
Amp
pEXBLA-ATa-AR
3447 bps
3000
500
2500
1000
2000
1500

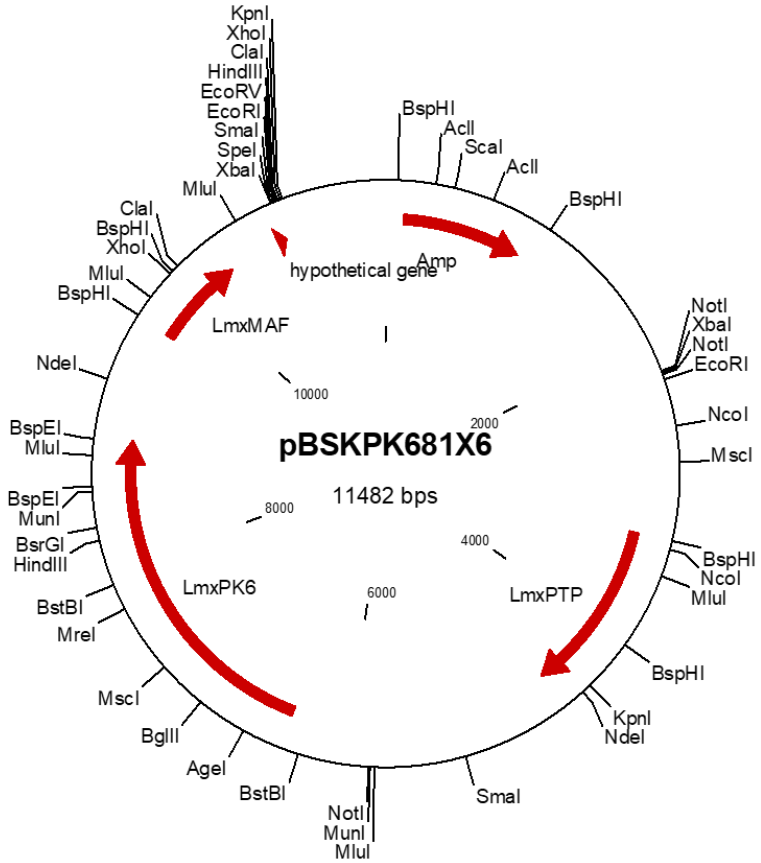
KpnI
XhoI
ClaI
HindIII
EcoRV
EcoRI
SmaI
SpeI
XbaI
MluI
ClaI
BspHI
XhoI
MluI
BspHI
NdeI
BspEI
MluI
BspEI
MunI
BsrGI
HindIII
BstBI
MreI
MscI
BglII
AgeI
BstBI
NotI
MunI
MluI
SmaI
KpnI
NdeI
BspHI
NcoI
MluI
BspHI
MscI
NotI
XbaI
NotI
EcoRI
NcoI
BspHI
AclI
ScaI
AclI
BspHI
hypothetical gene
Amp
LmxMAF
LmxPK6
LmxPTP
pBSKPK681X6
11482 bps
10000
2000
8000
4000
6000

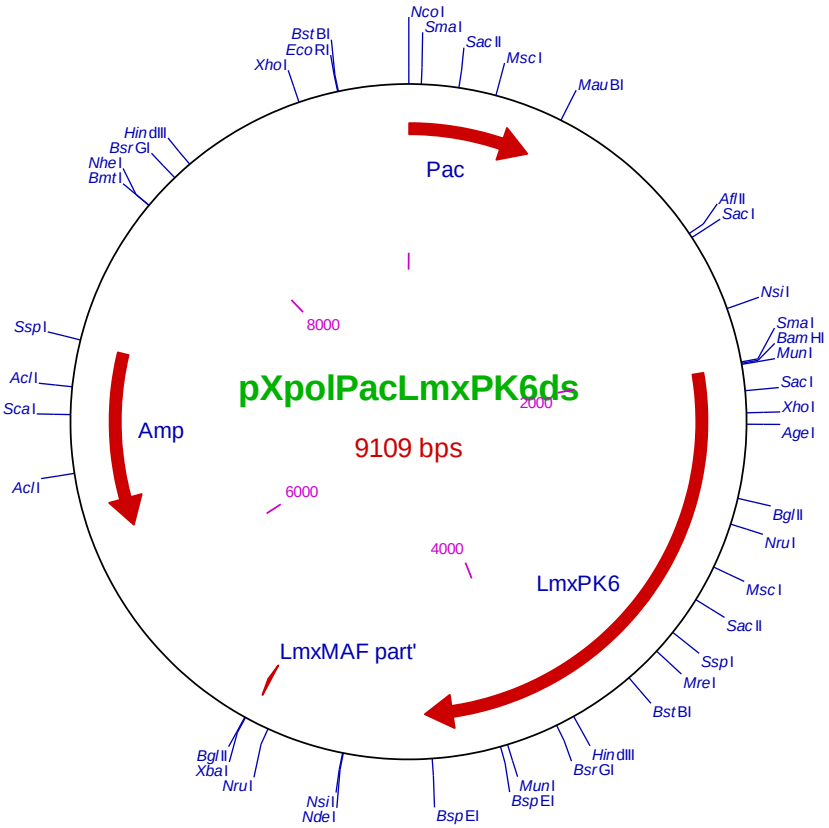
NcoI
SmaI
SacII
MscI
MauBI
AflII
SacI
NsiI
SmaI
BamHI
MunI
SacI
XhoI
AgeI
BglII
NruI
MscI
SacII
SspI
MreI
BstBI
HindIII
BsrGI
MunI
BspEI
NsiI
NdeI
BglII
XbaI
NruI
AclI
ScaI
AclI
SspI
HindIII
BsrGI
NheI
BmtI
BstBI
EcoRI
XhoI
Pac
LmxPK6
LmxMAF part'
Amp
8000
2000
4000
6000
pXpolPacLmxPK6ds
9109 bps

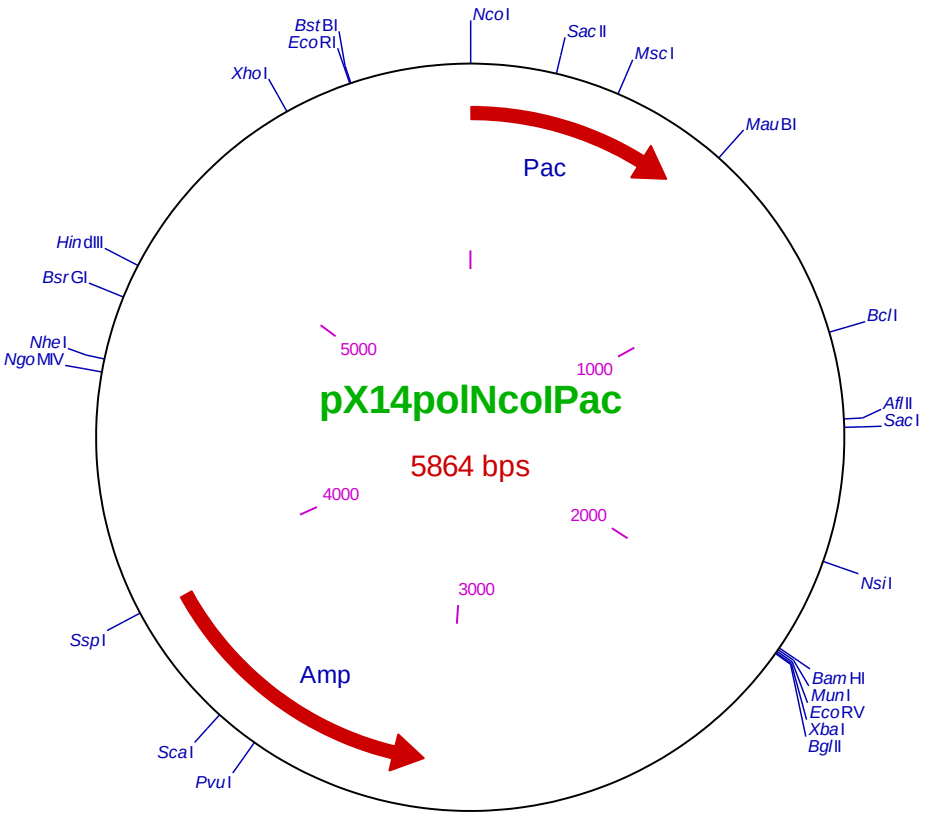
NcoI
SacII
MscI
MauBI
BclI
AflII
SacI
NsiI
BamHI
MunI
EcoRV
XbaI
BglII
PvuI
ScaI
SspI
HindIII
BsrGI
NheI
NgoMIV
BstBI
EcoRI
XhoI
Pac
Amp
1000
2000
3000
4000
5000
pX14polNcolPac
5864 bps

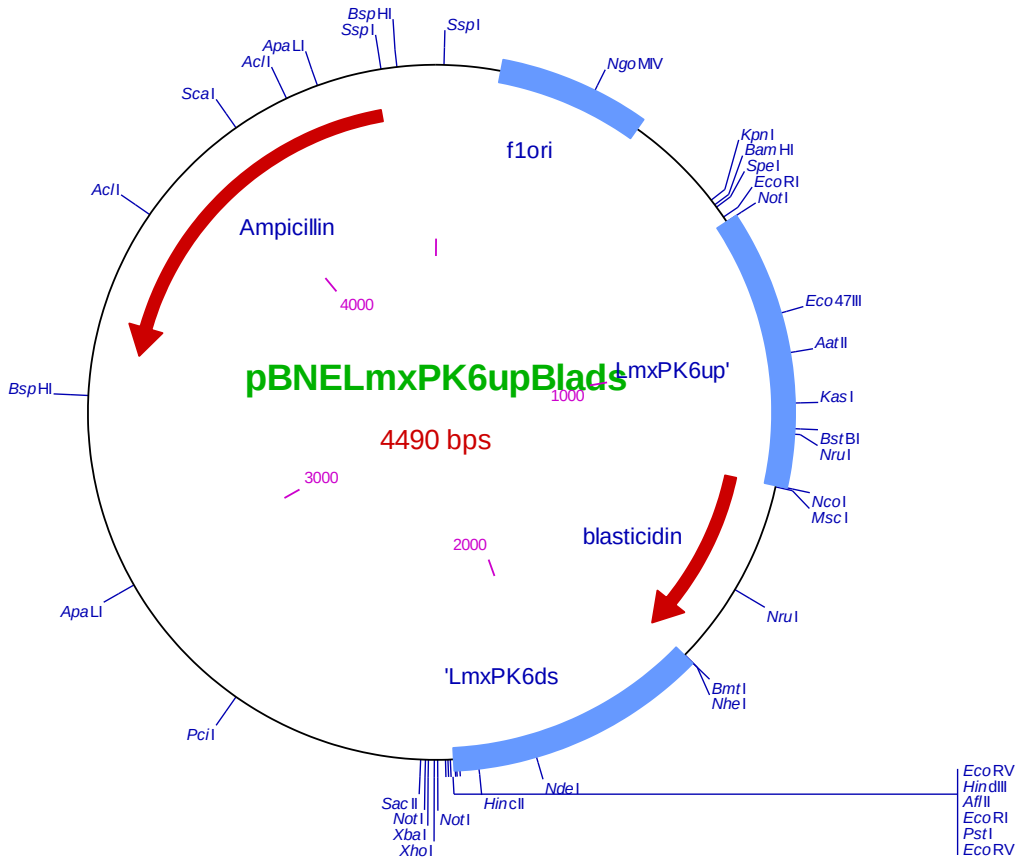
pBNELmxPK6upBlads
4490 bps
f1ori
Ampicillin
'LmxPK6up'
blasticidin
'LmxPK6ds
1000
2000
3000
4000
BspHI
SspI
SspI
ApaLI
AclI
ScaI
AclI
BspHI
ApaLI
PciI
SacII
NotI
XbaI
XhoI
NotI
HincII
NdeI
BmtI
NheI
NruI
NcoI
MscI
BstBI
NruI
KasI
AatII
Eco47III
NgoMIV
KpnI
BamHI
SpeI
EcoRI
NotI
EcoRV
HindIII
AflII
EcoRI
PstI
EcoRV

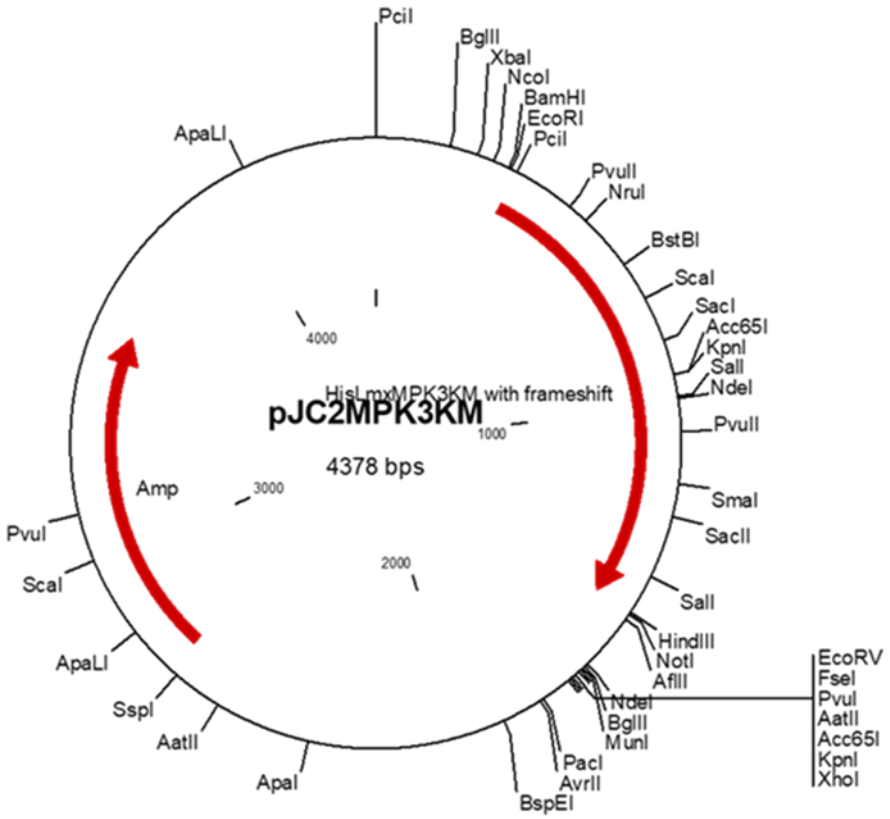
PciI
BglII
XbaI
NcoI
BamHI
EcoRI
PciI
PvuII
NruI
BstBI
ScaI
SacI
Acc65I
KpnI
SalI
NdeI
PvuII
SmaI
SacII
SalI
HindIII
NotI
AflII
NdeI
BglII
MunI
PacI
AvrII
BspEI
ApaI
AatII
SspI
ApaLI
ScaI
PvuI
ApaLI
EcoRV
FseI
PvuI
AatII
Acc65I
KpnI
XhoI
4000
1000
2000
3000
HisLmxMPK3KM with frameshift
pJC2MPK3KM
4378 bps
Amp

9.2 Animal experiment data analysis for LmxPK3

Table Analyzed	Data 1
Column A	**WT**
vs	**vs**
Column B	**LmxPK3+/- K1**
Unpaired t test	
P value	0.7306
P value summary	ns
Are means signif. different? (P < 0.05)	**No**
One- or two-tailed P value?	Two-tailed
t, df	t=0.3492 df=20
How big is the difference?	
Mean ± SEM of column A	0.7378 ± 0.1783 N=9
Mean ± SEM of column B	0.6554 ± 0.1526 N=13
Difference between means	0.08239 ± 0.2360
95% confidence interval	-0.4098 to 0.5746

Table Analyzed	Data 1
Column A	**WT**
vs	**vs**
Column C	**LmxPK3-/- K1D8**
Unpaired t test	
P value	0.3133
P value summary	ns
Are means signif. different? (P < 0.05)	**No**
One- or two-tailed P value?	Two-tailed
t, df	t=1.041 df=16
How big is the difference?	
Mean ± SEM of column A	0.7378 ± 0.1783 N=9
Mean ± SEM of column C	1.033 ± 0.2209 N=9
Difference between means	-0.2956 ± 0.2839
95% confidence interval	-0.8974 to 0.3063